Triassic eosauropterygians from Southwest China

Dissertation

zur

Erlangung des Doktorgrades (Dr. rer. nat.)

der

Mathematisch-Naturwissenschaftlichen Fakultät

der

Rheinischen Friedrich-Wilhelms-Universität Bonn

von

Qiang Li

aus

Anhui, China

Bonn, 2023

Angefertigt mit Genehmigung der Mathematisch-Naturwissenschaftlichen Fakultät

der Rheinischen Friedrich-Wilhelms-Universität Bonn

Gutachter: Prof. Dr. Thomas Martin

Gutachter: Prof. Dr. Jun Liu

Tag der Promotion: 26. 01. 2024

Erscheinungsjahr: 2024

Acknowledgments

During my time in Bonn, particularly while crafting this doctoral dissertation, I've been fortunate to encounter numerous individuals who've offered invaluable support and engaging discussions. Foremost among them is Prof. Dr. P. Martin Sander, whose guidance in bone histology has been instrumental. His unwavering support, insightful discussions, and invaluable suggestions have significantly enriched my academic journey. I extend my gratitude to Prof. Dr. Jun Liu from Hefei University of Technology, my Master's supervisor, for his consistent guidance and support throughout my career. My appreciation also goes to the supervisors and commission members, notably Prof. Dr. Thomas Martin, for his thorough review of this work and great supports on my submission. A special mention to all my co-authors, with Dr. Frank Tomaschek standing out for our enlightening discussions on fossilization. The Section of Paleontology, Institute of Geosciences, University of Bonn has provided an enriching academic environment over the past four years, for which I am deeply thankful. I'm indebted to Olaf Dülfer and Nils Jung for their expertise in thin section preparation. My colleagues in both Bonn and Hefei supported me a lot, especially during research and fieldwork. I would also like to thank the CSC, NSFC, and DFG (Research Unit FOR 2685) for financial and research supports.

Throughout this journey, my friends have been a constant source of motivation, offering both a listening ear and timely distractions. Lastly, my profound gratitude goes to my family. To my wife, our little boy, and my parents: your unwavering support, encouragement, and understanding have been my anchor over these years.

Summary

Bone histology of Triassic marine eosauropterygians, which reveals insights into their ontogeny, the burial conditions that influenced fossil preservation, and the significance of morphology in understanding the paleoenvironment during the Anisian stage, are discussed in this dissertation.

Chapter 2 summarizes the stages of fossil preservation in the SW Chinese fossil Lagerstätten and identifies key factors influencing bone preservation. Observations of different bone tissue sections reveal that the poor preservation of some thin sections is due to specific burial conditions. In order to investigate the reasons behind the various preservation, dozens of materials from the Xingyi area were sampled. The results reveal that some bones in this region have undergone low-grade metamorphism. Additionally, this chapter reported for the first time that the formation of fluorite and a continuous apatite phase transformation within vertebrate fossils. These findings tell the primary signal in the difficult to understand *Keichousaurus* histology. On the other hand, it provides crucial support for selecting appropriate fossils when studying the bone histology of eosauropterygians across the different localities in southwestern China.

Insights from Chapter 2 allow the successful study of *Keichousaurus* histology for the first time, These findings tell the primary signal in the difficult to understand *Keichousaurus* histology. On the other hand, it provides crucial support for selecting appropriate fossils when studying the bone histology of eosauropterygians across the different localities in southwestern China.The new pachypleurosaur described in Chapter 5 puts *Keichousaurus* into a phylogenetic and evolutionary perspective, providing new understanding of the intragroup relationships of eosauropterygians based on the discovery of new materials and comparative morphological study of different eosauropterygian taxa. The new nothosaur in Chapter 6 further contributes to the themes of sexual dimorphism, limb function, especially in conjunction with the track record, and the high diversity in the Chinese Middle Triassic Eosauropterygia and their importance for understanding eosauropterygian evolution in the Triassic.

In summary, the combination of methods applied across different chapters will establish useful methods for future research on the bone histology, morphology, and phylogenetic relationships of eosauropterygians in different Middle Triassic biotas from southwestern China. It will also facilitate a comprehensive exploration of the evolution of eosauropterygians from eastern and western Tethyan regions.

Structure of the dissertation

The dissertation consists of seven chapters. Chapter 1 provides an overview of the research problem, i.e., the introduction of several Middle Triassic marine reptile faunas from Southwest China and the geological background. It also provides a brief review of previous studies on sexual dimorphism, bone histology, and fossilization of marine reptiles.

Chapters 4 and 5 have already been published or accepted by peer-reviewed journals. Chapter 4 was published in *Current Biology*, and Chapter 5 was accepted by the *Swiss Journal of Palaeontology.* According to the regulations, chapters 4 and 5 are present only in a summarized form in this dissertation, and the originally published papers can be found in the appendices. Additionally, author contributions and a summary of the publication are presented at the beginning of chapters 4 and 5.

Chapters 2, 3, and 6 are finished manuscripts. These three chapters are prepared in submitted format with modifications of headings and figure numbering to adapt to the dissertation format.

Chapter 7 is produced following the dissertation format requirement.

Contents

Chapter 1

General Introduction

1.1 The Triassic Southwest Chinese faunas

The Triassic (Eastern Tethys) marine deposits of southwestern China have preserved a highly diverse assemblage of marine reptile fossils, as well as fishes, invertebrates, and plants. These deposits provide an exceptionally continuous record of marine reptile fossils. Notable fossil assemblages from this region include the Middle Triassic Panxian Fauna, Guizhou (Anisian), Luoping Biota (Anisian), Xingyi Fauna (Ladinian), and Late Triassic Guanling Biota (Carnian). Fossils from these four localities cover the major marine reptile taxa of the Triassic Ocean (Benton et al. 2013). Among the four known localities, the Luoping Biota, Panxian Fauna, and Xingyi Fauna preserved diverse eosauropterygians.

The Luoping Biota (Zhang et al. 2008, 2009, Hu et al. 2010, Benton et al. 2013) is a comprehensive marine ecosystem consisting of multiple taxa. The Luoping Biota is extensive and spectacular, including arthropods as the most abundant fossils, followed by fishes, marine reptiles, bivalves, gastropods, echinoderms, brachiopods, conodonts, foraminifers, and plants. This rich assemblage of marine reptiles has been documented by Hu et al. (2010), Benton et al. (2013), and Liu et al. (2011). The fossils are primarily found in rocks belonging to the Upper Member of the Guanling Formation, which dates to the early Middle Triassic (Anisian), about 235 million years ago (Xie et al. 2013). The depositional environment of this formation is thought to have been a shallow marine basin, which contributed to the exceptional preservation of the fossils (Zhou et al. 2014) in the Luoping Biota.

Recently, new marine reptile fossils have been reported from Luxi County, Yunnan Province (see chapters 5 and 6). The county is located about 60 km southwest of Luoping County. Vertebrate fossils from Luxi County were only briefly mentioned by Wen et al. (2020) with fragments of Nothosauroidea and Mixosauroidea. The stratigraphic age of the Luxi fossil beds is similar to that of the Luoping Biota embedded in the Upper Member of the Guanling Formation sensu Wen et al. (2020) and Hu et al. (2022).

The other Anisian fossil fauna is the Panxian Fauna from Yanjuang Village, Panzhou City, Guizhou Province. Since the discovery of marine reptiles in 1999, several groups of marine reptiles have been reported from this fauna. These include sauropterygians, including *Nothosaurus rostellatus* (Shang et al. 2006), *Nothosaurus yangjuanensis* (Jiang et al. 2006), *Lariosaurus hongguoensis* (Jiang et al. 2006), *Placodus inexpectatus* (Jiang et al. 2008),

Wumengosaurus delicatomandibularis (Jiang et al. 2008), *Atopodentatus unicus* (Cheng et al. 2014), and several other groups such as saurosphargids (*Largocephalosaurus qianensis* Li et al. 2013), ichthyosaurs (e.g., *Mixosaurus panxianensis* Jiang et al. 2006), protorosaurs (*Dinocephalosaurus orietalis* Li 2003), and archosaurs (*Qiansuchus mixtus* Li et al. 2006).

So far, there are ten pachypleurosaur-like forms that have been published from the Middle Triassic of Southwest China: *Keichousaurus hui* (Young 1958), *Wumengosaurus delicatomandibularis* (Jiang et al. 2008), *Dianopachysaurus dingi* (Liu et al. 2011), *Diandongosaurus acutidentaus* (Shang et al. 2011), *Qianxisaurus chajiangensis* (Cheng et al. 2012), *Dianmeisaurus gracilis* (Shang and Li 2015), *Dawazisaurus brevis* (Cheng et al. 2016), *Panzhousaurus rotundirostris* (Jiang et al. 2019), *Honghesaurus longicaudalis* (Xu et al. 2022), *Luopingosaurus imparilis* (Xu et al. 2023). In addition, a total of nine nothosaurid species have been reported, including *Sanqiaosaurus dengi* (Young 1965), *Lariosaurus xingyiensis* (Li and Rieppel 2002), *Nothosaurus youngi* (Li and Rieppel 2004), *Nothosaurus rostellatus* (Shang et al. 2006), *Nothosaurus yangjuanensis* (Jiang et al. 2006), *Lariosaurus hongguoensis* (Jiang et al. 2006), *Brevicaudosaurus jiyangshanensis* (Shang et al. 2020), and *Nothosaurus luopingensis* (Shang et al. 2022). Yet another species is newly described in this thesis (see Chapter 6).

The Xingyi Fauna was first reported by Zhongjian Yang in 1958 through the naming of *Keichousaurus hui* (Young 1958). Since then, many new fossils have been found in Xingyi City and adjacent areas, including Sauropterygia, Thalattosauria, and Tanystropheidea (Rieppel et al. 2003, Li et al. 2007, Zhao et al. 2008, Shang et al. 2020). The most diverse group is Sauropterygia, which consists of Placondontia, Pistosauria, Pachypleurosauria, and Nothosauroidea (Benton et al. 2013). The Xingyi Fauna is characterized by an abundance of marine reptile fossils, particularly *Keichousaurus hui*, and includes a diverse range of vertebrate and invertebrate species. This fauna is considered to represent a late stage of the Triassic ecosystem evolution, highlighting the flourishing marine ecosystem during this period.

In summary, the Triassic marine deposits in Southwest China have yielded a wealth of marine reptile fossils that have contributed significantly to our understanding of the diversity and evolutionary history of these ancient marine reptiles.

1.2 Geological background of Southwest China Yunnan and Guizhou

The paleoenvironment and fossils in Southwest China cover various sedimentary facies and biological species from coastal regions to pelagic habitats, respectively (Wang et al. 2008, Jiang

et al. 2009, Luo et al. 2013, Lu et al. 2018). This region was located along the convergent margins of the South China and Indochina plates since the Mesozoic, with the initial plate collision attributed to the Indochina Movement during the Middle and Late Triassic (Metcalfe 2006, Zheng et al. 2013, Faure et al. 2014). This tectonic movement resulted in the deposition of shallow-water carbonate sediments typified by the Yangliujing Formation. The deeper-water nodular limestones and mudstones, such as the Zhuganpo Formation (also known as the Zhuganpo Member of the Falang Formation), accumulated in the upper part of this sequence.

Fossil assemblages from the Xingyi area have been found in Dingxiao and Wusha towns in Xingyi City, Guizhou Province, with additional finds in nearby regions such as Fuyuan and Luoping in Yunnan Province, all contributing to the rich fossil record of the region. The primary fossil-bearing formation is located in the lower part of the Zhuganpo Formation (Zeng et al. 2013). However, there is an ongoing debate about the age of this formation. Chen (1985) initially suggested a late Ladinian age for *Keichousaurus hui*, while Dong (1997) assigned the Zhuganpo Formation, which he called the Zhuganpo Member, to a position between the late Ladinian and early Carnian within the Falang Formation. Conodont studies by Wang et al. (1998) eventually supported the Carnian age for the *Keichousaurus*-bearing beds. Further research by Ma et al. (2013) used ammonite fossils from the Wusha area of Xingyi to tentatively place the Xingyi fauna in the late Ladinian. Thus, the age of the Xingyi fauna could be confirmed as late Ladinian.

1.3 Sexual dimorphism and bong histology of pachypleurosaurs

Sexual dimorphism has been reported mainly from one group of Middle Triassic marine reptiles. Good examples are the small-bodied pachypleurosaurs *Neusticosaurus* and *Keichousaurus* from Europe and China, which show broadened distal humeral ends in adult males compared to females as well as proportional differences (Sander 1989, Lin and Rieppel 1998, Cheng et al. 2004). To understand sexual dimorphism in pachypleurosaurs, several methods have been applied to studies of *Neusticosaurus* and *Keichousaurus* (Sander 1989, Rieppel 1989, Lin and Rieppel 1998, Cheng et al. 2004, 2009, Xue et al. 2015). However, all these studies are based on external morphological characters. The determination of the ontogenetic stage in these studies is based on skeletal ratios formed by allometric growth during different size stages. Although sexual morphological dimorphism is pronounced in these extinct marine reptiles after sexual maturity, juveniles exhibit similar morphological features in both sexes, and juvenile male pachypleurosaurs may have previously been misidentified as females (Sander 1989, Motani et al. 2015, Xue et al. 2015).

Furthermore, additional investigations of bone histology of European pachypleurosaurs, such as *Neusticosaurus* and *Serpianosaurus*, have attempted to examine the potential correlation between sexual maturity and microstructural features, as evidenced by studies by Sander (1990) and Hugi et al. (2011). Klein and Griebeler (2018) proposed a possible onset of sexual maturity based on differences in growth rates between the two sexes in European pachypleurosaurs. These studies focused primarily on microanatomy and growth patterns observed in midshaft sections of long bones. However, despite these efforts, a comprehensive understanding of the histological evidence for sexual maturation and its relationship to external dimorphism in pachypleurosaurs remained elusive (see Chapter 4).

On the other hand, it is worth noting that the bone histology of pachypleurosaurs from the eastern Tethyan region has not yet been documented or reported. The considerable amount of available material, especially that of *Keichousaurus*, provides a promising opportunity to delve into bone histology and explore possible histological dimorphism between the two sexes in these extinct marine reptiles. However, the main reason why this resource is only beginning to be explored is the poor and sometimes peculiar preservation of the bone histology of the Southwest Chinese Triassic marine reptiles (see Chapter 2).

1.4 Fossilization and late diagenesis of fossil vertebrates

Fossils from Southwest Chinese faunas and biotas show different preservation conditions. Considering the different paleoenvironments of these fossil deposits and the geological background of Southwest China, the variation in fossil preservation could be a result of fossilization or subsequent diagenesis of the fossils.

Fossils come in various forms, including hard tissues, soft tissues, and traces, and they can be found in a range of sediment types, such as sandstone, mudstone, limestone, and even metamorphosed sediments (Chapter 2), each with its own complex geological characteristics (Benton and Harper 2009). The process of fossilization involves both internal and external factors, and analysis of the mineral composition of fossilized bones provides valuable insights into the past (Berna et al. 2004, de Sousa et al. 2020). During diagenesis, which involves various geological changes over time, bones undergo changes in their physical, chemical, and mineralogical properties (Keenan et al. 2015, de Sousa et al. 2020).

For decades, researchers have conducted burial experiments to study how fossils form and change over time (Briggs and McMahon 2015, Purnell et al. 2018). These experiments have helped to understand the early stages of fossil formation (Deline and Parsons-Hubbard 2013, Mähler et al. 2022). In addition, studies focusing on later diagenesis have used maturation

experiments to simulate the transformation of organic molecules in fossils (Stankiewicz et al. 2000, Glass et al. 2013, Saitta et al. 2018).

Fresh bone is primarily composed of bioapatite, represented by the formula $[(Ca)_{10-x}[(PO_4)_{6-x}(CO_3)_x](OH)_{2-x}]$, intertwined with an organic collagen matrix (Wopenka and Pasteris 2005, Li and Pasteris 2014, Reznikov et al. 2018). The initial transformation of bioapatite into either carbonate- or fluorine-enriched fossil apatite (FAp) is a topic that has been explored in several studies (Trueman et al. 2008, Hinz and Kohn 2010, Keenan 2016). In particular, fossil bones from ancient times, especially those that pre-date the Pleistocene, are predominantly preserved as FAp. However, they retain the original orientation of the bone crystallites. The discipline of paleohistology is fundamentally based on this preservation mechanism. On the histological scale, the preservation of bone tissue remains consistent regardless of its geological age (Buffrénil et al. 2021). Surprisingly, recrystallization of bone apatite from the bone crystallite FAp has not been previously reported, in contrast to calcite or aragonite fossils where this recrystallization is ubiquitous. Gogáin et al. (2022) reported idiomorphic apatite caused by low-grade metamorphism of a coal swamp deposit in Jarrow, Ireland. However, they do not show that this apatite results from direct recrystallization of the bone FAp in situ that is described in Chapter 2 of this dissertation.

1.5 Aim of the dissertation

The aim of this dissertation is to contribute to a deeper understanding of the Southwest Chinese Triassic eosauropterygian faunas, taking a variety of (sometimes novel) approaches. One aim is to establish a link between bone histology and morphology (i.e., environmental adaptation). The novelty of this study is based on multiple methods, including paleohistology, morphology, and systematic paleontology. In addition, the peculiar preservation of fossils from different localities prompts reflection on the paleoenvironment and subsequent changes in these faunas and biotas. The analysis of bone preservation also provides a potential methodology for sample selection in future paleohistological studies of eosauropterygians from southwest China. Furthermore, the morphology of two newly discovered eosauropterygians from the Luxi locality gives insights into the morphological adaptation and taxonomical diversity of the shallow marine environment in Luxi-Luoping area. Finally, the interrelationships within the Eosauropterygia clade are also examined based on the newly described materials.

1.6 Description of the chapters

As noted, bone histological studies of the Chinese marine reptiles fossils have been challenging. In Chapter 2, the underlying reasons for the different levels of preservation observed in the histological thin sections from Southwest China are revealed. A total of twenty-six marine reptile specimens from two distinct Middle and Late Triassic black shale fossil beds, the Xingyi Fauna and the Guanling Biota, were examined. The examination methods included polarized light microscopy, BSE-SEM imaging, wavelength dispersive X-ray spectroscopy, and Raman spectroscopy. Fluorite as a diagenetic mineral and the continuous transformation of apatite phases are described for the first time in fossilized bones. These findings have provided valuable insights into the relationship between the duration of exposure to high temperatures and the degree of alteration in bone apatite crystals, suggesting a process similar to low-grade metamorphism. Humeri partially replaced by fluorite or recrystallized apatite shows less histological information than unaltered humeri. This chapter also tells that the pre-burial environment (the shallow marine habitat) and the early fossilization of *Keichousaurus* from the Xingyi fauna are not the main factors that affected bone microanatomy.

Chapter 3 describes the bone histology of *Keichousaurus hui* from the Xingyi Fauna of southwestern China. Dozens of humeri were histologically sampled from three nearby localities. The bone tissue deposited in *Keichousaurus* humeri belongs to the lamellar-zonal type. Bone compactness is high in both sexes, and there are no differences. As in other pachypleurosaurs, the very small medullary cavity of the humerus indicates an osteosclerotic-like condition, also known as bone mass increase (BMI), which is consistent with the morphological evidence for secondary aquatic adaptation in *Keichousaurus*. The microanatomy of the humeral midshafts clearly records the onset of sexual maturity for the first time in eastern Tethys pachypleurosaurs. Sexual maturity occurred in the second annulus, corresponding to the second year of life in *Keichousaurus*. In males, the cross section of the shaft changes from round to triangular in the second year. No difference in growth rate between the two sexes was observed in this study, which may be due to the small sample size. The life history data also show an earlier sexual maturity of *K. hui* males compared to other pachypleurosaurs, which may reflect a competitive environment in the Xingyi Fauna.

Chapter 4, published as Li et al. (2023), reports on puberty in *Keichousaurus* based on the microanatomy of the humerus. This is the first report of puberty in a fossil amniote. A combination of bone histology and morphology was used to identify four distinct life stages in *Keichousaurus*, one of which is puberty, as highlighted by Ball and Wade (2013). Among adult *Keichousaurus* individuals, males exhibit more robust humeri compared to females, with

pronounced muscle insertion sites and a triangular shaft cross-section. Examination of mid-shaft sections of male humeri reveals a transformation from the initially rounded juvenile cross-section to the triangular adult cross-section, as evidenced by growth mark patterns. This change in shape is attributed to differential bone apposition along the periosteum, likely influenced by sex hormones, similar to the process observed in humans as described by Callewaert et al. (2010). These changes in bone structure are further influenced by shifts in the loading regime during puberty.

Chapter 5, to be published as Hu et al. (in press), provides insight into a new species of pachypleurosaur from the southwestern Chinese Luxi area in Yunnan Province. The new species, named *Dianmeisaurus mutaensis*, comes from a recently discovered deposit in the Upper Member of the Guanling Formation. The new phylogenetic analysis, using a new data matrix, positions the new taxon as a sister group to *Dianmeisaurus gracilis*, a diminutive pachypleurosaur from the Luoping Biota. This updated phylogenetic analysis also collapsed the monophyly of the traditionally recognized Eusauropterygia. In this new arrangement, Pistosauroidea, *Majiashanosaurus*, and *Hanosaurus* are identified as successive sister groups of a new clade that includes Pachypleurosauria and Nothosauroidea. The result identifies a monophyletic Pachypleurosauria, with the clade formed by *Dianmeisaurus* and *Panzhousaurus* occupying the most basal position. Furthermore, the clade formed by *Dawazisaurus* and *Dianopachysaurus* is identified as the sister group to the other pachypleurosaurs examined in this study. Because *Dianmeisaurus*, *Panzhousaurus*, *Dawazisaurus*, and *Dianopachysaurus* are all uniquely found in southern China, this chapter supports the hypothesis that pachypleurosaurs originated in the eastern Tethys.

Chapter 6 discusses a new species of notosaur (Eosauropterygia) also from the Upper Member of the Guanling Formation of Luxi. The disarticulated partial skeletons give this species a reconstructed body size of 2.5 meters. The comparison and phylogenetic analysis were performed to recognize the relationships within the eosauropterygians. Surprisingly, this analysis recovered a monophyletic genus *Nothosaurus*, unlike the previous one. This discrepancy between the two studies may be due to the addition of this new taxon of nothosaur but also reflects the inherent instability of the nothosauroidea tree. The new nothosaur from the Luxi locality shows a peculiar adaptation to the shallow marine habitat like the much smaller eosauropterygians from the Luoping Biota, apparently related to foraging on the shallow sea or lagoonal bottom.

Chapter 7 offers a synthetic perspective on the research results of this thesis. The topics are the bone histology and ontogeny of Middle Triassic pachypleurosaurs, fossil preservation and its implications for sampling material selection, and the implications of the two new

Chinese eosauropterygians. The chapter also rethinks the environmental adaptation within Chinese eosauropterygians through the correlations between paleohistology, morphology, and paleoenvironment of Chinese eosauropterygians. The study of fossilization and diagenesis provides useful approaches for recognizing available materials for bone histology research. Furthermore, future perspectives and possibilities of applying a combination of paleohistological, geochemical, and morphological methods to similar case studies in other Triassic marine reptiles from southwestern China are discussed.

Chapter 2

Fossilization and low-grade metamorphism of Triassic marine reptiles from Southwest China: A continuum of apatite transformation and fluorite precipitation

2.1 Authors and their contributions

Qiang Li, Jun Liu, Fabian Gäb, and P. Martin Sander. Fossilization and low-grade metamorphism of Triassic marine reptiles from Southwest China: A continuum of apatite transformation and fluorite precipitation. Submitted to *Palaeogeography, Palaeoclimatology, Palaeoecology* in November 2023.

QL, PMS, and JL designed the study. QL and PMS did the optical observation. QL collected the data and made the analysis. JL and FG helped with program investigation and improved the visualization. QL and PMS wrote the preliminary manuscript. QL prepared the figures and plates. QL, JL, PMS, and FG revised the manuscript for final submission.

2.2 Abstract as submitted to Palaeogeography, Palaeoclimatology, Palaeoecology

Models for successful fossilization and later alteration have not been established yet. Meanwhile, fossil bones from different localities vary greatly, making it challenging to ascertain different stages during alteration. Twenty-six specimens of marine reptiles from two Middle and Late Triassic black shale deposits (Xingyi Fauna and Guanling Biota) of southwest China were examined by polarized light microscopy, BSE-SEM imaging, wavelength dispersive X-ray spectroscopy, and Raman spectroscopy. Fluorite and continuous apatite phase transformation were observed in fossil bones for the first time. Our results revealed a correlation between the duration of high-temperature exposure and increased alteration levels of bone apatite crystals, suggesting low-grade metamorphism. We defined five stages of preservation among sampled fossils and established a corresponding model with increasing diagenesis and metamorphic alteration of bone histology. Stage I represents no alteration beyond diagenetic mineral precipitation in bone pores. Stage II shows a slight loss of apatite crystallite birefringence and the beginning of fluorite precipitation. Stage III encompasses the migration of kerogen from host shale into fossil bone, further loss of bone structure, and more fluorite formation. Stage IV shows recrystallization of fossilized bone apatite to idiomorphic apatite. Stage V is the complete loss of bone matrix structure and replacement by idiomorphic apatite. The correlation of alteration processes with temperature and the sources of F and Ca

that formed the fluorite is also explained. This study provides reference results for different stages of bone alteration during real geo-history, essential for studying bone diagenetic processes in dependence on high temperatures and fluids.

2.3 Introduction

Fossils, which are remains or traces of extinct creatures, play a crucial role in understanding Earth's long history (Rudwick 2008). The preservation of dead organisms as fossils is the exception and not the rule (Muscente et al. 2017). Fossils, preserved as hard tissues, soft tissues, and traces, are embedded in various geological materials, including sandstone, mudstone, limestone, and meta-sedimentary rocks (Benton and Harper 2009). To explore the diagenetic and metamorphic processes that occurred during the fossilization and later alteration, burial experiments addressing specific types of preservations have been applied for decades (Briggs and McMahon 2015, Purnell et al. 2018) and have significantly contributed to our understanding of early fossil diagenesis (e.g., Deline and Parsons-Hubbard 2013, Mähler et al. 2022). Studies have also been conducted on the later diagenesis of fossils, including maturation experiments that reveal changes in organic molecules and simulated diagenetic processes (Stankiewicz et al. 2000, Glass et al. 2013, Saitta et al. 2018). However, changes in temperature, pressure, and fluid conditions during or after late diagenesis (especially low-grade metamorphism) are quite challenging to evaluate and have not commonly been reported before.

Most importantly, although experimental processes can be accelerated by increasing the temperature and pressure, only changes in organic composition can usually be observed (Saitta et al. 2018). For inorganic components, the geological conditions and long fossilization time cannot be reproduced appropriately under simulation settings. Bennett et al. (2011) proposed a model based on six diagenetic stages for Carboniferous ostracods observing the degree of recrystallization in their carapaces. Nevertheless, this study does not offer detailed steps explaining the transition from fresh bone to severely altered fossils since it is merely based on the final mineralogy stage of diagenesis and on a carbonate, not a phosphate, mineral system.

Over the centuries, vertebrate fossil assemblages have been excavated around the globe, and the continued discoveries provide abundant knowledge of the biological evolution, adaptions, and paleoenvironments of prehistoric Earth. Vertebrate fossils are usually preserved as fossilized bones. The fossilization of bones involves endogenous and exogenous processes, and the mineral composition of fossil bones is a valuable path to the past (Berna et al. 2004, Sousa et al. 2020). During diagenesis, the alteration of bone results in changes on various scales in physical, chemical, and mineralogical properties (Keenan et al. 2015, Sousa et al. 2020).

Because of the overprinting effects of diagenetic and possible metamorphic processes, determining how fossil bones formed and were altered is rarely straightforward.

Fresh bone is a complex combination of bioapatite ($[(Ca)_{10-x}[(PO4)_{6-x}(CO3)_x](OH)_{2-x}]$), here termed 'BAp', and an organic collagen matrix (Wopenka and Pasteris 2005, Li and Pasteris 2014, Reznikov et al. 2018). The early-stage transformation from bioapatite to carbonate-enriched or fluorine-enriched fossil apatite (FAp) has been discussed in several studies (e.g., Trueman et al. 2008, Hinz and Kohn 2010, Keenan 2016), and fossil bones from deep time (i.e., pre-Pleistocene) are overwhelmingly preserved as FAp but keep the original crystallite orientation. The entire field of bone paleohistology is based on this mode of preservation, where at the histological level, bone tissue is preserved independently of geologic age (Buffrénil et al. 2021). Surprisingly, recrystallization of bone apatite from the bone crystallite FAp has not been reported before, unlike in calcitic or aragonitic fossils, where this recrystallization is ubiquitous. Although Ó Gogáin et al. (2022) reported idiomorphic apatite in bone porosity caused by low-grade metamorphism of a coal swamp lagerstätte (Jarrow, Ireland), they do not show that this apatite results from direct recrystallization of the bone FAp in place. Here, we describe this "third generation" of apatite derived from FAp, which was derived from BAp in reptile fossils from the Triassic marine faunas of SW China. We term this mineral phase of recrystallized fossilized bone apatite 'RAp'.

2.3.1 Triassic marine vertebrate faunas and regional geology of the SW China

Since 1945, several world-famous Middle and early Late Triassic marine biotas have been successively reported from southwest China (Benton et al. 2013). The localities are mainly distributed in Guizhou and Yunnan provinces, including Luoping Biota, Panxian Biota, Xingyi Fauna, and Guanling Biota (Benton et al. 2013). The paleoenvironment and fossils in SW China cover a variety of sedimentary facies and biological species from coastal regions to pelagic habitats, respectively (Wang et al. 2008, Jiang et al. 2009, Luo et al. 2013, Lu et al. 2018). Tectonically, southwest China has been located on the convergent margins of the South China and Indochina plates since the Mesozoic (Metcalfe 200, Zheng et al. 2013). The plate collision was caused by a tectonic event called the Indo-China Movement during the Middle and Late Triassic (Faure et al. 2014). The subsequent Yanshan Movement, which influenced the forming of the present China, also significantly impacted the regional tectonics of southwest China (Dong et al. 2008). Faults formed by extensive tectonic activity and the associated magmatic intrusion promoted hydrothermal deposits in the region (Mao et al. 2013, Li et al. 2020). These deposits are associated with extensive low-grade regional metamorphism in several provinces of southwest China (Li et al. 2018). Due to this geological setting, sediments in southwest China have undergone varying degrees of alteration after initial diagenesis.

Here we investigate the preservation of fossil bones from the Xingyi Fauna and the adjacent Guanling Biota, where tens of thousands of marine reptiles and associated fossils have been unearthed. Sufficient fossil materials, diverse burial conditions, and well-studied geological backgrounds provide perfect conditions for research on bone diagenesis and metamorphic alteration. The influences of various factors on the burial environment (such as fluids, temperature, and organic content) were assessed to understand the transitions of fossils during late diagenesis and low-grade metamorphism, i.e., beyond the standard FAp preservation. The organic matter preserved in the fossilized bones and their matrix allows the application of the Raman carbonaceous matter (CM) geothermometer (see Methods). Petrological thin sections, Raman spectroscopy, BSE-SEM imaging, and Wavelength dispersive X-ray spectroscopy (WDX) were used to understand bone microstructural changes at different diagenetic levels and diagenetic environments. Furthermore, a model correlating burial conditions and bone preservation and mineralization was established to explain the unusual fossil bone preservation from the Triassic of SW China.

Institutional abbreviations: HFUT, Hefei University of Technology; IGPB, Section Paleontology, Institue of Geosciences, University of Bonn.

Locality abbreviations: DQT, Daqingtou Village, Yunnan Province; GL, Guanling County, Guizhou Province; JYS, Jiyangshan Village, Yunnan Province; LG, Longguang Town, eastern Xingyi County, Guizhou Province; XY, Xinheini, western Xingyi County, Guizhou Province.

2.4 Material and Methods

2.4.1 Material

The 26 fossil reptile skeletons used in this study are from several Triassic localities in southwest China (Fig. 2.1, Table S1). They represent three taxa, i.e., the pachypleurosaur *Keichousaurus hui*, the thalattosaurs *Anshunsaurus* sp., and the thalattosaurs *Xinpusaurus* sp. Twenty-five sampled specimens are held at the Hefei University of Technology collections (21 *K. hui*, one *Anshunsaurus* sp., and three *Xinpusaurus* sp.) and one (*K. hui*) held at the University of Bonn.

The *Keichousaurus* specimens are from the late Ladinian (late Middle Triassic) Xingyi Fauna, hosted by the Zhuganpo Member of the Falang Formation (Zou et al. 2015a) cropping out in remote southwestern Guizhou and adjacent Yunnan provinces. An alternative term used in other studies is Zhuganpo Formation (Zeng et al. 2013). Eighteen samples, including the IGPB sample, show the typical pattern of Xingyi Fauna preservation, with black bones embedded in a dark grey shale matrix. The shales are indurated, and some specimens show white tectonic veins. Of these 18 specimens, seven were excavated at Xinheini (locality

abbreviation ‘XY’) and ten at Jiyangshan (locality abbreviation ‘JYS’) villages. Although the *Keichousaurus hui* (IGPB R-670) housed at IGPB lacks accurate locality information, its preservation in indurated dark grey shale with white tectonic veins suggests it belongs to the Xingyi Fauna. However, three specimens from Longguang (locality abbreviation ‘LG’) show a rather different preservation: light-colored bone embedded in a light reddish laminated rock.

Among the thalattosaurs, the single *Anshunsaurus* sp. specimen HFUT DQT-20-001 is also from the Xingyi Fauna and was collected at Daqingtou (locality abbreviation ‘DQT’), located on an adjacent hillside to Jiyangshan (Fig. 2.1). The three *Xinpusaurus* specimens, on the other hand, are from the Guanling area (locality abbreviation ‘GL’) in southwestern Guizhou Province, from the lower member of the Xiaowa Formation (Carnian, early Late Triassic) and are associated with the Guanling Biota (Wang et al. 2008).

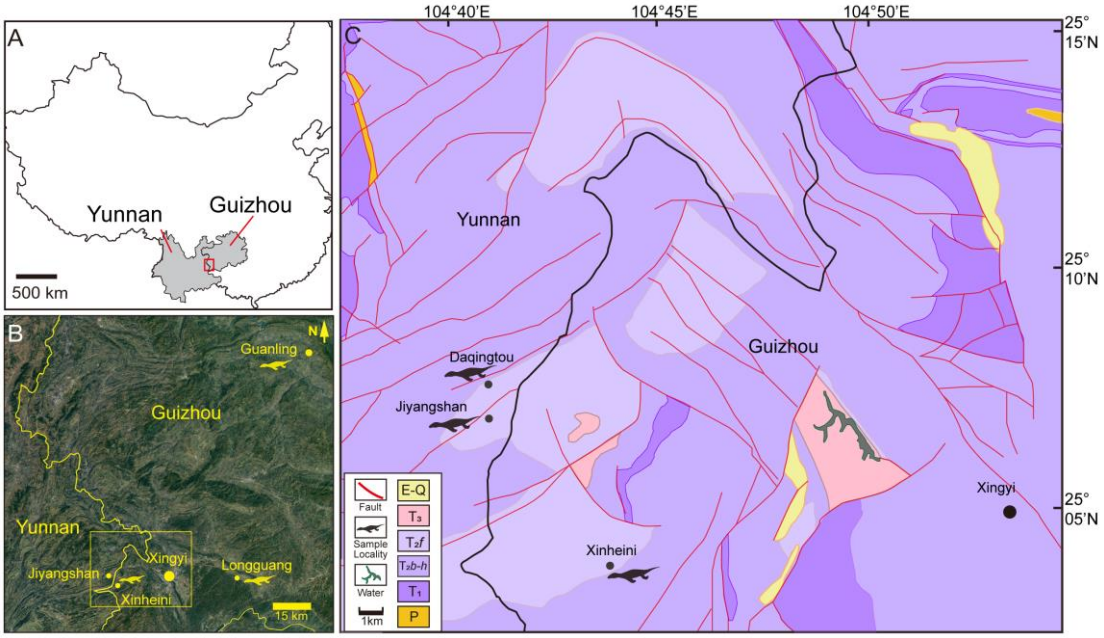

Figure 2.1. (A) Map of China with Guizhou and Yunan provinces highlighted; red square indicates the study area in map B. (B) Google Earth image showing fossil localities; note that ‘Xinheini’ represents the locality of XY samples. (C) Geological map of Yunnan and Guizhou provinces (yellow box in B, with the three fossil localities of the Xingyi Fauna from which the fossils in this study came; updated after Zhou et al. 2021); note the extensive faulting and folding in the region. Abbreviations: E-Q, Paleogene and Quaternary; T3, Upper Triassic; T2f, Falang Formation (fossils are hosted by the Zhuganpo Member), Middle Triassic; T2b-h, Baifeng Formation to Hekou Formation, lower Middle Triassic; T1, Lower Triassic; P, Permian.

2.4.2 Methods

Thin sectioning and polarized light microscopy

Samples for thin section preparation were obtained by core drilling at the prescribed position in humeral midshafts or ribs (Stein and Sander 2009). Cores were embedded in synthetic epoxy resin (Araldite 2020 A/B, Huntsman, Cambridge) and then sectioned along the previously marked transverse plane. Thin sections were prepared using standard petrographic methods (Lamm and Padian 2013) and ground to 30 to 80 μm thick. Thickness depended on translucency, as was noticed in a previous study on the *K. hui* material (Li et al. 2023). Optical microscopy was done on all thin sections in transmitted light mode using a Leica® DM750P polarizing microscope and a digital camera (Leica® DFC420). Photomicrographs were taken using ImageAccess easyLab 7.0 software. Some thin sections were left uncovered to permit further analysis by Raman spectroscopy, WDX element mapping, and cathodoluminescence (CL) observation in the electron microprobe.

Raman spectroscopy

Raman spectroscopy was used to study organic matter, specifically the organic carbon (carbonaceous matter, CM), in the fossils after petrographic thin section analysis of the bones. Organic matter gradually transforms into stable graphite with burial and metamorphic processes (Beyssac and Rumble 2014), and the degree of graphitization is only related to the peak metamorphic temperature and is irreversible. Raman spectra of CM exhibited a systematic change with the degree of metamorphism and provided a reliable geothermometer for metamorphic rocks in previous studies (e.g., Beyssac et al. 2002, Rahl et al. 2005, Lahfid et al. 2010, Kouketsu et al. 2014).

The Raman spectrometer used in this study is a Horiba Scientific HR800 confocal Raman spectrometer from the Institute of Geosciences at the University of Bonn. The spectrometer is equipped with an Olympus BX41 microscope and three different lasers. The 532 nm laser with a power output from 1 mW to 3 mW (3 mW for mineral content analysis) was used. However, some observation sites were slightly etched or burnt at 2 mW and 3mW. Thus, only spectra analyzed with 1 mW laser energy are considered.

The Raman scattering was detected with a 100x long working distance objective and an EMCCD detector over an acquisition time of 10 seconds. The grating was set to 600 grooves/mm and 200 holes per minute. Six thin sections from the Xingyi Fauna and two from the Guanling Biota were tested without coverslips. The identification of mineral content is based on the RRUFF database (Lafuente et al. 2015) using the software CrystalSleuth Application Version: May 19, 2008 (Laetsch and Downs 2006).

The peak fitting of CM for temperature determination focuses on the first-order region (1000-1750 cm^{-1}), which is associated with up to five discriminative bands for CM (G, D1, D2, D3, and D4). The raw data were fixed to range from 1000-1750 cm^{-1} in Excel. Peak fitting and spectra temperature estimation were done automatically using Python codes developed by Kaneki and Kouketsu (2022), modified from Kouketsu et al. (2014).

Raman spectra of the stage I-a fossil (HFUT LG-21-003) show a low intensity and high fluorescence background in the wavelength ranges of 1000–1750 cm^{-1}, leading to the inaccuracy of the peak fitting. Hence, the CM temperature of this sample could not be reliably obtained. For the remaining samples, the equation T[°C] = -2.30* FWHM-D1 + 486 from Kaneki and Kouketsu (2022) is applied in our study. The 95% prediction intervals of peak temperature were approximately ±30°C in 150-400°C using the auto fitting function (Kaneki and Kouketsu 2022).

Electron probe microanalyzer

To understand the petrography of the samples at high resolution, wavelength dispersive X-ray spectroscopy (WDX) was applied to the samples after the Raman spectroscopy. The instrument is a Jeol JXA-8200 SuperProbe high-resolution SEM with an element analyzer in the Institute of Geosciences of the University of Bonn. Carbon coating was applied to the samples before using the instrument. We performed BSE, CL imaging, and element maps on all carbon-coated, uncovered thin sections to detect the abundance and distributions of minerals. The SuperProbe was used in element mapping mode with 15 kV accelerating voltage and 15 nA beam current for all analyses.

Element distribution maps were recorded using WDX with 100–150 ms dwell time. The resolution of the elemental maps is 2 mm per step. The WDX recognized the following elements: C, Ca, F, P, S, Si, Cl, Na, Mg, Al, K, Fe, Ba, Sr, and Ti. For each element, there is one map that shows both distribution and relative concentration. The spatial overlap of different elements in the maps is used to detect specific minerals; e.g., a match in the distribution of Fe and S on the maps is taken to indicate pyrite (FeS_2). The instrument also provides backscattered electron (BSE) images of the mapped area. The distribution (but not composition) of minerals, organics, matrix, and embedding medium can be viewed in a single BSE image (e.g., Fig. 2.3B, C).

2.5 Results

The patterns of alteration of 26 fossil specimens were conceptualized as five alteration stages based on the optical preservation of the bone tissue, the organic matter content, the minerals found as bone porosity fill and tissue replacement, and the apatite phases. The degree of bone tissue alteration and recrystallization increases from stage I to stage V (Fig. 2.2).

Figure 2.2. Thin section images of eight samples representing five alteration stages caused by diagenesis and low-grade metamorphism. Each pair of images has the plane polarized light image on the left and cross-polarized light with lambda filter on the right. (A) Alteration stage I (I-a), HFUT LG-21-003; (B) Stage I (I-b), HFUT GL-17-004; (C) Stage II, HFUT XY-18-003; (D) Stage III, HFUT JYS-15-023; (E) Stage IV (IV-a), IGPB R-670; (F) Stage IV (IV-b), HFUT GL-17-001; (G) Very late stage IV (IV-a), HFUT DQT-20-001; (H) Stage V, HFUT GL-17-003. Scale bars equal 200 μm.

2.5.1 Five stages of bone alteration

Stage I, unaltered fossilized bones.

Stage I is represented by unaltered fossil bone tissue, meaning that the fossilized bone fibers consist of FAp only, as indicated by full birefringence under cross-polarized light. The fossils of stage I can be assigned to two substages, i.e., stage I-a (samples with low organic content, all from Longguang) and stage I-b (a sample from Guanling with high organic contents). A

representative fossil of stage I-a is HFUT LG-21-003. It shows fewer organics but more iron oxides than the other stages. The thin sections show strong birefringence of the bone mineral in cross-polarized light, which means the bone tissue is well preserved, and the apatite was not altered. Both the humerus and rib samples keep adequate histological information. Bone pores (osteocytes, vessels, and cracks) are occupied by red iron oxides and calcite (Fig. 2.3A). The BSE image (Fig. 2.3A, B) reveals the tiny spherical morphology of the iron oxides, which are attached to the inner wall of pores. The red iron oxides (Fig. 2.3A) were confirmed as hematite through Raman spectra. The elemental maps show a ubiquitous high concentration of C in the bone matrix (Fig. 2.3D). When combined with the Ca distribution, the P and F maps reveal that the fossil bone is mainly FAp (Fig. 2.3E, F). Calcite appears in some of the porosity (Fig. 2.3D), as already recognized by optical microscopy. The highest intensity of carbon (Fig. 2.3G) is correlated with pores and fractures filled with epoxy resin, as displayed in the BSE image (Fig. 2.3B, C). Consistent with light microscopy, the Fe map shows hematite enrichment in some bone pores (Fig 4.3B, H). Based on the mapping result of the selected area, the relatively high concentration of Si may represent some clay minerals filling in the spaces (Fig. 2.3I) between the iron oxides.

The *Xinpusuarus* specimen (HFUT GL-17-004) shows a similar alteration stage as the Longuang specimens, but it lacks hematite, and thus it is defined as alteration stage I-b (Fig. 2.2B). The thin section of the specimen is relatively dark in plain polarized light, possibly indicating higher CM contents in this bone compared to the LG samples. The structures of bone tissues and osteons in fossils of stage I-b are also finely preserved, which means the bone is not affected by metamorphism. The fractures within the bone are filled with calcite, resulting from diagenetic compression (sediment compaction) of the fossil.

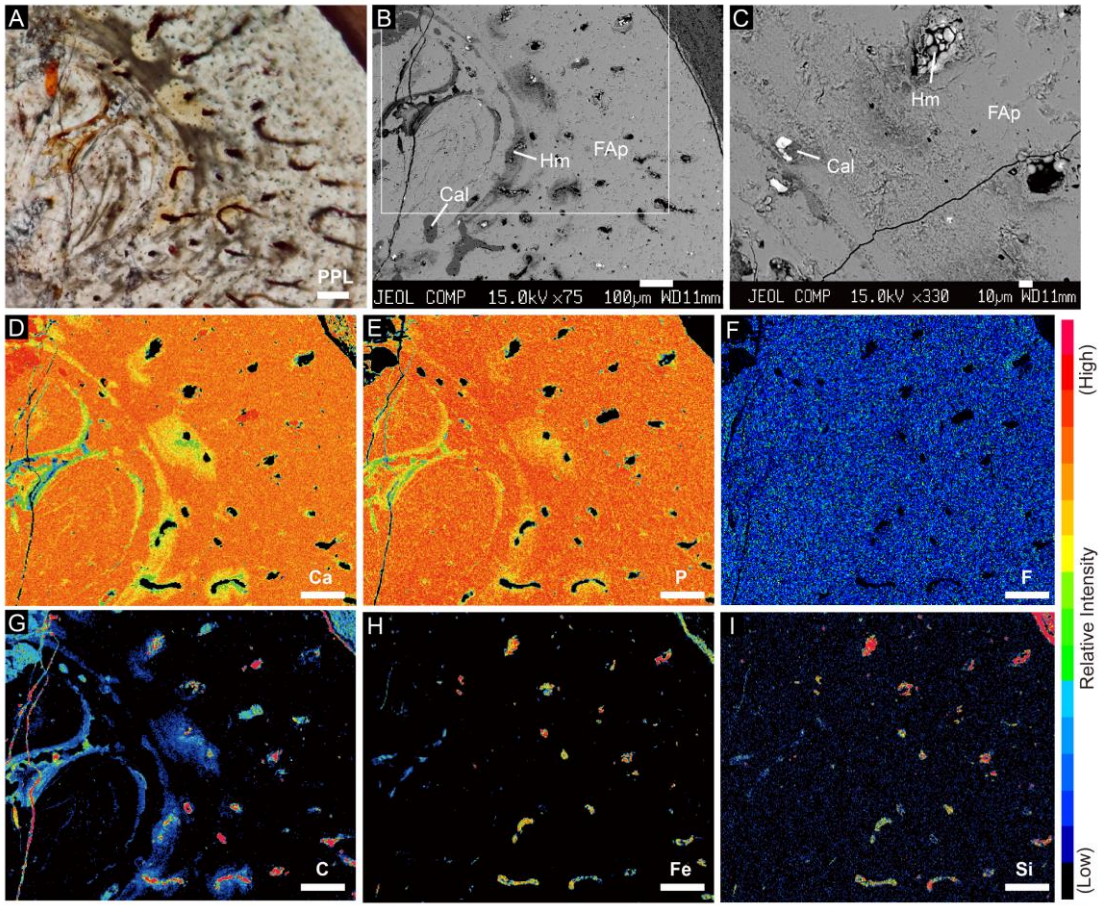

Figure 2.3. Alteration stage I (I-a, see also Fig. 2.2A): light microscopy imaging, SEM-BSE imaging, and WDX mapping of selected elements in the humeral thin section of sample HFUT LG-21-003 with low organic content. (A) Thin section in plane-polarized light (PPL). (B) SEM-BSE image with WDX mapping area indicated by box. (C) BSE image of spherical hematite and calcite infillings. (D-I) Element maps of Ca, P, F, C, Fe, and Si distribution in selected areas. The element maps show that the fossilized apatite is fluorapatite. Bone pores and fractures are infilled by hematite, calcite, and clay minerals. High intensity in the C map indicates results from epoxy introduced during sectioning. Scale bar equals 100 µm if not specified otherwise. Abbreviations: Cal, calcite; FAp, bone apatite fossilized as fluorapatite; Fl, fluorite; Hm, hematite; PPL, plane polarized light.

Stage II, slightly altered bones

Fossils of alteration stage II show slight alteration. The distinguishing feature of stage II specimens, compared to those of stage I, is the presence of the mineral fluorite and slightly altered bone tissue. The tissue appears bright under PPL but strikingly shows fluorite as a pore fill of microtunnels and needle-like (acicular) fluorite crystals. Fluorite as a mineral has not been reported in fossil bones before, to our knowledge. Specific examples of alteration type II-a include HFUT XY-18-003 and HFUT XY-18-004, both from Xinheini. HFUT XY-18-003 has a similar optical microscopic appearance to the Longguang specimens, but the CM content is

high. The bone apatite is slightly altered in the region with fractures, losing part of its birefringence. Both specimens show tiny needle-like crystallites inside the bone matrix, which can be recognized as long acicular crystals of fluorite (around five mm in width). These acicular crystallites are more concentrated near the vascular canals (both radial and longitudinal) and reach a length of up to 200-300 mm. In the thin section of HFUT XY-18-004, the acicular crystallites surrounding the pore spaces show an intersectional growth angle near 90° (Fig. 2.4B). The micro-tunnels that are filled with fluorite may have been caused by bioerosion through the growth of fungal hyphae or algae. The tunnels vary in diameter from 5 to 30 micrometers.

Combined with the elemental maps, the BSE images reveal that the main pore-filling materials consist of fluorite, calcite, CM, and clay minerals. Baryte and pyrite are rare occurrences (Fig. 2.4A, C). The BSE image of HFUT XY-18-003 especially shows fluorite-filled pores (Fig. 2.4C). The correlated distribution of Ca and F in the elemental maps (Fig. 2.4D, F) shows that the bone tissue of this specimen is mainly FAp, slightly altered near the fractures where there is a lower P intensity (Fig. 2.4D, E). The cracks, which show two kinds of element combinations, can be divided into two stages based on the cross-cutting pattern. Fractures of the earlier stage show a lower level of P than the bone matrix, whereas the Ca is at a higher level (Fig. 2.4D).

The later fractures are mainly filled by calcite. High fluorine and calcium levels in bone porosity, such as vascular canals, again indicate filling by fluorite (Fig. 2.4F). The CM component is revealed by the C map combined with the S map because of the sulfur content of the CM (Fig. 2.4G, I). The Si map suggests the presence of clay minerals in the small medullary cavity, which were deposited before the calcite (Fig. 2.4G, H) because the latter intersects the former. On the left part of the S map, a high sulfur level is correlated with iron and indicates pyrite (Fig. 2.4I). The Sr map shows low intensity in the bone matrix, whereas the calcite veins lack Sr (Fig. 2.4J). The simultaneous appearance of S and Ba at the margins of bone pores represents Baryte (Fig. 2.3K), which usually appears in the form of small grains and is attached to calcite.

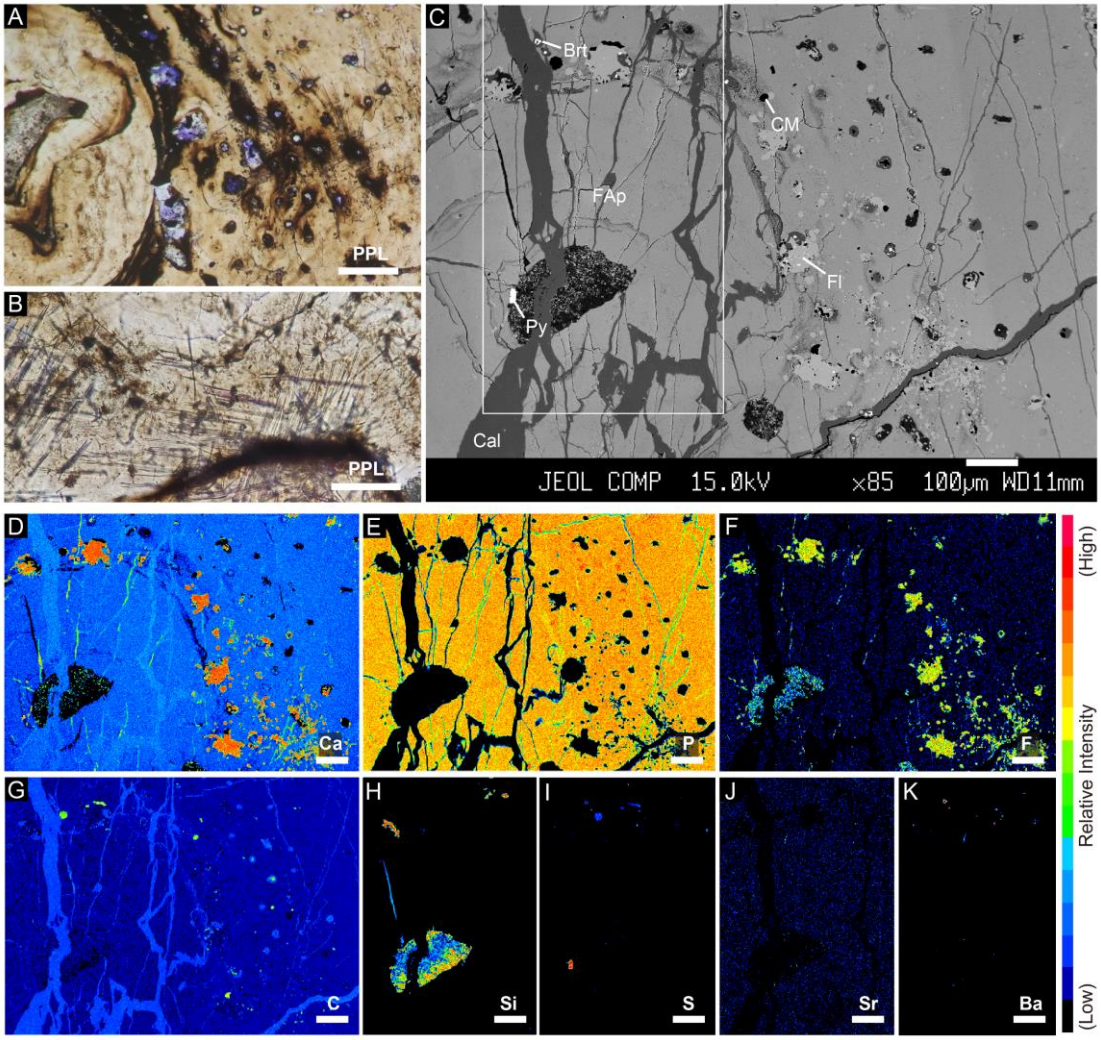

Figure 2.4. Alteration stage II (see also Fig. 2.2C): light microscopy imaging, SEM-BSE imaging, and WDX mapping of selected elements in the humeral thin section of sample HFUT XY-18-003. (A) Thin section showing violet fluorite infillings of bone pores in PPL. (B) Thin section showing intersectional needle-like fluorite surrounding bone pores such as blood vessels in PPL. (C) BSE image showing the distribution of different minerals and components. Box indicates the area of WDX element maps in H to K. (D-G) Element maps of Ca, P, F, and C of the area in panel C), revealing distributions of calcite, fluorite, and FAp. (H-K) Elemental maps of Si, S, Sr, and Ba in the medullary region (box in panel C) revealing the distribution of clay minerals (Si) and baryte (S and Ba). Scale bar equals 100 μm if not specified otherwise. Abbreviations: Brt, baryte; Cal, calcite; CM, carbonaceous matter; FAp, bone apatite fossilized as fluorapatite; Fl, fluorite; PPL, plane polarized light.

Stage III, moderately altered bones

Fossils in stage III show stronger alteration and a higher CM concentration than stage II. However, acicular fluorite crystallites and fluorite in microtunnels are also observed in stage III samples, with a greater volume of fluorite present in this stage. The thin sections of stage III fossils from Jiyangshan exhibit alternating dark and bright bands in the humeral midshaft

section (Fig. 2.2D, 2.5A), corresponding to the previous growth cycles. The original histology (i.e., fiber arrangement and microstructure) is partially lost in the bright bands and strongly compromised in the dark bands.

The elemental maps display a clear interaction among five main elements (C, Ca, F, P, and S). The high intensity of Ca and P in the bright bands indicates that the bone apatite was only slightly altered (Fig. 2.5D, E). On the other hand, the dark bands (Fig. 2.5A, E) have a lower P concentration and may have experienced phosphorus loss during alteration. The distribution of Ca and F in the elemental maps shows a large amount of fluorite and tiny calcite in the bone pores (Fig. 2.5D, F).

A similarly high carbon intensity can be observed in the bone pores and the dark bone bands. In the pores, the C is part of the calcite, whereas in the dark bone bands, it signifies a high concentration of organic matter (Fig. 2.5G). Notably, the enrichment of C is mirrored by that in S and found in areas with low phosphorus levels. These opaque regions in optical microscopy, which coincide with the highest intensity (red regions) in the elemental maps of C and S, indicate sulfur-rich pure CM occurrences in the fossil (Fig. 2.5G, H).

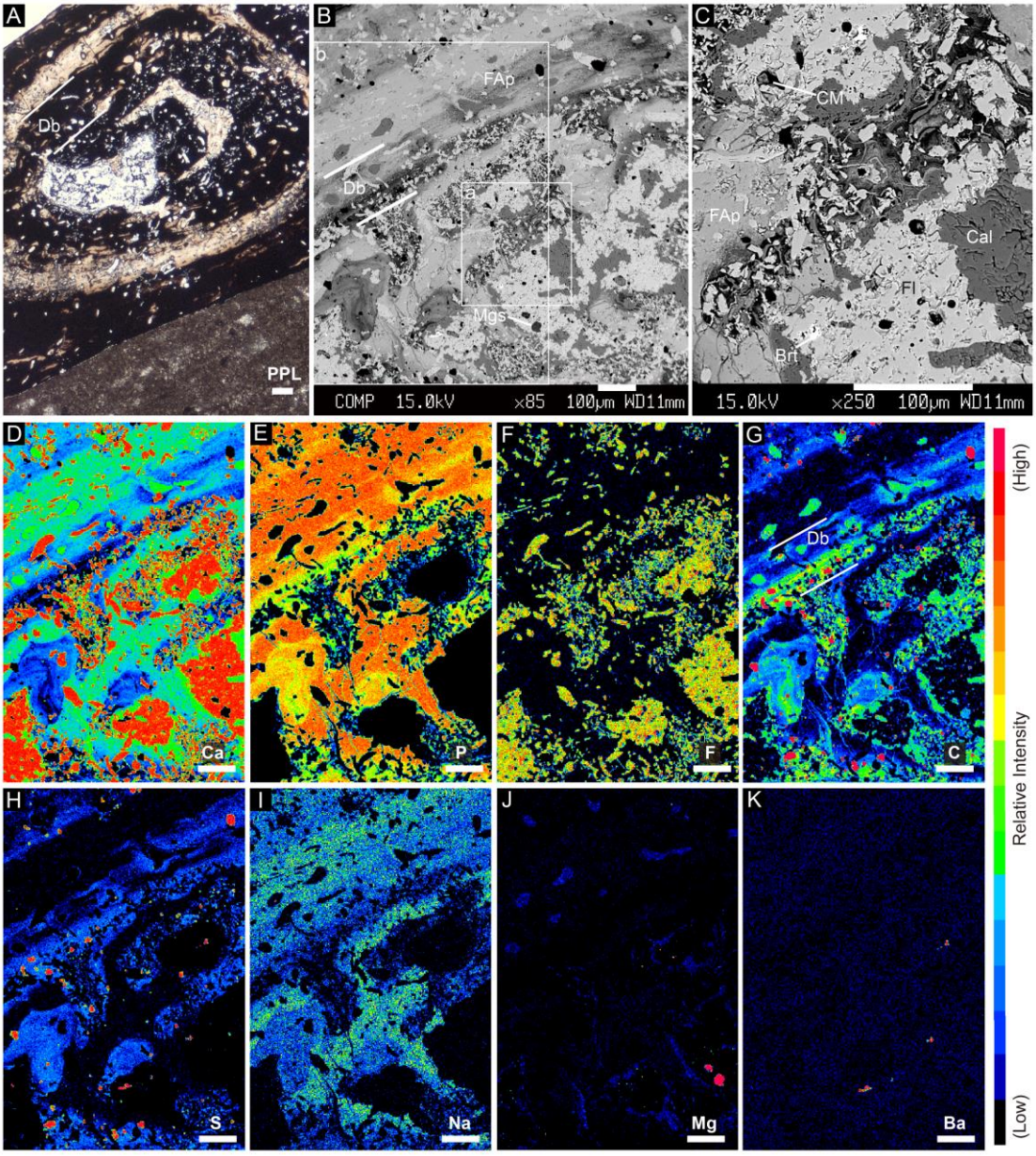

Figure 2.5. Alteration stage III (see also Fig. 2.2D): light microscopy imaging, SEM-BSE imaging, and WDX mapping of selected elements in humeral thin section of sample HFUT JYS-15-002. (A) Thin section showing cyclical dark bands (Db) with worse preservation in PPL. (B) BSE image with box a and box b showing areas selected for display of mineral contents and elemental mapping, respectively. (C) BSE image of medullary region showing distribution of different components and minerals. (D-G) Element maps of Ca, P, F, and C distribution in box b in panel B, revealing distribution of calcite, CM, fluorite, and FAp. (H-I) Element maps of S and Na showing a higher concentration in more organic-rich areas, i.e., the dark bands in thin sections. The areas with the highest intensity in the sulfur map are mainly pyrite with a little baryte. (J-K) Mg and Ba maps showing distribution of magnesite and baryte which cover only a few areas. Scale bar equals 100 μm if not specified. Abbreviations: Brt, baryte; Cal, calcite; CM, carbonaceous matter; Db: dark band; FAp, bone apatite fossilized as fluorapatite; Fl, fluorite; Mgs, magnesite; PPL, plane polarized light.

Interestingly, the intensity of Na, relatively high in unaltered regions, shows a negative correlation with the distribution of carbon and sulfur (Fig. 2.5I). The reduced Na intensity may result from a greater degree of bone alteration in the more organic-rich areas. (Fig. 2.5I). Magnesium appears in C and Ca-rich areas of the pore fill, indicating that the calcite is an Mg-rich calcite. However, high concentrations of Mg that match high C intensity may suggest magnesite deposition in the pore space during burial or later metamorphism (Fig. 2.5J). Baryte in HFUT JYS-15-002 is located in the medullary region and surrounded by fluorite, and it may have a metamorphic or hydrothermal origin.

Stage IV, strongly altered bone tissue with recrystallized apatite

The decisive feature of stage IV fossils is the presence of recrystallized apatite (RAp). The fossils from the Xingyi Fauna show recrystallized apatite (RAp) and numerous microtunnels filled with fluorite (Fig. 2.2E, G). We designate alteration substage IV-a for these specimens. As alteration intensifies in this substage, recrystallized apatite (RAp) extends from the outer cortex towards the inner bone regions. This expansion is observable through optical microscopy in specimens IGPB R-670, HFUT JYS-16-001, and HFUT DQT 21-001. One sample from Guanling (HFUT GL 17-006) also shows the coexistence of FAp and RAp, so we assigned it to alteration stage IV (Fig. 2.2F). However, we defined substage IV-b for this specimen since it lacks fluorite.

The thin section of stage IV-a fossil IGPB R-670 shows intense alteration of the bone tissue and has a relatively high CM content, especially in the dark bands (Fig. 2.2E, 2.6A). The BSE image shows a distinct brightness contrast between fluorite and FAp but not between fluorite and RAp (Fig. 2.6B). However, this difference can be resolved by cathodoluminescence microscopy in the SEM, revealing a zone of RAp at the outer margin of the bone. Dark grey RAp can be easily differentiated from bright fluorite and black FAp (Fig. 2.6C).

Elemental maps reveal information about all calcium-containing mineral phases, such as FAp, RAp, calcite, and fluorite based on the intensity of Ca (Fig. 2.6D). The P map shows two levels of phosphorus in the bone area, and they can be recognized as FAp and RAp because the latter shows a higher P intensity (Fig. 2.6E). The RAp is mainly distributed in the outer bone cortex, but also in small patches deep inside the bone. A possible explanation for the higher P content of the RAp compared to the FAp is that the late-precipitated RAp is pure fluorapatite. In contrast, the FAp in the fossil bone may contain a mix of other components, such as carbonaceous material (CM) and additional carbonate groups, which are either original or were incorporated during fossilization and diagenesis. Fluorite is widely distributed in sample IGPB R-670, forming large idiomorphic crystals (Fig. 2.6D, F). Low-level F concentrations are ubiquitous in the remaining bone tissue, indicating that all apatites are fluorapatite. There is no

difference between FAp and RAp in the level of F intensity (Fig. 2.5F), indicating the RAp is fluorapatite as well.

The C map, in combination with the Ca map, reveals calcite in bone pores and sediments. The overlapping areas in the C and S maps indicate that sulfur correlates with diffuse organics inside the bone but not in the sediment (Fig. 2.6G, H). There seems to be no pyrite. A distinct enrichment of Sr appears in the RAp (Fig. 2.6I), and at least two generations of RAp can be discerned through the intensity of strontium. The Sr map indicates an early crystallization of Sr-riched RAp, and the less Sr-rich RAp grew outward from the early crystals, presumably resulting from a gradual depletion of the pore fluid in strontium.

Another fossil, *Anshunsaurus* HFUT DQT-20-001 (Fig. 2.2G), represents further alteration beyond the alteration stage IV-a seen in IGPB R-670. Optical microscopy of the thin section of HFUT DQT-20-001 shows impressive alteration and an advanced grade of mineral recrystallization. The bone was crushed by sediment compaction, and all veins and bone porosity were filled with calcite. A large amount of RAp and little remaining of FAp indicate the sample to be of very late stage IV. Only a few histological structures (e.g., bone fibers, growth marks) are preserved, and FAp is replaced by recrystallized minerals. We cannot detect if microtubes were present because most original structures were obliterated by apatite recrystallization. However, fluorite layers, surrounding small islands of CM or distributed inside black rings as tiny crystallites, are pretty common (Fig. 2.2G). Fluorite shows a complex interaction with calcite veins and infillings. The calcite, which usually is closely associated with the purple fluorite layers, is more widely distributed. The calcite and fluorite layers surrounding CM islands show a mixture of minerals in most areas and display a light violet color (Fig. 2.2G). The stage IV-b fossil is also very dark, indicating that CM migration from the host sediment into the fossil also occurred in the Guanling samples. HFUT GL 17-006 shows heavy destruction of the bone tissue in areas with RAp formation. However, the areas without RAp were only slightly altered and the bone structures are still visible (Fig. 2.2F). The vascular canals are infilled by calcite. Where RAp crystals replace the bone tissue, the calcite-infilled canals are unaffected, indicating an in-situ replacement of FAp by RAp (Fig. 2.2F). Thus, the canals were filled with calcite first and then the FAp got replaced by RAp.

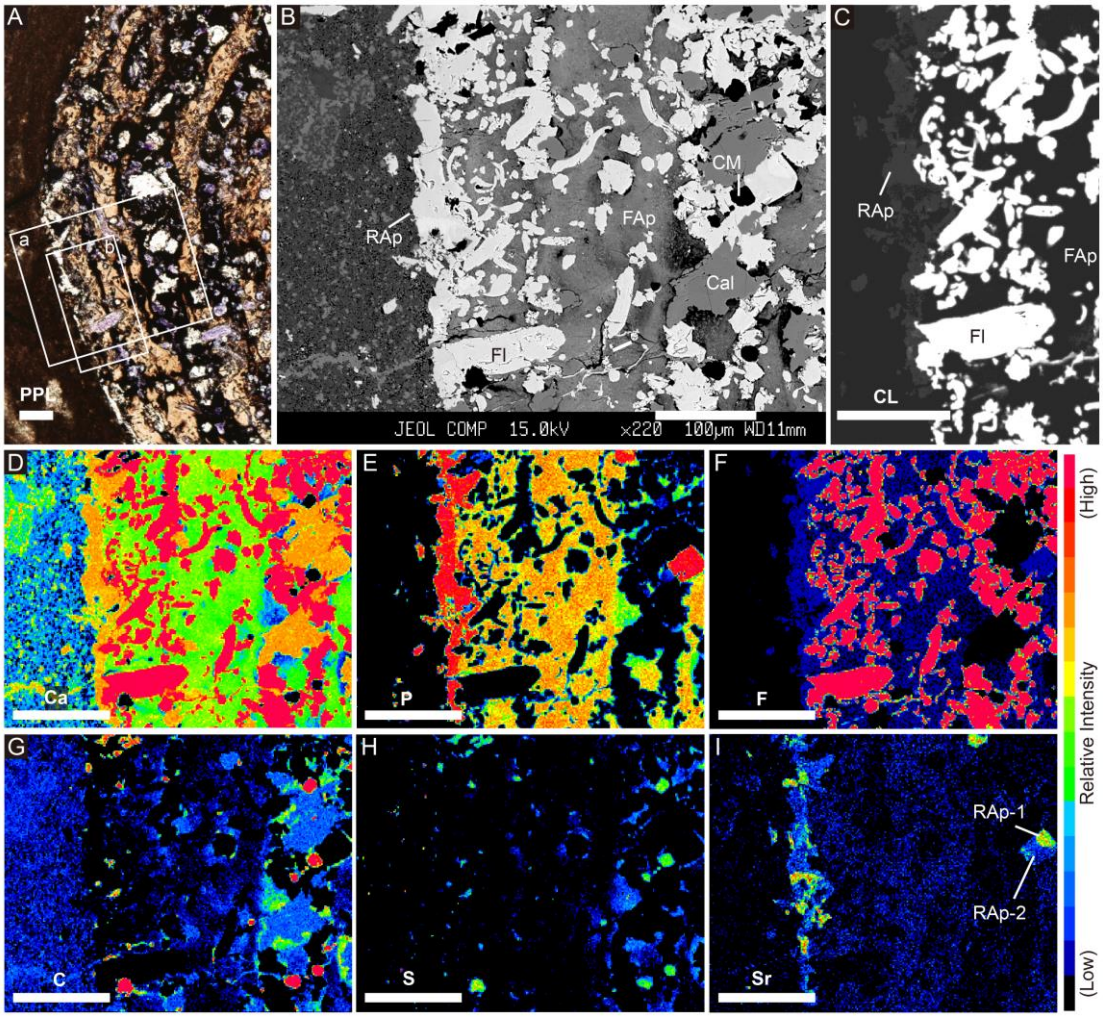

Figure 2.6. Alteration stage IV (see also stage IV-a, Fig. 2.2E): light microscopy imaging, SEM-BSE imaging (including cathodoluminescence), and WDX mapping of selected elements in humeral thin section of sample IGPB R-670. (A) Thin section showing medium alteration of bone with cyclical dark bands. Box a and box b indicate areas of panels B and C, respectively. (B) BSE image showing distribution of different minerals and other components in elemental mapping area. (C) SEM cathodoluminescence image showing the distribution of RAp (in dark grey), fluorite (in white), and other components (in black). (D-H) Element maps of Ca, P, F, C, and S in box a in panel A, showing distribution of calcite, CM, FAp, and RAp. The RAp mostly distributes in the outermost cortex of the bone. I, The Sr map showing two levels of Sr enrichment in RAp, which shows high and relatively low Sr intensity in early and late generations of RAp. FAp also shows the massive distribution of Sr but quite low. Scale bar equals 100 μm if not specified otherwise. Abbreviations: Cal, calcite; CM, carbonaceous matter; FAp, bone apatite fossilized as fluorapatite; Fl, fluorite; PPL, plane polarized light; RAp, recrystallized apatite RAp-1, the first generation of RAp; RAp-2, the second generation of RAp.

Stage V, entirely altered bones without FAp remaining

An extreme stage of bone alteration, also the final stage observed in this study is represented by fossilized bone that has lost all original structures to the growth of idiomorphic apatite

crystallites, i.e., RAp (Fig. 2.2H, 2.7C). In fossils of stage V (e.g., HFUT GL 17-003), the blurred boundary between fossil bone and sediment indicates massive ion exchange between the bone and environment. The thin section shows RAp, which replaces the original bone, aligned alternatingly with calcite that replaced vascular canals. The reasonable explanation for the phenomenon could be that apatite recrystallized and took the place of the old bone matrix, and subsequently, calcite formed in the original vessel and pore spaces (Fig. 2.7C).

All fossil bone apatite was replaced by RAp, which shows an outward radiating arrangement (Fig. 2.7A, B), probably determined by the original histology of radial vascular canals or radially oriented trabeculae. The cathodoluminescence image in the SEM shows apparent differences between calcite and RAp but also reveals slight changes in two generations of RAp through the brightness of luminescence (Fig. 2.7C). RAp appears even to have been precipitated in the host sediment near the bone (Fig. 2.7E, F). However, considering that the outer bone surface is quite open and blurred, it is also possible that those scattered RAp crystallites are the last remains of the original bone.

Magnesium-containing calcite is widely distributed in bone and sediments, which can be recognized by the overlap of Ca, C, and Mg in the elemental maps (Fig. 2.7D, G, J). The Mg-containing calcite fills the bone pores, revealing the original trabecular architecture despite the heavy alteration of the sample. Elemental maps of C and S showed that the organics fill the interstices between the calcite and RAp crystals (Fig. 2.7G, H). This can also be seen in optical microscopy. Possibly, the carbon was displaced by the growing idiomorphic crystals. Carbon concentration is also correlated to sulfur concentration, as in stages II and III fossils, indicating the organic nature of the carbon. The highest concentrations in the S map (Fig. 2.7H) correspond with Fe, suggesting that pyrite is massively distributed in the sediment. As in stage IV-a fossils, two phases of RAp are identified in the Sr map (Fig. 2.7I). The first generation, RAp-1, usually forms the corners of apatite crystals and provides a base for the growth of RAp-2. Additionally, Sr is also found in the calcite near the RAp in the medullary region, indicating either concurrent precipitation of calcite crystals or later metasomatism between these two minerals (Fig. 2.7I).

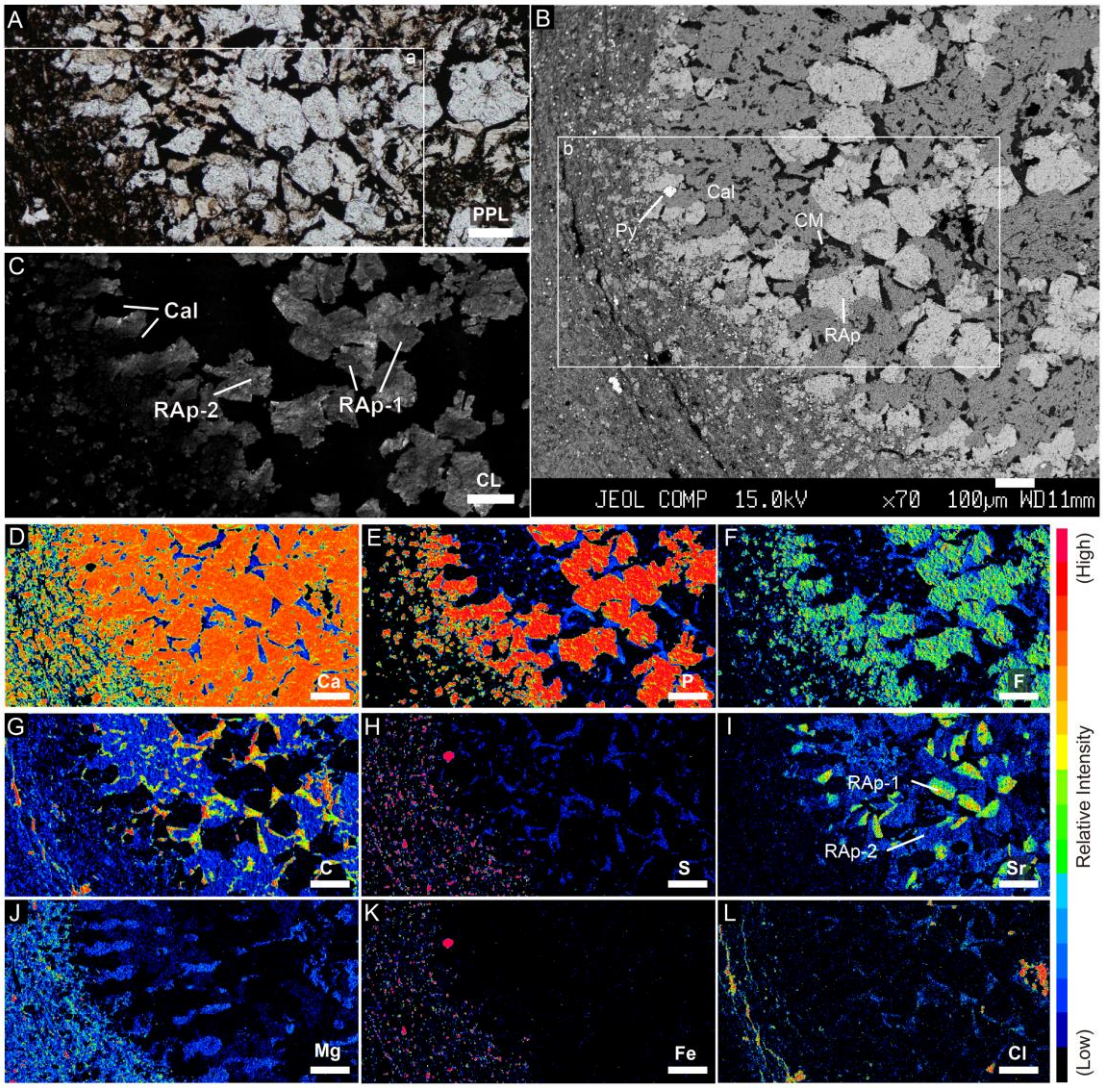

Figure 2.7. Alteration stage IV (see also Fig. 2.2H): light microscopy image, SEM-BSE imaging (including cathodoluminescence) and WDX mapping of selected elements of humeral thin section of sample HFUT GL-17-003. (A) Thin section showing fully altered bones in PPL. Box indicates the area of element maps. (B) BSE image with box showing areas selected for analysis of mineral contents and elemental mapping, respectively. (C) The BSE cathodoluminescence image showing the distribution of RAp (in grey) and other contents (in black). Two generations of RAp can be recognized through the darkness of the grey. (D-H) Element maps showing Ca, P, F, C, and S distribution, revealing the distribution of calcite, CM, and RAp. Note that the lower intensity of S is associated with CM and the higher intensity indicates the pyrite distribution when combined with Fe. I, The Sr map shows two levels of Sr enrichment in RAp, which indicates two generations of RAp formation. (J-K) Element maps of Mg and Fe representing Mg-rich calcite and pyrite (together with the high S intensity), respectively. (L) The high intensity in the Cl map showing epoxy resin infilling of pores and fractures. Scale bar equals 100 μm if not specified otherwise. Abbreviations: Cal, calcite; CM, carbonaceous matter; PPL, plane polarized light; Py, pyrite; RAp, recrystallized apatite; RAp-1, the first generation of RAp; RAp-2, the second generation of RAp.

2.5.2 Auxiliary mineral identification by Raman spectroscopy

Samples of stage I-a (HFUT LG-21-003 from Longuang), stage IV (IGPB R-670 from Xingyi), and stage V (HFUT GL-17-003 from Guanling) were analyzed for their mineralogical composition using Raman spectroscopy. This series of samples shows the progressive loss of bone microstructure and the appearance of RAp with increasing alteration stages (Fig. 2.8A, B, C). Raman spectra of the stage I-a sample HFUT LG-21-003 show a signal of apatite of bone tissue but no CM peak in the FAp matrix (Fig. 2.8D). CM is present only in the surrounding sediment. The hematite recognized uniquely in the stage I-a Longguang sample is corroborated by Raman peak searching. The stage IV fossil IGPB R-670 shows clear peaks of CM (D- and G-band position) in the FAp and dark bands in the bone (Fig. 2.8E). The simple spectra of the RAp indicate pure apatite crystals without CM interference (Fig. 2.8E), unlike the spectrum of FAp with CM presents. All purple fluorite areas show a broad band from 100 cm^{-1} to 500 cm^{-1}, different from synthetic fluorite Raman peaks that usually appear at the 332 cm^{-1} position. However, such broad bands below 500 cm^{-1} have been recorded by Čermáková et al. (2015) in hydrothermal fluorite. They associated the broad band feature with radiation-induced damage, and the intensity increased with increasing violet color saturation among their specimens.

Raman spectra of the stage V fossil HFUT GL-17-003 also show clear CM within the first-order region, spanning 1000-1800 cm^{-1}, which correspond to the darker areas and bands of the sample (Fig. 2.8F). The co-occurrence of RAp and broad peaks within the CM band-1 may suggest that CM is distributed in interstices between the RAp crystals. For a detailed view of the peaks, see Figure S1.

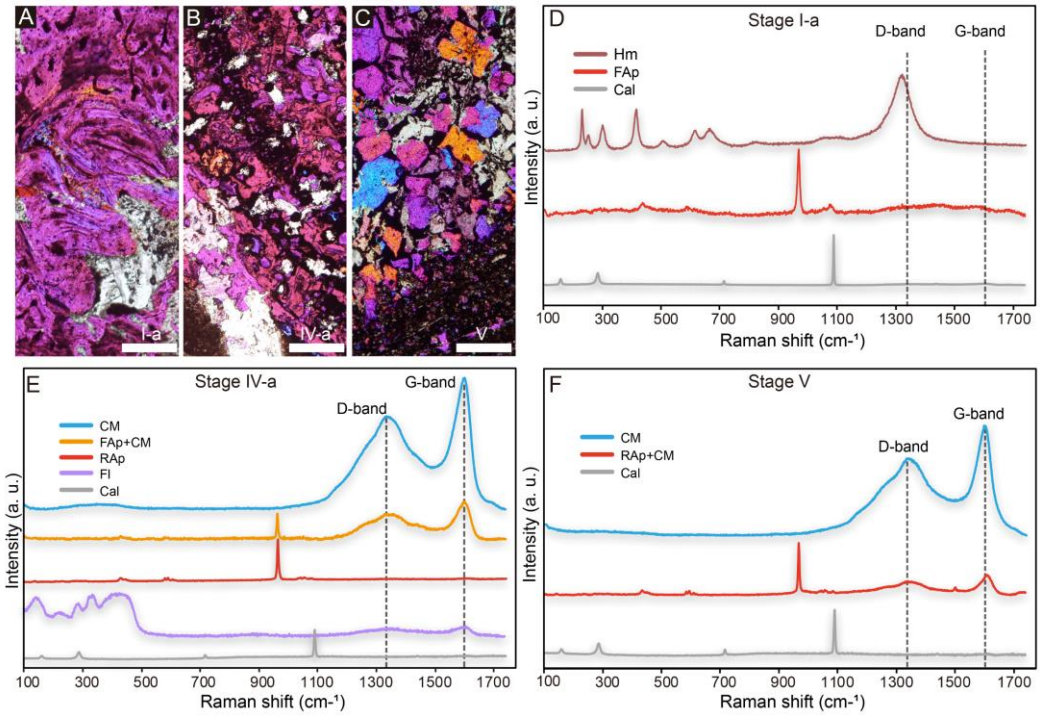

Figure 2.8. Three thin sections in cross-polarized light plus λ filter and Raman spectra showing apatite transformation and main contents from samples HFUT LG-21-003 (stage I) via IGPB R-670 (stage IV) to HFUT GL-17-003 (stage V). (A) Thin section of HFUT LG-21-003 showing well-preserved bone (stage I-a with low organic contents). (B) Thin section of IGPB R-670 showing medium alteration of bone and first appearance of RAp. (C) Thin section of HFUT GL-17-003 showing entirely altered bone. (D) Raman spectra of HFUT LG-21-003 (stage I) showing the low CM content of the bone matrix. Bone pores are filled by hematite and calcite. (E) Raman spectra of IGPB R-670 (stage IV) showing peaks of calcite, CM, fluorite, FAp, and RAp. (F) Raman spectra of sample HFUT GL-17-003 (stage V) showing peaks of calcite, CM, and RAp. The peaks in the D- and G-band positions reflect the existence of CM in fossils of stages IV and V. The scale bar equals 100 μm.

2.5.3 Temperature estimation

Raman spectroscopy analysis demonstrated the presence of CM in all tested samples, either in the bone or in the sediment only (Longguang specimen). To investigate the peak temperature and relevant effects during diagenesis and alteration, Raman spectra of the CM were used as a geothermometer (following Kaneki and Kouketsu 2022). Sediment, bone matrix, and porosities filled by organics were measured for temperature evaluation. The CM band-1 of all samples (one for each specimen) was plotted together to reveal the evolution of the temperature (Fig. 2.9A).

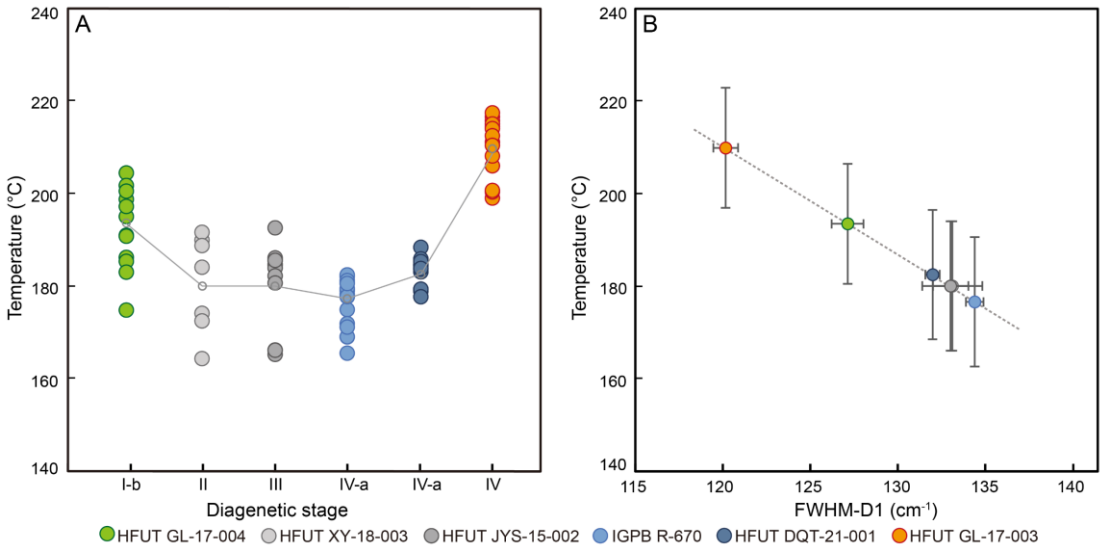

Figure 2.9. Peak temperature estimation of six samples from the five alteration stages showing that peak temperatures experienced by all tested samples are over 160 °C during diagenesis. The GL fossils experienced higher temperatures than the others. The temperatures are based on the Raman CM geothermometer, and the calculation follows equations in Kaneki and Kouketsu (2022). (A) estimated peak temperatures of six specimens of four alteration stages, temperature calculation based on FWHM-D1 band. The grey line indicates the average peak temperature of sampled plots of each specimen. (B) FWHM of D1-band plotted against estimated peak metamorphic temperature for the samples studied here. Error bars represent standard error, and the error range (approximately ±15°C) followed Kaneki and Kouketsu (2022).

As noted, the stage I-a fossil HFUT LG-21-003 from Longguang shows low CM intensity in sediments. It also showed a high fluorescence background which led to inaccurate peak fitting for the sample. The average temperatures experienced by stage I-b sample HFUT GL-17-004 from Guanling is 193°C and, surprisingly, is higher than that inferred for the four specimens from different localities of the Xingyi Fauna (XY, JYS, DQT, and IGPB) (Table 2.1, Fig. 2.9). Nonetheless, this temperature is still lower than the 209°C average temperature recorded for the stage V specimen from Guanling, HFUT GL-17-003. The fossils of stage II to IV-a, all from the Xingyi Fauna, show a slight average temperature increase from 177°C to

182°C with increasing alteration stage (Fig. 2.9B). Thus, the fossils from Guanling experienced higher temperatures compared to those from Xingyi. For the latter, the average peak temperatures do not significantly differ among stages II, III, and IV-a, even considering the strongly altered HFUT DQT-20-001 (advanced stage IV-a). Data for FWHM-D1, FWHM-D1, and estimated temperatures of all sample sites are listed in Table S2.

Table 2.1. Summary of the inferred peak temperature and FWHM of the D1-band of each sample.

Preservation	Sample ID	Temperature (°C)	Mean (cm^{-1})	SD (cm^{-1})	SE (cm^{-1})	Number of data
Stage I-b	HFUT GL-17-004	193 ± 30	127.2	3.0	0.9	11
Stage II	HFUT XY-18-003	180 ± 31	133	4.2	1.7	7
Stage III	HFUT JYS-15-002	180 ± 30	132.9	3.6	1.0	16
Stage IV-a	IGPB R-670	177 ± 30	134.5	1.9	0.5	17
Stage IV-b	HFUT DQT-20-001	182 ± 30	132	1.3	0.4	14
Stage V	HFUT GL-17-003	209 ± 29	120.3	2.6	0.7	14

SD is the standard deviation, and SE is the standard error. The error range of the temperature is the 95% prediction interval.

2.6 Discussion

2.6.1 General features of the five alteration stages

The preservation of fossils from Southwest China examined in this study shows broad compositional variance and levels of alteration across five alteration stages. High levels of CM are observed in all materials except for those from Longguang (stage I-a). Two kinds of apatite appear in the fossil bones, i.e., FAp (stage I to stage IV) and RAp (stage IV and stage V), suggesting a strong increase in metamorphic alteration of the bone. Minerals such as calcite, fluorite, pyrite, hematite, magnesite and baryte reveal a complex history of alteration during and after fossilization (Table 2.2). Fluorite is particularly intriguing because it is abundant but has not been observed in any fossil bone before.

Table 2.2. Minerals and stages of alteration of investigated fossils.

Preservation	Sample ID	Bone tissue preservation	Minerals and CM
Stage I-a	HFUT LG-21-003	Good	FAp, hematite, calcite, clay mineral
Stage I-b	HFUT GL-17-004	Good	FAp, calcite, CM
Stage II	HFUT JYS-16-003	Good-medium	FAp, fluorite, calcite, baryte, CM, pyrite
Stage II	HFUT XY-18-003	Good-medium	FAp, fluorite, calcite, CM, baryte, pyrite, clay mineral
Stage III	HFUT JYS-15-002	Medium	FAp, fluorite, calcite, CM, baryte, magnesite, pyrite
Stage III	HFUT JYS-15-023	Medium	FAp, fluorite, calcite, CM
Stage IV-a	IGPB R-670	Poor	FAp, RAp, fluorite, calcite, CM
Stage IV-a	HFUT DQT-20-001	Poor-none	FAp, RAp, fluorite, calcite, CM
Stage IV-b	HFUT GL-17-001	Medium	FAp, RAp, calcite, CM
Stage V	HFUT GL-17-003	None	RAp, calcite, CM
Stage V	HFUT GL-17-006	None	RAp, calcite, CM

2.6.2 FAp and RAp

The simplified chemical composition of bioapatite (BAp) is usually given as $Ca_{10}(PO_4)_6(OH)_2$, where calcium contributes 39.68%, and phosphorus contributes 18% (Pasero et al. 2010). The early F^- and CO_3^{2-} immigration during fossilization stabilizes bioapatite (Keenan 2016) and forms FAp (usually fluorapatite). Here we identified a new type of apatite, termed recrystallized apatite (RAp), within our fossil samples. RAp is fluorapatite formed during low-grade metamorphism by recrystallization (often as idiomorphic crystals) at the micrometer scale.

During the fossilization process, the bone apatite takes up fluorine from the pore water, i.e., the environment. This uptake of F^- may transform bone apatite into a more stable fluorapatite phase in early diagenesis (Trueman et al. 2008, Keenan 2016). Evidence for such a transformation in our samples is provided by the extensive presence of low-level fluoride

within the fossil bone, which is indicative of the typical diagenetic transition from bioapatite to fluorapatite (i.e., FAp).

We emphasize again that RAp, or recrystallized fossil fluorapatite, has not been reported in other fossil bones. RAp is not to be confused with the idiomorphic apatite found in a Carboniferous coal measure deposit, Jarrow in Ireland (Ó Gogáin et al. 2022). There, the apatite crystals occur as a void fill, not as a replacement of the bone tissue. In addition, the Jarrow fossils do not exhibit the fluorite found in the Guanling samples. Randomly oriented recrystallized apatite similar to RAp appears in highly metamorphic rocks, such as shocked apatite (McGregor et al. 2019, McGregor et al. 2021). There is no evidence that fossils from the SW China experienced such metamorphic processes leading to shocked apatite, and the presence of RAp is a clear indicator of FAp dissolution and reprecipitation, presumably caused by low-grade metamorphism. Interestingly, the fluorine intensities are close in FAp and RAp in IGPB R-670.

2.6.3 Fluorite

Fluorine-, phosphorus-, and calcium-containing compounds appear in all of our samples, but fluorite is only present in fossils from the Xingyi Fauna localities. In the case of fluorite (CaF_2), where Ca and F share 51.1% and 48.9% of the molecular weight, respectively, the fluorine content is much higher than in FAp. This mass balance argument suggests that the extra fluorine ions (F^-) came from environmental sources (extrinsic source hypothesis) rather than from the FAp (intrinsic source hypothesis) itself. At least in stages III and IV-a, the fluorine must be extrinsic because of the large amount of fluorite present (Fig. 2.6). In stage II, the volume of fluorite is much less, and an intrinsic origin remains a possibility. Other instances of continuous FAp recrystallization, hitherto unreported, would have to be investigated to see if they are also associated with fluorite.

Unlike the fossilized biogenic fluorite statoliths in mysid crustaceans (Wittmann and Ariani 1996), abiogenic fluorite precipitation is rarely reported as a mineral in fossils and never in fossil bone before. Witke et al. (2004) described fluoridized wood from the Permian petrified forest of Chemnitz, Germany. This occurrence was interpreted as evidence of a multi-stage process where hot (< 250 ºC) fluorine-bearing fluids infiltrated the wood along cracks and decayed areas (Mustoe 2018, Rößler 2021). The remaining examples, such as fluoritized corals and nummulitic fossils mentioned by Worley (1976) and Genç (2006), were also discovered in hydrothermal ore deposits in Derbyshire, England, and central Anatolia, Turkey. In summary, fluoritized fossils (except for the biological mineralization) reported so far all experienced

hydrothermal conditions such as volcanic eruption entombment or low to medium metamorphism.

Fluorites of several morphologies, including some truly enigmatic ones, are present in our samples. The acicular fluorite crystallites, which vertically intersect with each other, surround vessels in the cortex (Fig. 2.4B). It is noteworthy that idiomorphic fluorite crystallizes in the isometric cubic habit. Octahedral and more complex isometric forms are also not unusual (Franke 2015), but needle-shaped micro-fluorites have rarely been mentioned (Lowenstam 1981, Mouhovski et al. 2014). Wyllie et al. (1962) reported the appearance of apatite needles with a cavity containing fluorite in igneous rock. However, the micro-crystals in our samples show a vertical intersection with each other three-dimensionally, which is impossible for a hexagonal structure in apatite. Hence, the acicular micro-fluorites may suggest a primary euhedral growth of cubic fluorite.

Fluorites with shapes of microtubes are xenomorphic, which reveals later precipitation in in-vivo and post-mortem but pre-burial bone porosity in stage II to stage IV fossils. The known crystallizing temperature of fluorite varies from 80 to 200 °C (Haschke et al. 2021, Zou et al. 2022), which is covered by estimated peak temperature intervals of our samples and may indicate direct precipitation of fluorite from the fluids. However, in the stage IV specimen HFUT DQT-21-001, the presence of CM islands encircled by an inner ring of fluorite and an outer band of calcite may suggest later fluorite precipitation occurring at the interface between organic material and calcite. The replacement of calcite by fluorite has applications in multiple studies of various conditions and is ubiquitous in hydrothermal deposits (e.g., Megaw 2013, Zou et al. 2022). Those zonal structures may also reveal the metasomatism between early-stage calcite and fluoride-rich fluids.

Furthermore, the appearance of fluorite could also indicate F^--rich burial conditions. Considering the absence of fluorite in bones entirely replaced by RAp (stage V), it is plausible that the Guanling fossils were not subjected to F^--rich solutions during the later stages of alteration. Nevertheless, the fluorite and its distribution in our samples remain enigmatic.

2.6.4 Hematite and low CM

Keichousaurus fossils from the Middle Triassic Xingyi Fauna are almost always embedded in thin to medium-bedded muddy micrite (Lu et al. 2018) and black shales. Thus, those fossils are usually preserved in a matrix with a high CM content. However, specimens in a bleached or oxidized black shale from Longguang display low organic content, unaltered bone apatite, and hematite microspheres in voids.

Pyrite is common in *K. hui* fossils and relevant sediments, while hematite is not. The hematite microspheres here have a diameter of 10 micrometers and are attached to the inner wall of vessels. The concurrent precipitation of hematite and calcite happens under an oxidizing environment (Holz and Schultz 1998). Thus, a stillwater anoxic burial condition is possible due to the aquatic environment in which *Keichousaurus* perished. However, the simultaneous appearance of pyrite, calcite, and hematite (the latter resulting from the later oxidation of pyrite) is more common during fossilization (Wings 2004). For example, hematite and pyrite are preserved in fossils from Aust Cliff, England (Wings 2004, Milroy et al. 2019).

The hematite deposition and low organics content must indicate an oxidizing event for the Longguang fossils belonging to stage I. It may be hypothesized that these fossils were buried in more oxidizing conditions than the others, such as lower sea levels mentioned by Zou et al. (2015b). However, this appears unlikely because the sediment is laminated, and the skeletons are fully articulated, similar to those found within black shales. Such conditions suggest an absence of benthic organism activity, which is typical in anoxic environments inhibiting bottom life. Fossils from Longguang were collected near a fault, providing a reasonable oxygenic condition for the near-surface oxidization of organic matter and pyrite. However, without further field and geochemical work, the loss of the organic matter from the rock at Longguang and its fossils remains mysterious.

2.6.5 Calcite, pyrite, baryte, and magnesite

Calcite is present in the voids of all samples and occurs mainly in the form of sparite. In general, calcite is the most common diagenetic, porosity-filling mineral in fossil bone (Wings 2004, PMS, pers. obs.). Pyrite and baryte are also common in fossil bones. The Guanling Biota bones show more pyrite in the sediment than the Xingyi Fauna ones, suggesting a more anoxic depositional environment, consistent with the dominance of fossils of pelagic reptiles in Guanling (Wang et al. 2008).

The area with baryte is tiny in the samples from Xingyi Fauna. The Guanling bones lack baryte, possibly indicating a limited supply of Ba^{2+} ions. Krumbein and Garrels (1952) described the presence of calcite, pyrite, and baryte in chemical sediments as indicators of slightly alkaline conditions of pH 7-pH 8. In all Xingyi samples, there is a probability that the minerals precipitated under anoxic conditions since most materials are preserved in organic-rich laminated limestones or shales. Magnesite often forms in sedimentary or metamorphic magnesium-rich carbonate rocks (Zheng et al. 2015). The rare magnesite occurrence in our samples (Fig. 2.5J) is likely precipitated from hydrothermal fluids during the low-grade metamorphism.

Discussion of diagenetic temperature

Several studies have proposed Raman CM geothermometers (Beyssac et al. 2002, Rahl et al. 2005, Lahfid et al. 2010, Kouketsu et al. 2014). Rahl et al. (2005) and Kouketsu et al. (2014) expanded the lower temperature limit of the thermometer to 100°C and 150°C, respectively. Kaneki and Kouketsu (2022) suggested that estimates based on FWHM-D1 can cover the range of 150-400°C and show an error of around ±30°C, whereas the corresponding error is around ±35°C for FWHM-D2. Although our estimated peak temperatures based on FWHM-D1 and FWHM-D2 are different, both equations suggest temperatures of over 150°C in our specimens, even considering the maximum errors. In general, this suggests that all fossils (except for the Longguang ones) have passed through the oil window (65-150ºC), the temperatures at which kerogen will migrate (Selley 1998).

Estimates based on FWHM-D1 indicate that all samples experienced high peak temperatures of over 177° C (-30°C, lower limit of 95% prediction intervals), and the temperature variation between the two faunas is distinctive. Since the specimens from Guanling show two extremes of alteration stages yet must have experienced similarly high temperatures, it is likely that hydrothermal fluids played an essential role in the metamorphic alteration of the Guanling fossils. The well-preserved Guanling stage I-b sample, of which the mean temperature is about 25 ºC lower than the stage IV sample from the same area, may also indicate an influence of temperature.

No trend of temperature increases from alteration stage II to stage IV from the same locality can be recognized in the results based on FWHM-D1 (Fig. 2.9). Possibly, the samples indeed experienced similar peak temperatures, but the highly altered ones may have been heated for a longer period or been exposed to fluids with different composition. Indeed, it would be surprising if a relatively modest increase in temperature were the sole factor explaining the differences from stages II to IV-a.

Moreover, the stage II to IV-a fossils from the Xingyi area experienced lower temperatures yet showed more profound alteration than the stage I-b sample from Guanling. Also, the sample HFUT DQT-21-001, which is at a very late stage IV, is close in the degree of RAp crystallization to stage V but experienced a distinctly lower temperature (approximately 35 ºC) than stage V. The preservational differences among the five stages suggest that peak temperature may not have been the key factor influencing bone alteration (especially for apatite transformation) in our samples. Instead, the duration of the exposure to the hydrothermal environment could have been the controlling factor.

Table 2.3. Summary of alteration stages

Stages (alteration stage)	Features of the process	Samples
Stage 0 (fresh bone)	• BAp: a compound material of hydroxyapatite (HAp) and collagen • Non-mineralized components (bone cells, blood vessels)	
Stage I (unaltered)	• Loss of collagen from BAp • BAp transformed to FAp • Minor CM infiltration possible • Porosity filled by calcite and iron minerals	• I-a (Xingyi Fauna) HFUT LG-21-001 HFUT LG-21-002 HFUT LG-21-003 • I-b (Guanling Biota) HFUT GL-17-004
Stage II (slightly)	• Appearance of violet fluorite as pore fill and acicular crystals • Moderate loss of birefringence in the FAp • Always CM infiltration	(Xingyi Fauna) HFUT JYS-15-001, HFUT JYS-15-004, HFUT JYS-15-007, HFUT JYS-15-016, HFUT JYS-16-003, All XY samples
Stage III (moderately)	• Appearance of violet fluorite as large crystals, possibly pseudomorphs • Fluorite pore fill and acicular crystals • Bands of strong CM infiltration combined with complete loss of birefringence in FAp.	(Xingyi Fauna) HFUT JYS-15-002, HFUT JYS-15-006, HFUT JYS-15-014, HFUT JYS-15-023
Stage IV (strongly)	• Appearance of RAp (idiomorphic apatite crystals) replacing FAp from outside and pores • Few original bone tissue remains, indicated by osteocyte lacunae • More fluorite crystals (IV-a) • No change in CM	• IV-a (Xingyi Fauna) HFUT JYS-16-001, HFUT DQT-20-001, IGPB R-670 • IV-b (Guanling Biota) HFUT GL-17-001
Stage V (fully)	• All FAp has been transformed to RAp, no more birefringence • No original bone tissue, such as osteocyte lacunae • Idiomorphic apatite replaces both altered bone and calcite pore fill • Original bone porosity preserved as ghost • CM squeezed into interstitial spaces	(Guanling Biota) HFUT GL-17-003 HFUT GL-17-006

2.6.6 Diagenesis and metamorphism model of studied fossils

The fossils from the Xingyi Fauna represent four stages of alteration (stage I to stage IV) from different localities (LG, XY, JYS, DQT) and show a stepwise loss of bone apatite and an increase in fluorite mineralization. The specimens from the Guanling Biota display three alteration stages (stage I, IV, and V) but lack fluorite. The similar regional low-grade metamorphism and continuous phase change of apatite make it possible to build a fossil preservation and alteration model in this area.

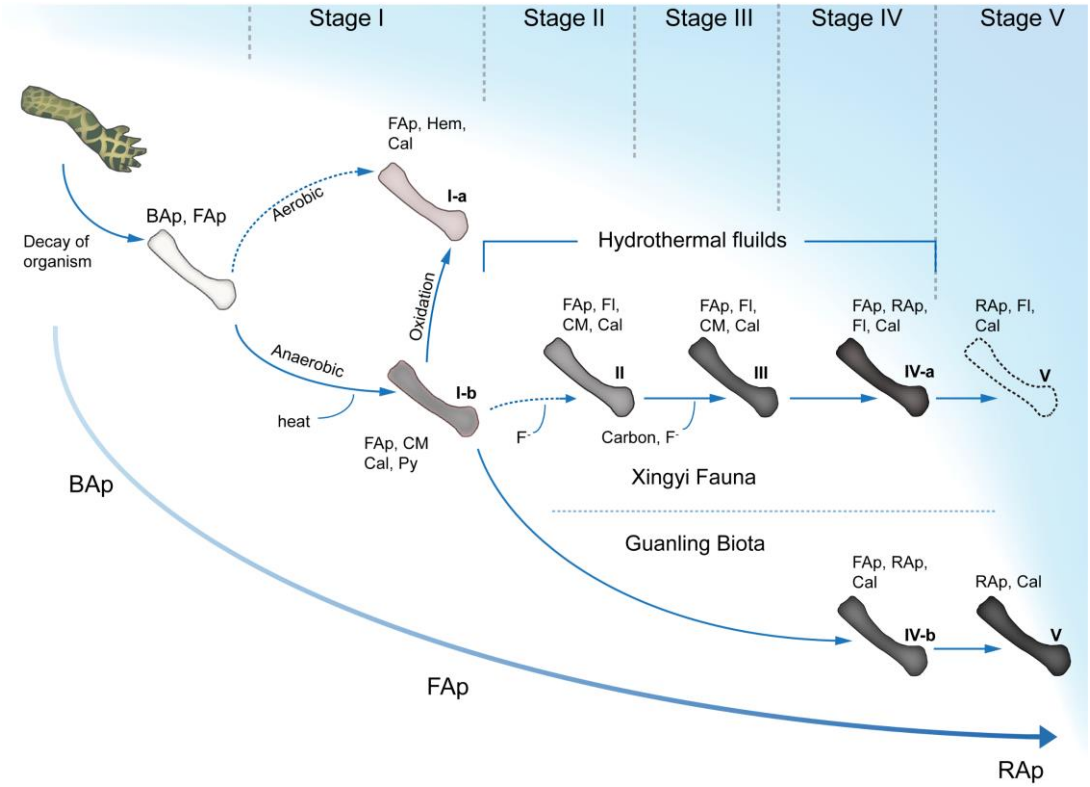

Figure 2.10. Model that shows five stages of diagenesis and metamorphic alteration of fossils from the Xingyi and Guanling areas. Seven different alteration (sub-) stages that the fossils experienced are marked by Roman numerals and a letter. The model follows the route of apatite transformation from BAp via FAp to RAp and other mineral precipitation during bone diagenesis and low-grade metamorphosis. Dashed lines indicate possible processes. The dotted bone of stage V is a very advanced stage IV-a sample (HFUT DQT-21-001).

Starting with fresh bone, the first step involves the decay of the carcass and the early diagenesis of the bones, i.e., the decomposition of collagen and other organic components in bone and the initial transformation of BAp to FAp (Fig. 2.10). In early diagenesis, microorganisms and bacteria in seawater contribute to the decomposition of organic phase (Sousa et al. 2020, Dal Sasso et al. 2016). This process opens up the BAp lattice, creating pathways for fluid movement that can occur before or during sediment deposition, leading to a

more stable thermodynamic phase, as described by Hinz and Kohn (2010) and Keenan et al. (2017).

Stage I, to the end of late diagenesis

The second step, roughly covered by the concept of "late diagenesis", is a further alteration of the bioapatite, and it ends with fossils of alteration stage I in our study. This is also the step during which the enclosing sediment turns to rock. The bulk of fossil bone tissue is FAp by the end of stage I.

In the case of the stage I-b sample from Guanling, the high temperature it experienced (209°C) is not reflected in bone alteration. Thus, some stage I fossils may experience temperature conditions typical of low-grade metamorphism without alteration. The diagenetic mineralization of bone (Trueman and Tuross 2002, Keenan 2016) reduces porosity and forms recrystallized apatite (specifically early FAp). This process probably was finished before the infiltration by organic carbon. Organic carbon uptake by the fossil bone must have occurred later during diagenesis since kerogen only migrates when the host rocks enter the oil window (Schobert 2013).

The Longguang fossils (substage I-a) and rocks stand out because of their low organic content compared to the higher levels in all other specimens. This raises the question of whether the substages I-a and I-b represent distinct fossilization pathways (aerobic vs. anaerobic) or steps in a single diagenetic sequence. The two-pathway hypothesis is unlikely given that the Longguang fossils are from laminated sediment and are well-articulated skeletons. It is typical for still water conditions and suggests an absence of oxygenated conditions at the seafloor. Instead, the Longguang rock may have undergone an oxygenation event (see discussion of hematite), leading to the loss of organics and formation of hematite. This oxygenation event possibly involved dry heating of the rock, resulting in the decay of organics into a gaseous phase that was then lost from the rock. Unfortunately, the lack of organic carbon in the bone tissue of the specimens makes it challenging to test this hypothesis with a carbon thermometer.

Stage II, slight alteration in early metamorphism

Metamorphic alteration began at stage II, apparently involving hydrothermal processes. At this stage, the fossilized bone begins to lose its original structures during the metamorphic progression. The fluorite precipitation occurred through hydrothermal fluids at this stage, increasing in volume from stage II to stage III with increasing metamorphism. However, the pathways for the hydrothermal fluids could be restricted to tectonic cracks and microcracks because the original black shale sediment was of low porosity.

Stage III: moderate alteration and further CM migration

Further organic carbon (kerogen) migration is possible, forming the dark ring structures in alteration stage III. Also, the stage III fossils show more fluorite inside the bone pores and a higher level of bone tissue destruction than stage II, which indicates a stronger alteration. Although the exact cause of the microtunnels (or Wedl tunneling) infilled by fluorite is still mysterious, these microstructures are more concentrated in organic areas, especially in dark bands with looser bone fibers (see Li et al. 2023).

Stage IV: from FAp to RAp

The dissolution of FAp and crystallization of RAp started in alteration stage IV (Fig. 2.10). Notably, the authigenic apatite in IGPB R-670 first appeared at the outer bone surface, replacing the FAp in the outer cortex from the outside in. This pattern of initial RAp mineralization suggests that apatite dissolution and recrystallization are closely related to the fluid environment and ions available in the host rock and fluids. Specimen HFUT DQT-21-001, in which RAp largely replaced the FAp, represents a very advanced stage IV and close to stage V. The stage IV-b fossil from Guanling (HFUT GL-17-001) displays an intermediate stage between I-b and V, with no fluorite observed. The differences in preservation between Xingyi and Guanling fossils are not yet well understood and require further study (Fig. 2.10).

Stage V: only RAp in bone

Alteration stage V presumably is the last stage before the complete destruction of the fossils since RAp has entirely replaced FAp. Almost all structures of the fossil bones and their histology (even the border between bone and sediment) are lost at this stage because of the idiomorphic growth of the RAp crystals. Although the stage V material from Guanling was collected geographically far from stage IV-a sample from Jiyangshan, the two RAp phases revealed by Sr distribution indicate similar recrystallization processes for the fossils from Jiyangshan and Guanling. The pathway connecting stages IV-a and V (Fig. 2.10) is reasonable, even though no fluorite has been found in our stage V sample.

2.6.7 Regional low-grade metamorphism and bone alteration

The organic carbon thermometer indicates that the specimens from both study regions experienced peak temperatures in the low-grade metamorphism range. However, the source of these temperatures approaching and exceeding 200º C is currently unclear for Guanling. For Xingyi, hydrothermal fluids are the most likely heat source because of the complex tectonic activity in SW China after the Middle Triassic (Goldfarb et al. 2021) and the well-known hydrothermal ore deposits in the Xingyi area (Qiu et al. 2022). We thus propose that

hydrothermal processes were important in the low-grade metamorphic alteration, leading to extensive fluorite precipitation in the bones and culminating in the complete replacement of FAp by RAp. Similarly, a new taphonomic model for the Jarrow Lagerstätte (Ó Gogáin et al. 2022) also calls for hydrothermal fossil alteration.

The story of the Guanling Biota fossils appears different but is insufficiently understood at present because of insufficient sample size. Our findings suggest elevated temperatures consistent with low-grade metamorphism, not immediately evident from field observations of the rock. Possibly, differences in the length of "baking" time of the different Guanling specimens (long for HFUT GL-17-001, 003, and 006 vs. short for HFUT GL-17-004) led to the different alteration stages observed in these specimens. The Guanling fossils are essential because they reveal that RAp formation can occur without fluorite precipitation and may be more common than previously recognized.

The source of the high temperatures at Guanling remains mysterious. Temperatures of low-grade metamorphism generally correspond to several kilometers of burial, a depth from which the rock typically does not rise again. The geothermal gradient of 25-30º C per km (away from plate boundaries, see DiPietro 2013) would mean that the lowest temperature we measured for the unaltered (stage I-b) Guanling specimen of 193º C ± 30º C is equivalent to a burial depth of around 6 km. Thus, other sources of the elevated temperatures need to be invoked for Guanling, such as hydrothermal fluids (for which there is no evidence), as in the case of the Xingyi Fauna, and possibly regional tectonic heating from the Himalayan front (Myrow et al. 2003).

2.7 Conclusion

The conclusion can be summarized to:

1. Low-grade metamorphic alteration of fossils of marine reptiles from two regions, Xingyi and Guanling (SW China), is identified in this study. We recognize five alteration stages of the bone tissue, from unaltered (except for normal fossilization) to near-complete destruction of the bone tissue. The five alteration stages are described in a simple sequential model.

2. Fossils from the Xingyi Fauna show fluorite precipitation inside the bones, which suggests a hydrothermal origin during late diagenesis or low-grade metamorphism. The origin of F^- ions is probably from the hydrothermal fluids. This is the first time that fluorite-replacing fossil bone tissues has been reported.

3. In fossils from both regions, we observed a continuous apatite phase transformation from fluorapatite (FAp) to recrystallized bone apatite (RAp). Two RAp generations with different Sr intensities are recorded. The hypothesis that apatite recrystallization is influenced by hydrothermal fluids needs further investigation.

4. The alteration of the fossils is correlated with low-grade metamorphism and associated high temperatures. Peak temperatures of 177-209 °C ± 30°C were detected based on mineral composition and the Raman CM geothermometer. The Guanling fossils experienced higher peak temperatures than those from the Xingyi Fauna. However, there is no correlation between elevated temperatures and increased bone alteration, at least in fossils from stages II to IV-a.

5. These temperatures are likely attributable to hydrothermal activities in the Xingyi region, similar to what is observed at the Jarrow lagerstätte. However, the source of such temperatures in Guanling remains uncertain due to the absence of mineralogical indicators of hydrothermal activity.

2.8 Acknowledgments

We thank Frank Tomaschek for the help on data collection and initial suggestions on manuscript revisions. We are also grateful to Nils Jung and Olaf Dülfer (IGPB) for the production of thin sections. Funding for this research was provided by grants GE 1094/24-1 and SA 469/54-1 from the German Research Council (DFG) to Thorsten Geisler and P. Martin Sander, respectively, as part of Research Unit FOR 2685 (contribution No. 55). This project was also supported by the National Natural Science Foundation of China under Grant numbers 42172026 and 41772003, the China Scholarship Council (201906690046), the Fundamental Research Funds for the Central Universities of China under Grant number PA2020GDKC0022, and the Department of Natural Resources of Anhui Province under Grant number 2021-g-2-16.

2.9 Supporting Information

Additional Supporting Information can be found online:

Google Drive link: https://drive.google.com/drive/folders/1-Ngg9MCyYf1NReX_lNHqDtrgU6iGu04g?usp=drive_link

Figures S1. Raman spectra of representative sample and Image of Raman spectra fitting.

Table S1. Fossils sampled for this study.

Table S2. Estimated peak temperature data of Equations T1 and T2.

Chapter 3

Bone histology and sexual maturation of *Keichousaurus hui* (Diapsida, Eosauropterygia) from southwestern China

3.1 Abstract

Keichousaurus hui is a small pachypleurosaur from the late Ladinian Xingyi fauna of the southwestern Chinese Guizhou and Yunnan provinces. The taxon is known from thousands of specimens, including entire growth series and gravid females. Like many other pachypleurosaurs, *Keichousaurus* exhibits distinct sexual dimorphism, particularly in the shape of the humerus.

Here we first describe the histology of the long bones of *Keichousaurus*. In addition, the microanatomy of the humeral midshafts clearly show the start of sexual maturity in *Keichousaurus*, too. Sexual maturity occurred in the second annuli, corresponding to the second year of life in *Keichousaurus*. In males, the cross-section of the shaft changes from round to triangular in the second year. Interestingly, the less organized bone tissue of the second cycle occurs in both sexes, but females continue to grow with a round or oval cross-section. However, sex determination is still impossible histologically in juvenile specimens. No distinct difference in growth rate was observed between the two sexes in this study, which may be due to the small sample size. Our life history data also show an earlier sexual maturity of *K. hui* males compared to other pachypleurosaurs. The estimated maximum age is more than nine years.

The bone tissue deposited in *K. hui* humeri belongs to the lamellar-zonal type. As in other pachypleurosaurs, the very small medullary cavity of the humerus suggests osteosclerosis, which fits with the morphological evidence for secondary aquatic adaptation in *Keichousaurus*.

3.2 Introduction

Sexual maturation, i.e., the ability of an organism to reproduce, is one of the most important ontogenetic stages of all gamogenetic organisms. The maturation of individuals is generally controlled by physiological processes and exhibits sex characteristics that differ between sexes (i.e., primary sex characteristics, secondary sex characteristics, and non-reproductive characteristics; see Darwin 1859, Padian and Horner 2011). In living animals, for example, they differ in color, body shape, and structure. Thus, sexual dimorphism provides reliable approaches to studying the maturation and ontogeny of living organisms. Typically, the onset

of reproduction is easily observed in living mammals, birds, and reptiles. However, identifying sexual maturity in fossil vertebrates from the Mesozoic is difficult. Most cases of sexual dimorphism have been considered as the result of sexual selection, such as the highly ornamented tails of male peacocks, larger noses in Mirounga, or antlers in deer. In some birds, females appear to be larger than males and are thought to lay more eggs and defend the brood better (Ralls 1976). In reptiles, in addition to differences in reproductive structure between the two sexes, there is confirmation of sexual maturity (Cox et al. 2007, Kaliontzopoulou et al. 2007). The body sizes of living alligators are sexually dimorphic, with males generally larger than females and growing longer after sexual maturity (Hutton 1987, Tucker et al. 2006). However, sex differences are usually expressed in the parts that have not been preserved (e.g., the color of fur, sex organs, or head crest), whereas we are limited to the osteological features when examining fossils (Sander 1989, Xue et al. 2015).

The Pachypleurosauria first appeared in early Anisian in the Germanic basin (Gürich 1884, Rieppel 2000). This clade then prospered during Anisian-Ladinian in Monte San Giorgio (Italy, Switzerland) and China (e.g., Sander 1989, Rieppel 1989, Rieppel 2000, Liu et al. 2011, Jiang et al. 2019). *Neusticosaurus* and *Keichousaurus*, small-bodied eosauropterygians from Europe and China known as pachypleurosaurs, show broadened distal humeral ends in adult males compared to those of females (Sander 1989, Lin and Rieppel 1998, Cheng et al. 2004). Although sexual size and morphological dimorphism are pronounced in these extinct marine reptiles after sexual maturity, the juveniles exhibit similar morphological features in both sexes, and juvenile male pachypleurosaurs may have been misidentified as females previously (Motani et al. 2015, Xue et al. 2015).

The previous studies on pachypleurosaurs mainly focused on external morphology. More recently, individual ontogeny and sexual dimorphism have been given more attention (Sander 1989, Klein and Griebeler 2018). Cheng et al. (2009) examined 70 essentially complete skeletons and estimated the possible length at sexual maturity of *Keichousaurus hui* according to the previous study (Lin and Rieppel 1998). The study by Cheng et al. (2009) was based on multivariate analysis (principal component methods, discriminant analysis) and provided a more accurate result for the sex determination of *K. hui*. Then, further quantitative analyses were conducted to understand the ontogenetic history and sex determination in Chinese *K. hui* (Motani et al. 2015, Xue et al. 2015) that could determine the range of adult size of the two sexes. However, ontogenetic stage determination in these studies is based on skeletal ratios formed by allometric growth during different size stages. The possibility that subadult males were misidentified as female may still result in a lower male proportion. Thus, life history and the exact stage of onset of sexual dimorphism were not subject to stringent control, and more

information is needed to address this issue (Cheng et al. 2009, Motani et al. 2015, Xue et al. 2015).

Bone histology is one of the most important sources of information on the physiology, lifestyle, and paleoecology of extinct marine reptiles (Houssaye 2013, Houssaye et al. 2016). Such studies have been well conducted to understand the ontogenetic history of European sauropterygians (Sander 1989, 1990, Klein 2010, Hugi et al. 2011, Krahl et al. 2013, Klein et al. 2015a, Klein et al. 2015b) based on the microanatomy and growth patterns in midshaft sections of long bones. Klein and Griebeler (2018) explained the possible start of sexual maturity by the different growth rates of the two sexes in European pachypleurosaurs. Nevertheless, the histological evidence of sexual maturation and its relations with external dimorphism is not well understood among pachypleurosaurs or even sauropterygians.

Keichousaurus hui inhabited the eastern Tethys and is represented by extremely abundant material. Here, we test dozens of *K. hui* individuals sampled from humeral midshafts by thin sectioning, which helps to identify the sexual maturity and microstructure based on bone histology. According to bone histology and microanatomy records morphogenesis, we want to offer a new perspective on the evolution of sexual dimorphism and ontogeny in Triassic marine reptiles.

3.3 Geological settings

During the late Middle Triassic to early Late Triassic, the Indosinian Orogeny caused the collision of the North China Plate and the South China Plate. The latter was wholly uplifted, resulting in a regression of the sea in area near the collision zone (Metcalfe 2006, Zheng et al. 2013). Meanwhile, regions further away from the collision zone experienced a marine transgression event (Luo et al. 2013, Lu et al. 2018). This event is characterized by shallow-water carbonate sedimentation, with the Yangliujing Formation as a typical example. In the upper part of this sequence, deep-water nodular limestone and mudstone, such as the Zhuganpo Formation (also known as the Falang Formation Zhuganpo Member), were deposited.

Fossil assemblages from the Xingyi area are primarily found in the Dingxiao and Wusha Town of Xingyi City, Guizhou Province. Additionally, the nearby regions, such as Fuyuan in Yunnan, have also yielded fossils from the same layers (see Figure 2.1). Fossil specimens used in this study were collected from Ji Yangshan Village of Fuyuan County, Qujing City, Yunnan Province, and Xinheini Village of Xingyi City, Guizhou Province. The distance between these two locations is approximately 35 kilometers.

The Xingyi fauna is mainly found in the lower part of the Xingyi Zhuganpo Formation (Zeng et al. 2013), although the age of this formation is currently under controversy. The Guizhou Geological Survey (1980) classified the lithology of the Zhuganpo Formation as middle-bedded nodular limestone, with the underlying strata being gray limestone and dolomite beds of the Yangliujing Formation of the Late Triassic. However, there exists a set of laminated mudstone, dolomite, limestone, and shale layers between the middle-bedded nodular limestone of the Zhuganpo Formation and the underlying Yangliujing Formation in Xingyi and Fuyuan area. These layers are the main fossil beds of the Xingyi fauna. Thus, it is important to determine whether this section belongs to the upper part of the Yangliujing Formation or the lower part of the Zhuganpo Formation.

The age of the Zhuganpo Formation has been discussed in previous studies. Chen (1985) proposed that the *Keichousaurus hui* was from the Late Ladinian of the Middle Triassic. Dong (1997) assigned the Zhuganpo Formation to the lower part of the Falang Formation, calling it the Zhuganpo Member, and placed it between the Late Ladinian and Early Carnian. Conodont studies (Wang et al. 1998) suggested that the correct age of *Keichousaurus*-bearing layers is indeed the Carnian.

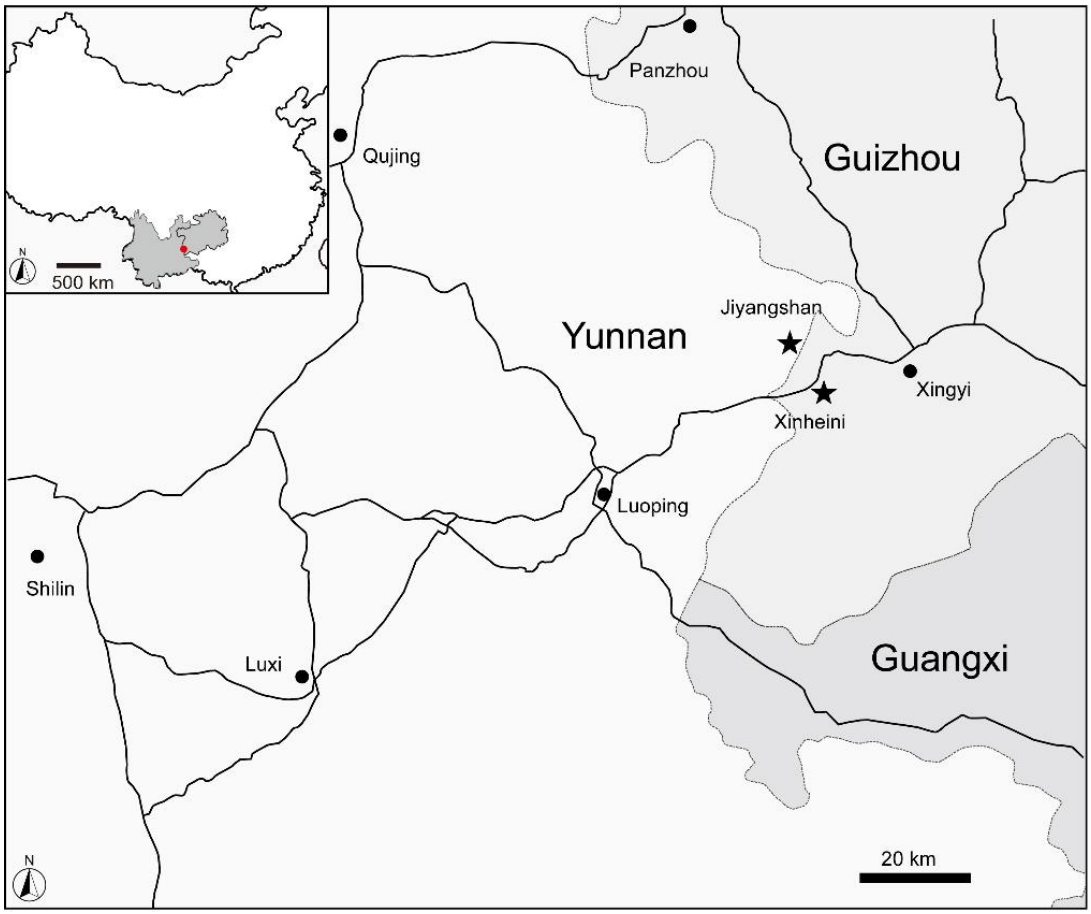

Figure 3.1. Traffic map of Fuyuan and Xingyi area. The fossil localities Jiyangshan (JYS) and Xinheini (XY) are indicated by stars.

Based on ammonite fossils collected from the Wusha area of Xingyi, Ma et al. (2013) preliminarily placed the Xingyi fauna in the Late Ladinian of the Middle Triassic. After further study by Zeng et al. (2013), the upper part of the Zhuganpo Formation was identified as gray, medium-bedded nodular micrite limestone with very thin shales and few nodules, while the lower section consisted of gray-green or gray laminated micrite limestone with occasional dolomite or dolomitic layers. The age of the Xingyi fauna, as determined by the laminated micrite limestone, was confirmed to be Late Ladinian (Zeng et al. 2013).

3.4 Material and Methods

3.4.1 Material

The sampled specimens are from the Middle Triassic (Ladinian) deposits of Zhuganpo Member of the Falang Formation. The fossils come from three different localities, i.e., Fuyuan, Yunnan Province, and Xingyi and Longguang, Guizhou Province, Southwest China. The linear distance between Fuyuan and Xingyi is about 20 kilometers (See Fig. 3.1 with fossil localities where specimens were collected for this study). A single specimen was collected 40 kilometers to the east from Longguang. The sampled *K. hui* specimens in this study are all well-articulated, and half of them are complete skeletons. All specimens are kept in the paleontology laboratory of Hefei University of Technology (HFUT). We drilled 18 humeral midshaft cores of *K. hui* (for coring method, see Sander 2000, Stein and Sander 2009) from 11 males (first identified as sex Y by Sander 1989), six females (first identified as sex X by Sander 1989), and one isolated fetus. Sex determination of the males was based on previously proposed principles (Lin and Rieppel 1998, Cheng et al. 2004, Cheng et al. 2009). Twenty-one thin sections of *Neusticosaurus* (*N. edwardsii*, *N. pusillus*, and *N. peyeri*) from Monte San Giorgia, kept at the University of Bonn, served as a comparison. These thin sections were previously examined histologically (Sander 1989, 1990, Klein and Griebeler 2018).

Due to the particular preservation of the dark gray, thin-bedded limestones of the Zhugangpo Member in the Xingyi area, the thin sections of *K. hui* generally exhibit poor preservation at the histological level and dark staining of some structures. Two different types of preservation were observed in the 18 thin sections from the three localities. Five Jiyangshan specimens are heavily affected by bioerosion and show dark rings in thin sections (Figs. 2.3D, H). The rest are bright under normal light, and some show postmortem filamentous structures of unknown origin under cross-polarized light (Figs. 2.3F-G). The thin sections with black diagenetic rings contain less histological information, which is possibly caused by hydrocarbon infiltration and loss of birefringence. In some specimens, there are tubular traces of unknown

origin that are denser in the dark layers. These traces inside the bone were probably formed by biogenic processes (Fig. 3.4E). Furthermore, diagenesis formed numerous tiny needle-like crystallites in most of the thin sections (Figs. 2.4A, D), also obscuring the original information in the bone tissue.

Table 3.1. Information for the sampled specimens in the HFUT collections. Abbreviations for measurements: FL = femur length, HL = humeral length, SL = standard length. Abbreviations for shape of cross-section: T = triangular, O = oval.

Specimen Number	Sampling Position	Sex	Preservation	SL /mm	HL /mm	FL /mm	Cross Section
HFUT JYS-15-001	Slightly distal	Male	normal	17.00	25.90	25.57	T
HFUT JYS-15-002	Slightly distal	Male	dark	13.45	22.31	18.55	T
HFUT JYS-15-004	Mid	Male	normal	19.65	27.1	23.02	T
HFUT JYS-15-006	Slightly distal	Male	dark	13.11	22.8	19.37	T
HFUT JYS-15-007	Mid	Female	normal	14.67	18.22	17.31	O
HFUT JYS-15-014	Mid	Female	dark	12.02	14.08	14.88	O
HFUT JYS-15-016	Mid	Fetus	normal	/	/	/	/
HFUT JYS-15-023	Mid	Male	dark	/	9.31	/	T
HFUT JYS-16-001	Mid	Male	dark	12.87	22.36	17.94	T
HFUT JYS-16-003	Mid	Male	normal	14.30	21.43	17.86	T
HFUT XY-18-002	Mid	Male	normal	13.08	18.7	17.15	T
HFUT XY-18-003	Mid	Male	normal	14.61	21.63	19.05	T
HFUT XY-18-004	Mid	Male	normal	14.43	19.79	16.72	T
HFUT XY-18-005	Mid	Female	normal	18.74	22.43	22.23	O
HFUT XY-18-007	Mid	Juvenile	normal	/	17.10	/	sub-T
HFUT XY-18-008	Mid	Female	normal	/	23.74	/	O
HFUT XY-18-009	Mid	Male	normal	/	19.10	/	T
HFUT LG-21-003	Mid	Female	normal	12.94	/	/	O

3.4.2 Methods

Macro-photography and measurement

All specimens examined here were prepared with pneumatic tools prior to photography. Photographs of the specimens and the coring positions were taken with a Mi 6 camera before and after the removal of the cores. Measurements of the long bones, glenoid, standard length (Sander 1990), and torso length were made with calipers (accuracy of 0.2 mm) to provide different body size proxies.

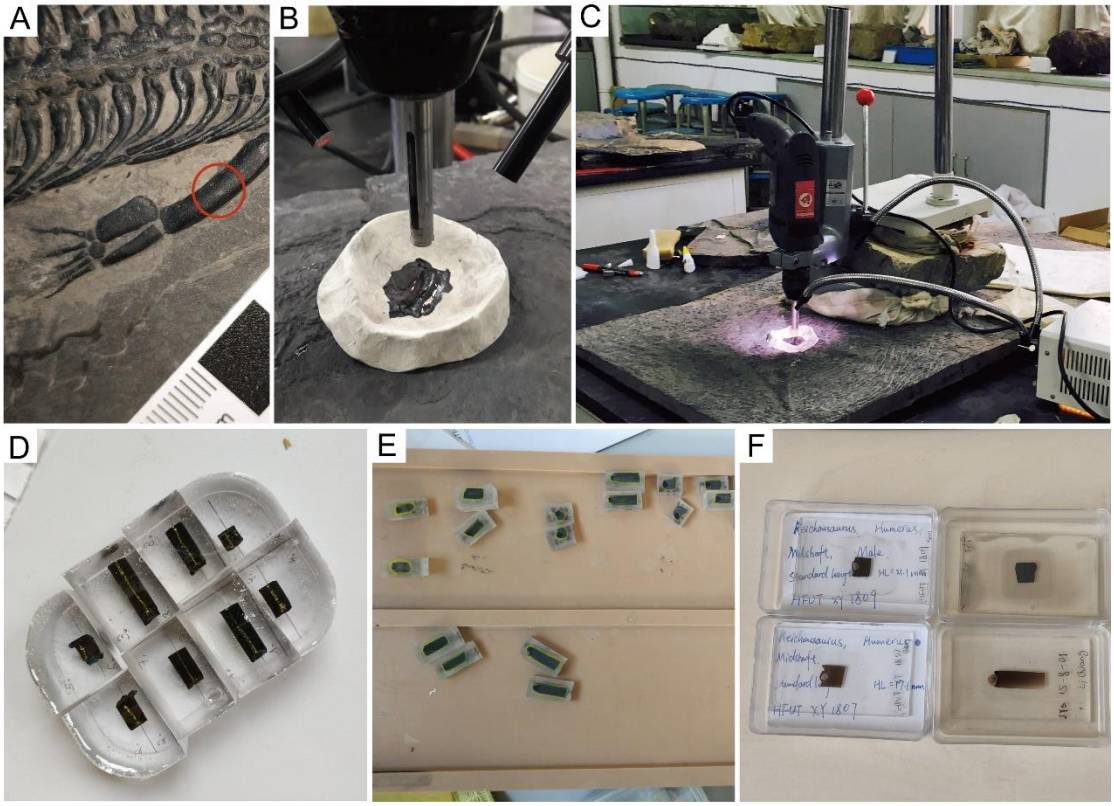

Figure 3.2. The sampling and thin sectioning methods. (A) prepared *K. hui* specimen HFUT JYS-15-007 and red mark for drilling; (B) Prepared humerus of HFUT JYS-16-001 protected by a layer of glue and surrounded by a clay dam; (C) The core drilling set-up; (D) Several cores embedded in epoxy blocks ready for sectioning; (E) Polished sections; (F) Thin sections.

Sampling by coring and thin sectioning

Based on previous studies of the histology of the long bones of tetrapods, the center of the humerus is an ideal location to obtain microstructure and a complete growth report. This is due to appositional cortical growth in the mid-shaft region, where the growth record is the longest and most complete. Therefore, the cores with clear annulus and minimal remodeling are most likely to be found in the middle of the shaft (see Fig. 1 of Stein and Sander 2009).

Since all humeri used for sampling were still at least partially embedded by sediment, the central shaft area was stabilized by a layer of superglue (Fig. 3.2A). To protect the drills from overheating and guarantee constant lubrication during drilling, water is poured into a circular plasticine dam surrounding the drill site. For drilling, the electric drill was mounted in a drill press, and the specimen was securely placed on a sandbag that rested on the base of the drill press. The cores contain the entire midshaft of humeri and sediment matrix (Fig. 3.2B-C).

Thin sections were then prepared using standard petrographic methods (e.g., Lamm 2013). Cores were embedded in synthetic resin (Araldite 2020 A/B, Huntsman, Cambridge) and then sectioned along the previously marked transverse plane. One half of the core was then glued with araldite onto a glass slide, cut down to a few millimeters thickness with a rock saw, and ground to a thickness of 30 μm or less. Finally, a cover slip was placed on top of the slide with UV glue to provide better optical contrast and protection (Fig. 3.2D-F).

The thin sections were examined with a Leica® DM750P polarizing microscope and a digital microscope camera (Leica® DFC420) in transmitted light mode. Photographs were taken using Image Access easyLab 7.0 software. Annual growth marks and bone tissue were marked using Adobe Illustrator CS6.

Skeletochronology

Skeletochronology is based on growth marks observed in polished sections and thin sections with reflected light and transmitted light, respectively (Sander 1989, Sander 1990). Given the peculiar preservation of the specimens with poor histological information, polish lines (Sander 2000) are considered an additional method to study skeletal chronology. Polish lines were defined by Sander (2000) as growth lines in polished sections. Due to the slightly different hardness of bone matrix, the harder region (usually means slow growth or LAGs) becomes convex and appears to be finer than the softer parts after polishing. The polish lines usually imply an abrupt softening of the bone and lead to an abrupt decrease in the reflectance in bright-field illumination in an incident light compound microscope or a stereomicroscope. For our samples, polish lines thus offer a possibility of skeletochronology studies when bone tissue has been severely altered after diagenesis.

For the skeletochronological analysis, we used minimum shaft circumference (MSC) as a body size proxy. MSC increases in proportion to long bone length (and thus total body length). MSC is also linked to local bone apposition rates which are closely related to increasing body mass and size in mammals, birds, and dinosaurs (Anderson et al. 1985). The relationship between MSC and body mass was later tested in lizards, which have body shapes similar to pachypleurosaurs (Campione and Evans 2012). Thus, each growth mark that is laid down during ontogeny is associated with a particular bone length and, thus, with a particular body

mass (Klein et al. 2015b). To obtain accurate growth curves (Fig. 3.7), the five thin sections with the most complete growth records were analyzed (three males and two females). All of these showed more than four complete and clear annuli (Fig. 3.7). In the graphs, the number of annuli is the independent variable, and the dependent variable here is the outer circumference of each ring, i.e., the MSC at the end of each growth cycle. Due to the presence of prenatal bone tissue in the medullary region of these five individuals, the growth mark record is complete, as no remodeling happened in medulla. Thus, the growth curves did not need to be corrected for any missing annual growth mark.

3.5 Results

3.5.1 Ontogenetic changes in histology and microanatomy

In *Keichousaurus hui,* vascularity is relatively low in both sexes, and radial vascular canals that reach cortical surface are present in all specimens (Li 2019). The average bone compactness of the studied slides is high. Vascularity decreases with age in the two male humeri but is getting higher with age in some samples.

Based on the morphological differences between specimens, the sex determination of adult *K. hui* is quite straightforward, as discussed above. However, the thin sections of the humeri provide an unexpected new sexually dimorphic feature of *K. hui*. The humeral cross sections show two different shapes in the middle of the shaft: round-oval and triangular (or sub-triangular). All adult males have triangular humerus cross-sections, whereas the cross-sections of females or possibly juvenile (subadult) are more elliptical (Fig. 3.3). In males, the triangular shape of the cross sections forms in the second year and becomes more prominent in later annuli. Histologically, this transformation is visible in most male individuals, even if no true LAGs (lines of arrested growth) were observed. Although the bone tissue types are quite similar, the slight density and structural differences are enhanced by diagenetic processes. However, the vascular density of the cortex is similar before and after the first annulus (Figs. 2.3B-I). The change in vascularization and growth rate is not obvious in the female individuals (Figs. 2.3J-M). The first annulus with a triangular shape indicates the time of completion of sexual maturation (Fig. 3.3G, I) and provides the ontogenetically earliest evidence for sexual determination in *K. hui*. Considering the morphological ontogeny of the skeleton of *K. hui*, the first triangular annulus most closely matches the external morphology of the male. Disordered bone tissue on the lateroventral sides of the male humeri indicates synchronous and rapid growth during sexual maturation, resulting in the formation of the posteroventral crest (Fig. 3.3I, 6A).

One fetus specimen (HFUT JYS-15-016) was sampled in this study (Fig. 3.3A). Of particular note, the fetal specimen here also exhibits a triangular cross section. Although almost no microstructure is preserved, the compressed skeleton and large cavity inside the bone are most likely caused by deformation or cut orientation of the humerus.

The adult male HFUT XY-18-007 (Fig. 3.3B) was identified as female or juvenile with paedomorphic characteristics at first. The external morphology shows female and juvenile humeral features (the distal end of the humerus is not distinctly expanded; see Cheng et al. 2009). However, bone histology of HFUT XY-18-007 shows a distinct bone transform and triangular annuli after the completion of sexual maturation (Fig. 3.3B). Therefore, it is presumed that the specimen is male and represents a case where the sex differentiation has been expressed earlier in the histological level than in the external morphology.

Although sexual maturity is observed in most sections, the boundaries between the two stages (subadult and adult) are blurred in several specimens. The peculiar dark remains at Jiyangshan obscured the growth marks in HFUT JYS-15-002 and HFUT JYS-15-006 (Fig. 3.3D, H), which shows the triangular growth traces but no microstructure transition between the two stages.

The ontogenetic changes of microanatomy, and vascularity density in particular, led us to recognize four distinct live history stages in *K. hui*. These stages are 1) prenatal or fetal, 2) juvenile, 3) subadult, and 4) adult. Stage 1, the fetus is defined as from embryo to live birth. Stage 2, juvenile is defined as soon after birth and lasts till the boundary before the midshaft cross sections, starting the transition from round to triangular in males. Stage 3, subadult, is delimited by the histological onset and cessation of development of the secondary sexual characters, the midshaft shape changes from round to triangular in the males. The subadult stage in most individuals lasts for one cycle, but sometimes it lasts for two annuli. The histological subadult stage may still show a juvenile morphology in males (Fig. 3.3B). Stage 4, adult shows the growth after subadult and lasts till end of the individual's life.

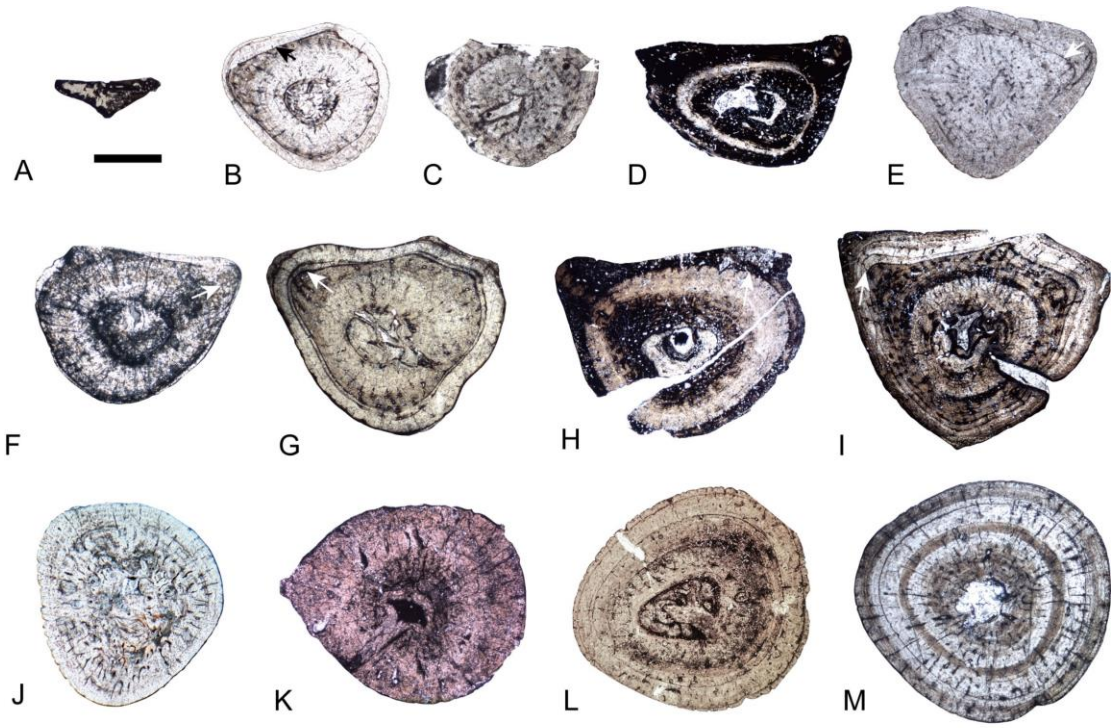

Figure 3.3. Microanatomy as preserved in whole thin sections of *K. hui* humeri, organized by size and sex. The sections are shown with the ventral sides up, and all thin sections are in cranial view. (A) Right humerus of HFUT JYS-15-016, fetus; (B) Right humerus of HFUT XY-18-007, adult male; (C) Right humerus of HFUT XY-18-002, male; (D) Right humerus of HFUT JYS-15-002, male; (E) Left humerus of HFUT XY-18-004, male; (F) Left humerus of HFUT XY-18-009, male; (G) Right humerus of HFUT JYS-16-003, male; (H) Right humerus of HFUT JYS-15-006, male; (I) Left humerus of HFUT JYS-15-004, male; (J) Left humerus of HFUT LG 21-003, female; (K) Left humerus of HFUT XY-18-005, female; (L) Left humerus of HFUT JYS-15-007, female; (M) Left humerus of HFUT XY-18-008, female. Note the triangular cross section of the male humeri (A-I). The arrows indicate the achieve of sexual maturation, and the scale bar corresponds to 1 mm for all thin sections.

3.5.2 Histological description

The medullary cavity of *K. hui*, which is normally surrounded by bone from the periosteum, varies in size but is always very small (Fig. 3.4). HFUT JYS-15-001 was not cut exactly in the middle shaft. Thus, the cavity is irregular and surrounded by a thick layer of endosteal bone (Fig. 3.4A). HFUT XY-18-003 has a medulla filled with thick, less oriented tissue and a thin layer of hatchling bone (Fig. 3.4B). The medullar region is also very small and has a sharp line around the bone of the endosteum (see Fig. 3.4C) in HFUT JYS-15-007. However, no calcified cartilage is present in our samples. HFUT JYS-15-002 and HFUT JYS-15-014 have the largest medullary cavities of all specimens, extending into the periosteal region, and have less endosteal bone (Fig. 3.3D, 3.4D). In HFUT XY-18-007, resorption of the bone and free cavities

are visible (Fig. 3.4E). There are four specimens that show the nutrient canal entering the bone, indicating proper midshaft positions of these cross sections. HFUT XY-18-002 and HFUT XY-18-005 show that the nutrient canal extends from the center of the medullary region, whereas in HFUT JYS-15-014, the canal extends to the surface of the bone (Fig. 3.4F). This suggests that the nutrient canals are oblique in orientation. In some large individuals, the number of small erosional cavities is high, indicating active remodeling of the inner cortex. HFUT JYS-15-002 shows a high degree of primary bone remodeling (erosion cavities along the cortical bone). HFUT XY-18-009 also shows a small free cavity and multiple erosion cavities surrounded by endosteal bone and a discontinuous nutrient canal (Fig. 3.4F). The inner bone structure of the fetal specimen (HFUT JYS-15-016) is not visible, only some trabecular remains are preserved in the medullary cavity (Fig. 3.3A).

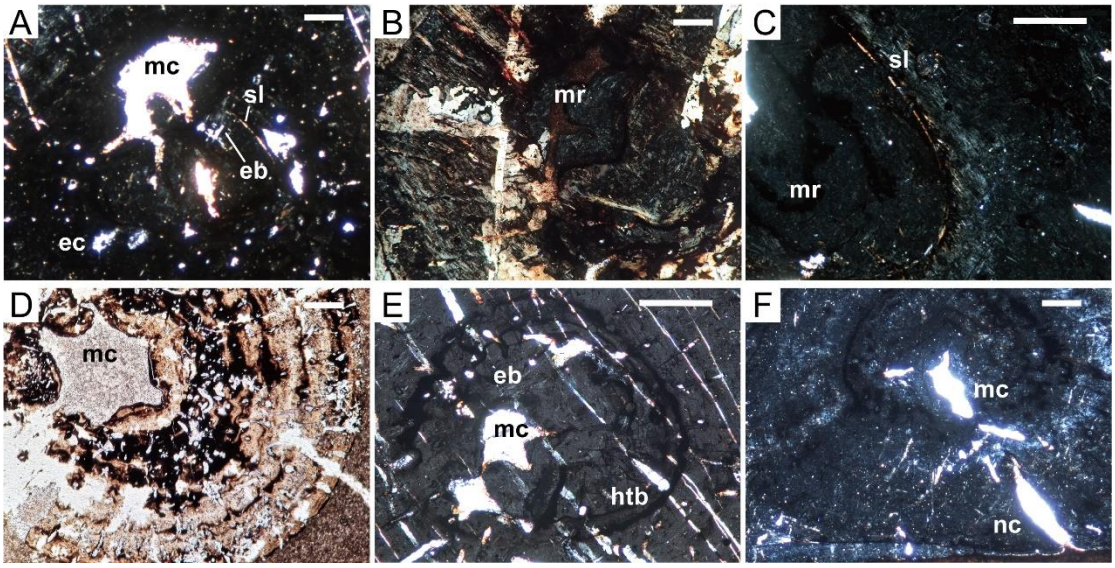

Figure 3.4. Details of medulla, bone tissue, and vascularization of *K. hui* humeri. (a) Medullary cavity of HFUT JYS-15-001. (b) Medullary cavity of HFUT XY-18-003 showing a filled cavity. (c) Medulla and inner cortex of HFUT JYS-15-007 in cross polarized light. (d) Medulla of HFUT JYS-15-014 in normal light. (f) Medulla of HFUT XY-18-007. (f) Medulla of HFUT XY-18-007 in cross polarized light with nutrient channel. Abbreviations: eb, endosteal bone; ec, erosion cavities; htb, prenatal bone tissue; mc, medullary cavity; mr, medullary canal; nc, nutrient canal; sl, sharp line. All figures except (d) are shown in cross polarized light, and the scale bar corresponds to 0.2 mm.

The bone tissue of *K. hui* is dominated by parallel-fibered bone with variable fiber arrangement levels, and no woven bone is present in midshafts of the humeri examined as mentioned by Li (2019). The organization of the tissue varies from section to section but increases from the interior to the outer cortex in general. The cortex is subdivided by cyclic growth marks (zones and annuli). However, no detectable external fundal system (EFS) was

observed in any thin section. In several sections, growth marks are incomplete along the circumference of the bone. These circumferentially incomplete growth marks indicate a slower rate of local bone deposition (e.g., Fig. 3.3B, E) than in the region without growth marks. Multiple incomplete marks record locally uneven apposition. This eventually leads to a different cross-sectional shape in males and is the morphogenetic process that leads to their triangular shaft cross-section.

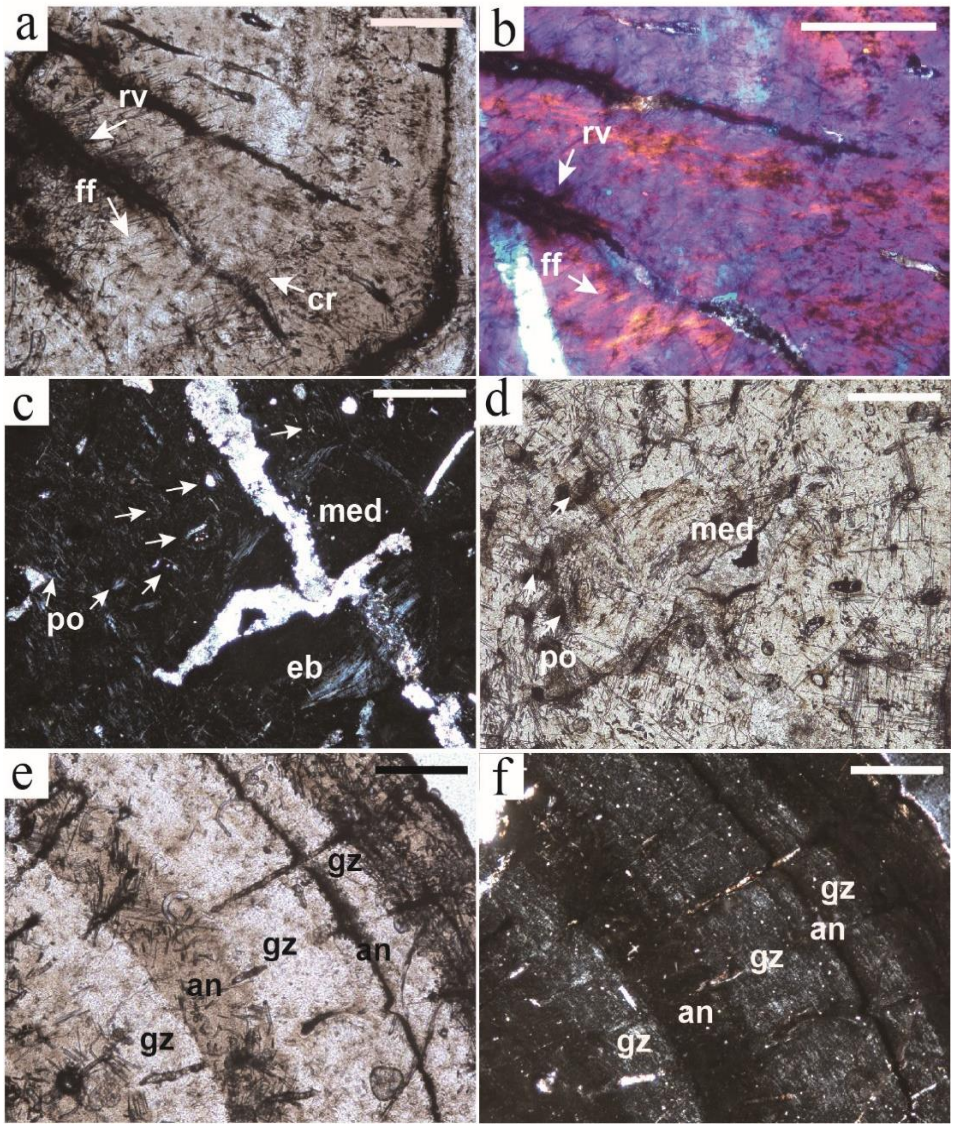

Figure 3.5. Bone tissues and different preservation under normal light and cross polarized light. (A) Details of HFUT XY-18-003 in normal light. (B) HFUT XY-18-003 shows "funnel-shaped fibers" surrounding radial vessels under cross polarized light. (C) HFUT XY-18-004 showing primary osteons and endosteal bone in cross polarized light. (D) Medulla of HFUT XY-18-004 showing irregular crystal needles inside the bone in normal light. (E) Various fungal hyphae of HFUT XY-18-008 in normal light. (F) Fungal hyphae-rich zones of HFUT XY-18-008 in cross polarized light. Abbreviations: an, annulus; cr, crystallites; eb, endosteal bone; fh, fungal hyphae; gz, fast growth zone; ff, funnel-shaped fibers; rv, radial vessel. Scale bar corresponds to 0.2 mm.

The loosely organized bone tissue in the innermost cortex of *K. hui* is similar to that of *Dactylosaurus* and aff. *Neusticosaurus pusillus* was described most recently by Klein and Griebeler (2018). Here, we refer to the earlier studies of Francillon-Vieillot et al. (1990) and Stein and Prondvai (2014) on woven bone. In HFUT JYS-15-007, a layer of highly organized fibers is preserved (Fig. 3.4C), surrounding the medullary cavity. The bone tissue appears dark under normal light and shows very bright circles, which are identified as lamellar bone under cross polarized light. In HFUT JYS-15-001, only part of the sharp line surrounding the medullary region is preserved (Fig. 3.4A).

Some radial vascular canals originating from the inner cortex are surrounded by highly organized fibers, creating a funnel and crossed structures (Figs. 2.5A-B). Funnel structures are defined as parallel-fibered surrounding the vascular canals and sunken toward the center of the bone. These well-arranged fibers, also observed in *N. pusillus* and some nothosaurs, were thought to be an early sign of the later primary osteons (Klein 2010). The funnel structures formed where the vascular canals existed. The likely interpretation is that during the deposition of the bone matrix, the pit grew outward and resulted in a funnel shape (Krahl et al. 2013, Klein et al. 2016). In terms of other features of vascular architecture, there are rare longitudinal primary osteons in some thin sections (Fig. 3.5D) similar to those in *N. pusillus*.

3.5.3 Analysis of the growth record of *K. hui*

Some annuli and LAGs appear as cyclic zones with different colors and diffuse patterns under normal or cross polarized light in sampled *K. hui* specimens. Subcycles, which in other pachypleurosaurs (e.g., *N. pusillus* and *Dactylosaurus*) normally consist of thin layers of highly organized bone tissue, are also common in *K. hui*. The midshafts of several specimens have inner rings (or portions thereof) of prenatal bone tissue (Figs. 2.4A, C), indicating that growth in this region was completed before birth. As noted above, the histological start of sexual maturity was recorded by clear annuli (Fig. 3.3) in the inner cortex. Triangular annuli are present in all males at the second ontogenetic stage, whereas annuli remain oval in females.

Polished sections observed in bright field illumination in reflected light were used for additional ontogenetic information about *K. hui* (see Methods section). Strong diagenesis is present in all specimens, resulting in poor preservation of bone tissue and sometimes a diffuse preservation of the growth pattern. However, the alternating zones and distribution of vascular canals are more evident when viewing the polished sections in reflected light than in the thin sections viewed in transmitted light. Two different reflection types are present in polished sections of *K. hui*, and the boundaries of different luminance are counted as growth marks. In HFUT JYS-15-002, however, the distinct growth marks at the posterolateral corner result from

a sampling position distal to the mid-shaft (Fig. 3.6A). Therefore, this specimen is not included in the growth curve, although the growth marks are visible under cross polarized light (Fig. 3.6B). The histology of HFUT XY-18-005 and HFUT XY-18-009 was strongly affected by diagenetic processes and was not visible in the thin section. However, the ages of the two specimens can conservatively be estimated to four and five based on the polished sections (Fig. 3.6C). The largest and smallest cycle numbers for all samples are eight for HFUT JYS-15-004 and zero for HFUT JYS-15-016 (Figs. 2.3A, 2.6E). Although the outermost growth marks of the oldest sample converged, no external fundamental system (EFS) is detectable in both thin sections and polished sections (Horner et al. 2001). Thus, the evidence for reaching the asymptotic size, normally provided by the presence of a typical layer of lamellar bone on the outside of the cortex, the EFS, was not found.

HFUT JYS-15-004 is the largest male individual whose outermost cycle, which looks very similar to EFS, is the eighth. The largest female (HFUT XY-18-008) has six growth marks and thus was presumably seven years old. It has a smaller body size than HFUT JYS-15-004. HFUT JYS-15-007 is another female that deposited five complete growth cycles (Fig. 3.6H). The growth curves of the five *K. hui* specimens show that the juvenile stage lasted for one year. At the beginning of the second year, there is the onset of sexual maturation, i.e., the subadult stage begins. Growth speed is rapid in the second year (in some individuals also in the third year), after which growth levels off. There are no signals suggesting differences between the two sexes, either in growth rate or final size when sexual maturity is achieved. It could be due to the small sample size we applied to growth analysis. Although the oldest specimen (HFUT JYS-15-004) shows a very low growth rate in the outer cortex, an unequivocal EFS has not been observed.

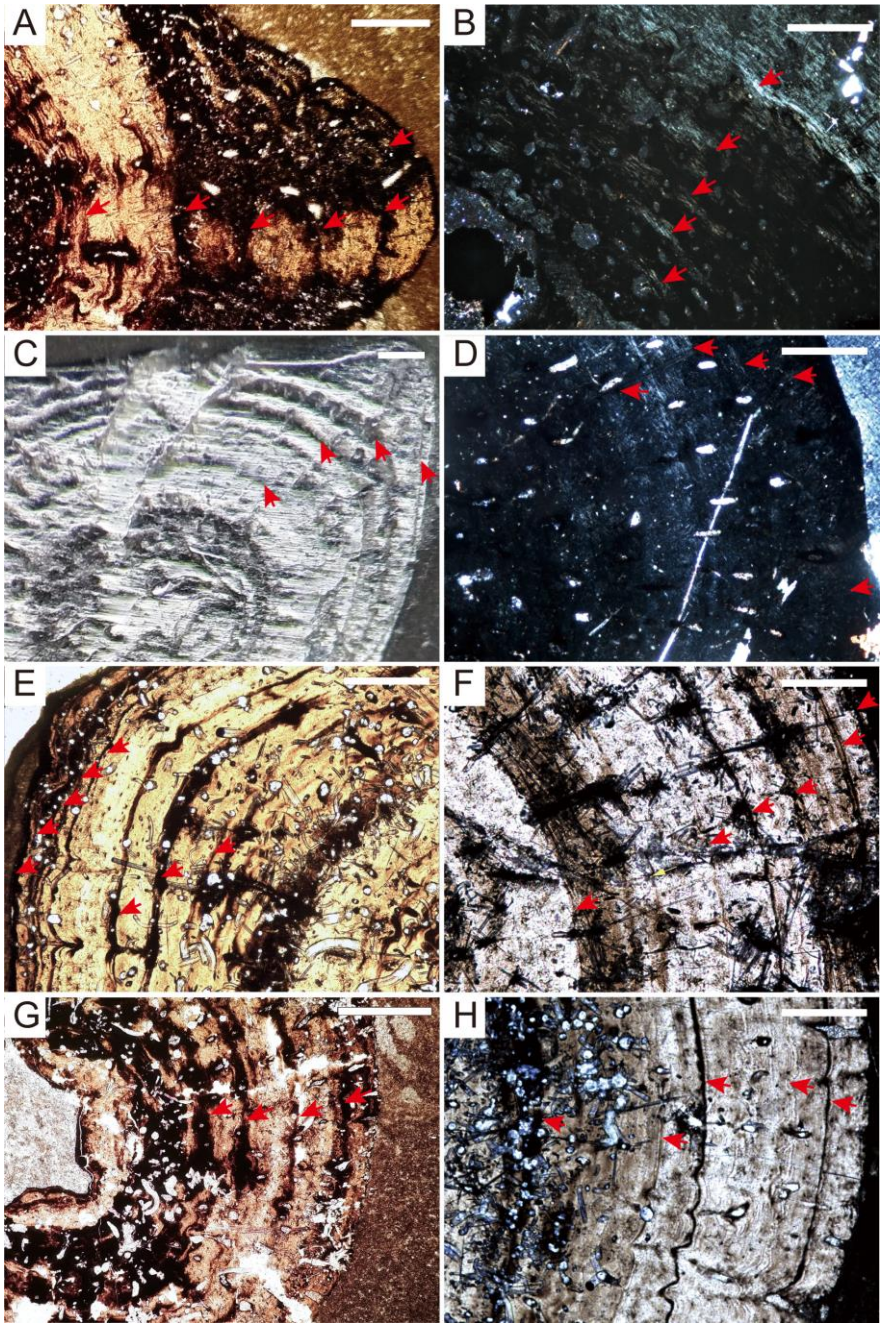

Figure 3.6. Records of growth marks in the humeri of *K. hui*. All samples are thin sections except for HFUT XY-18-009, which is a polished section. (A) Outer cortex of HFUT JYS-15-006 in normal light, note the growth marks at the posterolateral corner of the thin section. This is because the plane of the section is off midshaft and intersects the base of the crest extending to the ectepicondyle. (B) Inner cortex of HFUT JYS-15-006 in cross polarized light with several sub-annuli. (C) HFUT XY-18-009, polished section seen in incident light in brightfield illuminations. (D) HFUT JYS-15-001 in cross polarized light shows five (sub-)annuli. (E) HFUT JYS-15-004 in normal light shows very closely spaced annuli in the outermost cortex. (F HFUT XY-18-008 shows the annuli and colour change between growth zone and annulus zone. (G) HFUT JYS-15-004 in normal light shows four (sub-)annuli. (H) Thin section of HFUT JYS-15-007 in normal light shows five (sub-)annuli. Red arrows indicate (sub-)annuli. Scale bars correspond to 0.2 mm.

3.6 Discussion

3.6.1 Sexual maturity and dimorphism in histology

Based on hundreds of specimens from the Alpine region and China, the morphological sex separation of three species of *Neusticosaurus* from Monte San Giorgio, Switzerland, and Italy (Sander 1989), *Serpianosaurus mirigiolensis* (Rieppel 1989, Sander 1989) and *Keichousaurus hui* is well understood. Nevertheless, sexual dimorphism has not been documented with certainty in other pachypleurosaurs, presumably because only a few specimens of *Anarosaurus* (Klein 2010), *Dactylosaurus*, and aff. *N. pusillus* (Klein and Griebeler 2018) are known.

Some individuals of sexually dimorphic species have a relatively longer, morphologically more differentiated humerus with a conspicuously expanded distal end and a well-developed deltoid crest (sex y of Sander 1989, see also Rieppel 1989, and Lin and Rieppel 1998) than other individuals (sex x). The sex of the more differentiated individuals was initially suggested to be female, based on the argument that stronger forelimbs were needed for oviposition on land (Sander 1989). However, Cheng et al. (2004) reported a gravid *K. hui* individual with the sex x characteristics. Thus, "sex y" of *K. hui* is the male, and "sex x" is the female. Presumably, this applies to the other species as well.

In a previous bone histological study of *Neusticosaurus edwardsii* and *Serpianosaurus mirigiolensis* by Hugi et al. (2011), the onset of sexual maturity (i.e., the completion of sexual maturation) was recognized by microstructural changes (e.g., a sudden decrease in growth zone thickness or a change in vascularization), and it was hypothesized that this corresponded to the first appearance of the sexual dimorphism. In other words, the identification of sexual dimorphism was not possible based on microanatomical data alone. Similar studies on Pachypleurosauria from Central Europe also identified the time of onset of sexual dimorphism based on growth curves (Klein and Griebeler 2018). The triangular-shaped cross-sections of the humeral midshafts of male *K. hui* have never been observed in any of the pachypleurosaurs, nor other vertebrates. The triangular cross-section thus also represents a new morphological feature for sex determination. Histologically, the onset of sexual maturity (the last round growth cycle before the appearance of the triangular cycle) and individual maturation (change in bone tissue after the first triangular cycle) can be read directly from the microstructures in males. Although the growth marks are analogous in female specimens, the onset of sexual dimorphism is visible in thin sections (e.g., HFUT JYS-15-007, HFUT XY-18-005) as well when compared

with male ones. Thus, the long bone histology of *K. hui* can be used independently for sex determination once sexual maturity sets up.

Distinction between juveniles and females is difficult to be recognized in *K. hui* and other pachypleurosaurs. Although statistical analyses for allometric growth have been applied to the sex determination of females and juveniles, identifying females from juveniles is still difficult (Cheng et al. 2009, Motani et al. 2015, Xue et al. 2015). The adult specimen HFUT XY-18-007 (first identified as juvenile or female based on external morphology), which histologically shows male characteristics but externally shows female humeral characteristics, suggests that this microanatomical feature of *K. hui is* a powerful diagnostic method for sexing adults. However, additional juvenile specimens for further comparison are still needed, and sex recognition of fetuses is not possible.

The prominent angles of HFUT JYS-15-006 cross section show a sample out of midshaft (slightly toward the distal end) and explain the distal extension after sexual maturity. Nevertheless, the allometric growth of the midshaft on the ventral and dorsal sides is more pronounced in *K. hui* than in *Neusticosaurus.*

3.6.2 Bone histology of *Keichousaurus*

Similar bone microstructures exist in *K. hui* and European pachypleurosaurs. The bone tissue of *K. hui* can be summarized as lamellar-zonal bone (i.e., alternation of annuli of lamellar bone with vascular zones). Due to the strong diagenetic alteration of our material, it is difficult to observe birefringence and, thus to differentiate fiber orientation. So, following Klein and Griebeler (2018), we describe the bone tissue in *K. hui* as loosely organized, parallel-fibered bone. The tissue of *K. hui* is less organized than that of *Neusticosaurus* and *Dactylosaurus* in thin sections, which is thought to be the result of relatively rapid growth. Compared to the incipient fibrolamellar bone (Klein 2010) of *Anarosaurus*, which indicates a higher growth rate than other pachypleurosaurs, the growth rate of *K. hui* is lower. Bone tissue in the innermost cortex of *K. hui*, which shares the same characteristics with Alpine pachypleurosaurs (Hugi et al. 2011), generally shows less change between the (pre)hatch bone (if present) and the periosteal parts. In contrast to *K. hui* humeri, the rapid ontogenetic transition in the bone tissues of pachypleurosaurs from the Germanic Basin is thought to be a result of birth or dietary change during birth (Klein and Griebeler 2018).

The distinct sharp line in *K. hui* is not interpreted as an annulus because it is rare in specimens with prenatal tissue. Moreover, this layer of highly organized fibers is clearly different from the normal annuli. Therefore, we suggest the boundary between two different growth regions (in males) and the transitional bone tissue (in both males and females, Fig. 3.6)

to be the first growth mark in all specimens. The subtype of bone tissue during adult *K. hui* ontogeny, i.e., the appearance of less regular bone tissue and higher vascular density at the onset of sexual maturation, is reversed after sexual maturation ends.

The inner terminus of the nutrient canals, indicating the site of earliest bone growth, is well preserved in our specimens. Compared to aff. *N. pusillus* (e.g., SMNS 92125, Klein and Griebeler 2018), the nutrient canals in some cross sections of *K. hui* are quite large. *Anarosaurus* is the only European pachypleurosaur to date with a large medullary cavity, which is a plesiomorphic feature considering the condition of terrestrial reptiles (Canoville and Laurin 2010). The large nutrient canals, the dense vascular canals in the humeri, and the nature of the bone tissue in the thin sections of *Anarosaurus* indicate rapid growth. The specimens of *K. hui* have a similar size of nutrient canals (in proportion) as *Anarosaurus*. However, the bone tissue type here is much closer to *Neusticosaurus,* and the vascular patterns of *K. hui* are less dense than the aforementioned species.

The finely organized fibers between medulla and cortex in multiple specimens have also been observed in other Triassic sauropterygians (e.g., Sander 1990, Klein 2010, Hugi et al. 2011). The sharp line, considered to be the boundary between the periosteal and endosteal domains, was hypothesized to be homologous in structure to Kastschenko's line of amphibian long bones (Castanet and Smirina 1990) by Klein and Griebeler (2018). The remains of Kastschenko's line indicate that the earliest periosteal deposition was not replaced by remodeling of the endosteal bone in amphibians and separates the endosteal domain from the periosteal domain (Francillon-Vieillot et al. 1990, O'Keefe et al. 2019).

3.6.3 Microanatomy and secondary aquatic adaptation

Microanatomy shows an osteosclerotic condition in *K. hui*, a typical secondary aquatic adaptation as in other pachypleurosaurs (*Dactylosaurus*, *Neusticosaurus* spp., and *Serpianosaurus*), except for *Anarosaurus* (Sander 1989, Sander 1990, Klein 2010, Hugi et al. 2011, Klein and Griebeler 2018). The midshafts of *K. hui* have an internal structure similar to midshafts of pachypleurosaurs from the western Tethys, including *Dactylosaurus*, *Neusticosaurus* spp., and *Serpianosaurus.* The endosteal bone in the medullary cavity reduces the decentralized cavities and results in an increase in density of the bone in *K. hui* humeri, i.e., bone mass increase. Meanwhile, only a few erosional cavities are present, also indicating an increase in bone mass, as in those pachypleurosaurs described by Hugi et al. (2011). Other pachypleurosaurs, such as *Dactylosaurus* from the early Anisian of Poland, aff. *Neusticosaurus pusillus* from the early Ladinian of southern Germany, and *Neusticosaurus* spp. and *Serpianosaurus* from the Alpine Triassic of the Anisian/Ladinian all have small medullary

cavities. Together, these features indicate a shallow-water habitat (Klein et al. 2018).

3.6.4 The growth mark record in the *K. hui* humeri

In pachypleurosaurs, the males have dilated ends and well-developed articular surfaces (Rieppel 1989, Sander 1989, Lin and Rieppel 1998). However, the dimorphism of the humeri midshafts is pronounced only in *K. hui.* As noted, the cross-sections of the humeri are triangular in males from the beginning of the maturation process onwards. In females, oval midshaft cross sections occur at all life stages. Therefore, life history events are apparent from histological information in males, whereas they are more difficult to explain in females (see the discussion above on microanatomy).

The diameters of the inner region containing the prenatal bone tissue are approximately the same as the "minimum width of the humeral shaft" of the fetus in Cheng et al. (2009, "Measurement 15"), whereas the thickness of the first cycle is greater than 2 millimeters in all cases. Thus, the tissue deposited after the first cycle cannot be assumed to be the bone tissue deposited before birth. The width of the midshaft and the remnants of prenatal bone demonstrate that most specimens have a complete growth record, resulting in a maximally accurate growth mark count. Since we use the minimum shaft circumference (MSC) as the dependent variable, the cross-sectional shape changes between ontogenetic stages and sexes should also be considered. A triangular cross section has a greater circumference than an oval one and thus results in a higher growth rate if used as a size proxy, which then leads to an overestimation of body mass and size. However, it is unreasonable to quantitatively correct MSC of these irregular sub-circular, sub-triangular growth marks in the absence of an adequate sample size. Also, as the growth rate of both sexes is subject to individual variation, the growth rates of *K. hui* obtained in this study carry a large margin of error. Thus, the growth rate calculation based on MSC in our study is more appropriate to show the rapid growth of individual ontogenetic stages rather than sexual dimorphism of size.

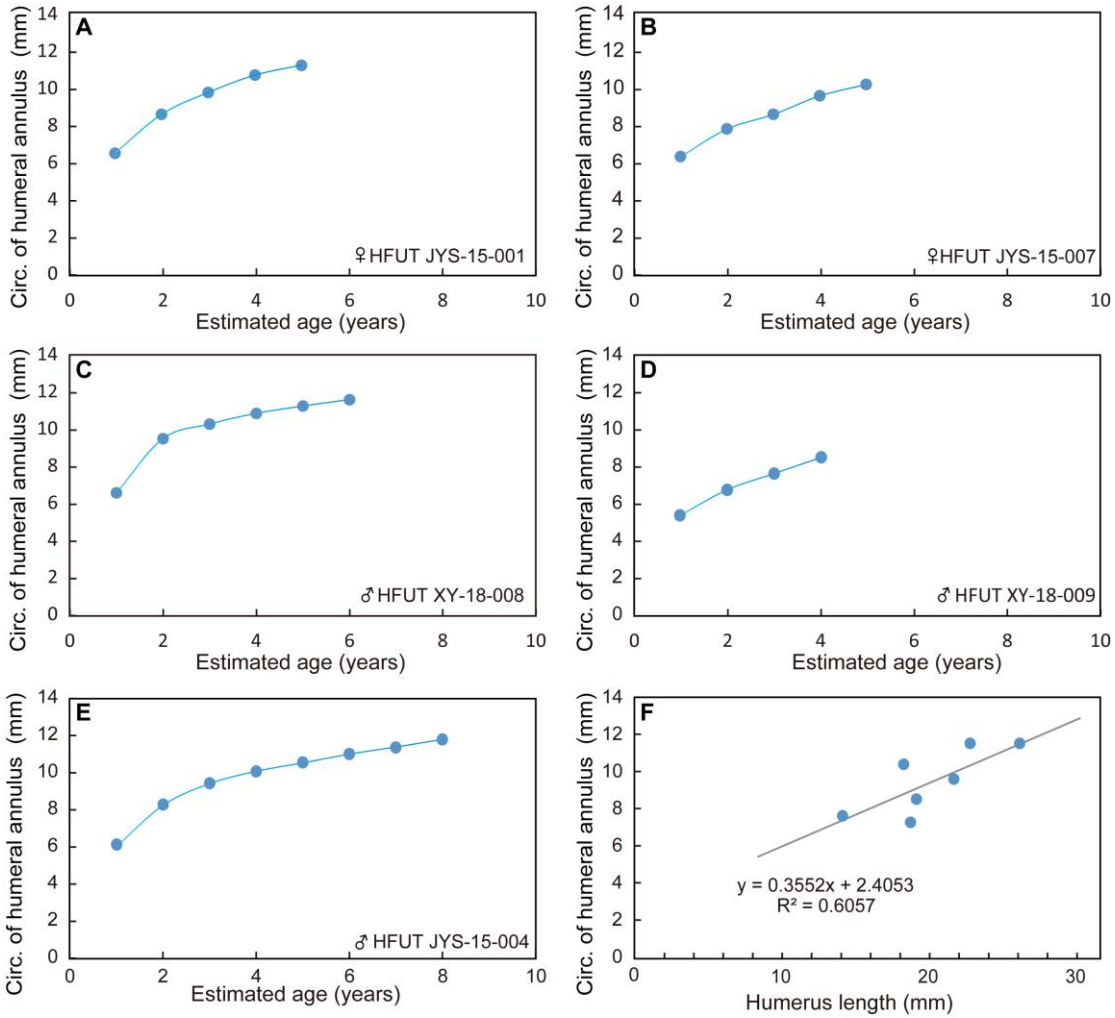

Figure 3.7. Growth curves for multiple individuals of *K. hui* and correlation between humeral mid-shaft circumferences and humerus length. Two females and three males with at least four complete growth cycles were selected for the growth curve. (A) female with five annuli, HFUT JYS-15-001. (B) female with five annuli, HFUT JYS-15-007. (C) male with six annuli, HFUT XY-18-008. (D) male with four annuli, HFUT XY-18-009. (E) male with eight annuli, HFUT JYS-15-004. (F) Ratio between humeral mid-shaft circumferences and humerus length of seven individuals with outmost growth marks preserved.

The maximum size of the sampled individuals is quite close to the largest published specimen (Cheng et al. 2009, Xue et al. 2015), which suggests that *K. hui* may reach full body size soon after age nine, although no unequivocal EFS has been observed (see HFUT JYS-15-004). The radian of the growth curves based on the circumferences of the humeral midshafts shows that the asymptotic age of *K. hui* at death is greater than nine years (Fig. 3.7E). The growth data of *K. hui* indicate rapid maturation and long life after maturation. Based on the life history data, the growth pattern of *K. hui is* similar to that of *Dactylosaurus* and *Serpianosaurus*, which reached sexual maturity after the second or third year and lived for over 10 years (Klein and Griebeler 2018). The growth pattern of *K. hui* is close to the European pachypleurosaurs except for *N. edwardsii*. The ontogenetic trajectory of *N. edwardsii* maintains a delay in sexual

maturity (i.e., a constant growth cycle thickness) until 5-6 years of age (Hugi et al. 2011) and is similar to the marine iguanas (*Amblyrhynchus cristatus)* living today, which feed exclusively in the sea (Trillmich and Trillmich 1986, Hugi and Sánchez-Villagra 2012). The similarity of ontogenetic process (timing of sexual maturity and full growth) and microanatomy between *K. hui* and aff. *N. pusillus* suggest similar habitats or lifestyle.

3.7 Conclusions

The bone tissue of *K. hui* is similar to that of *Serpianosaurus*, *Dactylosaurus*, and aff. *Neusticosaurus* (Sander 1989, Klein et al. 2010, Klein and Griebeler 2018) is generally dominated by parallel fibered bone. Small medullary cavities and low vascularity indicate an increase in bone mass, suggesting a similar lifestyle to European pachypleurosaurs.

The early cessation of sexual maturation is shown by distinct growth traces in all male specimens. The relatively short lifespan of *K. hui* with early sexual maturity suggests that the delay in sexual maturity in marine iguanas (*Amblyrhynchus cristatus*) living today does not occur here. Although no clear EFS occurs in our samples, the growth curve shows relatively rapid growth after sexual maturity and then declines after the sixth cycle (at least in the largest individual). The transition between bone tissues and the decline in growth rate during ontogeny of *K. hui* is hypothesized to be an integrative result of the ontogenetic stage and environment. Considering that the variation in bone structure is not pronounced in females, this could indicate a different growth rate (or strategy) between the two sexes of *K. hui*.

3.8 Acknowledgements

I would like to thank Jun Liu and P. Martin Sander for their help on sample preparation, thin section observation, and manuscript revision of this chapter.

Chapter 4

Puberty in a Mesozoic Reptile

Li, Q., Liu, J., Klein, N., Nakajima, Y., and Sander, P. M. 2023. Puberty in a Mesozoic reptile. *Current Biology*, 33(14), 3011-3016 e3013. doi:10.1016/j.cub.2023.05.073.

4.1 Authors and their contributions

JL, YN, and PMS. designed the study. QL, JL, and PMS made the drill cores and histological sections. QL, NK, and PMS performed the thin section observation. QL and PMS wrote the preliminary manuscript and prepared all the figures and plates. PMS and JL revised the manuscript and guided the research with their excellent supervision. All authors reviewed the final draft of the manuscript.

4.2 Article Summary

Sexual maturation is the ability of an organism to reproduce. The histology of bone can be preserved virtually unaltered for hundreds of millions of years in fossils from all environments and all vertebrate taxa, giving rise to the flourishing field of paleohistology (Buffrénil et al. 2021). The shafts of long bones are formed by the apposition of periosteal bone tissue, similar to the growth of wood, and preserve (an often cyclical) record of the growth of the individual and events in its life history. One such event is sexual maturation or puberty, during which hormonal changes transform the juvenile into a sexually mature adult. Puberty has been well studied in humans and some other living vertebrates. A prerequisite for detecting puberty is secondary sex characters, which however, have been difficult to detect in dinosaurs and other reptiles from deep time (e.g., Sander 1989, Cheng et al. 2004, Motani et al. 2015). An exception is the pachypleurosaur *Keichousaurus* which is known from thousands of specimens, from fetus to large adult. In adults, sex determination is quite straightforward (Cheng et al. 2004, Motani et al. 2015).

Here we describe puberty in *Keichousaurus*, a small sexually dimorphic and live-bearing marine reptile from Middle Triassic rocks of SW China, about 240 million years old. To understand the transition from juvenile to adult during puberty, we histologically sampled (by coring at midshaft) 18 humeri, pertaining to 11 males, six females, and one isolated fetus of *Keichousaurus*. From the thin and polished sections of each specimen, we recorded bone tissue type, bone compactness, age based on growth cycles, and onset and end of puberty. A combination of bone histology and morphology detected puberty (Ball and Wade 2013) as one

of four life stages (the others being fetus, juvenile, and adult) was applied in this chapter. The first stage, termed the "fetus," encompasses the period from the onset of ossification to birth. Although a clear-cut neonatal line is absent, the dimensions of 40 fetuses derived from 12 gravid females (Wen et al. 2022) establish a maximum size threshold for this estimation. Following this, the "juvenile" stage ensues, marking the interval post-birth and leading up to puberty; this stage appears to last for a singular year. The third stage, termed "puberty," is distinctly identifiable in the histological records, capturing the transformation of the midshaft profile from round to triangular, a feature especially pronounced in males during their second year of life. Lastly, the "adult" phase kicks in post-puberty and spans through the entirety of the organism's life.

Based on our results, adult *Keichousaurus* males have a more robust humerus than females, with pronounced muscle attachment sites and a triangular shaft cross section. Mid-shaft sections of the humeri of the males show the transition from the rounded juvenile cross section to the triangular adult cross section, as reflected in the contour of the growth marks. Upon histological examination, it becomes evident that differential bone apposition is responsible for the observed morphological alterations, particularly in a majority of male specimens. During the secondary growth phase, there's an enhanced rate of bone deposition at the anterior, posterior, and central dorsal regions of the shaft. This deposition pattern leads to the development of three distinct ridges. Notably, regions of accelerated bone deposition exhibit increased porosity and a less structured arrangement of bone fibrils, contrasting with the inter-ridge regions. Based on the growth curves of five specimens, all the individuals grew quickly in their first year. They continued to grow fast in the second year, with males reaching puberty during this time. By the third year, growth slowed down, suggesting they were mature enough to reproduce. The bone compactness analysis further corroborates the puberty idea, as illustrated in Figure 3 of Li et al. (2023). There is a subtle shift in primary compactness throughout ontogeny, evident from the figures: juveniles exhibit a compactness range of 96.9-98.9%, which during puberty transitions to 97.1-97.8%, and then further elevates to 98.4-99.7% in adults. The reduced bone compactness observed during puberty suggests an accelerated growth rate during this phase.

In summary, the puberty growth of humerus in *Keichousaurus* is presumably triggered by sex hormones, as in humans (Callewaert et al. 2010), and influenced by changes in the loading regime during puberty. This is the first report of puberty in a fossil amniote.

Chapter 5

A new pachypleurosaur (Reptilia: Sauropterygia) from the Middle Triassic of southwestern China and its phylogenetic and biogeographic implications

Hu, Y. W., Li, Q., and Liu, J. 2023 A new pachypleurosaur (Reptilia: Sauropterygia) from the Middle Triassic of southwestern China and its phylogenetic and biogeographic implications. Accepted by *Swiss journal of Palaeontology* in September 2023

5.1 Authors and their contributions

JL designed the research. YWH prepared all figures and tables. QL and YWH compiled the new data matrix for phylogenetic analysis, and YWH performed phylogenetic analyses. YWH and JL wrote the manuscript. YWH, QL, and JL revised and approved the final manuscript.

5.2 Article Summary

Following the catastrophic Permo-Triassic Mass Extinction, the nascent Triassic seas witnessed the emergence of numerous formidable reptilian marine predators. The Sauropterygia stands out as the most prolific clade in terms of species diversity among the Mesozoic marine reptiles, encompassing both the iconic Plesiosauria of the Jurassic and Cretaceous periods, as well as the basal Placodontia and Eosauropterygia of the Triassic (Kelley et al. 2014, Li and Liu 2020, Motani 2009, Rieppel 2000, Stubbs and Benton 2016). Historically, Eosauropterygians have been categorized into three major groups: the Pachypleurosauria, Nothosauroidea, and Pistosauroidea (Rieppel 2000). This conventional classification posits a monophyletic Pachypleurosauria as the sister clade to the Eusauropterygia clade, which integrates both the Nothosauroidea and Pistosauroidea (Lin et al. 2021, Liu et al. 2011, Neenan et al. 2013, Rieppel 2000). Subsequent to Rieppel's review (2000), an influx of newly identified genera of basal eosauropterygians from the Triassic strata of China and Europe (e.g., Cheng et al. 2006, Cheng et al. 2012, Cheng et al. 2016, Dalla Vecchia 2006, Renesto et al. 2014, Shang et al. 2020, Xu et al. 2022) has nuanced our understanding of eosauropterygian phylogenetics.

Although many new Triassic basal eosauropterygian species have been thoroughly described, the phylogenetic analyses accompanying these descriptions have predominantly relied on slightly augmented data matrices stemming from the work of Rieppel et al. (2002). As such, it becomes imperative to understand the morphological information derived from

comparative examinations of these new materials to understand the intricate phylogenetic ties among eosauropterygians. Pachypleurosaurs have been identified across disparate regions: both in the western Tethys, which encompasses the Germanic Basin, Alpine Triassic, and the Iberian Peninsula (e.g., Čerňanský et al. 2018, Miguel Chaves et al. 2020, Klein et al. 2022), and the eastern Tethys, notably in South China and Myanmar (e.g., Liu et al. 2011, San et al. 2019, Shang and Li 2015, Jiang et al. 2019). Based on a phylogenetic result indicating *Keichousaurus* from China as the sister clade of all European pachypleurosaurs, Rieppel and Lin (1995) postulated an eastern Tethyan genesis for the pachypleurosaurs. Their hypothesis got support from subsequent studies by Liu et al. (2011) and Renesto et al. (2014). Consequently, the paleobiogeographic origins of the pachypleurosaurs appear more multifaceted than previous estimations, needing a reevaluation (Klein et al. 2022).

This article introduces a novel species of Pachypleurosauria, titled *Dianmeisaurus mutaensis* sp. nov., sourced from a recently identified Lagerstätte in the Upper Member of the Anisian Guanling Formation. The type specimen of this new species was unearthed in a quarry near Muta village, situated in Luxi County, Yunnan Province, South China. Characteristically, *Dianmeisaurus mutaensis* manifests several autapomorphic characters, such as a postfrontal that extends posteriorly up to the midpoint of the parietal table and also being precluded from the upper temporal fenestra. It also shows a robust last dorsal rib that's comparatively shorter than the first sacral rib, coupled with the presence of two sacral vertebrae. The phylogenetic study, based on a newly revised data matrix, positions this taxon as a sister group to *Dianmeisaurus gracilis*—a tiny pachypleurosaur from the Middle Triassic Luoping Biota. The data matrix encompasses 203 characters, with 182 being informative, curated for 43 taxa. Additionally, the new data matrix incorporated several newly-identified taxa of eosauropterygians from recent discoveries. Heuristic analysis of this data matrix yielded five most parsimonious trees, with tree length equating to 811, a consistency index of 0.3169, and a retention index of 0.6139.

The new phylogeny also challenges the monophyly of the long-standing recognized Eusauropterygia. The Pistosauroidea, *Majiashanosaurus*, and *Hanosaurus* are suggested as successive sister groups, leading to a novel clade including Pachypleurosauria and Nothosauroidea. This analysis corroborates the existence of a monophyletic Pachypleurosauria, wherein the clade encompassing *Dianmeisaurus* and *Panzhousaurus* is posited at the most basal positions. Moreover, the clade inclusive of *Dawazisaurus* and *Dianopachysaurus* is described as the sister group to the other pachypleurosaurs within this research. Intriguingly, our findings agreed with those of Xu et al. (2022, 2023), revealing that two middle Anisian pachypleurosaurs, specifically *Qianxisaurus* and *Honghesaurus* from South China, are deeply

embedded within the European pachypleurosaurs. In comparison with other Chinese pachypleurosaurs, both *Qianxisaurus* and *Honghesaurus* display evolved character states: a conspicuously extended snout; a ratio of the longitudinal diameters of the upper temporal to the orbit being less than 0.5; a pronounced deltopectoral crest; and the posterior projection of the postfrontal approaching the median region of the cranial table. Given that taxa like *Dianmeisaurus*, *Panzhousaurus*, *Dawazisaurus*, and *Dianopachysaurus* are solely identified from South China, this study strengthened the proposition that the origin of pachypleurosaurs lies in the eastern Tethys.

Chapter 6

Nothosaurus sp. nov. (Sauropterygia) from the Middle Triassic of Luxi, Yunnan Province, China

6.1 Abstract

A new nothosaur species, represented by a single specimen from Member II of the Guanling Formation (Anisian, Middle Triassic) in Luxi, Yunnan Province, China, is reported here. The new specimen consists of a partial postcranial skeleton, preserving half of a pectoral girdle, half of a pelvic girdle, some gastral ribs, and limbs. The specimen is assigned to *Nothosaurus* based on characteristics such as the presence of a preaxial crest on a curved humerus, middle constriction of the coracoid, and a blunt tip on the dorsal blade of the scapula. The new material also exhibits a set of derived characters, including a long dorsal process of the scapula, a massive humerus, and hindlimbs featuring expanded ungual phalanges. The phylogenetic analysis recovered a monophyletic *Nothosaurus* with the new species as the sister group of *Nothosaurus jagisteus*. The ungual phalanx observed in *Nothosaurus* and small-sized eosauropterygians from Luoping-Luxi areas may indicate habitat adaptation in this region.

6.2 Introduction

Sauropterygia is a diverse group of diapsid reptiles that inhabited the Mesozoic oceans and can be broadly divided into two subgroups: Eosauropterygia (Rieppel 1994) and Placodontiformes (Neenan et al. 2013). The former consists of Pistosauroidea, pachypleurosaur-like forms, and Nothosauroidea (Cheng et al. 2012, Liu et al. 2014, Ma et al. 2015). Within the Nothosauroidea, two well-known genera are *Nothosaurus* and *Lariosaurus*, which were widely distributed in Middle-Late Triassic faunas across the eastern and western Tethys (Lin and Rieppel 1998, Rieppel 2000, Li and Rieppel 2004, Jiang et al. 2006b, Liu et al. 2014, Shang et al. 2022).

The systematics of nothosaurid sauropterygians have been well studied in past decades, yet the monophyly of *Nothosaurus* and *Lariosaurus* has remained controversial (Liu et al. 2014, Klein et al. 2015, Lin et al. 2017, Li and Liu 2020, Shang et al. 2022). The cladistic analysis by Liu et al. (2014) showed that the genera *Nothosaurus* and *Lariosaurus* are both non-monophyletic due to the presence of mixed morphologies in several Chinese taxa (Rieppel et al. 2003, Ji et al. 2014). The assignment of *N. youngi* to *Nothosaurus* was questioned and it was

found within the *Lariosaurus* clade together with European *N. juvenilis* and *N. winkelhorsti* by Klein et al. (2016) and Lin et al. (2017), respectively. Afterwards, *Nothosaurus* and *Lariosaurus* were found to be nonmonophyletic after the redefinition of these three species (Hinz et al. 2019, Lin et al. 2021). Finally, the latest study on the subject of *N. luopingensis* (Shang et al. 2022) recovered the monophyly of *Nothosaurus* and *Lariosaurus* again.

Luxi County, the place of origin of the specimen described here, is located approximately 60 km southwest of Luoping County in Yunnan Province, southwestern China. Luxi County thus is geographically close to the well-documented Middle Triassic Luoping Biota. Vertebrate fossils from Luxi County were only briefly mentioned by Wen et al. (2020), including fragmentary material of Nothosauroidea and Mixosauroidea. The stratigraphic position of the fossil beds in Luxi is the Upper Member of the Anisian Guanling Formation sensu Wen et al. (2020) and Hu et al. (2022). So far, three unquestionably Anisian *Nothosaurus* species have been documented from Southwest China, i.e., *N. luopingensis* and *N. zhangi* from the Luoping Biota and *N. yangjuanensis* from the Panxian Fauna (Jiang et al. 2006a, Liu et al. 2014, Shang et al. 2022). Although Shang et al. (2006) initially described *N. rostellatus* as a new species from the Panxian Fauna, later work by Yin et al. (2014) proposed it to be a juvenile form of *N. yangjuanensis*, an assignment later accepted by Klein et al. (2022).

Here, we describe new Anisian *Nothosaurus* material as *Nothosaurus* sp. nov. based on a postcranial skeleton from Xiaoapeng Village, Luxi County, Yunnan Province. The specimen is the first large-sized nothosaur from Luxi County and the second large-sized nothosaur from the Luoping-Luxi area. Moreover, we conducted a phylogenetic analysis that includes the new specimen to test its position within the Nothosauroidea clade. We also discuss the morphological diversity of the humeri with regard to phylogeny in the two genera of Nothosauridae (i.e., *Nothosaurus* and *Lariosaurus*).

6.3 Materials and Methods

The specimen was collected from the Upper Member of the Guanling Formation (Anisian) in Xiaoapeng Village, Luxi County, Yunnan Province, China, by a local collector. The material was then donated to the Geological Museum of Hefei University of Technology (HFUT) in 2022 and given the collection number HFUT XAP-22-007. The skeleton was covered with a thin layer of matrix prior to collection and was prepared using pneumatic pens and mounted needles, mainly from the top of the slab. Photographs were taken with a NIKON D7200 camera. Measurements were taken with a digital caliper with an accuracy of 0.05 mm and are listed in Table 1. The character matrix for phylogenetic analysis was constructed using NDE version

0.5.0. The data matrix was analysed using PAUP* version 4.0a169 for Windows (Swofford 2021).

To evaluate the body length of HFUT XAP-22-007, the proximodistal length of the humerus is applied as a proxy within Nothosauridae and Pachypleurosaur-like forms. A database was assembled, encompassing humerus and total body lengths of extant complete Triassic eosauropterygian specimens, with the exclusion of Pistosauroidea due to its unique body plan.

6.4 Systematic paleontology

Sauropterygian Owen 1860
Eosauropterygia Rieppel 1994
Nothosauridae Baur, 1889
Nothosaurus Münster, 1834
Nothosaurus sp. nov.

Holotype. HFUT XAP-22-007, an incomplete skeleton preserving limbs, gastralia, partial pectoral girdle, and pelvic girdle bones.

Locality. Xiaoapeng Village, Luxi County, Yunnan, China.

Horizon. Upper Member of Guanling Formation, Anisian, Middle Triassic.

Diagnosis. A large-sized *Nothosaurus* that can be distinguished from other *Nothosaurus* species by the following combination of characters: dorsal process of scapula long and tapering to a blunt point, up to 3/5 of scapula length; distinct preaxial crest of humerus, with anterior region equal to 1/3 of humerus length; width of region between proximal end and mid-shaft twice the width of mid-shaft; the ectepicondylar groove is open and anteriorly notched; the iliac blade is reduced but projects slightly beyond the level of the posterior margin of the acetabulum of the ilium; the width of the ulna at mid-diaphysis is equal to that of the radius; the pedal digit V is subequal to IV; the ungual phalanx of the pes is expanded.

6.5 Description

HFUT XAP-22-007 is an incomplete skeleton that preserves the left forelimb, scapula, coracoid, half of the pelvic girdle, partial right autopodium, several pairs of gastralia, and two hindlimbs.

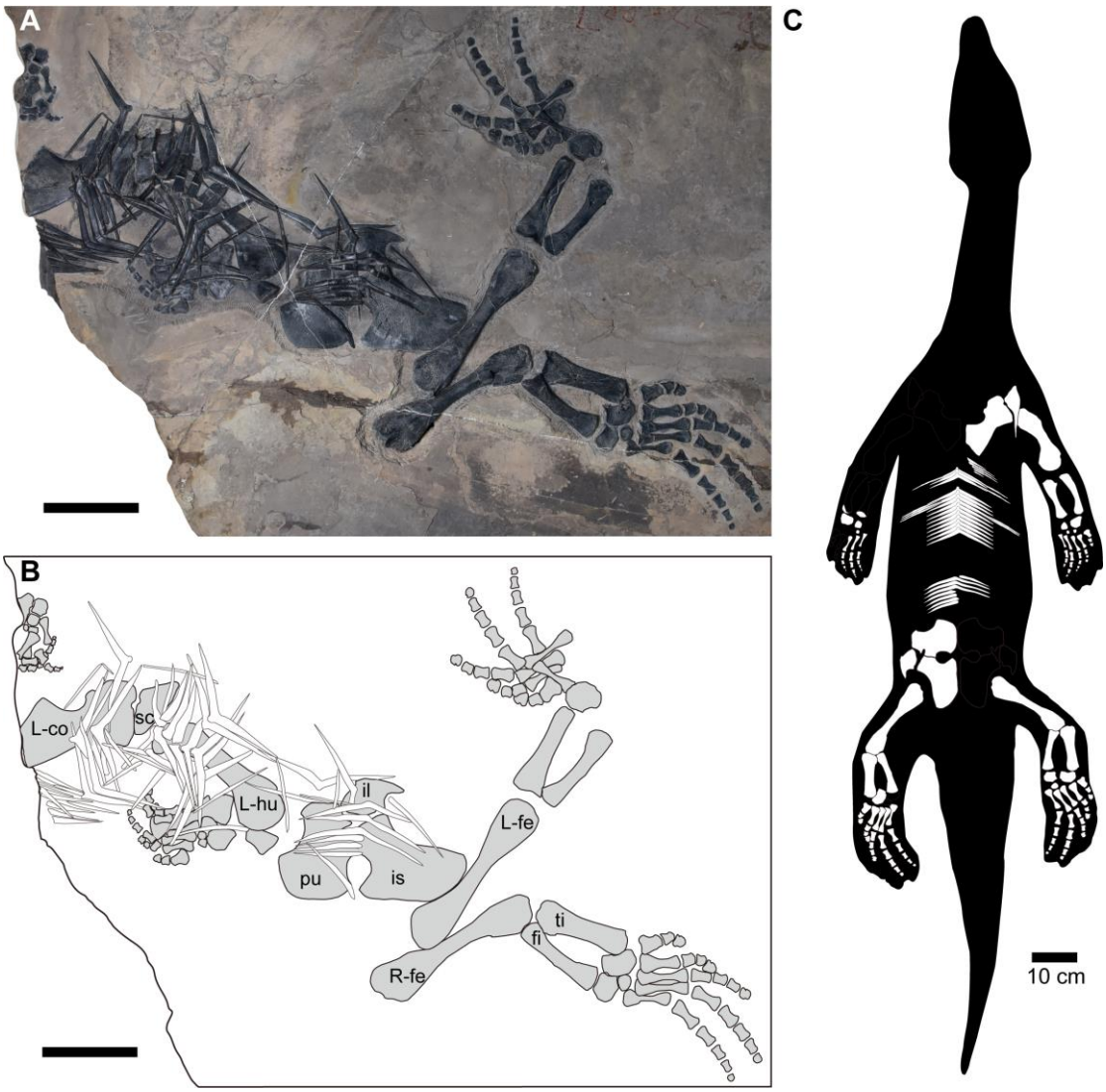

Figure 6.1. *Nothosaurus* sp. nov. (HFUT XAP-22-007). (A) Photo showing the original exposed side of the fossil. (B) Interpretative drawing. (C) Skeletal reconstruction in ventral view with known elements highlighted in white. Abbreviations: fi, fibula; il, ilium; L-co, left coracoid; L-fe, left femur; L-hu, left humerus; ti, tibia; R-fe, right femur; sc, scapula. Scale bars equal 10 cm.

6.5.1 Axial skeleton

Gastralia

At least 17 sets of gastral ribs are preserved. Each gastral rib is composed of five elements: a central medioventral element and two lateral elements on each side (see articulated elements

overlying the pelvic girdle). In the anterior gastral ribs, the medial elements have an angular shape with short processes that are absent in the posterior ones.

6.5.2 Appendicular skeleton

Pectoral girdle

The left scapula and coracoid of the pectoral girdle are exposed in ventral view (Fig. 6.2A, B). The scapula has been prepared from both sides (Fig. 6.2B) for better observation. These elements show characteristic synapomorphies of Nothosauridae as described by Peyer (1939) and confirmed by Rieppel (2000).

The ventrally expanded glenoid and the slender dorsal process of the scapula are obvious features of Nothosauridae. The dorsal process is long and tapers to a blunt point (Fig. 6.2B), reaching 3/5 of its length. A distinct notch on the post-medial margin of the glenoid part interlocks with a corresponding recess on the coracoid to house the coracoid foramen. The coracoid shows lateral and medial expansion and is distinctly waisted in the center. The coracoid foramen appears as an open notch on the lateral aspect of the glenoid. In the anterior margin (Fig. 5.2A), a small protruding structure can be seen, which is probably the result of compression during the fossilization process. The symphyseal region of the right coracoid is partially damaged due to previous destruction of the specimen.

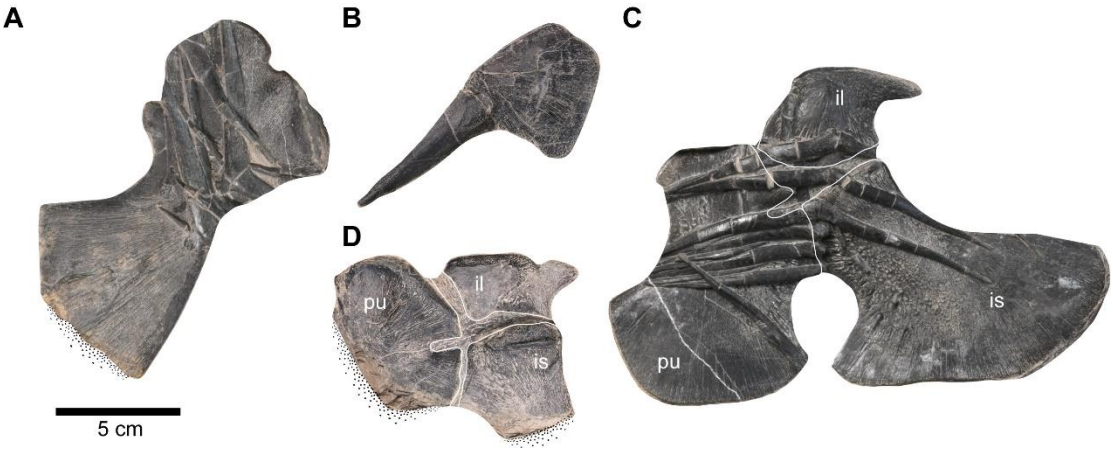

Figure 6.2. Pectoral and pelvic girdle of *Nothosaurus* sp. nov. (HFUT XAP-22-007) after preparation from both sides. (A) Left coracoid in mediodorsal view. (B) Left scapula in lateral view. (C) The right half of the pelvic girdle in mediodorsal view. (D) The articular portion of the right half of the pelvic girdle in a lateroventral view. Abbreviations: il, ilium; is, ischium; pu, pubis. Scale bar equals 5 cm.

Table 6.1. Measurements (in mm) of the appendicular skeleton of *Nothosaurus* sp. nov. (HFUT XAP-22-007).

Bone	Length	Proximal width	Mid-shaft width	Distal width
Left humerus	165.2	34.9	23.9	50.4
Left radius	95.8	21.2	12.5	23.3
Left ulna	95.1	33.0	12.3	25.1
Left femur	183.0	45.4	16.0	41.4
Right femur	183.2	45.9	16.0	/
Left fibula	98.8	24.2	14.5	26.2
Right fibula	96.8	23.3	15.5	27.9
Left tibia	96.2	34.2	18.9	20.6
Right tibia	98.9	/	21.84	27.91

Pelvic girdle

The right half of the pelvic girdle is well preserved and exposed in the dorsal (medial) view (Fig. 6.2C). In addition, the well-articulated girdle shows the connection of the pubis, ischium, and ilium after partial preparation from the ventral (lateral) view (Fig. 6.2D).

The plate-shaped pubis is exposed in the dorsal (medial) view and is overlain by several gastric ribs. The obturator foramen is invisible from the dorsal view but appears slit-like and open from the ventral view. The pubic bone is biconcave and convex in the middle. In contrast to the morphology seen in *N. jagisteus* (Rieppel 2001), the prepubic structure in the medial margin of the pubis is absent in HFUT XAP-22-007.

The right ilium was exposed in the medial view and has also been prepared from the opposite side. The iliac blade is reduced but projects slightly beyond the posterior margin of the acetabular portion of the ilium, which is a deviation from typical nothosaur morphology.

In ventral view, the acetabular articular surfaces of the ischium are visible. Both the anterior and posterior margins show strong concavity. The ischial shaft is slender and constricts just posterior to the acetabular facets. The posterior process of the ischium is asymmetrical with a markedly enlarged medial portion. The thyroid fenestra, represented by the posterior margin of the pubis and the anterior margin of the ischium, is relatively small in HFUT XAP-22-007.

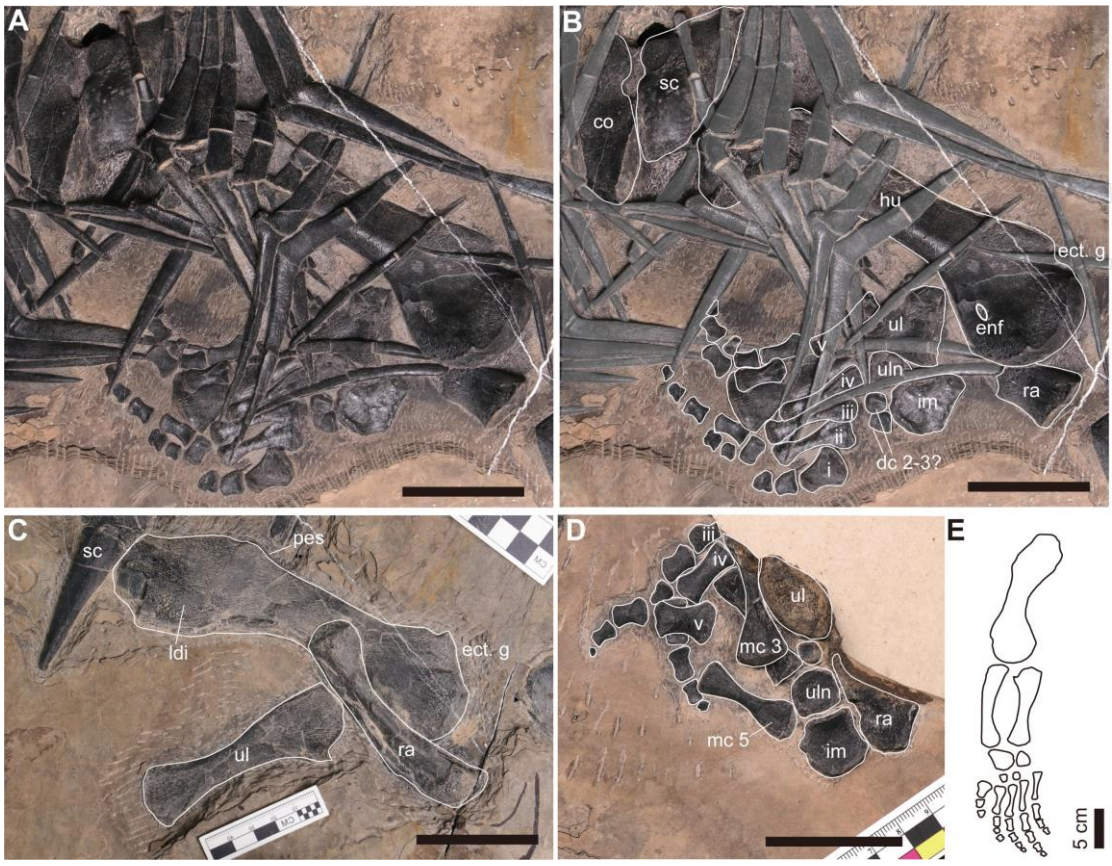

Figure 6.3. Forelimbs of *Nothosaurus* sp. nov. (HFUT XAP-22-007). (A), (B) Photographs of the left forelimb from the top of the slab, with the humerus in ventral view. (C) Photograph of the left humerus, ulna, and radius from the underside of the slab, with the humerus in dorsal view. (D) Part of the left autopodium. (E) Reconstruction of the left forelimb. Abbreviations: co, coracoid; dc, distal carpal; enf, entepicondylar foramen; ect. g, ectepicondylar groove; hu, humerus; im, intermedium; i-v, metacarpals i-v; ldi, latissimus dorsi insertion; pes, preaxial edge of shaft; ra, radius; sc, scapula; ul, ulna; uln, ulnare. Scale bars equal 5 cm.

Forelimbs

The forelimb (Fig. 6.3) is shorter than the hindlimb. The left forelimb is complete (Fig. 6.3A-C), while the right forelimb retains only three phalanges, three metapodials, and a few carpals (Fig. 6.3D). The proximal head of the left humerus is loosely articulated with the pectoral girdle and obscured by dislocated gastral ribs. The humerus has a robust appearance, with the distal end resembling Type III of *Nothosaurus* sp. as described by Bickelmann and Sander (2008). The dorsal side of the humerus shows a distinctive sauropterygian morphotype characterized by a convex preaxial margin and a concave postaxial margin (Romer 1956, Storrs 1991). The preaxial margin of the proximal shaft forms a straight angle, indicating a pronounced deltopectoral crest (covered mainly by gastral ribs, but can be inferred from the ventral side). On the dorsal side, the insertion of the latissimus dorsi muscle is prominent, although no distinct

crest is present. Near this insertion, a pitted surface area suggests a broad muscle insertion area. The length ratio of the pre-angulation region to the entire humerus is 32%. The pre-shaft region between the proximal end and the midshaft is massive, being twice as wide as the midshaft, distinguishing HFUT XAP-22-007 from other nothosaurs. The sharp edge of the preaxial margin results in a triangular cross-section of the humeral shaft. An oval entepicondylar foramen is located on the distodorsal portion of the humerus, measuring 10 mm by 5 mm (Fig. 6.3B). The ectepicondylar groove is open without a distal notch.

The ulna and radius are disarticulated and fully prepared on the ventral side of the slab. The proximal and distal regions of the right ulna are also exposed on the top of the rock matrix (Fig. 6.3B, C). The proximal facet for the humerus of the left ulna is relatively flat, while the distal articular facet for the carpals is convex. The ulna narrows along the shaft, with the proximal end being more expanded than the distal end. Although the preaxial and postaxial margins of the radius have similar degrees of concavity, the former has a sigmoidal curvature. In general, the width of the ulnar midshaft is 12.3 mm, approximately the same as that of the radius, which is 12.5 mm. The lengths of the ulna and radius are almost equal.

The right radius is dorsoventrally compressed in the preaxial portion when viewed from the ventral side of the slab. The proximal and distal articular facets of the radius are similar to those of the ulna, which is characterized by a flattened proximal head and a convex distal end. The lateral (preaxial) margin of the radius is slightly convex, while the medial (postaxial) margin is distinctly concave. The distal end of the radius is less expanded than that of the ulna.

Four carpals are ossified in the left forelimb, exceeding the traditional three carpals in *Nothosaurus* (Rieppel 2000). The intermedium is considerably larger than the ulnare and distal carpals 2 and 3, or alternatively, the displaced distal carpals 3 and 4. The ulnare is partially obscured by distal carpal 4. All metacarpals (except for metacarpal I) are elongated bones with narrow shafts and expanded ends. Metacarpal III is the most elongated of the series. Metacarpal V, which lacks a shaft, is significantly shorter than the other metacarpals and has a broad base. In the left manus, the intermedium has a rectangular shape, and the ulnare is round. The dimensions of the preserved distal carpals of the left manus are similar to those of the right manus.

The phalanges of the left forelimb are scattered, yet still accessible for study. The last two phalanges are reduced in length compared to the proximal phalanges of digits II through IV. In particular, the ungual phalanges of digits I and II show marked expansion. It is unclear whether the ungual phalanges of digits III through IV are unossified or simply not preserved in the left forelimb. Scattered gastral ribs partially obscure the terminal phalanx of digit IV, suggesting that the total number of phalanges in digit IV may exceed four. Three metacarpals are preserved

in the right manus and are probably correlated with digits III to V, analogous to the arrangement in the right forelimb. The phalanges of the right manus are assigned to digits II, III, and IV separately based on the morphology and length of each element (Fig. 6.3D). Digits IV and IV show additional ungual phalanges that are either not preserved or not ossified in the right manus. The phalangeal formula of the manus is 2-3-4-5-4.

Hindlimbs

Both hindlimbs are long and well articulated (Fig. 6.4). The femora are slender and relatively straight, with a slight sigmoidal curvature of the shaft. The expansion of the proximal head of the femur is pronounced but less distinct at the distal end. The intertrochanter is reduced, and there is no developed intertrochanteric fossa. Although the distal femoral condyles are reduced in size, the articular facets that interface with the tibia and fibula are still evident.

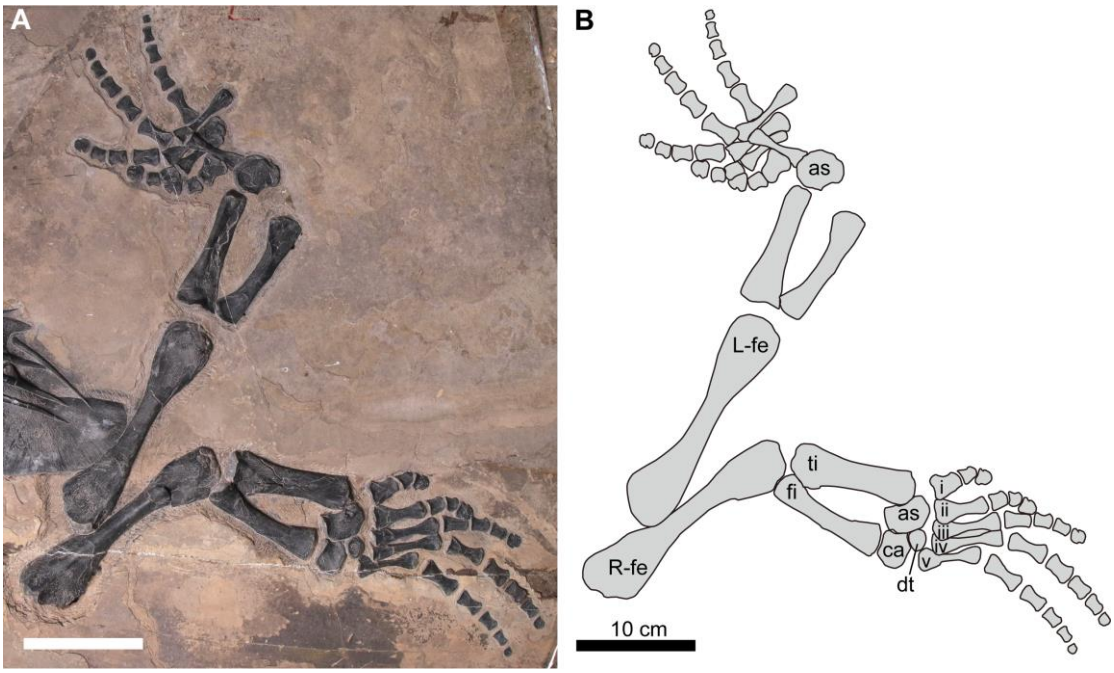

Figure 6.4. (A) Photograph and (B) interpretive drawing of the hind limbs of *Nothosaurus* sp. nov. (HFUT XAP-22-007). Abbreviations: as, astragalus; ca, calcaneum; dt, distal tarsal; L-fe, left femur; fi, fibula; i-v, metatarsals i-v; R-fe, right femur; ti, tibia. Scale bars equal 10 cm.

The tibia and fibula are approximately equal in length, each being approximately half the length of the femur, as shown in Table 6.1. The tibia is characterized by its straight and flat structure, with a slight constriction in the shaft. Notably, the proximal head of the tibia is wider than its distal part. In contrast, the fibula, which is concave along the preaxial margin and straight along the postaxial margin, is narrower than the tibia. The midshaft width of the fibula is about two-thirds that of the midshaft of the tibia.

The autopodium of the right leg is well articulated and consists of three tarsals, i.e., the astragalus, calcaneus, and distal tarsal 4. The astragalus is irregularly pentagonal in shape and has an anterior concavity. The calcaneus, which is approximately round in shape, articulates medially with both the astragalus and the distal tarsal. The articular surfaces for the distal fibula are prominently developed in the two proximal tarsals. Distal tarsal 4 is uniformly round and does not articulate distally with the metatarsals. In the left autopodium, only the astragalus is preserved between the tibia and the metatarsals.

All metatarsals are long and constricted in the middle, except metatarsal I (length 2.2 mm), which is stout and proximally expanded. Metatarsal IV (5.4 mm) is the longest of the metatarsals, followed by metatarsal III (5.2 mm). Metatarsal V is slightly shorter than mt III and IV, but is also long and slender.

The first toe is short, both in number and length of phalanges. The unguals in toes I and II are markedly robust and expanded, with a continuous decrease of this feature from digits III to IV, and are well developed and less expanded in digit V. The phalangeal formula of the pes is 2-3-4-5-5, indicating a hyperphalangy.

6.6 Phylogenetic analysis

To access the phylogenetic position of the new material within the Nothosauridae, we applied an analysis based on the data matrix of Hu et al. (2023), incorporating one new character. Araeoscelidia, Younginiformes, and Archosauromorpha were excluded from the contiguous outgroups because this study focuses primarily on Nothosauroidae. *Anarosaurus*, *Dactylosaurus*, *Serpianosaurus*, *Neusticosaurus*, *Dianopachysaurus*, and *Keichousaurus* are recognized as members of Pachypleurosauria. *Nothosaurus tchernovi* (Haas 1980), *N. edingerae* (Rieppel and Wild 1994), *N. haasi* (Rieppel et al. 1997), *N. winkelhorsti* (Klein and Albers 2009), *N. zhangi* (Liu et al. 2014), and *N. cristates* (Hinz et al. 2019) were not included in the analysis due to a lack of comparable skeletal remains for these species. To expand the dataset, operational taxonomic units (OTUs) were added to the previous data matrix, including HFUT XAP-22-007 and two recently described Nothosauridae species (*Brevicaudosaurus* and *N. luopingensis*). We coded characters based on the most recent published data matrices (Shang et al. 2020, Shang et al. 2022). The final data matrix contains 35 taxa and 204 characters. Our phylogenetic analysis was performed in PAUP 4.0a 169 using the same settings as Li and Liu (2020).

6.7 Body length estimation

The Triassic Nothosauroidea show a close correlation between humerus length (i.e., humerus length) and overall body length (Fig. 6.5). The congruence between humerus length and body lengths has also been corroborated in several studies (Cheng et al. 2009, Scheyer et al. 2014, Motani et al. 2015). The estimated total length of the adult individual HFUT XAP-22-007 is around 2.5 meters (Fig. 6.5). By contrast, the estimated body length of *N. zhangi*, as proposed by Liu et al. (2014), exceeds 5 meters, suggesting a substantial size disparity. Given the limited intraspecific size variation among adult individuals of one species and the adult status of HFUT XAP-22-007, it is not possible that the HFUT XAP-22-007 this specimen is unlikely to represent the same species. Meanwhile, when applying the same humerus-to-body length regression used in this study, the estimated body size of *N. luopingensis* approximates 1.5 meters.

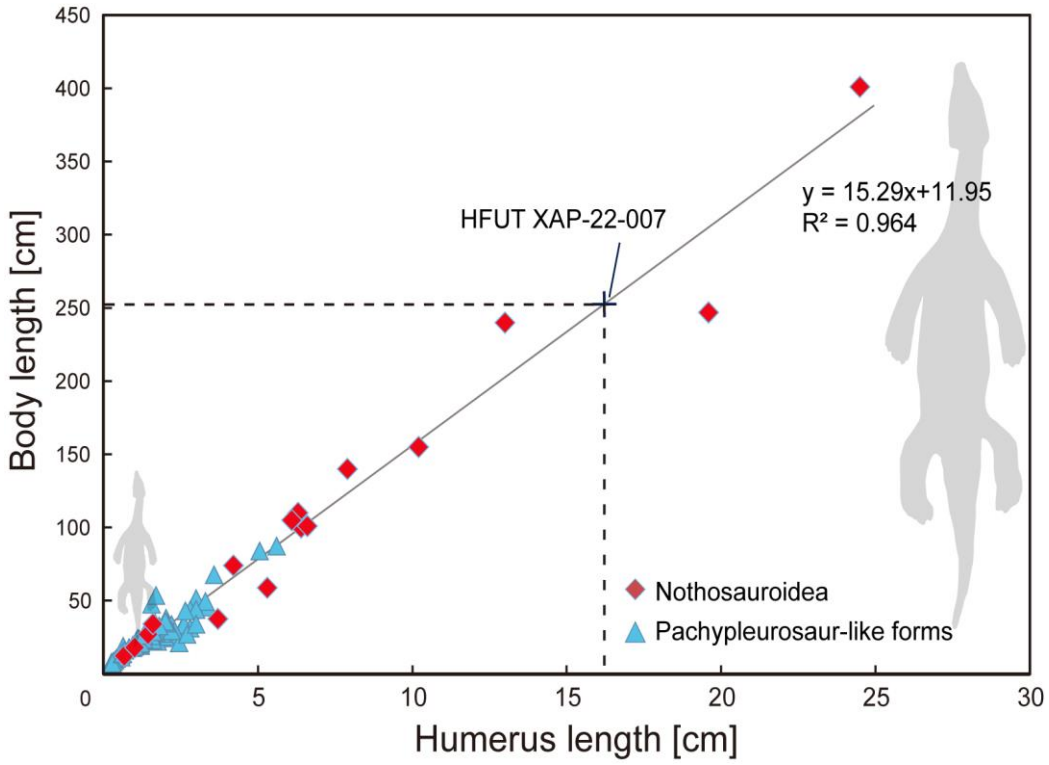

Figure 6.5. Humerus length-Body length relation in Triassic Nothosauridae and Pachypleurosaur-like forms. Body length of HFUT-XAP-22-007 is around 252 cm.

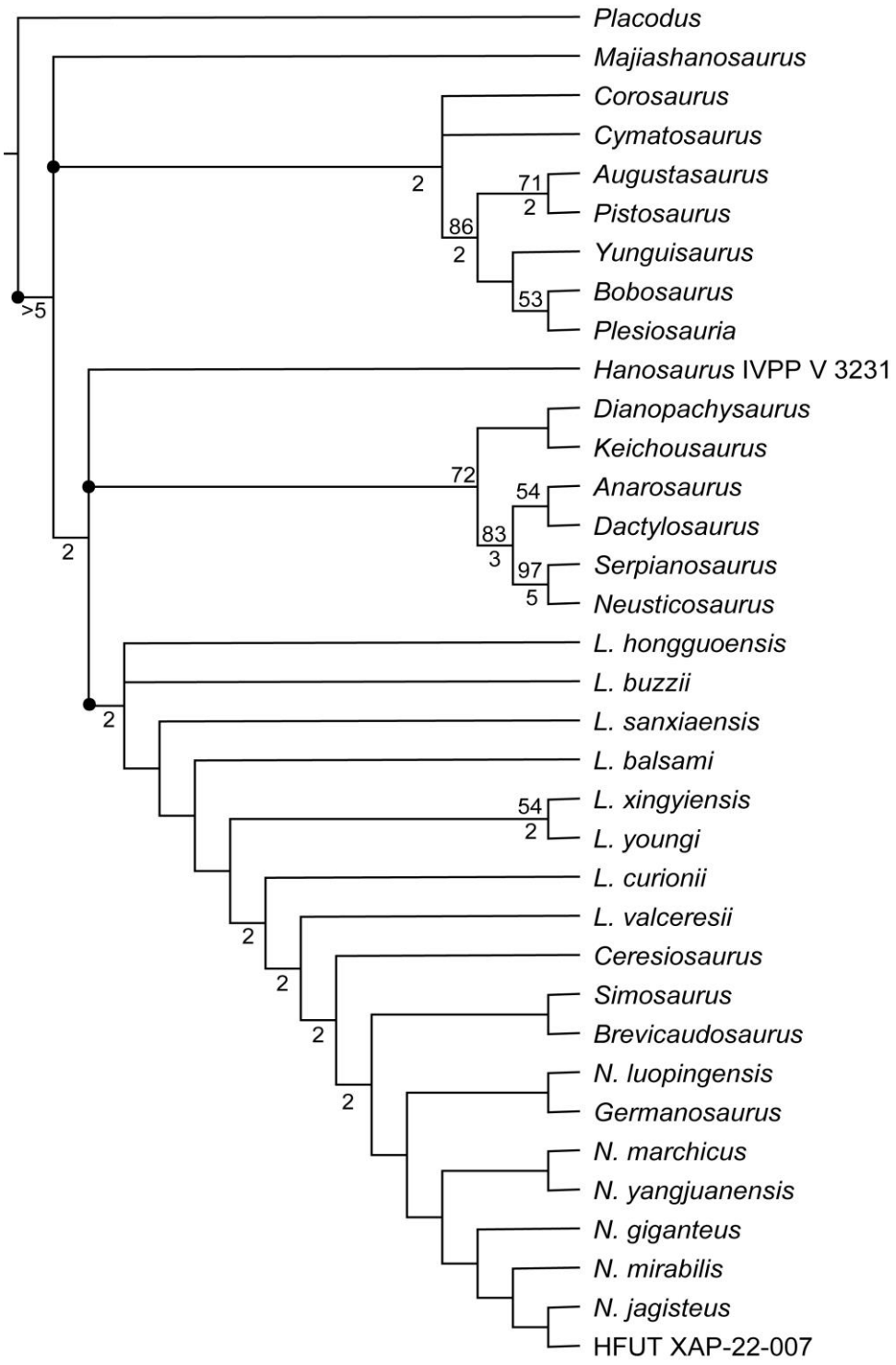

Figure 6.6. Strict consensus tree of four most parsimonious trees (MPTs) illustrating the phylogenetic position of *Nothosaurus* sp. nov. (HFUT XAP-22-007) with a tree length (TL) =631, consistency index (CI) = 0.342, and retention index (RI) = 0.584, indicating the relationships with other Triassic stem sauropterygians. Values above branches are bootstrap values over 50% (1000 replicates), and the values below the branches represent Bremer support values greater than 1. Abbreviations: *N*., *Nothosaurus*; L., *Lariosaurus*.

The heuristic search (1000 replicates) leads to a consensus tree, resulting in 4 MPTs with a tree length of 631 steps, the strict consensus of which is seen (in Figure 6.6). HFUT XAP-22-007 is recovered in a clade with *N. jagisteus*, forming the sister group of *N. mirabilis*. *N. giganteus* shares the most recent ancestor with the three species mentioned above. *N. luopingensis* is placed in a more basal position within the Notosauroidea than *N. yangjuanensis*. Our result provides insight into the presence of certain plesiomorphic characters specific to *N. luopingensis* but absent in *N. yangjuanensis*, as previously suggested by Shang et al. (2022).

Our analysis also supports the monophyly of Nothosauridae, with its relationships resolved. However, both Bootstrap and Bremer support values remain low in this analysis. A paraphyletic *Lariosaurus* lies in the basal Nothosauridae, and the monophyletic *Nothosaurus* sits at the apex. The monophyletic clade containing *Germanosaurus*, *N. luopingensis*, *N. marchicus*, *N. yangjuanensis*, *N. giganteus*, *N. mirabilis*, *N. jagisteus*, and HFUT XAP-22-007 is supported by six unambiguous synapomorphies: character 5, the ratio of the distance from the posterior margin of the external naris to the anterior margin divided by the width of the postorbital arch is less than 1.5 [state 1]; character 45, the longitudinal diameter of the upper temporal divided by that of the orbit is 2.0 or more [state 1]; character 78, the anterior fusion of the mandibular symphysis is present [state 1]; character 145, the insertion crest for the latissimus dorsi muscle is prominent [state 0]; character 159, the spina praeacetabuli is weakly developed [state 1]; character 195, a wedge-shaped (widest at the posterior orbit/skull table) skul1 shape [state 2]. The Early Triassic *Majiashanosaurus* is now repositioned in the basalmost position within Eosauropterygia. *Hanosaurus*, Pachypleurosauria, and the Notosauroidea form a monophyletic clade in an unresolved trichotomy. Similarly, there is an unresolved trichotomy at the base of Eosauropterygia.

The monophyly of Nothosauroidae does not change in our analysis compared to other studies (e.g., Neenan et al. 2013, Klein et al. 2016, Jiang et al. 2019), and relationships within Nothosauridae are also similar to those recovered in other recent studies (e.g., Li and Liu 2020). However, our analysis challenges the traditional view by suggesting a more basal paraphyletic *Lariosaurus* and a crown-positioned monophyletic *Nothosaurus*, thereby collapsing the long-held monophyly of both *Lariosaurus* and *Nothosaurus*. Our results also differ from those of Lin et al. (2021), who suggested a paraphyletic *Nothosaurus* and a monophyletic *Lariosaurus*. The controversy over the relationships between the two genera is unsurprising, considering that some Chinese taxa show mixed morphologies, such as an increased number of carpals and tarsals in members of the genus *Nothosaurus* (Yin et al. 2014, Shang et al. 2020, Shang et al. 2022). Surprisingly, the monophyletic genus *Nothosaurus* recovered in this analysis is different from the previous one (see Chapter 5), of which the paraphyletic nothosaurs displayed (Hu et

al. 2023). This discrepancy between the two studies may be due to the addition of this new taxon of nothosaur but also reflects the inherent instability of the nothosauroidea tree.

6.8 Discussion

HFUT XAP-22-007 can be classified as a new species of *Nothosaurus,* as suggested by morphological observations and phylogenetic analysis. The new species is diagnosed on the basis of the following characteristics: posterodorsal process long and accounting for 3/5 of the total length in the scapula; iliac blade reduced but projecting slightly beyond the level of the posterior margin of the acetabular portion of the ilium; a robust humerus with a distinct straight preaxial crest, curved at the 1/3 point of the humerus; width of ulna mid-diaphysis equal to that of radius.

Although HFUT XAP-22-007 lacks cranial bones, the preserved skeleton still provides distinguishable information. Typically, the dorsal process of the scapula tapers to a blunt tip in *Nothosaurus*. In HFUT XAP-22-007, this process extends to 3/5 of the length of the scapula, similar to *N. mirabilis* and *N. giganteus* (Diedrich 2012), and is longer than in species with more reduced dorsal processes, such as *N. jagisteus* and *N. luopingensis*. In addition, the anterior margin of the coracoid forms an obtuse internal angle at its extension lines, which may help to distinguish this new material. In contrast, species such as *N. jagisteus*, *N. cf. mirabilis*, *N. giganteus*, *N. luopingensis*, and *N. youngi* (listed as *L. youngi* in Lin et al. 2017 and adopted in this study) exhibit angles equal to or smaller than a right angle. (Peyer 1939, Rieppel 2001, Rieppel et al. 2003, Ji et al. 2014, Shang et al. 2022). However, this angle variation should be interpreted with caution as an autapomorphic character, as it could be influenced by ontogenetic stages or fossil compression of the fossils.

Furthermore, HFUT XAP-22-007 was established in Xiaoapeng Village, Luxi County, which is close to Luoping County, known for its Anisian Luoping Biota. To date, two species of Nothosauridae, namely *N. zhangi* and *N. luopingensis*, have been reported from the Luoping Biota. Considering the geographical proximity of the two localities, the nothosaurs from Luxi may be closely related to those from the Luoping Biota. It is noteworthy that N. zhangi is known only from fragmentary remains as well, including the mandible, several vertebrae, and ribs, whereas HFUT XAP-22-007 does not possess any of these bone elements. Nevertheless, a thorough examination of limb morphology suggests that HFUT XAP-22-007 represents an adult rather than a juvenile individual, i.e., the indentation on the most proximal tip of the deltopectoral crest, a well-developed ectepicondylar groove, and well-ossified carpals and tarsals.

In addition to the large size difference, HFUT XAP-22-007 also exhibits distinct morphological differences from *N. luopingensis,* particularly in limb structure, pectoral and pelvic girdles, and phalangeal formula of the manus. The humerus of HFUT XAP-22-007 is massive in appearance. Another significant feature that distinguishes it from *N. luopingensis* is the expanded region between the proximal end and the preaxial angle. Further differentiation can be seen in the morphology of the ulna: *N. luopingensis* has a convex preaxial margin at the ulnar mid-shaft, whereas HFUT XAP-22-007 has a concave ulnar preaxial margin. The iliac blade of HFUT XAP-22-007 extends slightly beyond the posterior margin of the acetabular portion of the ilium. In contrast, the iliac blade in *N. luopingensis* is more reduced and does not extend beyond the acetabular portion. Additionally, the ischium in the HFUT material is asymmetrical and has a widely extended posteromedial process, in contrast to the more symmetrical ischium of *N. luopingensis*. The manus phalangeal formulae of HFUT XAP-22-007 and *N. luopingensis* are 2-3-4-5-4 and 2-3-4-5-3, respectively, indicating a variation in the number of phalanges of the fifth digit.

Given that the autapomorphic features observed in the humerus of HFUT XAP-22-007 are within the genus *Nothosaurus*, such as a bulky proximal portion and a severely constricted midshaft (Fig. 6.3), a cladogram of Nothosauridae with simplified humeri sketches and silhouettes showing body sizes was generated (Fig. 6.7) for further comparison. The cladogram (Fig. 6.7) was derived from the strict consensus tree of the phylogenetic analysis (Fig. 6.6). The characteristic humeral features of nothosaurs recognized by Romer (1976), including curved humeri with a straight preaxial angle and postaxial concavity, are observed in HFUT XAP-22-007. It is evident that the humerus of the *Lariosaurus* clade (*L. honguoensis*-*Ceresiosaurus calcagnii*) tends to be less curved and lacks a straight preaxial angle (Fig. 6.7). An exception within this clade is *L. valceresii* (Tintori and Renesto 1990), which has a humeral morphology similar to that of *Nothosaurus*, but with reduced curvature and a less pronounced straight preaxial angle. Another taxon that presents an intermediate morphology between the nothosaurian and lariosaurian humeri is *C. calcagnii* (Peyer 1931), which is characterized by a relatively straight humerus. The morphological diversity of humeri in *Nothosaurus* and *Lariosaurus* could be due to taxonomic differences or even sexual dimorphism (Bickelmann and Sander 2008), although additional evidence is needed for further validation.

In the sister group of the Nothosauridae, the Pachypleurosauria, previous studies (e.g., Sander 1989, Lin 1994, Klein 2012, Liu et al. 2023) have shown that humeral morphology varies between species, ranging from straight to curved, and between sexes (curved with or without a straight preaxial angle). However, due to limited sample sizes, the relationship between humeral preaxial angulation and sex has only been conclusively established in a few

species, such as the three species of *Neusticosaurus* (Sander 1989), *Serpianosaurus* (Rieppel 1989), and *Keichousaurus* (Cheng et al. 2004). The hypothesis that all *Lariosaurus* lacking preaxial angulation represent females remains inconclusive. Therefore, the diversity in humerus preaxial angulation within *Nothosaurus* and *Lariosaurus* may be more plausibly explained by taxonomic differences between these genera (Bickelmann and Sander 2008).

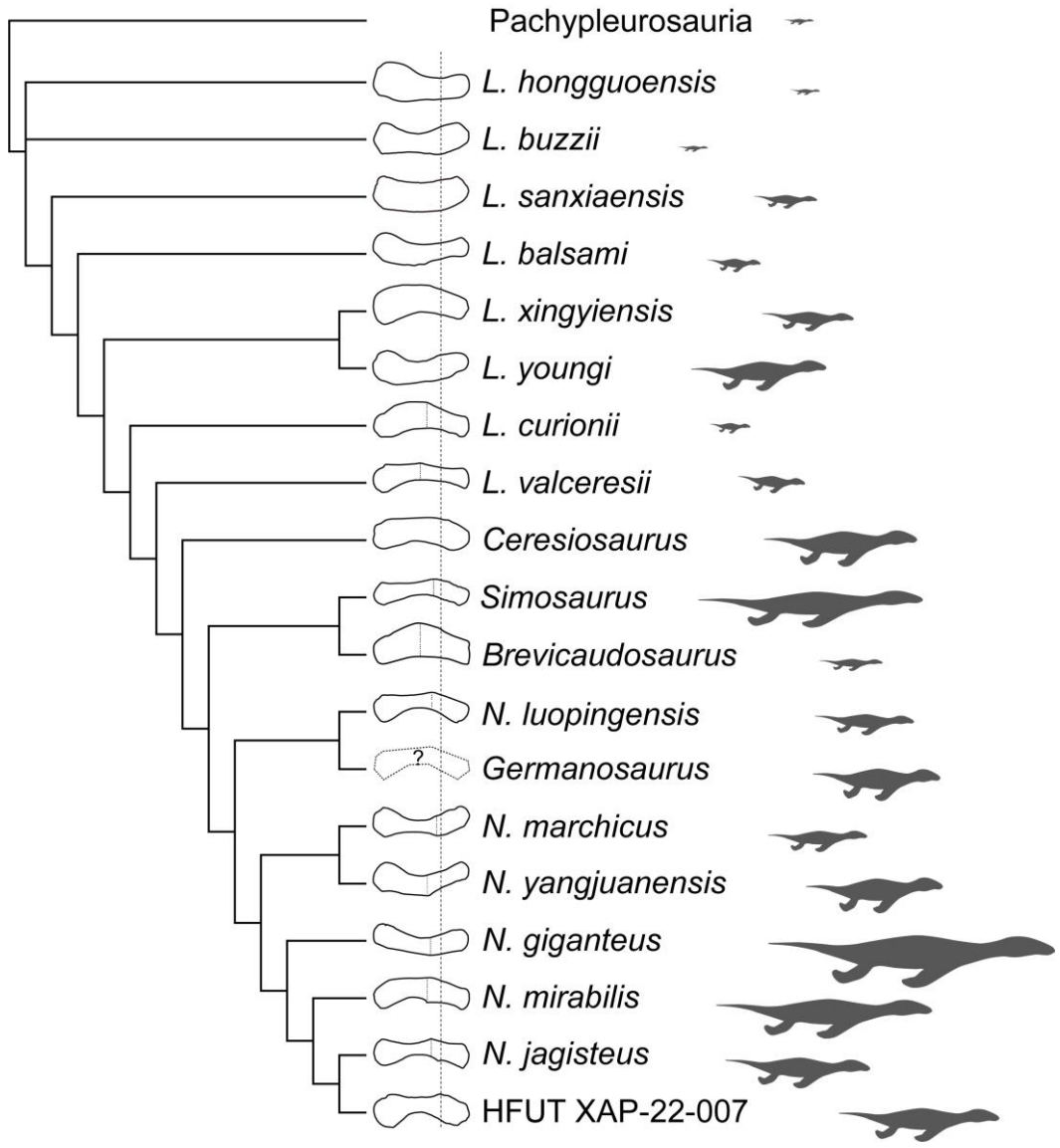

Figure 6.7. Phylogenetic relationships of Nothosauridae with humeri (with proximal end to the right) and relative body size comparison. The dotted lines show the positions of the "preaxial angle" of the humerus. The extended dotted line of HFUT XAP-22-007 indicates that the region between the proximal tip and the preaxial angle is shorter in HFUT XAP-22-007 than in other nothosaurs. Body size is based on the largest individuals of each species. Humerus of *Germanosaurus* is drawn in a dotted line since it is unknown.

The dorsoventrally broadened humerus and ulna suggest the use of the forelimb during swimming in most nothosaurids, suggesting a combination of paraxial propulsion and anguilliform swimming styles (Storrs 1993, Klein et al. 2015). However, the new material

presents a relatively slender ulna and radius, a morphological trait it shares only with *N. jagisteus*, which similarly lacks broadening in the ulna. This characteristic may correlate with their adaptation to shallow marine environments, specifically the lagoonal and intertidal environments of the Anisian of Yunnan (especially as compared to the deeper-water environment of the coeval Panxian Fauna of Guizhou. Comparable zeugopodial features have been identified in *N. luopingensis* and some eosauropterygians from the Luoping area (Liu et al. 2011, Shang et al. 2011, Shang et al. 2017).

The markedly expanded ungual phalanges and long pedal digit V in *N. luopingensis* were recognized as autapomorphies within the *Nothosaurus* (Shang et al. 2022). HFUT XAP-22-007 also displays a long pedal digit V and expanded ungual phalanges in digits I and II of both the manus and pes. Interestingly, HFUT XAP-22-007, *N. luopingensis*, and *N. yangjuanensis* all present phalangeal formula of 2-3-4-5-5 in their pes. Note that the pedal phalangeal formula of *N. yangjuanensis* was described as 2-3-4-5-6 by Yin et al. (2014) but later revised to 2-3-4-5-5 based on (personal observation of the holotype by Q. L.). Additionally, the expansion of the ungual phalanx of *N. yangjuanensi*s pes is less pronounced than in the new species. As mentioned by Shang et al. (2022), these hindlimb characteristics are also observed in various small to medium-sized Eosauropterygians from Luoping (Liu et al. 2011, Shang et al. 2011, Shang and Li 2015) and seem to be an adaptation to a shallow marine environment. Specifically, one would assume an environment in which limbs were used for propulsion that involved not only swimming but also pushing off the shallow bottom. Such an environment has indeed been documented from the Luoping area and uniquely preserves the spectacular and diverse foraging tracks described from Daaozi village in Luoping County (Zhang et al. 2014).

The robust humerus and extended hand unguals in Digit I and II of the new *Nothosaurus* species would have been the first part of the manus to touch the sea floor. This cycle of motion is indeed documented in the tracks, with the medial part of the manus touching the seabed first and deepest (Zhang et al. 2014), implementing the push-off motion recorded in the tracks. The elongated hand and pedal digits III to V would then have served a hydrodynamic function.

The similarities in pes characteristics between HFUT XAP-22-007 and the smaller Eosauropterygians from the Luoping-Luxi area may indicate convergent adaptation to this specific habitat. This is supported by the observation that the foraging tracks occur in two size classes (Zhang et al. 2014), attributed to the larger *Nothosaurus yangjuanensis* and the smaller *Lariosaurus hongguoensis*, both from the coeval Panxian fauna. However, based on new discoveries since the study by Zhang et al. (2014), the smaller tracks could have been made by *Diandongosaurus acutidentatus* (Liu et al. 2021) or *Nothosaurus luopingensis* (Shang et al. 2022), and the larger ones by the new species described here. Although in both nothosaur cases,

the preserved holotypes are larger than the reconstructed trackmaker (estimated forelimb of three species spread 40, 52, and 150 cm, respectively), the trackmakers could have been juveniles, as already suggested by Zhang et al. (2014).

Xin et al. (2020) reported twelve rows of *Dikoposichnus luopingensis* trackways in Member I of the Guanling Formation, located in Qinyuan, Guizhou Province. These trackways bear resemblance to those previously described by Zhang et al. (2014), exhibiting characteristics consistent with the nothosaur foraging traces. The widths of these twelve trackways range from 28.7 cm to 79.1 cm, suggesting the organisms are considerably smaller than HFUT XAP-22-007. Additionally, these trackways were found together with autopodial imprints, potentially attributable to placodonts or saurosphargids. This evidence, as outlined by Xin et al. (2020), suggests a paleoenvironment such as shallow coastal lagoons, where robust forelimbs would provide a substantial ecological advantage.

The foraging tracks from Da'aozi are too small to have been made by the animal described in this paper. Nonetheless, testing this intriguing hypothesis is challenging due to the absence of comparable extant examples and limited postcranial data from other nothosaur species, especially those originating from Europe.

The silhouettes representing body size variations among different nothosaur species (Fig. 6.7) suggest a potential trend of body size increase in some crown branches within the family (Fig. 6.7). Nevertheless, it could be unreal. A more rigorous verification of body size changes within the Nothosauroidea, or even in the Eosauropterygia clade, requires a more extensive fossil material and an evaluation of the stratigraphic origins of all Nothosauroidea.

6.9 Conclusion

HFUT XAP-22-007 represents a newly identified nothosaur species discovered in the Anisian strata of Luxi, Southwest China. The species shares postcranial autapomorphies with the genus *Nothosaurus* (Rieppel 2000). In particular, it emerges as the second large nothosaur from the Luoping-Luxi area, characterized by a number of derived features, including an elongated dorsal process of the scapula, a robust humerus, and hindlimbs with an extended ungual phalanx. The discovery of HFUT XAP-22-007 supports a monophyletic *Nothosaurus* and a paraphyletic *Lariosaurus*. The phylogenetic analysis resolved relationships within *Nothosaurus*, albeit with low support. However, it is important to highlight that more basal genera, such as *Simosaurus* and *Brevicaudosaurus,* occupy intermediate positions between the *Lariosaurus* and *Nothosaurus* clades in our cladogram. Future discoveries of more complete and articulated specimens are expected to significantly enrich our understanding of the nothosaurids in the

Luoping-Luxi region. These findings will shed light on the evolutionary relationships within this fascinating group and contribute to a deeper understanding of their phylogeny. Such findings will also contribute to a better understanding of the remarkable nothosaur foraging tracks from the Luoping, for which we offer a revised interpretation to the producers. Understanding the foraging tracks is important for the functional interpretation of unusual features in the limb anatomy of the Luoping Biota nothosaurs.

Chapter 7

Synthesis: How to improve our understanding of the revolution within Triassic eosauropterygians.

The previous chapters of this dissertation presented several research projects on eosauropterygians from the Southwest Chinese marine reptile fossil localities. This synthetic chapter aims to point out common themes in the different chapters of the dissertation and how it hopefully will be more than the sum of its parts. Common themes, not only in this work but in many similar research, are phylogeny, ontogeny, histology, adaptation, and paleoenvironment. An additional theme is bone fossilization (Chapter 2), rarely seen in connection with the other themes. In the special case of the marine reptile fossils from the Triassic of Southwest China, this theme turned out to play an important role, however, forming the point of departure for the remaining chapters. Description of new species and analysis of their phylogenetic relationship (chapters 5 and 6) require a sound understanding of the ontogenetic stage and sexes of the materials. These are most reliable obtained from bone histological analysis (Chapters 3 and 4), which was only possible through a comprehensive understanding of the diagenetic and metamorphic alteration of the bone tissue (Chapter 2). Thus, the circle of research questions and relevant methodologies is complete.

7.1 Fossil preservation and implications for histological sampling

It is no coincidence that there are virtually no osteohistological studies on Southwest Chinese Triassic marine reptiles despite the enormous body of morphological, anatomical, and phylogenetic work on these fossils. Preservation is generally poor, with a few exceptions (for a few samples of Chinese Triassic marine reptiles in a different context, see Wintrich et al. 2020). However, the histology of poorly preserved samples still can be understood if the observer is able to distinguish between the primary histological signal and the changes brought about by fossilization and post-fossilization geological history.

The paleoenvironment and fossils in Southwest China cover a variety of sedimentary facies and biological species from coastal regions to pelagic habitats, respectively (Wang et al. 2008, Jiang et al. 2009, Luo et al. 2013, Lu et al. 2018). Vertebrate fossils from these faunas and biotas are preserved in different conditions, but most of them are embedded in organic black shales, especially those from Xingyi Fauna and Guanling Biota (Wang et al. 2008, Ma et al. 2013, Zou et al. 2015). In addition, the preservational quality of vertebrate fossils from

different localities also varies. The boundary between the bones and matrix of some pachypleurosaurs from Fuyuan and thalattosaurs from Guanling is difficult to see during preparation (personal observation by Q.L.). Bone alteration after fossilization in some samples also caused difficulties in paleohistological study.

Fossil bones from deep time, especially from the pre-Pleistocene, are predominantly preserved as FAp, but retain the original bone crystallite orientation. Ó Gogáin et al. (2022) identified idiomorphic apatite within bone porosity as a result of low-grade metamorphism of a coal swamp deposit in Jarrow, Ireland. However, their results did not conclusively demonstrate that this apatite was derived from direct recrystallization of the bone FAp at its original site. Interestingly, specimen IGPB R-670 shows a rare "third generation" apatite derived from FAp, which in turn is derived from BAp, in reptile fossils from the Triassic marine faunas of SW China. This recrystallized phase of fossilized bone apatite, termed "RAp", is a new fossil discovery. Its presence provides insight into the obscured boundaries observed between bones and surrounding sediments.

Fluorite in fossils is rarely reported. Witke et al. (2004) described fluoridated wood from the Permian petrified forest of Chemnitz, Germany. This occurrence was interpreted as evidence of a multi-step process in which hot (< 250 ºC) fluoride-containing fluids infiltrated the wood along cracks and decayed areas (Mustoe 2018, Rößler 2021). The remaining examples, such as fluoridized corals and nummulite fossils mentioned by Worley (1976) and Genç (2006), have also been found in hydrothermal ore deposits in England and Turkey. Thus, the fluorite in HFUT and IGPB materials may also have experienced hydrothermal conditions such as volcanic eruption burial or low to moderate metamorphism. The occurrence of fluorite in bones, as well as the carbonaceous materials covering the original bone structures, indicate a hydrothermal condition during the later diagenesis of the fossils in Xingyi and Guanling areas.

These extreme patterns of bone preservation in the Southwest Chinese samples (Chapter 2) thus not only crucially helped in understanding their primary histology (Chapters 3 and 4) but offered substantial new insights into the still enigmatic process of bone fossilization.

7.2 Bone histology and ontogeny of Pachypleurosauria

The potential of paleohistology, in combination with an adequate sample size and preparatory work (Chapter 3), once again became apparent in the case of *Keichousaurus*. Despite the often poor preservation, the detection of puberty was achieved, as detailed in Chapter 4. This represents a first in the study of fossil reptiles, including dinosaurs, marking a significant milestone in paleontological research. Histology records the growth of the entire individual but

also morphogenesis and, thus also the ontogeny of sexual dimorphism. Puberty is the life history stage when such shape change develops most distinctly (Chapter 4).

In European pachypleurosaurids and nothosaurids, the microanatomy of long bones has been reported in several previous studies (Sander 1989, 1990, Klein 2010, Hugi et al. 2011, Krahl et al. 2013, Klein et al. 2015a, Klein et al. 2015b). Sander (1989) suggested that the marks of skeletal growth (MSGs) in *Neusticosaurus pusillus* and *Neusticosaurus peyeri* were annual in nature, and it was then applied in subsequent studies to identify the annulus of other pachypleurosaurs (Hugi 2011, Klein and Griebeler 2018). The thin sections of *Neusticosaurus* and *Serpianosaurus* both show pachyostosis (Ricqlès 1976, Hugi et al. 2011), which indicates increased bone density (Buffrénil and Schoevaert 1988). *Neusticosaurus* and *Serpianosaurus* both show a lamellar-zonal bone tissue type throughout the cortex. However, the cortex of *Neusticosaurus* consists of alternating bands of lamellar bone and parallel fibrous bone matrices, whereas the cortex of *Serpianosaurus mirigiolensis* consists of alternating bands of pure lamellar bone (Hugi 2011). *Anarosaurus* of the other European pachypleurosaur clade shows histological features closer to pistosaurids due to the abundance of fibrolamellar bone throughout the cortex (Klein 2010). This feature is usually associated with increased growth rates and possibly increased metabolic rates in fast-growing marine reptiles such as *Cymatosaurus* and *Rhaeticosaurus* (Klein 2010, Wintrich et al. 2017). It is worth noting that *Anarosaurus* has been defined phylogenetically as a genus of pachypleurosaurs (e.g., Rieppel 2000, Holmes et al. 2008, Klein et al. 2022), while paleohistology provides an interesting hypothesis for the origin of *Anarosaurus* (Klein 2010). Although not supported by further phylogenetic analysis, the hypothesis suggests a possible approach to exploring phylogeny through microanatomical information. The differences in bone tissue among European pachypleurosaurs may indicate a diversity of habitats and locomotion (Klein 2010, Hugi et al. 2011). The lamellar-zonal bone tissue (i.e., alternation of lamellar bone annuli with vascular zones) of *Keichousaurus* is similar to that of the small *Neusticosaurus pusillus* and *Neusticosaurus peyeri*. *Keichousaurus* also shares small medullary cavities with other Triassic pachypleurosaurs, such as *Dactylosaurus* from the Early Anisian of Poland, aff. *Neusticosaurus pusillus* from the Early Ladinian of southern Germany, and *Neusticosaurus* spp. and *Serpianosaurus* from the Alpine Triassic of the Anisian/Ladinian.

Keichousaurus reached sexual maturity around its second or third year, based on observed annuli. This pattern is similar to that of *Dactylosaurus* and *Serpianosaurus*, which also reached maturity after the second or third year and lived for over ten years (Klein and Griebeler 2018). The growth pattern of *K. hui* is consistent with European pachypleurosaurs, with the exception of *N. edwardsii*. The growth of *N. edwardsii* shows a delay in sexual maturity, with a consistent

growth cycle thickness until 5-6 years of age (Hugi et al. 2011). This pattern is similar to that of marine iguanas (*Amblyrhynchus cristatus*), which feed exclusively in the sea, as noted by Trillmich and Trillmich (1986) and supported by Hugi and Sánchez-Villagra (2012).

In Pachypleurosauria, some individuals of sexually dimorphic species have a longer and more distinct humerus with an expanded distal end and a developed deltoid crest (termed "sex y" by Sander 1989, see also Rieppel 1989, and Lin and Rieppel 1998) compared to other individuals (termed "sex x"). Originally, "sex y" individuals were thought to be female, based on the idea that stronger forelimbs would be required for land-based oviposition (Sander 1989). However, Cheng et al. (2004) found a pregnant *K. hui* with "sex x" characteristics. This means that in *K. hui*, "sex y" are males and "sex x" are females. This distinction may also apply to other species. Interestingly, the clear sexual differences in *Keichousaurus* can be seen in the cross section of the male humerus.

The end of the first growth cycle is marked by a change in growth as described by Ricqlès (1983), indicating a decrease in bone fiber organization, visible under cross-polarized light. On the other hand, the end of the second and later growth cycles is marked by an annulus, which is a thin layer of avascular lamellar bone. The slight differences in bone fiber orientation between the modulation and the zones and annulus in the higher cycles are accentuated by diagenesis, which manifests as chromatic differentiation, with the less organized fibers staining as a dark band (Li et al. 2023).

7.3 New marine reptile taxa from Luxi and eosauropterygian systematics

A further understanding of the morphology of an organism is obtained by considering the development and function of any anatomical feature. Ideally, this understanding informs taxonomical research at the level of alpha diversity, i.e., the description of new species (Chapters 5 and 6). Thus, the juvenile status of the holotype and only specimen of one of the two new eosauropterygians from the new locality of Luxi, *Dianmeisaurus mutaensis* (Chapter 5), could be immediately recognized and enter into the consideration of how to diagnose the new taxon. The other new species, as yet unnamed, adds to the diversity of *Nothosaurus* from Southwest China and is at the other end of the ontogenetic spectrum, showing clear indications of its fully adult status. However, the phylogenetic analyses, including the two new taxa (Chapters 5 and 6), led to contradictory results, suggesting that an incomplete understanding of ontogeny and sexual dimorphism is at play, as well as specific environmental adaptations (Chapter 6). The genera *Nothosaurus* and *Lariosaurus* are considered non-monophyletic

following the cladistic review by Liu et al. (2014) due to morphologies observed in several Chinese taxa (Rieppel et al. 2003, Ji et al. 2014). Following this analysis, *N. youngi* was placed within the *Lariosaurus* clade, along with the European *N. juvenilis* and *N. winkelhorsti*, as demonstrated in subsequent studies (Klein et al. 2016, Lin et al. 2017, Lin et al. 2021). However, the reclassification of these three "*Nothosaurus*" species as *Lariosaurus* in subsequent studies (Hinz et al. 2019, Lin et al. 2021, Shang et al. 2022) has left the monophyly of *Nothosaurus* and *Lariosaurus* in a state of controversy. A key study on Early Triassic *L. sanxiaensis* (Li and Liu 2020) proposed a monophyletic *Nothosaurus*, while *Lariosaurus* was considered paraphyletic. Specimen HFUT XAP-22-007, a new nothosaur from the Middle Triassic of southwestern China, confirms the monophyletic position of *Nothosaurus* proposed by Li and Liu (2020) and Shang et al. (2022).

However, the monophyletic genus *Nothosaurus* recovered in Chapter 6 is different from Chapter 5, although the latter mainly concentrates on pachypleurosaurids (Hu et al. 2023). The discrepancy between the two phylogenetic trees may be due to the addition of this new taxon of nothosaur but also reflects the inherent instability of the phylogeny. Such uncertainty may be addressed through further research involving new materials or alternative approaches such as paleohistology. One case is the pachypleurosaurids from eastern and western Tethys. As discussed in previous chapter (Chapter 3), the study highlights that *Keichousaurus* from southwest China has a long bone histology similar to certain European pachypleurosaurs, specifically *Neusticosaurus pusillus* and *Neusticosaurus peyeri*. However, it contrasts with the histology of *Anarosaurus* from earlier strata. The bone histology of different pachypleurosaur species did trigger further thinking of its correlation with the external morphology, as mentioned by Nicole et al. (2010).

On the other hand, although many genera and species have been reported from the aforementioned fossil localities, the phylogenetic relationships within Eosauropterygia remain unclear, especially regarding the European members. Paleohistological studies, previously applied to western Tethys eosauropterygians, represent a promising avenue to improve our understanding of the ontogeny, aquatic adaptation, and life history of Chinese eosauropterygians.

7.4 Implications for environmental adaptation based on new species and specimens

Function evolves as an adaptation to a specific environment, but such adaptations are often hypothetical and difficult to test. Searching for correlations between habitat and morphology is

one way. Another way is to look for “fossilized behavior”, i.e., ichnofossils. Chapter 6 offers an example of the latter, set against the background of the habitat represented by the rocks containing the Luoping Biota.

The marine reptile fossil deposits of southwest China show significant stratigraphic and environmental variability. The paleoenvironment of the Anisian Luoping Biota is thought to be a warm carbonate platform of a coastal internal basin, with organisms preserved in situ or nearly in situ (Zhang et al. 2009, Hu et al. 2010, Zhou et al. 2014). The Anisian Panxian Fauna is slightly younger and inhabited on a platform in a shallow marine environment. The Xingyi Fauna shows a transition from a Middle Triassic shallow marine environment to a more pelagic Late Triassic ecosystem (Benton et al. 2013, Zhou et al. 2015). It thus would be very interesting to test the morphological adaptation within the eosauropterygian clades in published species and new materials.

A case in point is the new *Nothosaurus* species based on HFUT XAP-22-007 (Chapter 6). The robust humerus of HFUT XAP-22-007 indicates strong forelimbs and increased mobility in this individual (Chapter 6). The distinctly broadened ungual phalanx and elongated pedal digit V in *N. luopingensis* are recognized as autapomorphies within *Nothosaurus* (Shang et al. 2022). HFUT XAP-22-007 also has an elongated pedal digit V and an elongated ungual phalanx. However, the expansion of the ungual phalanx in *N. yangjuanensis* (from the Panxian Fauna) is less pronounced. The variation in the pes between the three Anisian nothosaurs from the SW China may represent an adaptation to the shallow marine environment inhabited by the Luoping nothosaurs. Given that some small-sized eosauropterygians from the Luoping Biota also exhibit analogous pes features (Liu et al. 2011, Shang et al. 2011, Shang and Li 2015), these morphological congruencies might indicate a convergent adaptation to this environment rather than a closer phylogenetic relationship.

Adaptation to a special mode of foraging in the shallow and warm sea of the carbonate platforms and lagoons represented by the sediments hosting the Luoping Biota is documented by the spectacular sauropterygian swimming tracks from Daaozi (Luoping County), reported by Zhang et al. (2014). These authors reconstructed the mode of foraging involving punting with the forelimbs, and the expanded unguals of the new *Nothosaurus* appear to be adapted to this mode of propulsion (Chapter 6). The age-old problem of confidently assigning a producer to a given ichnofossil may thus have found its solution in this instance.

7.5 Future perspectives

Given the diversity of themes addressed in this dissertation, many perspectives for future work come to mind. For one, it is important to study the paleohistology and morphology of the same material in more detail. This will help determine whether some external features are the result of convergent evolution or represent a synapomorphy within an unresolved phylogenetic tree. Do the Anisian pachypleurosaurs from Luoping and Luxi show similar long bone histology to their European relatives, or do they show features more adapted to their habitat? Can the combination of bone histology and morphology help to resolve the evolutionary uncertainty in Chinese eosauropterygians? Moreover, will the bones from other localities all be good for paleohistological observation? These investigations pave the way for future explorations of the evolutionary trajectories of these diverse marine reptiles.

In addition, *Keichousaurus* from the Xingyi Fauna shows a distinct progression in bone preservation, ranging from the well-preserved Stage I to the poorly preserved Stage IV. In contrast, Guanling fossils predominantly show two polar states of preservation. This raises the question: Is there an intermediate state of alteration in the Guanling fossils? Furthermore, is it possible to develop a comprehensive preservation model that can be universally applied to fossils from Southwest China?

In general, this dissertation serves as an initial exploration that warrants further extension to additional fossils and localities. The development of a comprehensive diagenetic model encompassing different faunas will assist in the identification of fossils suitable for paleohistological study. Future studies should employ an integrated approach that combines morphological comparisons, phylogenetic analyses, and paleohistology. These methods will elucidate the evolutionary history and aquatic adaptation pathways of eosauropterygians from the unique Southwest Chinese fossil beds.

Complete literature list

Abdala, V., Manzano, A. S., and Herrel, A. (2008). The distal forelimb musculature in aquatic and terrestrial turtles: phylogeny or environmental constraints? *Journal of Anatomy*, *213*, 159-172.

Albers, P. C. H., and Rieppel, O. (2003). A new species of the sauropterygian genus *Nothosaurus* from the Lower Muschelkalk of Winterswijk, the Netherlands. *Journal of Paleontology*, *77*(4), 738-744.

Anderson, J. F., A. Hall-Martin and Russell D. A. (1985) Long-bone circumference and weight in mammals, birds and dinosaurs. *Journal of Zoology*, 207, 53-61.

Avens, L., Goshe, L. R., Zug, G. R., Balazs, G. H., Benson, S. R., and Harris, H. (2020). Regional comparison of leatherback sea turtle maturation attributes and reproductive longevity. *Marine Biology*, *167*, 1-12.

Ball, G. F., and Wade, J. (2013). The value of comparative approaches to our understanding of puberty as illustrated by investigations in birds and reptiles. *Hormones and behavior*, *64*(2), 211-214.

Benjamin, M., Toumi, H., Ralphs, J. R., Bydder, G., Best, T. M., and Milz, S. (2006). Where tendons and ligaments meet bone: attachment sites (‘entheses’) in relation to exercise and/or mechanical load. *Journal of Anatomy*, *208*(4), 471-490.

Bennett, C. E., Williams, M., Leng, M. J., Siveter, D. J., Davies, S. J., Sloane, H. J., and Wilkinson, I. P. (2011). Diagenesis of fossil ostracods: Implications for stable isotope based palaeoenvironmental reconstruction. *Palaeogeography*, *Palaeoclimatology*, *Palaeoecology*, *305*(1-4), 150-161.

Benton, M. J., and Harper, D. A. (2009). *Introduction to Paleobiology and the Fossil Record*. John Wiley and Sons.

Benton, M. J., Zhang, Q., Hu, S. X., Chen, Z., Wen, W., Liu, J., ... and Choo, B. (2013). Exceptional vertebrate biotas from the Triassic of China, and the expansion of marine ecosystems after the Permo-Triassic mass extinction. *Earth-Science Reviews*, *125*, 199-243.

Berna, F., Matthews, A., and Weiner, S. (2004). Solubilities of bone mineral from archaeological sites: the recrystallization window. *Journal of Archaeological Science*, *31*(6), 867-882.

Beyssac, O., and Rumble, D. (2014). Graphitic carbon: a ubiquitous, diverse, and useful geomaterial. *Elements*, *10*(6), 415-420.

Beyssac, O., Goffé, B., Chopin, C., and Rouzaud, J. N. (2002). Raman spectra of carbonaceous material in metasediments: a new geothermometer. *Journal of Metamorphic Geology*, *20*(8), 859-871.

Bickelmann, C., and Sander, P. M. (2008). A partial skeleton and isolated humeri of *Nothosaurus* (Reptilia: Eosauropterygia) from Winterswijk, the Netherlands. *Journal of Vertebrate Paleontology*, *28*(2), 326-338.

Briggs, D. E. G., and McMahon, S. (2015). The role of experiments in investigating the taphonomy of exceptional preservation. *Palaeontology*, *59*(1), 1-11.

Callewaert, F., Sinnesael, M., Gielen, E., Boonen, S., and Vanderschueren, D. (2010). Skeletal sexual dimorphism: relative contribution of sex steroids, Growth Hormone-Insulin-Like Growth Factor-I (GH-IGF-I) and mechanical loading. *Journal of Endocrinology*, *207*, 127-134.

Campione, N. E. and D. C. Evans (2012) A universal scaling relationship between body mass and proximal limb bone dimensions in quadrupedal terrestrial tetrapods. *BMC Biology 10*.

Canoville, A. and M. Laurin (2010) Evolution of humeral microanatomy and lifestyle in amniotes, and some comments on palaeobiological inferences. *Biological Journal of the Linnean Society 100*, 384-406.

Carvajal-Castro, J. D., López-Aguirre, Y., Ospina-L, A. M., Santos, J. C., Rojas, B., and Vargas-Salinas, F. (2020). Much more than a clasp: evolutionary patterns of amplexus diversity in anurans. *Biological Journal of the Linnean Society*, *129(3)*, 652-663.

Castanet, J. and E. Smirina. 1990. introduction to the skeletochronological method in amphibians and reptiles. In *Annales des Sciences Naturelles. Zoologie et Biologie Animale*, 191-196.

Čermáková, Z., Bezdička, P., Němec, I., Hradilová, J., Šrein, V., Blažek, J., and Hradil, D. (2015). Naturally irradiated fluorite as a historic violet pigment: Raman spectroscopic and X-ray diffraction study. *Journal of Raman Spectroscopy*, *46*(3), 236-243.

Čerňanský, A., Klein, N., Soták, J., Olšavský, M., Šurka, J., and Herich, P. (2018). A Middle Triassic pachypleurosaur (Diapsida: Eosauropterygia) from a restricted carbonate ramp in the Western Carpathians (Gutenstein Formation, Fatric Unit): paleogeographic implications. *Geologica Carpathica*, *69*(1), 3-16.

Chen, Z. F. (1985). Stratigraphic position of *Keichousaurus hui* Young of Middle Triassic and its significance in southwestern Guizhou. *Geology of Guizhou*, *2*(3), 289-290.

Cheng, Y. N., Holmes, R., Wu, X. C., and Alfonso, N. (2009). Sexual dimorphism and life history of *Keichousaurus Hui* (Reptilia: Sauropterygia). *Journal of Vertebrate Paleontology*, *29*(2), 401-408.

Cheng, Y. N., Sato, T., Wu, X. C., and Li, C. (2006). First complete pistosauroid from the Triassic of China. *Journal of Vertebrate Paleontology*, *26*(2), 501-504.

Cheng, Y. N., Wu, X. C., and Ji, Q. (2004). Triassic marine reptiles gave birth to live young. *Nature*, *432*(7015), 383-386.

Cheng, Y. N., Wu, X. C., Sato, T., and Shan, H. Y. (2012). A new eosauropterygian (Diapsida, Sauropterygia) from the Triassic of China. *Journal of Vertebrate Paleontology*, *32*(6), 1335-1349.

Cheng, Y. N., Wu, X. C., Sato, T., and Shan, H. Y. (2016). *Dawazisaurus brevis*, a new eosauropterygian from the Middle Triassic of Yunnan, China. *Acta Geologica Sinica-English Edition*, *90*(2), 401-424.

Cox, C. L., Hanninen, A. F., Reedy, A. M., and Cox, R. M. (2015). Female anoles retain responsiveness to testosterone despite the evolution of androgen-mediated sexual dimorphism. *Functional Ecology*, *29*, 758-767.

Cox, R. M., Butler, M., and John-Alder, H. (2007). The evolution of sexual size dimorphism in reptiles. In D. J. Fairbarin, W. U. Blanckenhorn and T. Szekely (Eds.), '*Sex, Size, and Gender Roles: Evolutionary Studies of Sexual Size Dimorphism*'. Oxford University: Oxford, pp. 38–49.

Cox, R. M., Skelly, S. L., and John-Alder, H. (2003). A comparative test of adaptive hypotheses for sexual dimorphism in lizards. *Evolution*, *57*, 1653–1669.

Currie, P. J. (1981). *Hovasaurus boulei*, an aquatic eosuchian from the Upper Permian of Madagascar. *Palaeontologia Africana*, 21, 99-168.

Currie, P. J., and Carroll, R. L. (1984). Ontogenetic changes in the eosuchian reptile *Thadeosaurus*. *Journal of Vertebrate Paleontology*, *4*(1), 68-84.

Dal Sasso, G., Lebon, M., Angelini, I., Maritan, L., Usai, D., and Artioli, G. (2016). Bone diagenesis variability among multiple burial phases at Al Khiday (Sudan) investigated by ATR-FTIR spectroscopy. *Palaeogeography*, *Palaeoclimatology*, *Palaeoecology*, *463*, 168-179.

Dalla Vecchia, F. M. (2006). A new sauropterygian reptile with plesiosaurian affinity from the Late Triassic of Italy. *Rivista Italiana Di Paleontologia E Stratigrafia*, *112*(2), 207-225.

Darwin, C. *On the Origin of Species by Means of Natural Selection, or the Preservation of Favored Races in the Struggle for Life* (J. Murray, 1859).

Buffrénil, V. de, and Schoevaert, D. (1988). On how the periosteal bone of the delphinid humerus becomes cancellous: ontogeny of a histological specialization. *Journal of Morphology*, *198*(2), 149-164.

Buffrénil, V. de, Ricqlès, A. J. de, Zylberberg, L., and Padian, K. (2021). *Vertebrate skeletal histology and paleohistology*. Boca Raton: CRC Press.

Miguel Chaves, C. de, Ortega, F., and Pérez-García, A. (2018). New highly pachyostotic nothosauroid interpreted as a filter-feeding Triassic marine reptile. *Biology Letters*, 14(8), 20180130.

Miguel Chaves, C. de, Ortega, F., and Pérez-García, A. (2020). The Iberian Triassic fossil record of Sauropterygia: an update. *Journal of Iberian Geology*, *46*, 445-464.

Sousa, D. V. de, Eltink, E., Oliveira, R. A. P., Félix, J. F., and de Moura Guimarães, L. (2020). Diagenetic processes in Quaternary fossil bones from tropical limestone caves. *Scientific Reports*, *10*(1), 1-16.

Delfino, M., and Sanchez-Villagra, M. R. (2010). A survey of the rock record of reptilian ontogeny. *Seminars in Cell and Developmental Biology*, 21(4), 432-440.

Deline, B., and Parsons-Hubbard, K. M. (2013). Experimentally observed soft-tissue preservation near a marine brine seep. *Palaeontology*, *56*(5), 893-900.

Diedrich, C. (2012). The Middle Triassic marine reptile biodiversity in the Germanic Basin, in the centre of the Pangaean world. *Central European Journal of Geosciences*, *4*(1), 9-46.

DiPietro, J. A. (2013). Keys to the interpretation of geological history. In DiPietro, J. A. (Eds.), *Landscape Evolution in the United States*. Amsterdam, The Netherlands: Elsevier, pp. 327-344.

Dong, S., Zhang, Y., Long, C., Yang, Z., Ji, Q., Wang, T., Hu, J., and Chen, X. (2008). Jurassic Tectonic Revolution in China and New Interpretation of the "Yanshan Movement". *Acta Geologica Sinica-English Edition*, *82*(2), 334-347.

Dong, W. P. (1997). *Stratigraphy (lithostratic) of Guizhou Province.* Beijing: China University of Geosciences Press.

Evans, L. (1951). Effects of male hormone upon the tail of the slider turtle, *Pseudemys scripta troostii*. *Science*, *114*, 277-279.

Faure, M., Lepvrier, C., Nguyen, V. V., Vu, T. V., Lin, W., and Chen, Z. (2014). The South China block-Indochina collision: Where, when, and how? *Journal of Asian Earth Sciences*, *79*, 260-274.

Francillon-Vieillot, H., Buffrénil, V. de, Castanet, J., Géraudie, J., Meunier, F., Sire, J., Zylberberg, L. and Ricqlès, A. de (1990) Microstructure and mineralization of vertebrate skeletal tissues. In Carter, J. G. (Eds.), *Biomineralization of the Skeleton: Patterns*, *Processes and Evolutionary Erends*, 1, 471-530.

Franke, W. A. (2015). The enigma of fluorite morphology revisited by dissolution experiments: In memory of Arkadij E. Glikin (1943–2012). *European Journal of Mineralogy*, *27*(3), 255-262.

Fröbisch, N. B. (2008). Ossification patterns in the tetrapod limb--conservation and divergence from morphogenetic events. *Biological Reviews*, *83*(4), 571-600.

Genç, Y. (2006). Genesis of the Neogene interstratal karst-type Pöhrenk fluorite–barite (±lead) deposit (Kırşehir, Central Anatolia, Turkey). *Ore Geology Reviews*, *29*(1), 105-117.

Glass, K., Ito, S., Wilby, P. R., Sota, T., Nakamura, A., Bowers, C. R., Miller, K. E., Dutta, S., Summons, R. E., and Briggs, D. E. (2013). Impact of diagenesis and maturation on the survival of eumelanin in the fossil record. *Organic Geochemistry*, *64*, 29-37.

Goldfarb, R. J., Mao, J., Qiu, K., and Goryachev, N. (2021). The great Yanshanian metallogenic event of eastern Asia: Consequences from one hundred million years of plate margin geodynamics. *Gondwana Research*, *100*, 223-250.

Griffin, C. T., Stocker, M. R., Colleary, C., Stefanic, C. M., Lessner, E. J., Riegler, M., ... Nesbitt, S. J. (2021). Assessing ontogenetic maturity in extinct saurian reptiles. *Biological Reviews*, *96*(2), 470-525.

Gürich, G. (1884) Ueber einige Saurier des oberschlesischen Muschelkalkes. *Zeitschrift der Deutschen Geologischen Gesellschaft*, 125-144.

Haas, G. (1980). Ein Nothosaurier-Schädel aus dem Muschelkalk des Wadi Ramon (Negev, Israel). *Annalen des Naturhistorischen Museums in Wien*, *83*, 119-125.

Haschke, S., Gutzmer, J., Wohlgemuth-Ueberwasser, C. C., Kraemer, D., and Burisch, M. (2021). The Niederschlag fluorite-(barite) deposit, Erzgebirge/Germany—a fluid inclusion and trace element study. *Mineralium Deposita*, 56, 1071-1086.

Hinz, E. A., and Kohn, M. J. (2010). The effect of tissue structure and soil chemistry on trace element uptake in fossils. *Geochimica et Cosmochimica Acta*, 74, 3213-3231.

Hinz, J. K., Matzke, A. T., and Pfretzschner, H.-U. (2019). A new nothosaur (Sauropterygia) from the Ladinian of Vellberg-Eschenau, southern Germany. *Journal of Vertebrate Paleontology*, *e1585364*.

Holmes, R., Cheng, Y. N., and Wu, X. C. (2008). New information on the skull of *Keichousaurus hui* (Reptilia: Sauropterygia) with comments on sauropterygian interrelationships. *Journal of Vertebrate Paleontology*, *28*(1), 76-84.

Holz, M., and Schultz, C. L. (1998). Taphonomy of the south Brazilian Triassic herpetofauna: fossilization mode and implications for morphological studies. *Lethaia*, 31, 335-345.

Horner, J. R., Padian, K. and Ricqlès, A. de (2001) Comparative osteohistology of some embryonic and perinatal archosaurs: developmental and behavioral implications for dinosaurs. *Paleobiology*, 27, 39-58.

Houssaye, A. (2013) Bone histology of aquatic reptiles: what does it tell us about secondary adaptation to aquatic life? *Biological Journal of the Linnean Society*, 108, 3-21.

Houssaye, A., Sander, P. M. and Klein, N. (2016) Adaptive patterns in aquatic amniote bone microanatomy-more complex than previously thought. *Integrative and Comparative Biology*, 56, 1349-1369.

Hu, S. X., Zhang, Q. Y., Chen, Z. Q., Zhou, C. Y., Lv, T., Xie, T., . . . Benton, M. J. (2010). The Luoping Biota: exceptional preservation, and new evidence on the Triassic recovery from end-Permian mass extinction. *Proceedings of the Royal Society B: Biological Sciences*, *278*(1716), 2274-2282.

Zhang, Q., Wen, W., Hu, S., Benton, M. J., Zhou, C., Xie, T., Lü, T., Huang, J., Choo, B., Chen, Z. Q., Liu, J., and Zhang, Q. (2014). Nothosaur foraging tracks from the Middle Triassic of southwestern China. *Nature Communications*, 5(3973): 1-12.

Hu, Y. W., and Liu, J. (2022). A new morphotype of nothosaurs (Sauropterygia: Nothosauridae) from the Middle Triassic of South China. *Historical Biology*, *35*(10), 1794-1803.

Hu, Y. W., Li, Q., Liu, J. (2023). A new pachypleurosaur (Reptilia: Sauropterygia) from the Middle Triassic of southwestern China and its phylogenetic and biogeographic implications. *Swiss Journal of Palaeontology* (In press).

Hugi, J. and Sánchez-Villagra, M. R. (2012) Life history and skeletal adaptations in the Galapagos marine iguana (*Amblyrhynchus cristatus*) as reconstructed with bone histological data-a comparative study of iguanines. *Journal of Herpetology*, 312-324.

Hugi, J., Scheyer, T. M., Sander, P. M., Klein, N., and Sánchez-Villagra, M. R. (2011) Long bone microstructure gives new insights into the life of pachypleurosaurids from the Middle Triassic of Monte San Giorgio, Switzerland/Italy. *Comptes Rendus Palevol*, 10, 413-426.

Hutton, J. M. (1987) Growth and feeding ecology of the nile crocodile *Crocodylus niloticus* at Ngezi, Zimbabwe. *Journal of Animal Ecology*, 56, 25-38.

Ji, C., Jiang, D. Y., Rieppel, O., Motani, R., Tintori, A., and Sun, Z. Y. (2014). A new specimen of *Nothosaurus youngi* from the Middle Triassic of Guizhou, China. *Journal of Vertebrate Paleontology*, *34*(2), 465-470.

Jiang, D. Y., Lin, W. B., Rieppel, O., Motani, R., and Sun, Z. Y. (2019). A new Anisian (Middle Triassic) eosauropterygian (Reptilia, Sauropterygia) from Panzhou, Guizhou Province, China. *Journal of Vertebrate Paleontology*, *38*(4), 1-9.

Jiang, D. Y., Maisch, M. W., Hao, W. C., Sun, Y. L., and Sun, Z. Y. (2006a). *Nothosaurus yangjuanensis* n. sp (Reptilia, Sauropterygia, Nothosauridae) from the middle Anisian (Middle Triassic) of Guizhou, southwestern China. *Neues Jahrbuch für Geologie und Paläontologie*, *Monatshefte*, *2006*(5), 257-276.

Jiang, D. Y., Maisch, M. W., Sun, Z. Y., Sun, Y. L., and Hao, W. C. (2006b). A new species of *Lariosaurus* (Reptilia, Sauropterygia) from the Middle Anisian (Middle Triassic) of southwestern China. *Neues Jahrbuch für Geologie und Paläontologie*, *Abhandlungen*, *242*(1), 19-42.

Jiang, D. Y., Motani, R., Hao, W. C., Rieppel, O., Sun, Y. L., Schmitz, L., and Sun, Z. Y. (2008). First record of Placodontoidea (Reptilia, Sauropterygia, Placodontia) from the Eastern Tethys. *Journal of Vertebrate Paleontology*, *28*(3), 904-908.

Jiang, D. Y., Motani, R., Tintori, A., Rieppel, O., Chen, G. B., Huang, J. D., Zhang, R., Sun, Z. Y. and Ji, C. (2014). The Early Triassic eosauropterygian *Majiashanosaurus discocoracoidis*, gen. et sp. nov. (Reptilia, Sauropterygia), from Chaohu, Anhui Province, People's Republic of China. *Journal of Vertebrate Paleontology*, *34*(5), 1044-1052.

Jiang, D. Y., Rieppel, O., Motani, R., Hao, W. C., Sun, Y. L., Schmitz, L., and Sun, Z. Y. (2008). A new middle Triassic eosauropterygian (Reptilia, Sauropterygian) from Southwestern China. *Journal of Vertebrate Paleontology*, *28*(4), 1055-1062.

Jiang, D., Motani, R., Hao, W., Rieppel, O., Sun, Y., Tintori, A., Sun, Z., and Schmitz, L. (2009). Biodiversity and sequence of the Middle Triassic Panxian marine reptile fauna, Guizhou Province, China. *Acta Geologica Sinica-English Edition*, 83, 451-459.

Jiang, D. Y., Lin, W. B., Rieppel, O., Motani, R., and Sun, Z. Y. (2019). A new Anisian (Middle Triassic) eosauropterygian (Reptilia, Sauropterygia) from Panzhou, Guizhou Province, China. *Journal of Vertebrate Paleontology*, *38*(4), 1-9.

Kaliontzopoulou, A., Carretero, M. A., and Llorente, G. A. (2007). Multivariate and geometric morphometrics in the analysis of sexual dimorphism variation in Podarcis lizards. *Journal of Morphology*, *268*(2), 152-165.

Kaneki, S., and Kouketsu, Y. (2022). An automatic peak deconvolution method for Raman spectra of terrestrial carbonaceous material for application to the geothermometers of Kouketsu et al.(2014). *Island Arc*, *31*(1), e12467.

Keenan, S. W. (2016). From bone to fossil: A review of the diagenesis of bioapatite. *American Mineralogist*, *101*(9), 1943-1951.

Keenan, S. W., and Engel, A. S. (2017). Early diagenesis and recrystallization of bone. *Geochimica et Cosmochimica Acta*, 196, 209-223.

Keenan, S. W., Engel, A. S., Roy, A., and Lisa Bovenkamp-Langlois, G. (2015). Evaluating the consequences of diagenesis and fossilization on bioapatite lattice structure and composition. *Chemical Geology*, 413, 18-27.

Kelley, N. P., Motani, R., Jiang, D. Y., Rieppel, O., and Schmitz, L. (2014). Selective extinction of Triassic marine reptiles during long-term sea-level changes illuminated by seawater strontium isotopes. *Palaeogeography*, *Palaeoclimatology*, *Palaeoecology*, *400*, 9-16.

Klein, N., and Griebeler, E. M. (2018). Growth patterns, sexual dimorphism, and maturation modeled in Pachypleurosauria from Middle Triassic of central Europe (Diapsida: Sauropterygia). *Fossil Record*, *21*(1), 137-157.

Klein, N. (2010) Long Bone Histology of Sauropterygia from the Lower Muschelkalk of the Germanic Basin Provides Unexpected Implications for Phylogeny. *PLoS ONE*, 5, e11613.

Klein, N. (2012). Postcranial morphology and growth of the pachypleurosaur *Anarosaurus heterodontus* (Sauropterygia) from the Lower Muschelkalk of Winterswijk, The Netherlands. *Paläontologische Zeitschrift*, *86*, 389-408.

Klein, N., and Albers, P. C. H. (2009). A new species of the sauropsid reptile *Nothosaurus* from the Lower Muschelkalk of the western Germanic Basin, Winterswijk, The Netherlands. *Acta Palaeontologica Polonica*, *54*(4), 589-598.

Klein, N., and Scheyer, T. M. (2014). A new placodont sauropterygian from the Middle Triassic of the Netherlands. *Acta Palaeontologica Polonica*, *59*(4), 887-902.

Klein, N., A. Houssaye, J. M. Neenan and T. M. Scheyer (2015a) Long bone histology and microanatomy of Placodontia (Diapsida: Sauropterygia). *Contributions to Zoology 84*(1), 59-S15.

Klein, N., and Griebeler, E. M. (2018). Growth patterns, sexual dimorphism, and maturation modeled in Pachypleurosauria from Middle Triassic of central Europe (Diapsida: Sauropterygia). *Fossil Record*, *21*(1), 137-157.

Klein, N., Furrer, H., Ehrbar, I., Torres Ladeira, M., Richter, H., and Scheyer, T. M. (2022). A new pachypleurosaur from the early Ladinian Prosanto Formation in the Eastern Alps of Switzerland. *Swiss Journal of Palaeontology*, *141*(1), 1-27.

Klein, N., J. M. Neenan, T. M. Scheyer and E. M. Griebeler (2015b) Growth patterns and life-history strategies in Placodontia (Diapsida: Sauropterygia). *Royal Society Open Science*2,, 140440.

Klein, N., P. M. Sander, A. Krahl, T. M. Scheyer and A. Houssaye (2016) Diverse aquatic adaptations in *Nothosaurus* spp. (Sauropterygia)-Inferences from Humeral Histology and Microanatomy. *PLoS ONE*, 11, e0158448.

Klein, N., Voeten, D. F. A. E., Haarhuis, A., and Bleeker, R. (2016). The earliest record of the genus *Lariosaurus* from the early middle Anisian (Middle Triassic) of the Germanic Basin. *Journal of Vertebrate Paleontology*, *36*(4), e1163712.

Klein, N., Voeten, D. F., Lankamp, J., Bleeker, R., Sichelschmidt, O. J., Liebrand, M., ... and Sander, P. M. (2015b). Postcranial material of *Nothosaurus marchicus* from the Lower Muschelkalk (Anisian) of Winterswijk, The Netherlands, with remarks on swimming styles and taphonomy. *Paläontologische Zeitschrift*, *89*(4), 961-981.

Kouketsu, Y., Mizukami, T., Mori, H., Endo, S., Aoya, M., Hara, H., Nakamura, D., and Wallis, S. (2014). A new approach to develop the Raman carbonaceous material geothermometer for low-grade metamorphism using peak width. *Island Arc*, *23*(1), 33-50.

Krahl, A., Lipphaus, A., Sander, M.P., Maffucci, F., Hochscheid, S., and Witzel, U. (2020). Humerus osteology, myology, and finite element structure analysis of Cheloniidae. Anat. Rec. *303*, 2177-2191.

Krahl, A., N. Klein and P. M. Sander (2013) Evolutionary implications of the divergent long bone histologies of *Nothosaurus* and *Pistosaurus* (Sauropterygia, Triassic). *BMC Evolutionary Biology*, *13*, 1-23.

Krumbein, W. C., and Garrels, R. (1952). Origin and classification of chemical sediments in terms of pH and oxidation-reduction potentials. *The Journal of Geology*, *60*, 1-33.

Laetsch, T., and Downs, R. (2006). Software for identification and refinement of cell parameters from powder diffraction data of minerals using the RRUFF Project and American Mineralogist Crystal Structure Databases. In *19th General Meeting of the International Mineralogical Association*, Kobe, Japan. 23-28.

Lafuente, B., Downs, R. T., Yang, H., and Stone, N. (2015). The power of databases: The RRUFF project. In Armbruster, T., and Danisi, R. M. (Eds.), *Highlights in Mineralogical Crystallography*. Berlin, Germany: W. De Gruyter. 1-30.

Lahfid, A., Beyssac, O., Deville, E., Negro, F., Chopin, C., and Goffé, B. (2010). Evolution of the Raman spectrum of carbonaceous material in low-grade metasediments of the Glarus Alps (Switzerland). *Terra Nova*, 22, 354-360.

Lamm, E. T., and Padian, K. (2013). Preparation and sectioning of specimens. In Lamm, E. T., and Padian, K. (Eds.), *Bone Histology of Fossil Tetrapods: Advancing Methods*, *Analysis*, *and Interpretation*. California, the USA: University of California Press. 55-160.

Li, C., Zhao, L. J., and Wang, L. T. (2007). A new species of *Macrocnemus* (Reptilia: Protorosauria) from the Middle Triassic of southwestern China and its palaeogeographical implication. *Science in China Series D-Earth Sciences*, *50*(11), 1601-1605.

Li, J. L., and Rieppel, O. (2004). A new nothosaur from Middle Triassic of Guizhou, China. *Veterbrate PalAsiatica*, *42*(1), 1-12.

Li, J., Hu, R., Zhao, C., Zhu, J., Huang, Y., Gao, W., Li, J., and Zhuo, Y. (2020). Sulfur isotope and trace element compositions of pyrite determined by NanoSIMS and LA-ICP-MS: new constraints on the genesis of the Shuiyindong Carlin-like gold deposit in SW China. *Mineralium Deposita*, *55*, 1279-1298.

Li, Q. (2019). *Research on Triassic Sauropterygians.* (Unpublished Master's thesis), Hefei University of Technology, Hefei, China. 1-89

Li, Q., and Liu, J. (2020). An Early Triassic sauropterygian and associated fauna from South China provide insights into Triassic ecosystem health. *Communications Biology*, *3*(1), 63.

Li, Q., Liu, J., Klein, N., Nakajima, Y., and Sander, P. M. (2023). Puberty in a Mesozoic reptile. *Current Biology*, *33*(14), 3011-3016 e3013.

Li, Y., He, D., Li, D., Lu, R., Fan, C., Sun, Y., and Huang, H. (2018). Sedimentary provenance constraints on the Jurassic to Cretaceous paleogeography of Sichuan Basin, SW China. *Gondwana Research*, *60*, 15-33.

Li, Z., and Pasteris, J. D. (2014). Tracing the pathway of compositional changes in bone mineral with age: Preliminary study of bioapatite aging in hypermineralized dolphin's bulla. *Biochimica et Biophysica Acta (BBA)-General Subjects*, *1840*, 2331-2339.

Li, Z. G, Sun, Z. Y., Jiang, D. Y., and Ji, C. (2016). LA-ICP-MS Zircon U-Pb age of the fossil layer of Triassic Xingyi Fauna from Xingyi, Guizhou, and its significance. *Geological Review*, *62*, 779–790. (in Chinese with English abstract).

Lin, K. (1994). Functional morphology and phylogeny of *Keichousaurus hui* (Sauropterygia, Reptilia). Ph. D. thesis, McGill University.

Lin, K. B., and Rieppel, O. (1998). Functional morphology and ontogeny of *Keichousaurus hui* (Reptilia, Sauropterygia). *Fieldiana (Geology) n.s*., *39*, 1-39.

Lin, W. B., Jiang, D. Y., Rieppel, O., Motani, R., Ji, C., Tintori, A., ... Zhou, M. (2017). A new specimen of *Lariosaurus xingyiensis* (Reptilia, Sauropterygia) from the Ladinian (Middle Triassic) Zhuganpo Member, Falang Formation, Guizhou, China. *Journal of Vertebrate Paleontology*, e1278703.

Lin, W. B., Jiang, D. Y., Rieppel, O., Motani, R., Tintori, A., Sun, Z. Y., and Zhou, M. (2021). *Panzhousaurus Rotundirostris* Jiang et al., 2019 (Diapsida: Sauropterygia) and the Recovery of the Monophyly of Pachypleurosauridae. *Journal of Vertebrate Paleontology*, e1901730.

Liu, J., Hu, S. X., Rieppel, O., Jiang, D. Y., Benton, M. J., Kelley, N. P., ... Lv, T. (2014). A gigantic nothosaur (Reptilia: Sauropterygia) from the Middle Triassic of SW China and its implication for the Triassic biotic recovery. *Scientific Reports*, *4*(7142), 1-9.

Liu, J., Rieppel, O., Jiang, D. Y., Aitchison, J. C., Motani, R., Zhang, Q. Y., Zhou, C. Y. and Sun, Y. Y. (2011). A new pachypleurosaur (Reptilia, Sauropterygia) from the lower Middle Triassic of SW China and the phylogenetic relationships of Chinese pachypleurosaurs. *Journal of Vertebrate Paleontology*, *31*(2), 292-302.

Liu, Q. L., Cheng, L., Stubbs, T. L., Moon, B. C., Benton, M. J., Yan, C. B., and Tian, L. (2023). Rapid neck elongation in Sauropterygia (Reptilia: Diapsida) revealed by a new basal pachypleurosaur from the Lower Triassic of China. *BMC Ecology and Evolution*, *23*(1), 44.

Liu, Q. L., Yang, T., Cheng, L., Benton, M. J., Moon, B. C., Yan, C., An, C. B. and Tian, L. (2021). An injured pachypleurosaur (Diapsida: Sauropterygia) from the Middle Triassic Luoping Biota indicating predation pressure in the Mesozoic. *Scientific Reports*, *11*(1), 21818.

Liu, X. Q., Lin, W. B., Rieppel, O., Sun, Z. Y., Li, Z. G., Lu, H., and Jiang, D. Y. (2015). A new specimen of *Diandongosaurus acutidentatus* (Sauropterygia) from the Middle Triassic of Yunnan, China. *Veterbrate PalAsiatica*, *53*(4), 281.

Lovern, M. B., McNabb, F. M. A., and Jenssen, T. A. (2001). Developmental effects of testosterone on behavior in male and female green anoles (*Anolis carolinensis*). *Hormones and Behavior*, *39*(2), 131-143.

Lowenstam, H. A. (1981). Minerals formed by organisms. *Science*, 211, 1126-1131.

Lu, H., Jiang, D., Motani, R., Ni, P., Sun, Z., Tintori, A., Xiao, S., Zhou, M., Ji, C., and Fu, W. (2018). Middle Triassic Xingyi Fauna: showing turnover of marine reptiles from coastal to oceanic environments. *Palaeoworld*, 27(1), 107-116.

Luo, M., Chen, Z., Hu, S., Zhang, Q., Benton, M. J., Zhou, C., Wen, W., and Huang, J. (2013). Carbonate reticulated ridge structures from the lower Middle Triassic of the Luoping area, Yunnan, southwestern China: Geobiologic features and implications for exceptional preservation of the Luoping Biota. *Palaios*, *28*(7), 541-551.

Ma, L. T., Jiang, D. Y., Rieppel, O., Motani, R., and Tintori, A. (2015). A new pistosauroid (Reptilia, Sauropterygia) from the late Ladinian Xingyi marine reptile level, southwestern China. *Journal of Vertebrate Paleontology*, *35*(1), e881832.

Ma, L. T., Ji, C., Sun, Z. Y., Yang, P. F., Zou, X. D. (2013). Biodiversity and strati-graphic distribution of the Triassic Xingyi marine reptile fauna, Guizhou province. *Journal of Stratigraphy*, *7*(2), 178–185 (in Chinese with English abstract).

Mähler, B., Janssen, K., Tahoun, M., Tomaschek, F., Schellhorn, R., Müller, C. E., Bierbaum, G., and Rust, J. (2022). Adipocere formation in biofilms as a first step in soft tissue preservation. *Scientific Reports*, *12*(1), 10122.

Mao, J. W., Cheng, Y. B., Chen, M. H., and Franco, P. (2013). Major types and time–space distribution of Mesozoic ore deposits in South China and their geodynamic settings. *Mineralium Deposita*, *48*(2), 267-294.

Marquez-Aliaga, A., Klein, N., Reolid, M., Plasencia, P., Villena, J. A., and Martinez-Perez, C. (2019). An enigmatic marine reptile, *Hispaniasaurus cranioelongatus* (gen. et sp. nov.) with nothosauroid affinities from the Ladinian of the Iberian Range (Spain). *Historical Biology*, *31*(2), 223-233.

McGregor, M., Erickson, T. M., Spray, J. G., and Whitehouse, M. J. (2021). High-resolution EBSD and SIMS U–Pb geochronology of zircon, titanite, and apatite: Insights from the Lac La Moinerie impact structure, Canada. *Contributions to Mineralogy and Petrology*, *176*(1), 76.

McGregor, M., Erickson, T., and Spray, J. (2019). Recrystallization and micro-twinning in apatite and titanite from the Lac La Moinerie impact structure, Canada: Implications for U-Pb impact chronology. *Large Meteor Impacts and Planetary Evolution VI Abst*, 5099.

Meers, M. B. (2003). Crocodylian forelimb musculature and its relevance to Archosauria. *The Anatomical Record Part A274*(2), 891-916.

Megaw, P. K. M. (2013). Mexican fluorite. *Rocks and Minerals*, *88*(2), 120-133.

Metcalfe, I. (2006). Paleozoic and Mesozoic tectonic evolution and palaeogeography of East Asian crustal fragments: The Korean Peninsula in context. *Gondwana Research*, *9*(1-2), 24-46.

Milroy, P., Wright, V. P., and Simms, M. J. (2019). Dryland continental mudstones: Deciphering environmental changes in problematic mudstones from the Upper Triassic (Carnian to Norian) Mercia Mudstone Group, south-west Britain. *Sedimentology*, *66*(7), 2557-2589.

Motani, R. (2009). The evolution of marine reptiles. *Evolution: Education and Outreach*, *2*(2), 224-235.

Motani, R., Jiang, D. Y., Rieppel, O., Xue, Y. F., and Tintori, A. (2015). Adult sex ratio, sexual dimorphism and sexual selection in a Mesozoic reptile. *Proceedings of the Royal Society B: Biological Sciences*, *282*(1815), 20151658.

Mouhovski, J., Vitov, O., Dimov, V., Kostova, B., and Gechev, S. (2014). High vacuum phase transformation of fluorspar vapors to crystal aggregates. *Bulgarian Chemical Communications*, *46*, 68-78.

Muscente, A. D., Schiffbauer, J. D., Broce, J., Laflamme, M., O'Donnell, K., Boag, T. H., Meyer, M., Hawkins, A. D., Huntley, J. W., McNamara, M., Mackenzie, L. A., Stanley, G. D., Hinman, N. W., Hofmann, M. H., and Xiao, S. (2017). Exceptionally preserved fossil assemblages through geologic time and space. *Gondwana Research*, *48*, 164-188.

Mustoe, G. E. (2018). Mineralogy of Non-Silicified Fossil Wood. *Geosciences*, *8*(3), 85.

Myrow, P. M., Hughes, N. C., Paulsen, T., Williams, I., Parcha, S. K., Thompson, K., Bowring, S. A., Peng, S. C., and Ahluwalia, A. (2003). Integrated tectonostratigraphic analysis of the Himalaya and implications for its tectonic reconstruction. *Earth and Planetary Science Letters*, *212*(3-4), 433-441.

Nakajima, Y., Hirayama, R., and Endo, H. (2014). Turtle humeral microanatomy and its relationship to lifestyle. *Biological Journal of the Linnean Society, 112*, 719-734.

Neenan, J. M., Klein, N., and Scheyer, T. M. (2013). European origin of placodont marine reptiles and the evolution of crushing dentition in Placodontia. *Nature Communications*, *4*, 1621.

Neenan, J. M., Li, C., Rieppel, O., and Scheyer, T. M. (2015). The cranial anatomy of Chinese placodonts and the phylogeny of Placodontia (Diapsida: Sauropterygia). *Zoological Journal of the Linnean Society*, *175*(2), 415-428.

Ó Gogáin, A., O'Sullivan, G., Clements, T., Hoare, B. C., Murray, J., and Wyse Jackson, P. N. (2022). Metamorphism as the cause of bone alteration in the Jarrow assemblage (Langsettian, Pennsylvanian) of Ireland. *Palaeontology*, *65*, e12628.

O'Keefe, F. R., Sander, P. M., Wintrich, T., and Werning, S. (2019). Ontogeny of polycotylid long bone microanatomy and histology. *Integrative Organismal Biology*, *1*(1), oby007.

Pasero, M., Kampf, A. R., Ferraris, C., Pekov, I. V., Rakovan, J., and White, T. J. (2010). Nomenclature of the apatite supergroup minerals. *European Journal of Mineralogy*, *22*(2), 163-179.

Peyer, B. (1931). Die Triasfauna der Tessiner Kalkalpen. 4. *Ceresiosaurus calcagnii* nov. gen. nov. spec. *Abhandlungen der Schweizerischen paläontolosichen Gesellschaft*, *51*, 1-68.

Peyer, B. (1939). Die Triasfauna der Tessiner Kalkalpen. XIV. *Paranothosaurus amsleri* nov. gen. nov. spec. *Abhandlungen der schweizerischen paläontologischen Gesellschaft*, *62*, 1-87.

Piñeiro, G., Ferigolo, J., Ramos, A., and Laurin, M. (2012). Cranial morphology of the Early Permian mesosaurid *Mesosaurus tenuidens* and the evolution of the lower temporal fenestration reassessed. *Comptes Rendus Palevol*, *11*(5), 379-391.

Purnell, M. A., Donoghue, P. J. C., Gabbott, S. E., McNamara, M. E., Murdock, D. J. E., and Sansom, R. S. (2018). Experimental analysis of soft-tissue fossilization: Opening the black box. *Palaeontology*, *61*(3), 317-323.

Qiu, L., Wu, Y., Wang, Q., Wu, L., He, Z., Peng, S., and Fan, Y. (2022). Metallogenic Mechanism of Typical Carbonate-Hosted Uranium Deposits in Guizhou (China). *Minerals*, *12*(7), 585.

Rahl, J. M., Anderson, K. M., Brandon, M. T., and Fassoulas, C. (2005). Raman spectroscopic carbonaceous material thermometry of low-grade metamorphic rocks: Calibration and application to tectonic exhumation in Crete, Greece. *Earth and Planetary Science Letters*, *240*(3-4), 339-354.

Ralls, K., 1976. Mammals in which females are larger than males. *The Quarterly Review of Biology*, *51*(2), 245-276.

Renesto, S., Binelli, G., and Hagdorn, H. (2014). A new pachypleurosaur from the Middle Triassic Besano Formation of Northern Italy. *Neues Jahrbuch für Geologie und Paläontologie-Abhandlungen*, *271*(2), 151-168.

Reznikov, N., Bilton, M., Lari, L., Stevens, M. M., and Kröger, R. (2018). Fractal-like hierarchical organization of bone begins at the nanoscale. *Science*, *360*(6388), eaao2189.

Ricqlès, A. J. de (1983). Cyclical growth in the long limb bones of a sauropod dinosaur. *Acta Palaeontologica Polonica*, *28*(1-2). 225-232.

Rieppel, O. (1989). A new pachypleurosaur (Reptilia: Sauropterygia) from the Middle Triassic of Monte San Giorgio, Switzerland. *Philosophical Transactions of the Royal Society of London B*, *323*(1212), 1-73.

Rieppel, O. (1992a). The skull in a hatchling of *Sphenodon punctatus*. *Journal of Herpetology*, *26*(1), 80-84.

Rieppel, O. (1992b). Studies on skeleton formation in reptiles. I. The postembryonic development of the skeleton in *Cyrtodactylus pubisulcus* (Reptilia: Gekkonidae). *Journal of Zoology*, *227*(1), 87-100.

Rieppel, O. (1993a). Studies on skeleton formation in reptiles. V. Patterns of ossification in the skeleton of *Alligator mississippiensis* Daudin (Reptilia, Crocodylia). *Zoological Journal of the Linnean Society*, *109*(3), 301-325.

Rieppel, O. (1993b). Studies on skeleton formation in reptiles: patterns of ossification in the skeleton of *Chelydra serpentina* (Reptilia, Testudines). *Journal of Zoology*, *231*(3), 487-509.

Rieppel, O. (1994). Studies on skeleton formation in reptiles. Patterns of ossification in the skeleton of *Lacerta agilis exigua* Eichwald (Reptilia, Squamata). *Journal of Herpetology*, *28*(2), 145-153.

Rieppel, O. (1994). The status of the sauropterygian reptile *Nothosaurus juvenilis* from the Middle Triassic of Germany. *Palaeontology*, *37*(4), 733-746.

Rieppel, O. (1999a). Phylogeny and paleobiogeography of Triassic Sauropterygia: problems solved and unresolved. *Palaeogeography, Palaeoclimatology, Palaeoecology*, *153*(1-4), 1-15.

Rieppel, O. (1999b). The Sauropterygian genera *Chinchenia*, *Kwangsisaurus*, and *Sanchiaosaurus* from the Lower and Middle Triassic of China. *Journal of Vertebrate Paleontology*, *19*(2), 321-337.

Rieppel, O. (2000). Sauropterygia I. In ed. P. Wellnhofer (ed.) *Encyclopedia of Paleoherpetology*, 134. munich: Verlag Dr. Friedrich Pfeil.

Rieppel, O. (2001). A new species of *Nothosaurus* (Reptilia: Sauropterygia) from the upper Muschelkalk (lower Ladinian) of southwestern Germany. *Palaeontographica Abteilung A*, *263*, 137-161.

Rieppel, O., and Hagdorn, H. (1997). Paleobiogeography of Middle Triassic Sauropterygia in central and western Europe. In M. Callaway Jack and L. Nicholls Elizabeth (Eds.), *Ancient Marine Reptiles* (pp. 121-144). San Diego, Academic Press.

Rieppel, O., and Lin, K. (1995). Pachypleurosaurs (Reptilia: Sauropterygia) from the Lower Muschelkalk, and a review of the Pachypleurosauroidea. *Fieldiana (Geology) n.s.*, *32*, 1-44.

Rieppel, O., and Wild, R. (1994). *Nothosaurus edingerae* Schultze, 1970: diagnosis of the species and comments on its stratigraphical occurrence. *Stuttgarter Beiträge zur Naturkunde B*, *204*, 1-13.

Rieppel, O. (1989). A new pachypleurosaur (Reptilia: Sauropterygia) from the Middle Triassic of Monte San Giorgio, Switzerland. *Philosophical Transactions of the Royal Society of London B, Biological Sciences*, *323*(1212), 1-73.

Rieppel, O., Li, J. L., and Jun, L. (2003). *Lariosaurus xingyiensis* (Reptilia: Sauropterygia) from the Triassic of China. *Canadian Journal of Earth Sciences*, *40*(4), 621-634.

Rieppel, O., Mazin, J.-M., and Tchernov, E. (1997). Speciation along rifting continental margins: a new Nothosaur from the Negev (Israël). *Comptes Rendus de l'Académie des Sciences-Series IIA-Earth and Planetary Science*, *325*(12), 991-997.

Rieppel, O., Sander, P. M., and Storrs, G. W. (2002). The skull of the pistosaur *Augustasaurus* from the Middle Triassic of northwestern Nevada. *Journal of Vertebrate Paleontology*, *22*(3), 577-592.

Romer, A. S. (1956). *The Osteology of the Reptiles*. Chicago, Illinois, University of Chicago Press.

Rößler, R. (2021). The most entirely known Permian terrestrial ecosystem on Earth–kept by explosive volcanism. *Palaeontographica Abteilung B*, *303*, 1-75.

Rudwick, M. J. (1985). *The meaning of fossils: Episodes in the history of palaeontology (2nd ed.)*. Chicago, Illinois, University of Chicago Press, 304pp.

Saitta, E. T., Clapham, C., and Vinther, J. (2018). Experimental subaqueous burial of a bird carcass and compaction of plumage. *Paläontologische Zeitschrift*, *92*(4), 727-732.

San, K. K., Fraser, N. C., Foffa, D., Rieppel, O., and Brusatte, S. L. (2019). The first Triassic vertebrate fossils from Myanmar: Pachypleurosaurs in a marine limestone. *Acta Palaeontologica Polonica*, *64*(2), 357-362.

Sander, P. M. (1988). A fossil reptile embryo from the Middle Triassic of the Alps. *Science*, *239*, 780-783.

Sander, P. M. (1989). The pachypleurosaurids (Reptilia: Nothosauria) from the Middle Triassic of Monte San Giorgio (Switzerland) with the description of a new species. *Philosophical Transactions of the Royal Society of London B*, *325*(1230), 561-666.

Sander, P. M. (1990) Skeletochronology in the small Triassic reptile *Neusticosaurus*. *Annales des Sciences Naturelles Zoologie Paris*, 11, 213-217.

Sander, P. M. (2000) Longbone histology of the Tendaguru sauropods: implications for growth and biology. *Paleobiology*, 26, 466-488.

Sato, T., Cheng, Y. N., Wu, X. C., and Li, C. (2010). Osteology of *Yunguisaurus* Cheng et al., 2006 (Reptilia; Sauropterygia), a Triassic pistosauroid from China. *Paleontological Research*, *14*(3), 179-195.

Sato, T., Zhao, L. J., Wu, X. C., and Li, C. (2014a). *Diandongosaurus acutidentatus* Shang, Wu and Li, 2011 (Diapsida: Sauropterygia) and the relationships of Chinese eosauropterygians. *Geological Magazine*, *151*(01), 121-133.

Sato, T., Zhao, L. J., Wu, X. C., and Li, C. (2014b). A new specimen of the Triassic pistosauroid *Yunguisaurus*, with implications for the origin of Plesiosauria (Reptilia, Sauropterygia). *Palaeontology*, *57*(1), 55-76.

Scharf, I., Feldman, A., Novosolov, M., Pincheira-Donoso, D., Das, I., Böhm, M., Uetz, P., Torres-Carvajal, O., Bauer, A., Roll, U., et al. (2015). Late bloomers and baby boomers: ecological drivers of longevity in squamates and the tuatara. *Global Ecology and Biogeography*, *24*, 396-405.

Scheyer, T. M., Romano, C., Jenks, J., and Bucher, H. (2014). Early Triassic marine biotic recovery: the predators' perspective. *PLoS ONE*, *9*(3), e88987.

Schobert, H. H. (2013). *Chemistry of fossil fuels and biofuels*. Cambridge, UK, Cambridge University Press, 130pp.

Selley, R. C. (1998). *Elements of petroleum geology*. Gulf Professional Publishing, 457pp.

Shang, Q. H. (2006). A new species of *Nothosaurus* from the early Middle Triassic of Guizhou, China. *Veterbrate PalAsiatica*, *44*(3), 237-249.

Shang, Q. H., and Li, C. (2015). A new small-sized eosauropterygian (Diapsida: Sauropterygia) from the Middle Triassic of Luoping, Yunnan, southwestern China. *Veterbrate PalAsiatica*, *53*(4), 265-280.

Shang, Q. H., Li, C., and Wang, W. (2022). *Nothosaurus luopingensis* sp. nov.(Sauropterygia) from the Anisian, Middle Triassic of Luoping, Yunnan Province, China. *Veterbrate PalAsiatica*, *60*(4), 249.

Shang, Q. H., Li, C., and Wu, X. C. (2017). New information on *Dianmeisaurus gracilis* Shang and Li, 2015. *Veterbrate PalAsiatica*, *55*(2), 145-161.

Shang, Q. H., Sato, T., Li, C., and Wu, X. C. (2016). New osteological information from a 'juvenile' specimen of *Yunguisaurus* (Sauropterygia; Pistosauroidea). *Palaeoworld*, *26*(3), 500-509.

Shang, Q. H., Wu, X. C., and Li, C. (2011). A new eosauropterygian from Middle Triassic of eastern Yunnan Province, southwestern China. *Veterbrate PalAsiatica*, *49*(2), 155-171.

Shang, Q. H., Wu, X. C., and Li, C. (2020). A New Ladinian Nothosauroid (Sauropterygia) from Fuyuan, Yunnan Province, China. *Journal of Vertebrate Paleontology*, e1789651.

Stankiewicz, B., Briggs, D., Michels, R., Collinson, M., Flannery, M., and Evershed, R. (2000). Alternative origin of aliphatic polymer in kerogen. *Geology*, *28*(7), 559-562.

Stein, K. and E. Prondvai (2014) Rethinking the nature of fibrolamellar bone: an integrative biological revision of sauropod plexiform bone formation. *Biological Reviews*, *89*, 24-47.

Stein, K., and Sander, P. M. (2009). Histological core drilling: a less destructive method for studying bone histology. In M. A. Brown, J. F. Kane, and W. G. Parker (Eds.), *Methods in Fossil Preparation: Proceedings of the First Annual Fossil Preparation and Collections Symposium*. Petrified Forest National Park. pp. 69-80.

Storrs, G. W. (1991). Anatomy and relationships of *Corosaurus alcovensis* (Diapsida: Sauropterygia) and the Triassic Alcova Limestone of Wyoming. *Bulletin of the Peabody Museum of Natural History*, *44*, 1-151.

Storrs, G. W. (1993). Function and phylogeny in sauropterygian (Diapsida) evolution. *American Journal of Science*, *293A*, 63-90.

Stubbs, T. L., and Benton, M. J. (2016). Ecomorphological diversifications of Mesozoic marine reptiles: the roles of ecological opportunity and extinction. *Paleobiology*, *42*(4), 547-573.

Sues, H. D., and Carroll, R. L. (1985). The pachypleurosaurid *Dactylosaurus schroederi* (Diapsida: Sauropterygia). *Canadian Journal of Earth Sciences*, *22*(11), 1602-1608.

Swofford, D. L. (2021). *PAUP: phylogenetic analysis using parsimony (and other methods)*, *version 4.0a. 169*. Sinauer Associates.

Tintori, A., and Renesto, S. (1990). A new *Lariosaurus* from the Kalkschieferzone (Uppermost Ladinian) of Valceresio (Varese, N. Italy). *Bollettino della Società Paleontologica Italiana*, *29*(3), 309-319.

Trillmich, K. G. and F. Trillmich (1986) Foraging strategies of the marine iguana, *Amblyrhynchus cristatus*. *Behavioral Ecology and Sociobiology*, 18, 259-266.

Trueman, C. N., and Tuross, N. (2002). Trace elements in recent and fossil bone apatite. *Reviews in Mineralogy and Geochemistry*, *48*, 489-521.

Trueman, C. N., Privat, K., and Field, J. (2008). Why do crystallinity values fail to predict the extent of diagenetic alteration of bone mineral? *Palaeogeography*, *Palaeoclimatology*, *Palaeoecology*, *266*(3-4), 160-167.

Tucker, A., C. Limpus, K. Mcdonald and H. Mccallum (2006) Growth dynamics of freshwater crocodiles (*Crocodylus johnstoni*) in the Lynd River, Queensland. *Australian Journal of Zoology*, 54, 409-415.

Wang, C. Y., Kang, P. Q., and Wang, Z. H. (1998). Conodont-based age of the *Keichousaurus hui* Yang, 1958. *Acta Micropalaeontologica Sinica*, *15*(2), 196-198. (in Chinese with English abstract)

Wang, X., Bachmann, G. H., Hans, H. D., Sander, P. M., Cuny, G., Chen, X., ... and Xu, G. (2008). The Late Triassic black shales of the Guanling area, Guizhou Province, south-west China: a unique marine reptile and pelagic crinoid fossil Lagerstätte. *Palaeontology*, *51*(1), 27-61.

Wang, X., Lu, H., Jiang, D. Y., Zhou, M., and Sun, Z. Y. (2019). A new specimen of *Yunguisaurus* (Reptilia; Sauropterygia) from the Ladinian (Middle Triassic) Zhuganpo Member, Falang Formation, Guizhou, China and the restudy of *Dingxiaosaurus*. *Palaeoworld*, *29*(1), 137-150.

Wen, Q. Q., Zhang, Q. Y., Min, X., Zhou, C. Y., Wen, W., Hu, S. X., and Huang J. Y. (2022). Characteristics of the newborns of *Keichousaurus hui*. (Reptilia Sauropterygia) from Xingyi Fauna (Ladinian, Middle Triassic), Guizhou Province. *Sedimentary Geology and Tethyan Geology*, *42*, 556-571. (in Chinese with English abstract)

Wen, W., Zhang, Q., Hu, S., Zhou, C., Huang, J., Ma, Z., and Min, X. (2020). Occurrence and Significance of Middle Triassic Luoping Biota from Luxi County, Yunnan Province. *Earth Science*, *45*(8), 3094-3103.

Wings, O. (2004). Authigenic minerals in fossil bones from the Mesozoic of England: poor correlation with depositional environments. *Palaeogeography*, *Palaeoclimatology*, *Palaeoecology*, *204*(3-4), 15-32.

Wintrich, T., Hayashi, S., Houssaye, A., Nakajima, Y., and Sander, P. M. (2017). A Triassic plesiosaurian skeleton and bone histology inform on evolution of a unique body plan. *Science Advances*, *3*(12), e1701144.

Wise, P. A., Vickaryous, M. K., and Russell, A. P. (2009). An embryonic staging table for in ovo development of *Eublepharis macularius*, the leopard gecko. *The Anatomical Record*, *292*(8), 1198-1212.

Witke, K., Göetze, J., Röessler, R., Dietrich, D., and Marx, G. (2004). Raman and cathodoluminescence spectroscopic investigations on Permian fossil wood from Chemnitz—a contribution to the study of the permineralisation process. *Spectrochimica Acta Part A: Molecular and Biomolecular Spectroscopy*, *60*(13), 2903-2912.

Wittmann, K. J., and Ariani, A. P. (1996). Some aspects of fluorite and vaterite precipitation in marine environments. *Marine Ecology*, *17*(1-3), 213-219.

Wopenka, B., and Pasteris, J. D. (2005). A mineralogical perspective on the apatite in bone. *Materials Science and Engineering: C*, *25*(2), 131-143.

Worley, N. E. (1976). Lithostratigraphical control of mineralization in the Blende Vein, Magpie Mine, Sheldon, near Bakewell, Derbyshire. *Proceedings of the Yorkshire Geological Society*, *41*(2), 95-106.

Wu, X. C., Cheng, Y. N., Li, C., Zhao, L. J., and Sato, T. (2011). New information on *Wumengosaurus delicatomandibularis* Jiang et al., 2008 (Diapsida: Sauropterygia), with a revision of the osteology and phylogeny of the taxon. *Journal of Vertebrate Paleontology*, *31*(1), 70-83.

Wyllie, P., Cox, K., and Biggar, G. (1962). The habit of apatite in synthetic systems and igneous rocks. *Journal of Petrology*, *3*(2), 238-243.

Xie, T., Zhou, C., Zhang, Q., Hu, S., Huang, J., Wen, W., and Cong, F. (2013). Zircon U-Pb age for the tuff before the Luoping Biota and its geological implication. *Geological Review*, *59*(1), 159-164.

Xing, L., Klein, H., Lockley, M. G., Wu, X. C., Benton, M. J., Zeng, R., & Romilio, A. (2020). Footprints of marine reptiles from the Middle Triassic (Anisian-Ladinian) Guanling Formation of Guizhou Province, southwestern China: The earliest evidence of synchronous style of swimming. *Palaeogeography, palaeoclimatology, palaeoecology, 558*, 109943.

Xu, G. H., Ren, Y., Zhao, L. J., Liao, J. L., and Feng, D. H. (2022). A long-tailed marine reptile from China provides new insights into the Middle Triassic pachypleurosaur radiation. *Scientific Reports*, *12*(1), 7396.

Xu, G. H., Shang, Q. H., Wang, W., Ren, Y., Lei, H., Liao, J. L., Zhao, L. J. and Li, C. (2023). A new long-snouted marine reptile from the Middle Triassic of China illuminates pachypleurosauroid evolution. *Scientific Reports*, *13*(1), 16.

Xue, Y. F., D. Y. Jiang, Z. Y. Sun, P. F. Yang and C. Ji (2015) New information on sexual dimorphism and allometric growth in *Keichousaurus hui*, a pachypleurosaur from the Middle Triassic of Guizhou, South China. *Acta Palaeontologica Polonica*, 32, 197-197.

Yin, C., Hao, W., Sun, Z., Sun, Y., and Jiang, D. (2014). New material of *Nothosaurus yangjuanensis* from the middle Anisian (middle Triassic) of Guizhou Province, Southwestern China. *Acta Scientiarum Naturalium Universitatis Pekinensis*, *50*(3), 467-475.

Young, C. C. (1958). On the new pachypleurosauroidea from Keichow, South-West China. *Veterbrate PalAsiatica*, *2*, 69-81.

Young, C. C. (1965). On the new nothosaurs from Hupeh and Kweichou, China. *Veterbrate PalAsiatica*, *9*(4), 315-356.

Zeng, X., Chen, X., Cheng, L., and Wang, J. (2013). Redefinition of the Zhuganpo Formation in the southest Yangtze platform. *Journal of Stratigraphy*, *37*(4), 479-484. (in Chinese with English abstract)

Zhang, Q. Y., Zhou, C. Y., Lv, T., Xie, T., Lou, X. Y., Liu, W., . . . Jiang, X. S. (2008). Discovery and significance of the Middle Triassic Anisian biota from Luoping, Yunnan Province. *Geological Review*, *54*(4), 523-526.

Zhang, Q., Zhou, C., Lu, T., Xie, T., Lou, X., Liu, W., . . . Zhao, L. (2009). A conodont-based Middle Triassic age assignment for the Luoping Biota of Yunnan, China. *Science in China Series D: Earth Sciences*, *52*(10), 1673.

Zhao, L. J., Li, C., Liu, J., and He, T. (2008). A new armored placodont from the Middle Triassic of Yunnan Province, southwestern China. *Veterbrate PalAsiatica*, *46*(3), 171-177.

Zhao, L. J., Sato, T., and Li, C. (2008). The most complete pistosauroid skeleton from the Triassic of Yunnan, China. *Acta Geologica Sinica-English Edition*, *82*(2), 283-286.

Zheng, Y., Xiao, W., and Zhao, G. (2013). Introduction to tectonics of China. *Gondwana Research*, *23*(4), 1189-1206.

Zheng, Z., Cui, X., Wang, D., Chen, Y., Bai, G., Li, J., and Liu, X. (2015). Review of the Metallogenic Regularity of Magnesite Deposits in China. *Acta Geologica Sinica-English Edition*, *89*(6), 1747-1761.

Zhou, C., Xie, T., Liu, S., Meng, F., Liu, W., Li, S., and Huang, X. (2021). *China Geological Survey: Geological Map Database of Xingyi County, Guizhou Province* (G48E018012) 1:50 000.

Zou, H., Li, M., Santosh, M., Zheng, D., Cao, H., Jiang, X., Chen, H., and Li, Z. (2022). Fault-controlled carbonate-hosted barite-fluorite mineral systems: The Shuanghe deposit, Yangtze Block, South China. *Gondwana Research*, *101*, 26-43.

Zou, X., Balini, M., Jiang, D., and Tintori, A. (2015a). Ammonoids from the Zhuganpo Member of the Falang Formation at Nimaigu and their relevance for dating the Xingyi fossil-Lagerstätte (Late Ladinian, Guizhou, China). *Rivista Italiana di Paleontologia e Stratigrafia*, *121*(1), 135-161.

Zou, X., Guo, W., Jiang, D., and Sun, Z. (2015b). Preliminary analysis of environment of fossils reservoir of Xingyi Fauna in Guizhou Province. *Acta Scientiarum Naturalium Universitatis Pekinensis*, *51*(3), 472-484.

Appendices

Appendix A1-A10

Li, Q., Liu, J., Klein, N., Nakajima, Y., and Sander, P. M. 2023. Puberty in a Mesozoic reptile. *Current Biology*, 33(14), 3011-3016 e3013. doi:10.1016/j.cub.2023.05.073.

Appendix B1-B32

Hu, Y. W., **Li, Q.**, and Liu, J. 2023 A new pachypleurosaur (Reptilia: Sauropterygia) from the Middle Triassic of southwestern China and its phylogenetic and biogeographic implications. Accepted by *Swiss journal of Palaeontology* in September 2023

Report

Current Biology

Puberty in a Mesozoic reptile

Graphical abstract

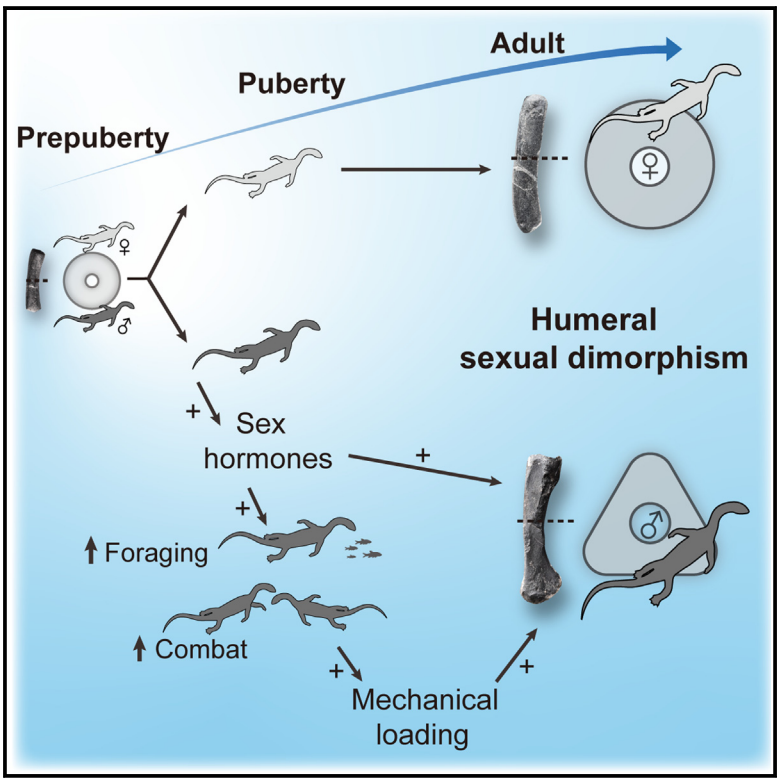

Highlights

- Puberty is recognized in a Triassic reptile called *Keichousaurus* by bone histology
- Shape change of male humeri in *Keichousaurus* starts from the onset of puberty
- Sex hormones may trigger puberty in *Keichousaurus*
- Loading regime during puberty can result in differential bone apposition in humeri

Authors

Qiang Li, Jun Liu, Nicole Klein, Yasuhisa Nakajima, P. Martin Sander

Correspondence

junliu@hfut.edu.cn

In brief

Li et al. report puberty for the first time in a fossil amniote. The bone thin sections show the onset of pubertal growth and reveal the development of sexually dimorphic features in a live-bearing marine reptile called *Keichousaurus* from the Triassic of South China.

Li et al., 2023, Current Biology *33*, 1–6
July 24, 2023
https://doi.org/10.1016/j.cub.2023.05.073

CellPress

Current Biology

CellPress

Report

Puberty in a Mesozoic reptile

Qiang Li,[1,2] Jun Liu,[1,2,5,*] Nicole Klein,[2] Yasuhisa Nakajima,[3] and P. Martin Sander[1,2,4]
[1]Division of Geology, School of Resources and Environmental Engineering, Hefei University of Technology, Hefei 230009, China
[2]Section Paleontology, Institute of Geosciences, University of Bonn, 53115 Bonn, Germany
[3]Department of Natural Sciences, Faculty of Science and Engineering, Tokyo City University, Tokyo 1588557, Japan
[4]The Dinosaur Institute, Natural History Museum of Los Angeles County, Los Angeles, CA 90007, USA
[5]Lead contact
*Correspondence: junliu@hfut.edu.cn
https://doi.org/10.1016/j.cub.2023.05.073

SUMMARY

The histology of bone can be preserved virtually unaltered for hundreds of millions of years in fossils from all environments and all vertebrate taxa, giving rise to the flourishing field of paleohistology.[1] The shafts of long bones are formed by the apposition of periosteal bone tissue, similar to the growth of wood, and preserve, an often cyclical, record of the growth of the individual and events in its life history. One such event is sexual maturation or puberty, during which hormonal changes transform the juvenile into a sexually mature adult. Puberty has been well studied in humans and some other living vertebrates. Here, we describe puberty in *Keichousaurus*, a small sexually dimorphic and live-bearing marine reptile from Middle Triassic rocks of SW China, about 240 million years old. Using a combination of bone histology and morphology, we detected puberty[2] as one of the four life stages (the others being fetus, juvenile, and adult). Adult *Keichousaurus* males have a more robust humerus than females, with pronounced muscle attachment sites and a triangular shaft cross section. Midshaft sections of the humeri of the males show the transition from the rounded juvenile cross section to the triangular adult cross section, as reflected in the contour of the growth marks. This shape change is produced by differential bone apposition of the periosteum, presumably triggered by sex hormones, as in humans,[3] and influenced by changes in loading regime during puberty. This is the first report of puberty in a fossil amniote.

RESULTS AND DISCUSSION

A prerequisite for detecting puberty is secondary sexual characteristics, which, however, have been difficult to detect in extinct reptiles from deep time.[4–6] An exception is the pachypleurosaur *Keichousaurus*, which is known from thousands of specimens, from fetus to large adult. In adults of several pachypleurosaur species, humerus shape is sexually dimorphic and sex determination based on humerus shape is well established.[5–8] The males have humeri with conspicuously expanded distal ends and well-developed deltoid crests as secondary sex characters. However, the exact function of these features is unknown.[4,6] Female humeri, on the other hand, retain the juvenile morphology into adulthood (Figure 1A). Note that the sex of juveniles cannot be determined this way because juveniles resemble females in morphology. A sexual size dimorphism is also found in *Keichousaurus*, as males are on average about 10% larger.[6]

To understand the transition from juvenile to adult during puberty, we histologically sampled (by coring at midshaft) 18 humeri, pertaining to 11 males, six females, and one isolated fetus of *Keichousaurus*. From the thin and polished sections of each specimen, we recorded bone tissue type, bone compactness, and age based on growth cycles and onset and end of puberty (STAR Methods; Figure S1).

Life history stages

Combining the diverse evidence from the analysis of the ontogenetic changes in histology, microanatomy, and compactness led us to recognize four distinct life history stages in *Keichousaurus hui*. These stages are (1) fetus, (2) juvenile, (3) puberty, and (4) adult. Stage 1, the fetus, is defined as from the onset of ossification to birth. There is no distinct neonatal line, but the size of 40 fetuses belonging to 12 pregnant females provides a lower bound of fetus maximum size.[9] Stage 2, the juvenile, is recognized as the period from birth to puberty and apparently only lasted 1 year. Stage 3, puberty, is recognized by the histological onset and conclusion of the midshaft shape change from round to triangular in the male during the second year. Stage 4, the adult stage, commences after puberty and continues to the end of the individual's life. Its record consists of increasingly narrower and less vascularized growth cycles of zones and annuli, grading into an external fundamental system in the oldest individual we studied.

Histological record of puberty

The humeral midshaft cross section of every specimen sampled, except for the fetus, shows a record of consecutive yearly growth cycles. The end of the first cycle is marked by a growth modulation[10] (Figure 1B), i.e., a decrease in bone fiber organization visible in cross-polarized light, whereas the

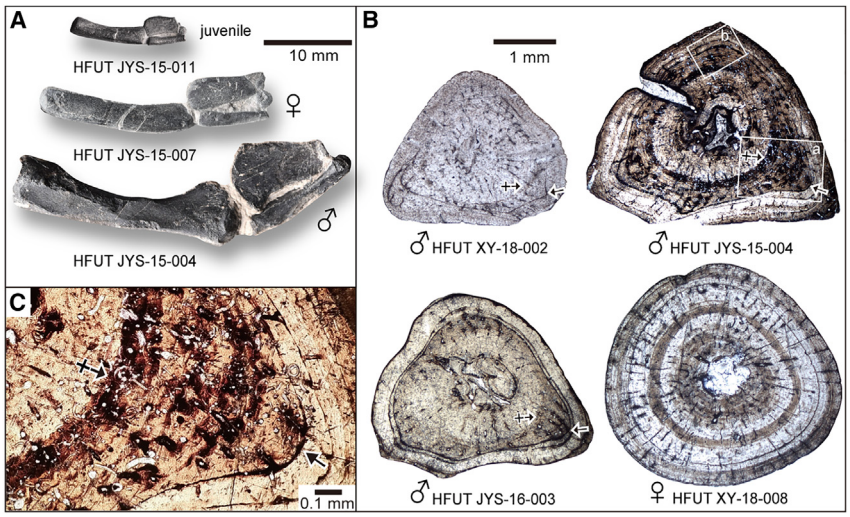

Figure 1. Fossil bone histology of the humerus midshaft revealing puberty and bone tissues in *Keichousaurus*

(A) Sexual dimorphism in *Keichousaurus* forelimbs with proximal ends to the left

(B) Entire shaft cross sections of *Keichousaurus*; all thin sections are dorsal side up. Arrows with "+" mark the onset of puberty; simple arrows indicate termination of puberty in the second year. Microscope photos in (B) and (C) are in normal light.

(C) Close up of the white-lined box "a" in (B) showing the shape change (between two arrows) of the humerus shaft during puberty in adult male HFUT JYS-15-004 by differential bone apposition.

second and all higher cycles end in an annulus (a thin layer of avascular lamellar bone). The slight differences in bone fiber arrangement between the modulation and the zones and annulus in the higher cycles were enhanced by diagenesis as color differentiation, with the less-organized fibers staining as a dark band (between arrows in Figures 1B and 1C). The modulation and annuli indicate the shape of the shaft at different ontogenetic stages. However, annuli have two different contours, rounded and triangular. All adult males have triangular contours, whereas those of the females are rounded (Figure 1B). All individuals start out with rounded contours, but during puberty the triangular contour develops from a rounded one in males. The triangular contour becomes more prominent in older males. Thus, bone histology reveals puberty in male *Keichousaurus*.

Histologically, this transformation is caused by the differential bone apposition around the contour, as can be observed in most male individuals. During the second growth cycle, local apposition rate increases at the anterior and posterior margins of the shaft and at the center of its dorsal surface, resulting in the formation of three ridges. The locally increased apposition is reflected by the higher porosity and less-ordered bone fibril arrangement compared with the areas between the ridges.

Growth curves and growth rate changes

To determine the growth rate before and after puberty, we constructed growth curves for five individuals (three males, two females) four years and older. We determined age in years by counting growth marks and increase in body size by measuring growth mark circumference because midshaft circumference closely correlates with body size in amniotes.[11] All individuals experienced fast growth in their first year. The growth rate remained high in their second year, during which males underwent puberty (Figure 2A; STAR Methods). Growth slowed down in the third year, indicating that sexual maturity was reached, with a shift of resource allocation from growth to reproduction. Presumably, females also underwent puberty in their second year of life, but direct morphological or histological evidence is lacking. In the largest male, the outermost complete annulus was formed in the eighth year (Figure 2B). The ever-closer spacing of the outer annuli indicates that this individual approached maximum body size, i.e., skeletal maturity.

Analysis of bone compactness also supports these conclusions (Figure 3). The primary compactness changes slightly during ontogeny (Figure 3), from juveniles (96.9%–98.9%) to puberty (97.1%–97.8%) to adults (98.4%–99.7%), and the lower bone compactness at puberty also indicates faster growth during this period. Because only three individuals are considered here, the low sample size may have biased these results.

Biology of *Keichousaurus* puberty

Sexually dimorphic features such as differences in body size may be ''foreshadowed'' in juvenile individuals of living species, but the distinct shape change in *Keichousaurus* humeri, underlain by localized differential bone apposition, is hypothesized to be associated with puberty because of the entire preserved growth record.

Secondary sex characters are usually related to combat and reproduction in amniotes, including extant squamates.[12,13] The dorsal ridges of *Keichousaurus* humeri are identified as attachment sites for the latissimus dorsi and triceps muscles, which serve in the abduction and extension of forelimbs.[14,15] The ventral deltopectoral crest is related to flexor muscles, such as the pectoralis, biceps brachii, and brachialis[14,16] (Figure 1A). These distinct ridges may indicate increased muscle attachments and mechanical load capacity of the forelimbs in male *Keichousaurus*.[17] This feature is probably related to reproduction behaviors, such as mating (e.g., with the forelimbs used in holding females during mating, like the amplexus of extant amphibians)[18] and combat between adult males, during which the male's skeleton encounters higher mechanical demands than the female's.[6] Potentially, the more muscular forelimb of the male could indicate increased foraging activity to support a more active lifestyle. Detailed myological reconstruction[16] and functional analysis of the pachypleurosaur forelimb and shoulder girdle will serve in testing hypotheses of reproduction-related function.

In mammals, sex hormones (both estrogens and androgens) have positive effects on periosteal expansion in male long bones.[3] In reptiles, testosterone affects bone growth during puberty[19,20] and increases activity levels in pubertal individuals[21] (which increases mechanical loads). Thus, the humeral

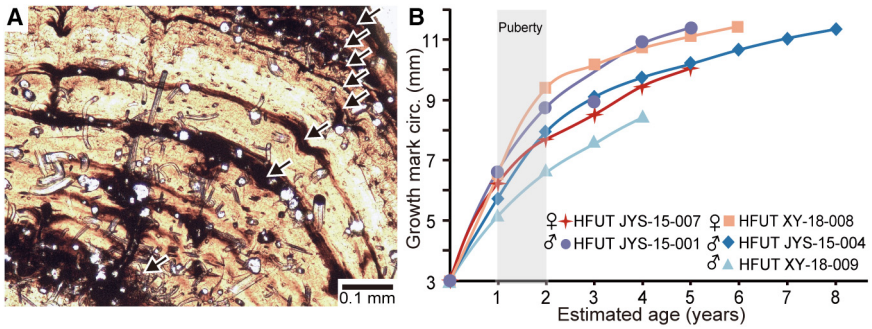

Figure 2. Growth marks and curves in *Keichousaurus*

(A) Close up of the white-lined box "b" in Figure 1B showing the humeral cortex of the largest and oldest sampled individual, HFUT JYS-15-004. Note the close spacing of the outer growth marks (arrows), indicating skeletal maturity.

(B) Growth curves of multiple individuals of *Keichousaurus*, plotting body size (proxy: humeral midshaft circumference) against age in years, derived from annual growth mark count. There is no apparent difference in growth trajectory between the sexes.

dimorphism developing during puberty by local differential periosteal expansion in *Keichousaurus* was probably caused by the combination of both sex steroid action internally and puberty-related behavior externally (Figure 4). Taking place during the second year of life, puberty came at an early age to *Keichousaurus*, as in other pachypleurosaurs and most reptiles of same size, presumably as an adaptation to strong predation pressure.[22,23]

Conclusions

Using bone histology, our study documents puberty in a fossil amniote for the first time. At the fetal and juvenile stages, *Keichousaurus* males and females followed a similar morphogenetic program, with even periosteal bone apposition. But then, presumably triggered by the combined effects of sex steroid regulation and the associated increase in mechanical loading, the male's morphogenetic program changed. Our work thus

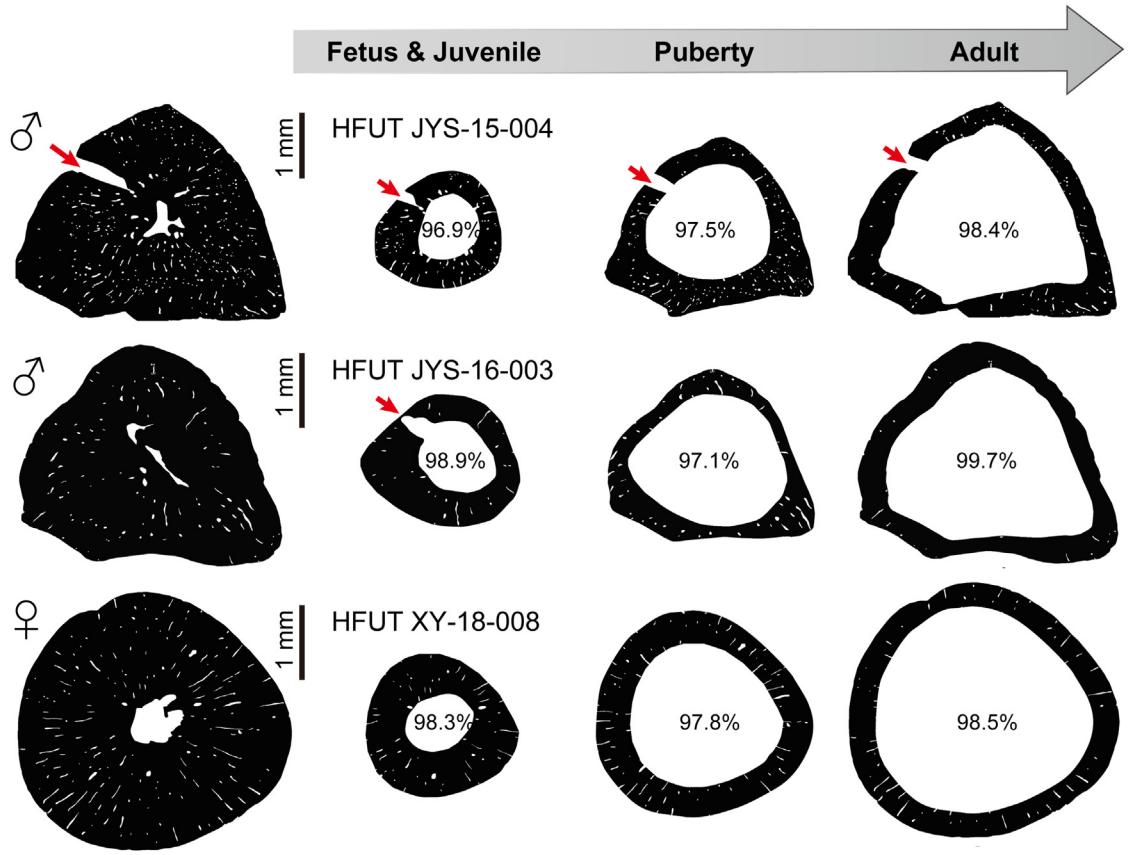

Figure 3. Graphic representation of the development of bone compactness of *Keichousaurus*

Bone compactness in two males and one female, graphically separated by ontogenetic stages (see STAR Methods section), from fetus to adult (see below for stage description). The first column shows the total cross sections of three individuals. The second column shows the fetal and juvenile stages of each individual. The third column represents the puberty of the two male individuals, during which sexual maturation occurs, as evidenced by the round inner margin and the triangular outer margin of this growth cycle. In the fourth column, the combined post-puberty cycles represent the adult stage to the end of the individual's life. The percent values in the figure represent bone compactness at each stage. Red arrows indicate nutrient canal, not included in porosity analysis.

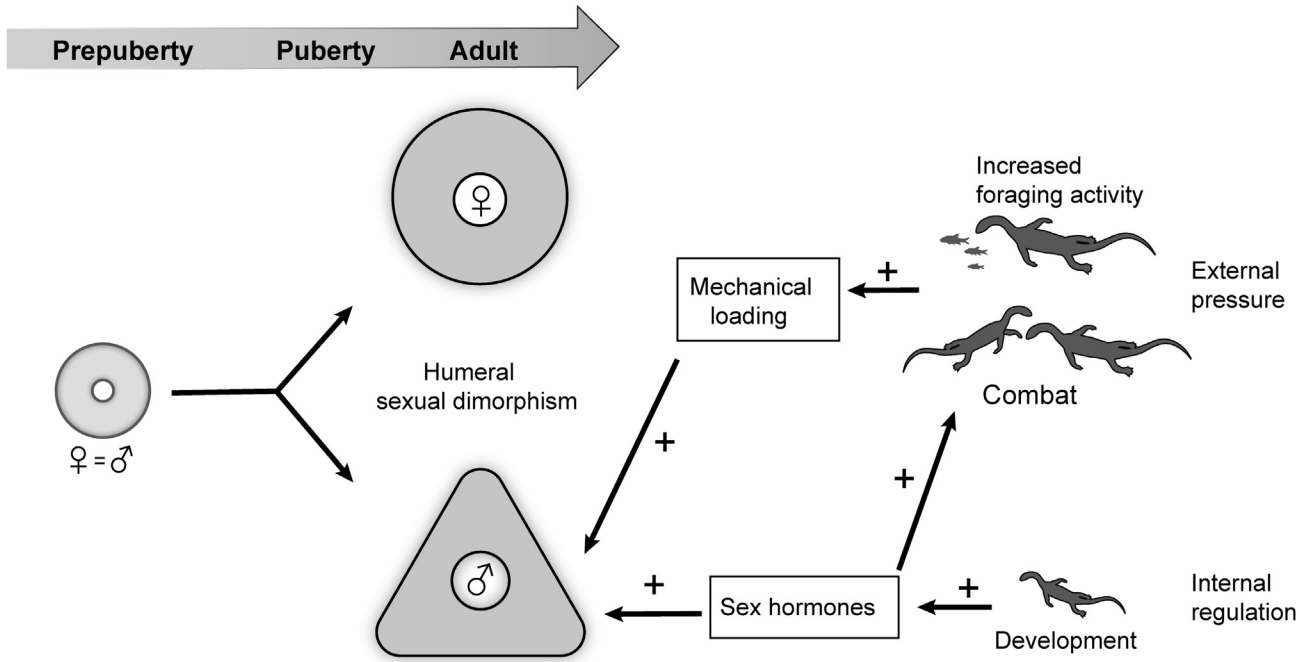

Figure 4. Cartoon showing the humeral sexual dimorphism in *Keichousaurus* males developed during puberty and the two major controlling factors

The shape change of humerus midshaft cross section results from differential local bone apposition rate, which is influenced by external stimulation (e.g., mechanical loading) and internal regulation of sex hormones. The external stimuli may be caused mainly by individual growth and reproduction-related behavior, such as increased foraging activity and combat between males. Internally, the secretion of sex hormones is regulated by an individual's sexual development during puberty.

offers a new perspective on morphogenesis and the evolution of sexual dimorphism in fossil vertebrates.

STAR★METHODS

Detailed methods are provided in the online version of this paper and include the following:

- KEY RESOURCES TABLE
- RESOURCE AVAILABILITY
  - Lead contact
  - Materials availability
  - Data and code availability
- EXPERIMENTAL MODEL AND SUBJECT DETAILS
- METHOD DETAILS
  - Fossil material
  - Sampling and thin-sectioning
  - Histological observation
  - Bone compactness analysis
  - Skeletochronology and growth analysis
- QUANTIFICATION AND STATISTICAL ANALYSIS
- ADDITIONAL RESOURCES

SUPPLEMENTAL INFORMATION

Supplemental information can be found online at https://doi.org/10.1016/j.cub.2023.05.073.

ACKNOWLEDGMENTS

We thank Olaf Dülfer (IGPB) for production of thin sections, Sudipta Kalita for discussion of the draft, and Alexandra Houssaye, Holly Woodward, and two anonymous reviewers for their helpful comments that improved the paper. This project was supported by the National Natural Science Foundation of China under grant numbers 42172026 and 41772003, the China Scholarship Council (201906690046), the Fundamental Research Funds for the Central Universities of China under grant number PA2020GDKC0022, and the Department of Natural Resources of Anhui Province under grant number 2021-g-2-16.

AUTHOR CONTRIBUTIONS

J.L., Y.N., and P.M.S. designed the study; Q.L., J.L., and P.M.S. made the drill cores and histological sections; Q.L., N.K., and P.M.S. performed the thin section observation; Q.L. prepared the figures; Q.L., J.L., and P.M.S. wrote the manuscript; all authors reviewed the final draft of the manuscript.

DECLARATION OF INTERESTS

The authors declare no competing interests.

INCLUSION AND DIVERSITY

We support inclusive, diverse, and equitable conduct of research.

Received: January 31, 2023
Revised: April 23, 2023
Accepted: May 31, 2023
Published: June 22, 2023

REFERENCES

1. Buffrénil, V.de., Ricqlès, A.J.de., Zylberberg, L., and Padian, K. (2021). Vertebrate Skeletal Histology and Paleohistology (CRC Press).
2. Ball, G.F., and Wade, J. (2013). The value of comparative approaches to our understanding of puberty as illustrated by investigations in birds and reptiles. Horm. Behav. *64*, 211–214. https://doi.org/10.1016/j.yhbeh.2013.05.002.
3. Callewaert, F., Sinnesael, M., Gielen, E., Boonen, S., and Vanderschueren, D. (2010). Skeletal sexual dimorphism: relative contribution of sex steroids, growth hormone-insulin-like growth factor-I (GH-IGF-I) and mechanical loading. J. Endocrinol. *207*, 127–134. https://doi.org/10.1677/JOE-10-0209.
4. Sander, P.M. (1989). The pachypleurosaurids (Reptilia: Nothosauria) from the Middle Triassic of Monte San Giorgio (Switzerland) with the description of a new species. Philos. Trans. R. Soc. Lond. B *325*, 561–666.
5. Cheng, Y.N., Wu, X.C., and Ji, Q. (2004). Triassic marine reptiles gave birth to live young. Nature *432*, 383–386. https://doi.org/10.1038/nature03050.
6. Motani, R., Jiang, D.Y., Rieppel, O., Xue, Y.F., and Tintori, A. (2015). Adult sex ratio, sexual dimorphism and sexual selection in a Mesozoic reptile. Proc. R. Soc. B. *282*, 20151658. https://doi.org/10.1098/rspb.2015.1658.
7. Lin, K., and Rieppel, O. (1998). In Functional Morphology and Ontogeny of *Keichousaurus hui* (Reptilia, Sauropterygia), *39* (Field Museum of Natural History), pp. 1–35.
8. Cheng, Y.N., Holmes, R., Wu, X.C., and Alfonso, N. (2009). Sexual dimorphism and life history of *Keichousaurus hui* (Reptilia: Sauropterygia). J. Vertebr. Paleontol. *29*, 401–408. https://doi.org/10.1671/039.029.0230.
9. Wen, Q.Q., Zhang, Q.Y., Min, X., Zhou, C.Y., Wen, W., Hu, S.X., and Huang, J.Y. (2022). Characteristics of the newborns of Keichousaurus hui. (Reptilia Sauropterygia) from Xingyi Fauna (Ladinian, Middle Triassic), Guizhou Province. Sediment. Geol. Tethyan Geol. *42*, 556–571. https://doi.org/10.19826/j.cnki.1009-3850.2022.04007.
10. Ricqlès, A.J.de (1983). Cyclical growth in the long limb bones of a sauropod dinosaur. Acta Palaeontol. Pol. *28*, 225–232.
11. Campione, N.E., and Evans, D.C. (2012). A universal scaling relationship between body mass and proximal limb bone dimensions in quadrupedal terrestrial tetrapods. BMC Biol. *10*, 60. https://doi.org/10.1186/1741-7007-10-60.
12. Cox, R.M., Skelly, S.L., and John-Alder, H.B. (2003). A comparative test of adaptive hypotheses for sexual size dimorphism in lizards. Evolution *57*, 1653–1669. https://doi.org/10.1111/j.0014-3820.2003.tb00371.x.
13. Cox, R.M., Butler, M., and John-Alder, H. (2007). The evolution of sexual size dimorphism in reptiles. In Sex, Size, and Gender Roles: Evolutionary Studies of Sexual Size Dimorphism, D.J. Fairbarin, W.U. Blanckenhorn, and T. Szekely, eds. (Oxford University Press), pp. 38–49.
14. Meers, M.B. (2003). Crocodylian forelimb musculature and its relevance to Archosauria. Anat. Rec. *274A*, 891–916. https://doi.org/10.1002/ar.a.10097.
15. Abdala, V., Manzano, A.S., and Herrel, A. (2008). The distal forelimb musculature in aquatic and terrestrial turtles: phylogeny or environmental constraints? J. Anat. *213*, 159–172. https://doi.org/10.1111/j.1469-7580.2008.00937.x.
16. Krahl, A., Lipphaus, A., Sander, M.P., Maffucci, F., Hochscheid, S., and Witzel, U. (2020). Humerus osteology, myology, and finite element structure analysis of Cheloniidae. Anat. Rec. *303*, 2177–2191. https://doi.org/10.1002/ar.24311.
17. Benjamin, M., Toumi, H., Ralphs, J.R., Bydder, G., Best, T.M., and Milz, S. (2006). Where tendons and ligaments meet bone: attachment sites ('entheses') in relation to exercise and/or mechanical load. J. Anat. *208*, 471–490. https://doi.org/10.1111/j.1469-7580.2006.00540.x.
18. Carvajal-Castro, J.D., López-Aguirre, Y., Ospina-L, A.M., Santos, J.C., Rojas, B., and Vargas-Salinas, F. (2020). Much more than a clasp: evolutionary patterns of amplexus diversity in anurans. Biol. J. Linn. Soc. Lond. *129*, 652–663. https://doi.org/10.1093/biolinnean/blaa009.
19. Evans, L.T. (1951). Effects of male hormone upon the tail of the slider turtle, *Pseudemys scripta troostii*. Science *114*, 277–279.
20. Cox, C.L., Hanninen, A.F., Reedy, A.M., and Cox, R.M. (2015). Female anoles retain responsiveness to testosterone despite the evolution of androgen-mediated sexual dimorphism. Funct. Ecol. *29*, 758–767. https://doi.org/10.1111/1365-2435.12383.
21. Lovern, M.B., McNabb, F.M.A., and Jenssen, T.A. (2001). Developmental effects of testosterone on behavior in male and female green anoles (*Anolis carolinensis*). Horm. Behav. *39*, 131–143. https://doi.org/10.1006/hbeh.2000.1637.
22. Klein, N., and Griebeler, E.M. (2018). Growth patterns, sexual dimorphism, and maturation modeled in Pachypleurosauria from Middle Triassic of central Europe (Diapsida: Sauropterygia). Foss. Rec. *21*, 137–157. https://doi.org/10.5194/fr-21-137-2018.
23. Scharf, I., Feldman, A., Novosolov, M., Pincheira-Donoso, D., Das, I., Böhm, M., Uetz, P., Torres-Carvajal, O., Bauer, A., Roll, U., et al. (2015). Late bloomers and baby boomers: ecological drivers of longevity in squamates and the tuatara. Glob. Ecol. Biogeogr. *24*, 396–405.
24. Zeng, X.W., Chen, X.H., Cheng, L., and Wang, J.P. (2013). Redefinition of the Zhuganpo Formation in the southest Yangtze platform. J. Stratigr. *37*, 479–484.
25. Zou, X.D., Balini, M., Jiang, D.Y., Tintori, A., Sun, Z.Y., and Sun, Y.L. (2015). Ammonoids from the Zhuganpo Member of the Falang Formation at Nimaigu and their relevance for dating the Xingyi Fossil-Lagerstaette (Late Ladinian, Guizhou, China). Riv. Ital. Paleontol. Stratigr. *121*, 135–161. https://doi.org/10.13130/2039-4942/6511.
26. Benton, M.J., Zhang, Q.Y., Hu, S.X., Chen, Z.Q., Wen, W., Liu, J., Huang, J.Y., Zhou, C.Y., Xie, T., Tong, J.N., et al. (2013). Exceptional vertebrate biotas from the Triassic of China, and the expansion of marine ecosystems after the Permo-Triassic mass extinction. Earth Sci. Rev. *125*, 199–243. https://doi.org/10.1016/j.earscirev.2013.05.014.
27. Wang, C.Y., Kang, P.Q., and Wang, Z.H. (1998). Conodont based age of the *Keichousaurus hui* Yang, 1958. Acta Micropalaeontol. Sin. *15*, 196–198. https://doi.org/10.1088/0256-307X/15/12/010.
28. Li, Z.G., Sun, Z.Y., Jiang, D.Y., and Ji, C. (2016). LA-ICP-MS zircon U-Pb age of the fossil layer of Triassic Xingyi fauna from Xingyi, Guizhou, and its significance. Geol. Rev. *62*, 779–790. https://doi.org/10.16509/j.georeview.2016.03.018.
29. Sander, P.M. (1988). A fossil reptile embryo from the Middle Triassic of the Alps. Science *239*, 780–783. https://doi.org/10.1126/science.3340859.
30. Francillon-Vieillot H., Buffrénil V.d.e., Castanet J., Géraudie J., Meunier F.J., Sire J.Y., Zylberberg L., Ricqlès A.J. de Microstructure and mineralization of vertebrate skeletal tissues. In: Carter J.G., editor. Biomineralization: Patterns and Evolutionary Trends, Volume 1. Van Nostrand Reinhold; 1990. p. 471–530.
31. Sander, P.M. (1990). Skeletochronology in the small Triassic reptile *Neusticosaurus*. Ann. Sci. Nat. Zool. *11*, 213–217.
32. Stein, K., and Sander, P.M. (2009). Histological core drilling: a less destructive method for studying bone histology. In Methods in Fossil Preparation: Proceedings of the First Annual Fossil Preparation and Collections Symposium, M.A. Brown, J.F. Kane, and W.G. Parker, eds. (Petrified Forest National Park), pp. 69–80.
33. Nakajima, Y., Hirayama, R., and Endo, H. (2014). Turtle humeral microanatomy and its relationship to lifestyle. Biol. J. Linn. Soc. Lond. *112*, 719–734. https://doi.org/10.1111/bij.12336.
34. Sander, P.M. (2000). Longbone histology of the Tendaguru sauropods: implications for growth and biology. Paleobiology *26*, 466–488. https://doi.org/10.1666/0094-8373(2000)026<0466:LHOTTS>2.0.CO;2.

35. Lamm, E.T. (2013). Preparation and sectioning of specimens. In Bone Histology of Fossil Tetrapods: Advancing Methods, Analysis, and Interpretation, K. Padian, and E.T. Lamm, eds. (University of California Press), pp. 55–160.

36. Avens, L., Goshe, L.R., Zug, G.R., Balazs, G.H., Benson, S.R., and Harris, H. (2020). Regional comparison of leatherback sea turtle maturation attributes and reproductive longevity. Mar. Biol. *167*, 1–12. https://doi.org/10.1007/s00227-019-3617-y.

37. Anderson, J.F., Hall-Martin, A., and Russell, D.A. (1985). Long-bone circumference and weight in mammals, birds and dinosaurs. J. Zool. *207*, 53–61.

STAR★METHODS

KEY RESOURCES TABLE

REAGENT or RESOURCE	SOURCE	IDENTIFIER
Chemicals, peptides, and recombinant proteins		
Synthetic resin	Huntsman, Cambridge	Araldite 2020 A/B
Deposited data		
Measurement of sampled specimens	This study	N/A
Software and algorithms		
Image Access easyLab 7.0	Leica	https://www.leica-microsystem.com
Adobe Illustrator CS6	Adobe	https://www.adobe.com
Excel	Microsoft	https://www.microsoft.com/en-us/
Bw-counter	Peter Göddertz	peter.goeddertz@uni-bonn.de

RESOURCE AVAILABILITY

Lead contact

Further information and requests for resources and reagents should be directed to and will be fulfilled by the lead contact, Jun Liu (junliu@hfut.edu.cn).

Materials availability

The fossil skeletons and the thin section samples produced from them are accessioned and accessible at the Geological Museum of Hefei University of Technology (HFUT), Hefei, China.

Data and code availability

All data used in the study are included in this publication with the supplemental information and are publicly available as of the date of publication. The present research did not use any updated codes.

EXPERIMENTAL MODEL AND SUBJECT DETAILS

The experimental subjects of this study comprise 18 fossil specimens belonging to the pachypleurosaurian species *Keichousaurus hui*. All *K. hui* specimens were sectioned for bone histology. The skeletochronology and growth analysis of *K. hui* are based on thin section observation of HFUT JYS-15-001, HFUT JYS-15-004, HFUT JYS-15-007, HFUT XY-18-008, and HFUT XY-18-009. The bone compactness analysis was based on thin section observation and calculation of HFUT JYS-15-003, HFUT JYS-15-004, and HFUT XY-18-008. All specimens and histological thin sections are stored at the Geological Museum of Hefei University of Technology, China.

METHOD DETAILS

Fossil material

We histologically sampled 18 individuals of the small pachypleurosaur (Eosauropterygia) *Keichousaurus hui*, a species which is known from thousands of individuals, allowing detailed paleobiological insights.[5–9] The specimens are all well-articulated, and half of them are complete skeletons. In the other half, incompleteness is due to collecting. All specimens are kept in the Geological Museum of Hefei University of Technology. Of the 18 individuals, 11 are males, six are females, and one is an isolated fetus. Sex determination of the males was based on the previously proposed principles.[4,5,7]

The 18 histologically sampled individuals of *Keichousaurus hui* are from the Xingyi Fauna, which is stratigraphically situated in the lower part of the Zhuganpo Formation.[24] An alternative term used in the literature is Zhuganpo Member of the Falang Formation.[25] The age of Xingyi Fauna is controversial[26] and an earliest late Triassic (Carnian) age was supported by conodont biostratigraphy.[27] The accuracy of this biostratigraphic age was questioned by Zou et al.,[25] however. Instead, a late Middle Triassic (late Ladinian) age is suggested by ammonite biostratigraphy[25] and, recently, by U-Pb dating of single zircon grains, which gave an age of 240.8 ± 1.8 Ma.[28] The fossils studied by us come from three different localities, i.e., Fuyuan County in Yunnan Province and Xingyi and Longguang counties in Guizhou Province.

We assembled a series of linear measurements from the sampled *Keichousaurus* fossils (Figure S1 [Overview of histological images of specimens sampled in the HFUT collection, organized by sex and size]). Our data includes sex identification of 18 specimens and measurements of humeral length and standard length.[4]

Sampling and thin-sectioning

All specimens examined here were prepared with pneumatic tools before photography. Measurements of the humerus and standard length[4,29] (i.e., length of the four last presacral centra) were taken with calipers (Figure S1). Based on previous studies of the histology of the long bones of tetrapods, the middle of the humerus is the ideal location to observe the microstructure and complete growth record.[30–32] This is because the appositional cortical growth record is most complete in the mid-shaft region. Therefore, histological sections with a clear growth record and minimal remodelling are most likely found in the middle of the humerus shaft (see Figure 1 of reference[32]). Some sections show the nutrient canal (NC) oriented towards the section center, justifying the sampling position as appropriate for preserving the complete periosteal bone growth record (Figure S1). The others did not contain an obvious NC in the section, but these sections are not regarded as ineligible for analysis because the NC may extend perpendicular or obliquely to the longitudinal axis of a long bone depending on the individual.[33]

We obtained the histological samples of the humerus at midshaft by core drilling,[32,34] choosing a coring bit with an internal diameter (10 mm) greater than the humerus shaft diameter. Since all humeri used for sampling were still partially embedded in sediment, the midshaft area was stabilized by a layer of cyanoacrylate glue before drilling. The electric drill with a low speed and low torque was mounted in a drill press, and the specimen was securely placed on a sandbag that rested on the base of the drill press. Water was poured into a circular plasticine dam surrounding the drill site to protect the drill bit from overheating and guarantee constant lubrication during drilling. The cores contain the entire midshaft of the humeri and the sediment matrix supporting it.

Thin sections were prepared using standard petrographic methods.[35] Cores were embedded in synthetic resin (Araldite 2020 A/B, Huntsman, Cambridge) and then sectioned along the previously marked transverse plane. One half of the core was then glued with Araldite onto a glass slide, cut down to a few millimetres thickness with a rock saw, and ground to a thickness of 80 to 30 μm, depending on the degree of diagenetic staining. Finally, a cover slip was placed on top of the slide with UV glue to provide better optical contrast and protection. The other half of the embedded core was prepared into a polished section.

Histological observation

Thin sections were examined with a Leica® DM750P polarizing microscope in transmitted light mode. Polished sections were observed with the same microscope in incident-light bright-field mode to reveal histological details, especially in the very dark sections. Photomicrographs were acquired with a digital microscope camera (Leica® DFC420) and Image Access easyLab 7.0 software. Annual growth marks and bone tissue modulations were traced on the photomicrographs using Adobe Illustrator CS6. Terminology follows the most recent review.[1]

The periosteal bone tissue in the primary growth cycle of *Keichousaurus* pertains to the lamellar-zonal bone type, growing in a cyclical fashion. The second and all higher cycles consist of a zone of poorly vascularized parallel-fibered bone matrix followed by an annulus of lamellar bone. Radial vascular canals developed to reach the outer bone surface in all specimens. There is no fundamental change in tissue type with ontogeny. In comparison with *Neusticosaurus* and *Dactylosaurus*,[22] the bone tissue of *Keichousaurus* is similarly organized. However, the growth rate of *K. hui* is lower than that of *Anarosaurus* because *Anarosaurus* shows incipient fibrolamellar bone.[22] In *Keichousaurus*, the medullary region is sharply set off from the periosteal domain. The medullary region is filled with endosteal bone, and no calcified cartilage is left.

The end of the first cycle is not marked by an annulus but by a more subtle kind of growth mark termed a "modulation"[10]. Although a neonatal line generally is not visible, we interpret the modulation as the end of the first postnatal growth cycle. We base this interpretation on the relatively large size of the animal attained at the end of the first cycle. Because there are many gravid females of *Keichousaurus hui*,[5,9] size at birth is known from many individuals.[9] These fetuses are too small for the modulation at the end of the first growth cycle to represent birth.

The second cycle, beginning after the modulation (between the arrows in Figure 1A), then, is the cycle during which puberty happens and the change in contour takes place, indicating change in humerus morphology. Histologically, this transformation is caused by the differential rates of local bone apposition. The less ordered parallel-fibred bone tissue on the lateroventral side of male humeri documents an increase in apposition rate, resulting in the formation of the posteroventral crest, and likely indicates puberty (Figure 1C). The transformation is visible in all male individuals, even if no actual annulus or LAG (lines of arrested growth) was formed at the end of the second cycle.

In modern reptiles and amphibians, the completion of reproductive maturation is often marked by a decrease in LAG spacing and an increase in organization of bone fibres.[36] In our *Keichousaurus* sample, often a clear color change from dark to lighter after the second cycle reflects more ordered bone fibre arrangement after puberty because the more ordered fibres were less affected by diagenetic staining. This stained bone tissue is also found close to the medullary cavity, vessels and outermost cortex. The dark stain results from the relatively open, or more porous structure that more easily incorporates kerogen from the surrounding sediment during fossilization.

Bone compactness analysis

To study bone porosity variation through ontogeny, the three best thin sections, i.e., those without diagenetic staining and damage caused by thin sectioning, were used. The additional requirement was that the sections preserve at least four growth marks (Figure 3). Individual growth stages were graphically separated with Photoshop on the photomicrographs of the sections in the .jpg file format via observation of the bone modulation and annuli by using the polarizing microscope. The .jpg image files were converted to black and white images, with pores assigned the white colour. Bone porosity was then calculated using the pixel-counting software 'bw-counter' developed by Peter Göddertz at the Institute of Geoscience of the University of Bonn (© Peter Göddertz, IGPB). We excluded the area of the nutrient canal, which is seen in some of the sections, from porosity analysis. Bone compactness is the inverse of porosity and expressed in percent where bone tissue covers a given area.

Skeletochronology and growth analysis

In pachypleurosaurs, skeletochronology is based on growth marks observed in thin sections and polished sections with transmitted and reflected light, respectively.[31,34] Given the peculiar preservation and dark staining of some specimens with poor histological information, polish lines[34] were also used for skeletochronology. Polish lines were defined by Sander[34] as subtle growth lines only visible in polished sections. Due to the subtle differences in hardness of the bone matrix, the harder region (usually meaning slow growth or LAGs) stands out. They also appear brighter than the softer parts after polishing. The polish lines usually are followed by an abrupt softening of the bone, leading to an abrupt decrease in the reflectance in bright-field illumination in an incident light compound microscope or a stereo microscope.

We used minimum shaft circumference (MSC) as the body size proxy in the skeletochronology analysis. MSC increases in proportion to long bone length (and thus total body length). MSC is also linked to local bone apposition rates, which are closely related to an increase in bone length and body mass in mammals, birds, and dinosaurs.[37] The relationship between MSC and body mass was tested in lizards, which have body shapes similar to pachypleurosaurs.[9] Thus, each growth mark laid down during ontogeny is associated with a particular MSC (i.e., the circumference of the growth mark) and, thus, with a specific body mass.[9] We did not estimate body mass, however, since we were only interested in relative growth.

We also considered the shape changes of the humeral cross sections in the males. Usually, the midshaft of long bones is oval or round. The triangular-shaped cross sections in adult males of *Keichousaurus* deviate from the normal situation and may cause an overestimation of the growth rate. Thus, the shape change during puberty will theoretically lead to a more prominent decline in growth rates in males than in females. However, this is not borne out by the data (Figure 2A) and may have been hidden by individual variation. In addition, the overestimation caused by greater MSCs in triangular cross section contours becomes more prominent in the outer annuli (because their shape is closer to a triangle which increases error) than inner ones. Despite this bias, the higher growth rate during puberty than after puberty still remains (Figure 2B).

To obtain the growth curves for *Keichousaurus hui* in Figure 2B, the five thin sections with the most complete growth record were analyzed, representing three males and two females. All of these have more than four full and clear annual growth marks in the form of annuli. In Figure 2B, the number of annuli is the independent variable, and the dependent variable is the outer circumference of each annulus, i.e., the MSC at the end of each growth cycle. Due to a sharp boundary between the medullary region and the cortex of these five individuals, the growth mark record is complete, as no remodeling has destroyed the inner cortex. Thus, the growth curves do not need to be corrected for any missing annuli.

In *Keichousaurus*, closer spacing of the annuli, which indicates slower growth after the second cycle, also supports that the males are sexually mature at this stage. The slow-down in growth reflects a change in resource allocation from growth to reproduction with sexual maturity. As indicated by ever more closely spaced growth marks, body size increase slowed down until the maximum body size was reached, although only one individual (HFUT JYS-15-004) shows this in our sample (Figure 2A). In fact, in this individual, growth cycles become so closely spaced as to representing an external fundamental system.

QUANTIFICATION AND STATISTICAL ANALYSIS

This study used no statistical analysis.

ADDITIONAL RESOURCES

There is no additional resource to report besides that in the above resource availability section.

Appendix B

A new pachypleurosaur (Reptilia: Sauropterygia) from the Middle Triassic of southwestern China and its phylogenetic and biogeographic implications

Yi-Wei Hu[1], Qiang Li[1,2], Jun Liu[1*]

[1] School of Resources and Environmental Engineering, Hefei University of Technology, Hefei 230009, China. [2] Institute of Geosciences, University of Bonn, Bonn 53115, Germany

[*]Correspondence: junliu@hfut.edu.cn

Abstract

After the devastating Permo-Triassic Mass Extinction, several new groups of large reptilian predators invaded the sea in the early part of the Triassic. Among these predators, sauropterygians, consisting of placodonts, pachypleurosaurs, nothosaurs and pistosaurs (including the iconic plesiosaurs), displayed the greatest diversity at both the generic and species levels, and persisted from the Early Triassic to the Late Cretaceous. Here we report a new species of Pachypleurosauria, *Dianmeisaurus mutaensis* sp. nov., from a recently discovered Lagerstätte in the Upper Member of the Anisian Guanling Formation. The only known specimen of the new species was collected from a quarry near Muta village, Luxi County, Yunnan Province, South China. Our new phylogenetic analysis based on a novel data matrix recovered the new taxon as a sister group to *Dianmeisaurus gracilis* – a small pachypleurosaur from the Middle Triassic Luoping biota. The new phylogenetic analysis also collapsed the monophyly of the traditionally recognized Eusauropterygia. Pistosauroidea, *Majiashanosaurus*, and *Hanosaurus* comprise the consecutive sister groups to a new clade including Pachypleurosauria and Nothosauroidea. A monophyletic Pachypleurosauria, within which the clade consisting of *Dianmeisaurus* and *Panzhousaurus* occupies the basal-most position, is recovered by this study. The clade consisting of *Dawazisaurus* and *Dianopachysaurus* forms the sister group to the remaining pachypleurosaurs included in this study. Since *Dianmeisaurus*, *Panzhousaurus*, *Dawazisaurus*, and *Dianopachysaurus* are all

exclusively known from South China, our study provides further evidence to the hypothesis that pachypleurosaurs had a palaeobiogeographic origin in the eastern Tethys.

Keywords: marine reptiles, Pachypleurosauria, *Dianmeisaurus*, phylogeny, palaeobiogeographic origin

Introduction

The Sauropterygia is the most flourishing clade among Mesozoic marine reptiles in terms of species diversity, and includes the iconic Plesiosauria from the Jurassic and Cretaceous and the stem-group Placodontia and Eosauropterygia from the Triassic (Kelley et al., 2014; Li & Liu, 2020; Motani, 2009; Rieppel, 2000; Stubbs & Benton, 2016). Eosauropterygians were traditionally divided into three groups, the Pachypleurosauria, the Nothosauroidea, and the Pistosauroidea (Rieppel, 2000). This traditional view holds that a monophyletic Pachypleurosauria comprises the sister group to the clade Eusauropterygia consisting of Nothosauroidea and Pistosauroidea (Lin et al., 2021; Liu et al., 2011; Neenan et al., 2013; Rieppel, 2000).

Since the review by Rieppel (2000), many new genera of basal eosauropterygians have been described from the Triassic of China and Europe (Cheng et al., 2006; Cheng et al., 2012; Cheng et al., 2016; Dalla Vecchia, 2006; de Miguel Chaves et al., 2018; Jiang et al., 2019; Jiang et al., 2008; Klein et al., 2022; Liu et al., 2011; Ma et al., 2015; Marquez-Aliaga et al., 2019; Renesto et al., 2014; Shang et al., 2020; Shang & Li, 2015; Shang et al., 2011; Xu et al., 2022; Xu et al., 2023), which has complicated eosauropterygian interrelationships. Holmes et al. (2008) restudied *Keichousaurus hui* and questioned the monophyly of Pachypleurosauria for the first time, which has been supported by several later studies (e.g., Cheng et al., 2012; Cheng et al., 2016; Jiang et al., 2014; Marquez-Aliaga et al., 2019; Shang et al., 2011; Shang & Li, 2015; Shang et al., 2017; Wu et al., 2011). Their results also showed the collapse of a monophyletic Eusauropterygia clade, which was supported by some independent studies (e.g., Li &

Liu, 2020; Liu et al., 2021; Neenan et al., 2013; Xu et al., 2022, 2023), although these studies recognized a monophyletic Pachypleurosauria. The study by Ma et al. (2015) supported the collapse of a monophyletic Pachypleurosauria, but still recognized a monophyletic Eusauropterygia clade instead. This finding was also supported by some other studies (e.g., Liu et al., 2015; Shang et al., 2020; Jiang et al., 2019).

Although the above-mentioned new Triassic basal eosauropterygian taxa have been well described, the phylogenetic analysis associated with the description of these new taxa primarily relied on slightly expanded data matrices that originated from Rieppel et al. (2002). Thus, the morphological information provided by comparative studies of these new materials of basal eosauropterygians still needs to be incorporated to examine the phylogenetic interrelationships of eosauropterygians. Additionally, the palaeobiogeographic origin of Pachypleurosauria is still controversial (Klein et al., 2022; Liu et al., 2011; Renesto et al., 2014; Rieppel, 1999a; Rieppel & Lin, 1995; Xu et al., 2023). Pachypleurosaurs have been reported in both the western Tethys (the Germanic Basin, Alpine Triassic, and Iberian Peninsula) (e.g., Čerňanský et al., 2018; de Miguel Chaves et al., 2020; Klein et al., 2022; Renesto et al., 2014; Rieppel, 1989; Sander, 1989; Sues & Carroll, 1985) and the eastern Tethys (South China and Myanmar) (e.g., Liu et al., 2011; San et al., 2019; Shang & Li, 2015; Jiang et al., 2019). Rieppel and Lin (1995) proposed an eastern Tethys origin of pachypleurosaurs based on the phylogenetic result that shows *Keichousaurus* from China forms the sister group of all European pachypleurosaurs. This hypothesis was supported by Liu et al. (2011) and Renesto et al. (2014). However, the earliest known pachypleurosaur is *Dactylosaurus* from the early Anisian of the Germanic Basin (Rieppel & Hagdorn, 1997). Thus, the palaeobiogeographic origin of pachypleurosaurs is more complex than previously believed and needs to be reassessed (Klein et al., 2022).

In this paper, we report a new species of Pachypleurosauria from Yunnan Province, China, represented by the part and counterpart of a single individual. The new specimen shares several synapomorphies with *Dianmeisaurus gracilis*, but also presents several

unique characteristics meriting the status of a new species. In addition to describing the new species in detail, we also aim to clarify the phylogenetic interrelationships of eosauropterygians by incorporating the morphological information from the recently described basal eosauropterygian taxa and discuss the palaeobiogeographic origin of pachypleurosaurs.

Materials and methods

The new specimen described here was collected from the Upper Member of the Anisian Guanling Formation in an abandoned quarry that is about one km northwest of Muta village, Luxi County, Yunnan Province (Fig. 1). The skeleton was split into two parts during collection and prepared with pneumatic tools and needles in the palaeontological lab of HFUT. The data matrix for the phylogenetic analysis was produced using the software Mesquite Version 3.6. The data matrix comprises 203 characters, of which 179 are from Li and Liu (2020), 17 from Lin et al. (2021), three from Klein et al. (2022), and four are new characters. Published character codings were carefully checked, and several errors were corrected (the character list and data matrix are given in Supplementary Data 1 and 2, respectively). Cladistic analysis was performed using the software PAUP Version 4.0a169 for Windows (Swofford, 2021). Heuristic search (ADDSEQ = RANDOM, NREPS = 1000, HOLD = 100, with other settings default) was performed to acquire the most parsimonious trees. Bootstrap support values were estimated by 1000 replicates and other settings were default. Measurements were collected using digital callipers and are provided in Table 1.

Appendix B

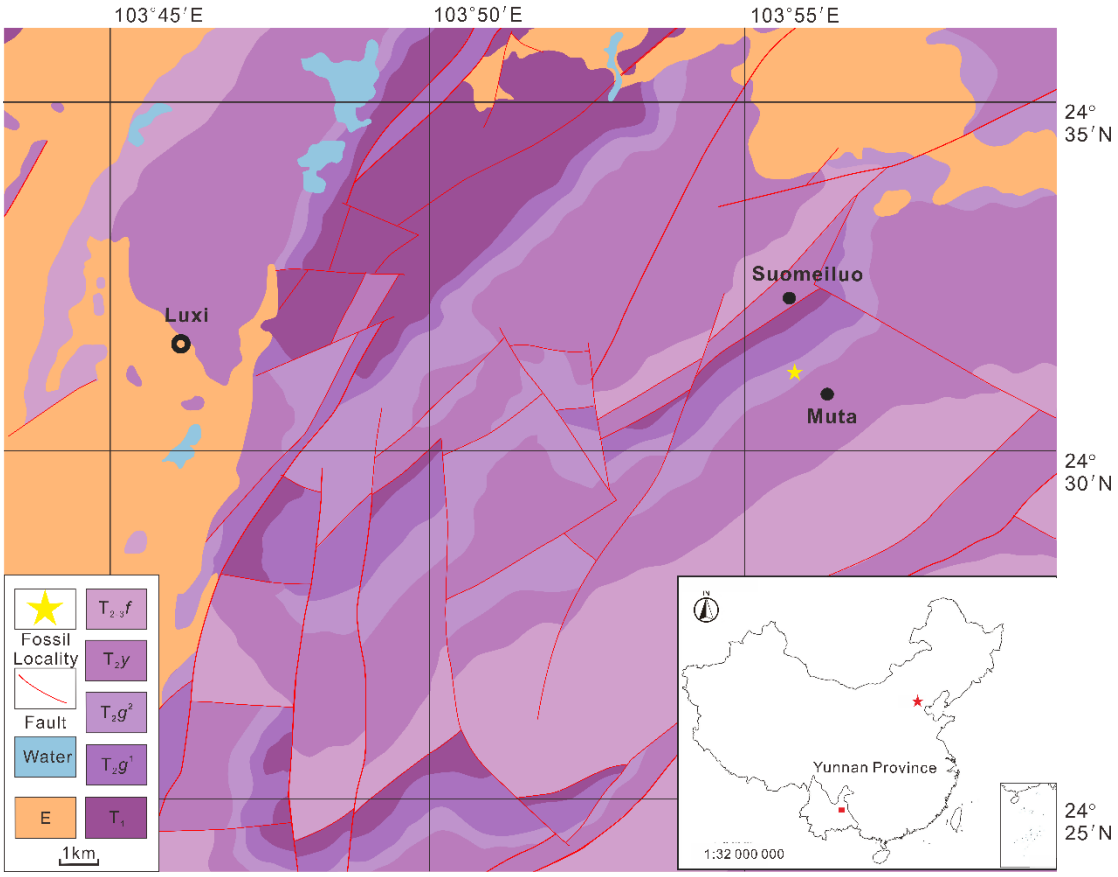

Figure 1. The geologic map showing the quarry where *Dianmeisaurus mutaensis* sp. nov. (HFUT MT-21-08-001) was discovered (updated after Hu & Liu, 2022). Abbreviations: E, Palaeogene; T_{2-3}f, Falang Formation, Ladinian-Carnian, Middle-Late Triassic; T_2y, Yangliujing Formation, Anisian-Ladinian, Middle Triassic; T_2g^2, Upper Member of Guanling Formation, Anisian, Middle Triassic; T_2g^1, Lower Member of Guanling Formation, Anisian, Middle Triassic; T_1, Lower Triassic.

Systematic palaeontology

Sauropterygia Owen, 1860

Eosauropterygia Rieppel, 1994

Pachypleurosauria Nopcsa, 1928

Dianmeisaurus Shang & Li, 2015

Revised diagnosis

Postfrontal with a distinct constriction behind the orbit (also present in *Anarosaurus*, *Honghesaurus*, and *Prosantosaurus*); distal end of sacral ribs distinctly expanded (also present in *Diandongosaurus* and *Qianxisaurus*); interorbital septum extremely narrowed and distinctly shorter than the distance between external nares (a synapomorphy of *Dianmeisaurus*); skull table with deeply concave posterior margin (also present in *Dawazisaurus* and *Diandongosaurus*).

***Dianmeisaurus mutaensis* sp. nov.**

Holotype

HFUT MT-21-08-001, a complete and articulated skeleton exposed in dorsal view (part and counterpart).

Ontogenetic evaluation

There are currently three known specimens of *Dianmeisaurus*, among which HFUT MT-21-08-001 represents the smallest individual with a total body length of 99.2 mm. It is much smaller than the two published specimens of *Dianmeisaurus gracilis* (315 mm for the holotype, see Shang & Li, 2015; 250 mm for IVPP V 17054, see Shang et al., 2017). Several morphological characters indicate that HFUT MT-21-08-001 is skeletally immature. First, the skull is poorly ossified. The skull has fontanelles, which generally indicates that the individual is at an early ontogenetic stage (Lin & Rieppel, 1998; Piñeiro et al., 2012; Rieppel, 1992a, 1992b; Rieppel, 1993a; Wise et al., 2009). Secondly, the distal end of the humeri is incompletely ossified since the entepicondylar groove is still present. The entepicondylar groove starts close and turns into a foramen when the individual becomes more mature (Currie & Carroll, 1984; Sander, 1989). Thirdly, among the carpals and tarsals of HFUT MT-21-08-001, only the astragalus is ossified, also indicating an early ontogenetic stage of the individual (Fröbisch, 2008;

Rieppel, 1992b; Sander, 1989). All these lines of evidence strongly support the conclusion that HFUT MT-21-08-001 is skeletally immature.

Type Locality

Muta Village, Luxi County, Yunnan Province, China.

Type Horizon

Upper Member of Guanling Formation, Anisian, Middle Triassic.

Etymology

Named after Muta village where the holotype was collected.

Diagnosis

A pachypleurosaur with following autapomorphies among pachypleurosaurs: 23 cervical vertebrae, 20 dorsal vertebrae, and two sacral vertebrae; postfrontal extending posteriorly to a level beyond the middle of parietal; last dorsal rib stout and shorter than the first sacral rib; phalangeal formula of manus and pes 2-3-4-4-2 and 1-2-3-4-3 respectively. In addition to the above mentioned autapomorphies, *Dianmeisaurus mutaensis* also differs from *D. gracilis* in the following morphological characters: maxilla enters the external naris; anterior process of the frontal does not extend beyond

the anterior margin of the orbit; postfrontal excluded from the upper temporal fenestra; coronoid process absent.

Figure 2. The holotype of *Dianmeisaurus mutaensis* sp. nov. (HFUT MT-21-08-001). A. the skeleton in dorsal view; B, the counterpart of A (natural mold). Scale bars equal 1 cm.

Description

The skeleton, embedded in the dark-grey micritic limestone, consists of a part and its counterpart. The specimen is well-preserved, with a total length of 99.2 mm. Adjacent to the specimen, there are scattered limb and rib bones from other individual(s), but the limited information available prevents further identification.

Skull

The skull of HFUT MT-21-08-001 is dorsoventrally compressed and slightly distorted (Fig. 3). The surface of the dermatocranial bones shows weak sculpturing. The preorbital region of the skull is slightly shorter than the postorbital region. The snout is very short and round anteriorly. The occipital portion is plate-like without an occipital crest.

Appendix B

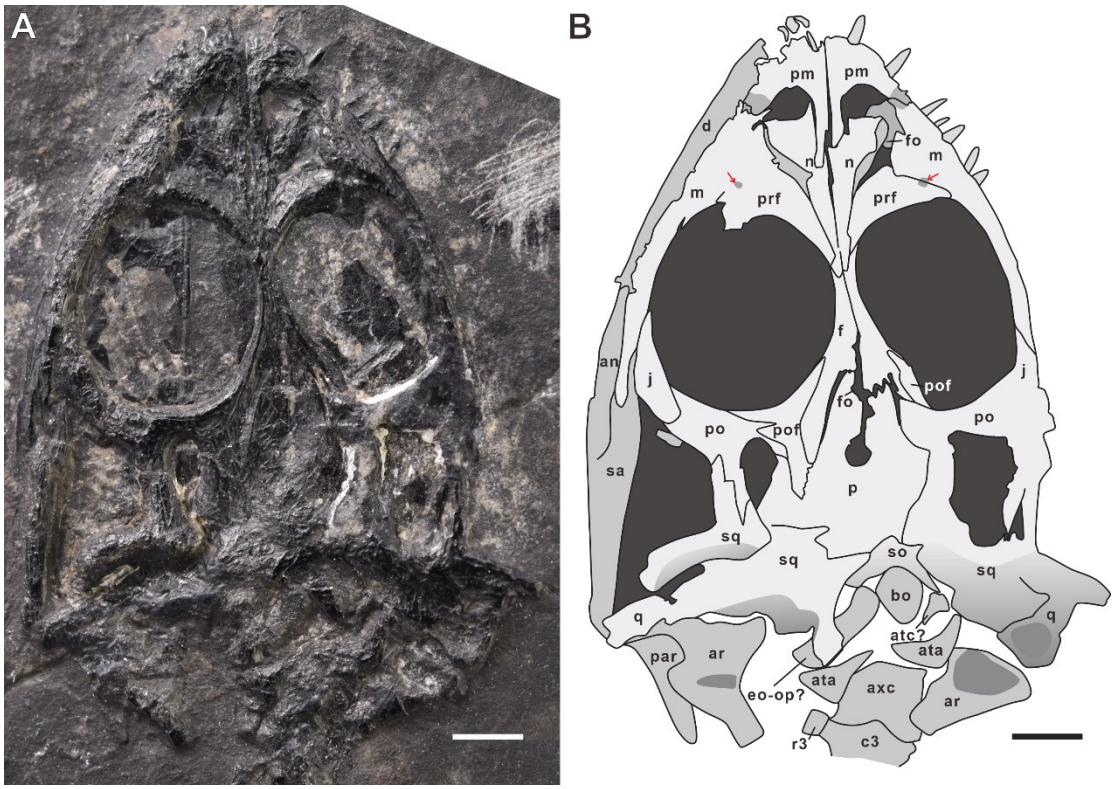

Figure 3. The skull of *Dianmeisaurus mutaensis* sp. nov. (HFUT MT-21-08-001). A. photo; B, interpreted drawing. Abbreviations: an, angular; ar, articular; ata, atlas arch; atc, atlas centrum; axc, axial centrum; bo, basioccipital; c3, 3rd cervical centrum; d, dentary; eo-op, exoccipital-opisthotic complex; f, frontal; fo, fontanelle; j, jugal; m, maxilla; n, nasal; p, parietal; par, prearticular; pm, premaxilla; po, postorbital; pof, postfrontal; prf, prefrontal; q, quadrate; r3, 3rd cervical rib; sa, surangular; so, supraoccipital; sq, squamosal. The red arrow marks the pit on the premaxilla-maxilla suture. Scale bars equal 1 mm.

Table 1. Measurements of *Dianmeisaurus mutaensis* sp. nov. (HFUT MT-21-08-001).

MEASUREMENT	**VALUE (MM)**
Body length	99.2
Condylobasal skull length	10.7
Length of skull (to posterior margin of the parietal	9.3
Maximum width of the skull	8.2

Appendix B

Diameter of right external naris (longitudinal×transverse)	0.5×0.8
Minimum width between external nares	0.5
Diameter of right orbit (longitudinal×transverse)	3.8×3.3
Minimum width between orbits	0.3
Diameter of pineal foramen	0.3
Distance from snout tip to anterior margin of external naris	0.9
Distance from snout tip to anterior margin of orbit (preorbital region)	3.0
Minimum distance between external naris and orbit (length from the posterior margin of the external naris to the anterior margin of the orbit)	1.6
Distance from snout tip to anterior margin of upper temporal fenestra	7.0
Minimum distance between orbit and upper temporal fenestra (minimum width of the postorbital arch)	0.4
Distance from posterior margin of orbit to the posterolateral end of the squamosal (postorbital region)	3.4
Length of right humerus	4.7
Proximal width of right humerus	1.4
Distal width of right humerus	1.5
Minimal width of right humerus	0.9
Length of left ulna	2.6
Length of left radius	3.0
Proximal width of left ulna	0.7
Distal width of left ulna	0.6
Proximal width of left radius	0.8
Distal width of left radius	0.5
Length of left femur	6.6
Proximal width of left femur	1.6
Distal length of left femur	1.1

Minimal width of left femur	0.9
Length of right tibia	3.2
Minimal width of right tibia	0.5
Length of right fibula	3.0
Minimal width of right tibia	1.0

The paired premaxillae constitute the short snout in front of the external nares and the anterior margin of the external nares. The posterodorsal processes of the premaxilla extend backward along the midline, separating the anterior part of the nasal. Each posterolateral process of the premaxilla contacts the maxilla around the lateral margin of the external naris, where the snout constriction is absent as in most pachypleurosaurs (Rieppel, 2000), but a depression is developed.

The maxilla forms the anterolateral margin of the orbit. The anterior process of the maxilla runs into the lateral corner of the external naris where it contacts the premaxilla. Dorsally, the ascending process of the maxilla is wedged between the nasal anteromedially and the prefrontal posteromedially. It almost reaches the level of the midpoint of the anterior margin of the orbit. A small pit is located at the maxilla-prefrontal suture, which is close to the anterolateral corner of the orbit. The posterior process of the maxilla abuts the lateral margin of the jugal and reaches the posterior margin of the orbit.

The external naris is located anteriorly, quite close to the tip of the snout, as is also the case in *Dianmeisaurus gracilis* and *Panzhousaurus* (Jiang et al., 2019). The length from the tip of the snout to the anterior margin of the external naris divided by the condylobasal skull length is 0.08. The longitudinal diameter of the external naris is less than its transverse diameter and the longitudinal diameter of the orbit. The lateral corner of the external naris shows an acute angle.

A pair of roughly triangular nasal bones meet along the midline, with the contact length comprising 3/4 of the total nasal length. Anteriorly, the nasal forms the posterior and part of the dorsal margin of the external naris. Anterodorsally, the

paired nasals embrace the posterior processes of the premaxillae. Anterolaterally, the nasals are not well ossified, leaving an open gap with the maxilla and prefrontal. This gap is interpreted as a morphological feature related to the early ontogenetic stage of the specimen, i.e. a fontanelle. The posterior processes of the nasal separate the posterior processes of the prefrontal and taper backward to overlie the frontal, almost reaching the midpoint of the medial margin of the orbit, which is an autapomorphy of the species. The surface of the nasal shows a few deep pits.

The circular orbit is large, about twice longer than the upper temporal fenestra. The interorbital septum is extremely narrow. The minimum width of the interorbital septum is distinctly shorter than the minimum distance between the external nares, a synapomorphy of *Dianmeisaurus*. The prefrontal forms the anterodorsal margin of the orbit. Laterally, the prefrontal contacts the maxilla. The posterior process of the prefrontal meets the frontal. The paired frontals form the dorsal margin of the orbit. The anterior process of the frontal almost extends to the midpoint of the medial margin of the orbit, which is convergently present in *Dianopachysaurus* among pachypleurosaurs (Liu et al., 2011). The anterior process of the frontal in other pachypleurosaurs extends very close to or beyond the anterior margin of the orbit (e.g., Cheng et al., 2016; Klein et al., 2022; Shang et al., 2011; Jiang et al., 2019; Xu et al., 2022). The well-developed posterolateral processes of the frontals are widely separated from the upper temporal fenestra and enter between the postfrontal and parietal.

The postfrontal forms the posterodorsal margin of the orbit. It has a roughly triradiate shape. The lateral margin of the postfrontal is distinctly constricted, which is also present in *Dianmeisaurus gracilis*, *Anarosaurus*, *Honghesaurus*, and *Prosantosaurus* among pachypleurosaurs (Klein, 2009; Klein et al., 2022; Shang et al., 2017; Xu et al., 2022). The postfrontal is separated from the upper temporal fenestra by the postorbital and parietal, which is otherwise only seen in *Honghesaurus* (Xu et al., 2022) among pachypleurosaurs. The posterior process of the postfrontal is embraced by the parietal

and extends beyond the midpoint of the skull table, a synapomorphy shared with *Panzhousaurus* (Jiang et al., 2019) among pachypleurosaurs.

The postorbital defines the lateral and the entire anterior margin of the upper temporal fenestra. The lateral process of the postorbital contacts the jugal. The dorsal process of the postorbital narrowly meets the parietal, separating the postfrontal from the upper temporal fenestra. The posterior process of the postorbital contacts the squamosal with an interdigitated suture.

The boomerang-shaped jugal constitutes the posterolateral corner of the orbit. The ventral margin of the jugal contacts the maxilla. The posterodorsal process of the jugal covers the postorbital, being separated from the squamosal by the postorbital.

The parietals are partly fused. A distinct suture is present in front of the pineal foramen, dividing the paired parietals, but the parietal is fully fused behind the pineal foramen. The parietal is very broad. Anteriorly, the interdigitated parietal-frontal suture is located anterior to the posterior margin of the orbit. A large unossified gap between the frontal and parietal indicates the existence of another fontanelle. Laterally, the parietal constitutes the posterodorsal margin of the upper temporal fenestra. Posteriorly, the parietal contacts the squamosal and the supraoccipital. The circular pineal foramen is in the middle of the parietal table.

Due to the postmortem alteration, the right upper temporal fenestra is completely covered by the right squamosal, and the left fenestra is incomplete. Even so, it is conclusive that the upper temporal fenestra is distinctly shorter than the orbit.

The large squamosal is irregular in shape due to its postmortem alteration. The forked anterior process of the squamosal forms half of the supratemporal arch. The lateral process of the squamosal caps the quadrate. Medially, the squamosal contacts the dorsal margin of the supraoccipital.

The quadrate is partially covered by the squamosal. The condylar portion of the left quadrate is exposed in lateral view. The quadrate shows a concave region on the right side of the skull.

The supraoccipital is exposed horizontally without a medial crest. The supraoccipital contacts the parietal anteriorly with a V-shaped suture and the squamosal laterally. Posteriorly, it meets the exoccipital-opisthotic complex. The basioccipital is located at the same level as the mandibular articulations.

The relationships between bones of the lower jaw are indeterminate due to the poor preservation of the exposed surface. However, a coronoid process is certainly absent, which is different when compared to *Dianmeisaurus gracilis*, *Diandongosaurus* and *Keichousaurus* (Holmes et al., 2008; Shang et al., 2011; Shang et al., 2017). The dentary extends posteriorly to the midpoint of the orbit and contacts the angular. Medially, the angular meets the surangular. Both of them contribute to the lateral and dorsal margins of the lower jaw. The articular shows a distinct trough in dorsal view, forming the dorsal part of the well-develop retroarticular process. The prearticular is disarticulated from the articular and constitutes the floor of the retroarticular process.

The dentition of the right side is better preserved than the dentition of the left side. Thus, the following description is based on the dentition of the right side. All teeth have a pointed apex. Two premaxillary teeth are visible and are similar in size. No premaxillary and maxillary fangs are present. Five maxillary teeth are visible, of which the second is distinctly smaller than the others, likely because it represents a replacement tooth.

Postcranial skeleton

Vertebrae

HFUT MT-21-08-001 comprises 23 cervical vertebrae, 20 dorsal vertebrae, only two sacral vertebrae, and at least 40 caudal vertebrae (Fig. 2). All zygapophyses are pachyostotic and no intercentra are present. The atlas is dislocated and covered by the basioccipital. Two triangular atlas arches are disarticulated and well exposed (Fig. 3). The cervical vertebrae have low neural spines. The neural spines of the dorsal region

are also low, and there is no elongated transverse process on the dorsal region. The caudal vertebrae become smaller posteriorly.

Ribs

The ribs are slender (Fig. 2). The distal end of the dorsal rib becomes flat and slightly expanded. The first dorsal rib is almost twice as long as the last cervical rib. The last (20^{th}) dorsal rib is short and robust. It is shorter than the sacral ribs and all other dorsal ribs, which represents an autapomorphy of the species among Pachypleurosauria. The distal end of last dorsal rib shows an expansion that is slightly more obvious than the distal expansion of other dorsal ribs. However, the last dorsal ribs are too short to articulate with the ilium and do not extend toward the ilium. Additionally, there is no evidence of dislocation for the last dorsal ribs (Fig. 6). So they can not be sacral ribs, but at the best be called transitional ribs (Romer, 1956). The left side of the sacral ribs are completely exposed (Fig. 6). The distal end of the sacral ribs is slightly expanded. The slender caudal ribs all taper to a point. The first caudal rib extends perpendicularly to the body axis. The third caudal rib is the longest among all caudal ribs. From the third caudal rib to the sixth, the length of the caudal rib is reducing gradually. The 1^{st}-6^{th} caudal ribs of this specimen are prominent. In *Dianmeisaurus gracilis*, the 1^{st}-9^{th} caudal ribs are prominent, while in *Panzhousaurus*, prominent caudal ribs are present on 1^{st}-11^{th} caudal vertebrae.

Pectoral girdle

Among the pectoral girdle elements (Fig. 4), the interclavicle and coracoid are completely covered by ribs and vertebrae. The left scapula is exposed in the lateral view, while the right scapula is exposed in the medial view. As in all other sauropterygians (Klein et al., 2022; Rieppel, 2000), the posterior margin of the clavicle is connected to the medial surface of scapula, a synapomorphy of sauropterygians. The posteriorly directed dorsal wing of the scapula is rod-like and tapers to a blunt tip, a synapomorphy of eosauropterygians (Rieppel, 2000).

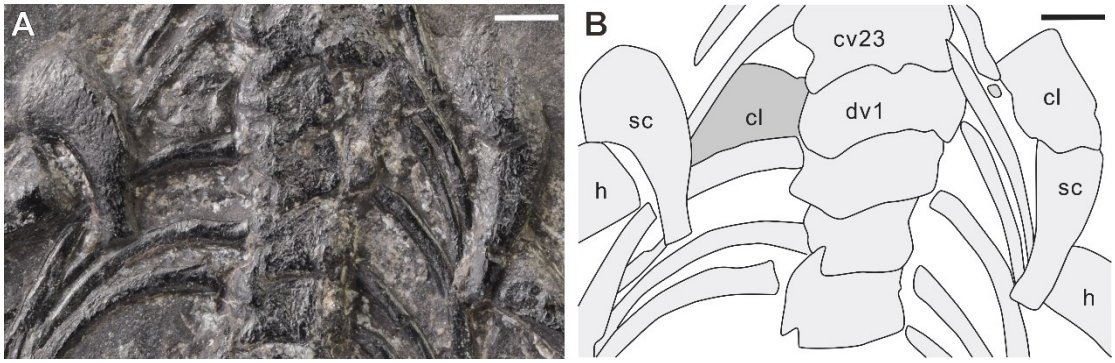

Figure 4. Pectoral region of *Dianmeisaurus mutaensis* sp. nov. (HFUT MT-21-08-001). A. photo; B, interpreted drawing. Abbreviations: cl, clavicle; cv23, 23rd cervical vertebra; dv1, 1st dorsal vertebra; h, humerus; sc, scapula. Scale bars equal 1 mm.

Forelimb

The right forelimb is preserved completely (Fig. 5). The humerus is curved as in all sauropterygians. Owing to the weakly developed deltopectoral crest, the preaxial margin of the humerus is slightly angulated. The distal end of the humerus is slightly broadened. Due to its early ontogenetic stage, an entepicondylar groove can be seen in this specimen, instead of the entepicondylar foramen (Sander, 1989). The ulna is shorter than the radius. The preaxial margin of the ulna is smoothly concave. Both ends of the ulna are slightly expanded. The radius is straight, with its proximal part slightly wider than the distal end. The proximal end and mid-shaft of the radius are approximately as broad as those of the ulna.

No carpal element is ossified. Metacarpal 1 is distinctly shorter and stouter than metacarpals 2- 4, of which metacarpal 3 is the longest. The phalangeal elements are tightly connected. The phalangeal formula of the manus is 2-3-4-4-2.

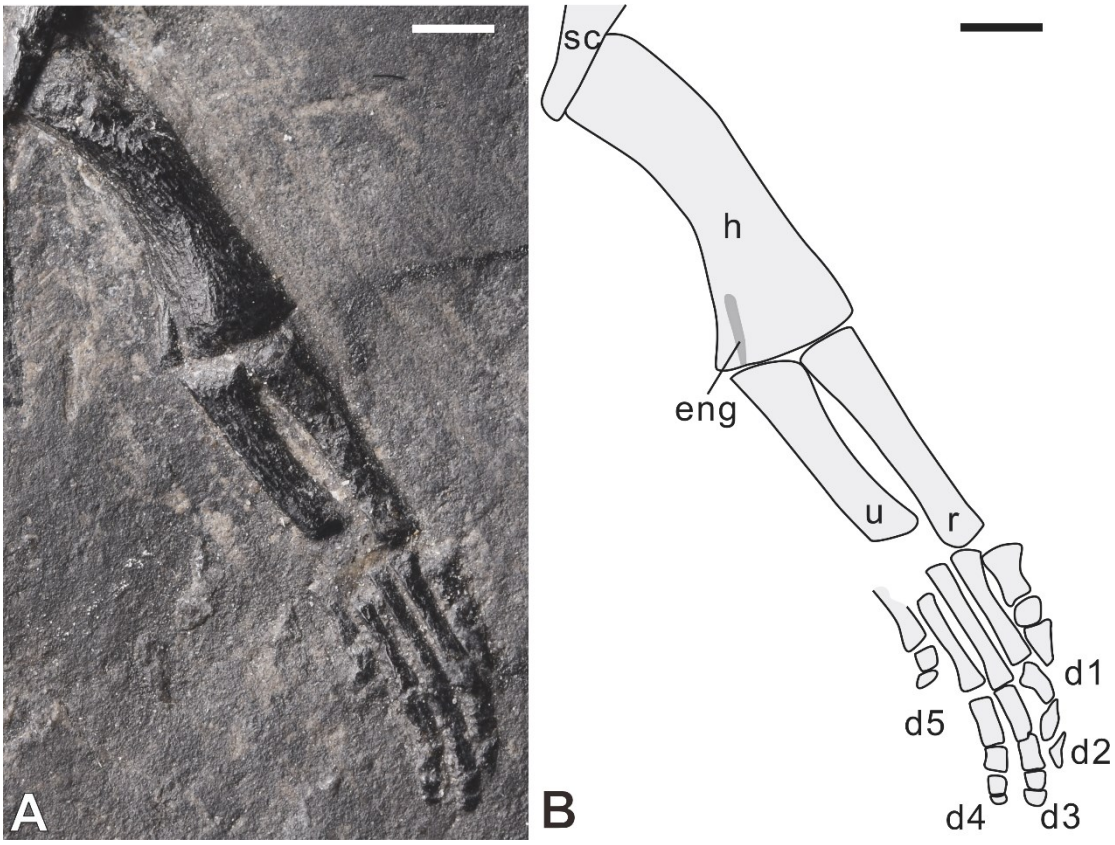

Figure 5. Right forelimb of *Dianmeisaurus mutaensis* sp. nov. (HFUT MT-21-08-001). A. photo; B, interpreted drawing. Abbreviations: d, digit; eng, entepicondylar groove; h, humerus; r, radius; sc, scapula; u, ulna. Scale bars equal 1 mm.

Pelvic girdle

The pelvic girdle is partially exposed in dorsal view (Fig. 6). The dorsal blade of the ilium is reduced to a simple stub. The pubis and ischium are flat bones, thickened dorsoventrally at the lateral margin. The ischium shows the concave postaxial margin.

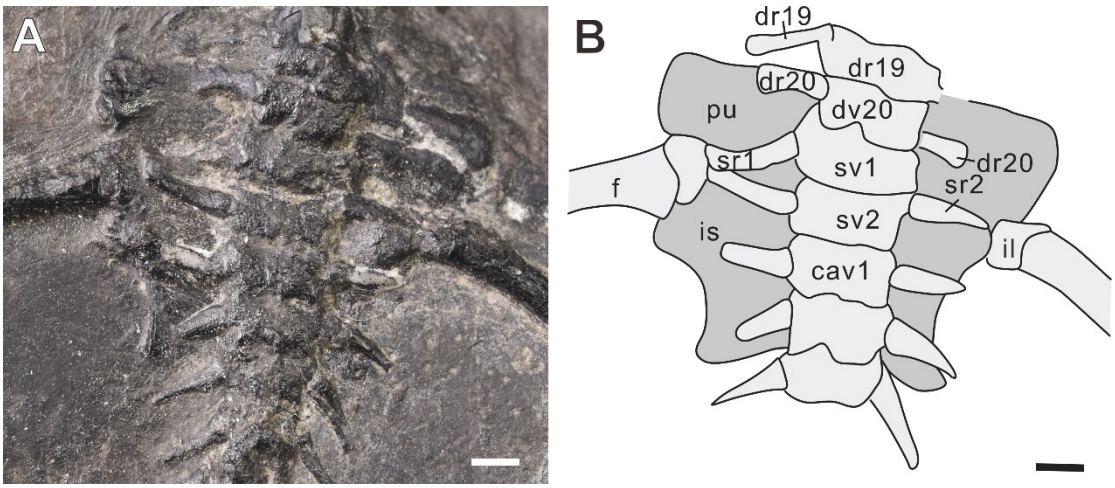

Figure 6. Sacral region of *Dianmeisaurus mutaensis* sp. nov. (HFUT MT-21-08-001). A. photo; B, interpreted drawing. Abbreviations: cav, caudal vertebra; dr, dorsal rib; dv, dorsal vertebra; fi, fibula; il, ilium; is, ischium; pu, pubis; sr, sacral rib; sv, sacral vertebra. Scale bars equal 1 mm.

Hindlimb

The hind limb is well preserved except for the distal portion of the left femur (Fig. 2). The femur is long and sigmoidally curved, and the ratio of femur length divided by humerus length is 1.39. The anterior and posterior femoral condyles are subequally extended. The internal trochanter is absent. The fibula and tibia are equal in length, but the flat tibia is much more broadened than the fibula. The small round astragalus is the only ossified tarsal bone. Metatarsal 1 is the shortest and stoutest element of the metatarsals, while others are long and slender. Metatarsals 3 and 4 are approximately the same length, slightly longer than metatarsals 2 and 5. The phalangeal formula of the pes is 1-2-3-4-3.

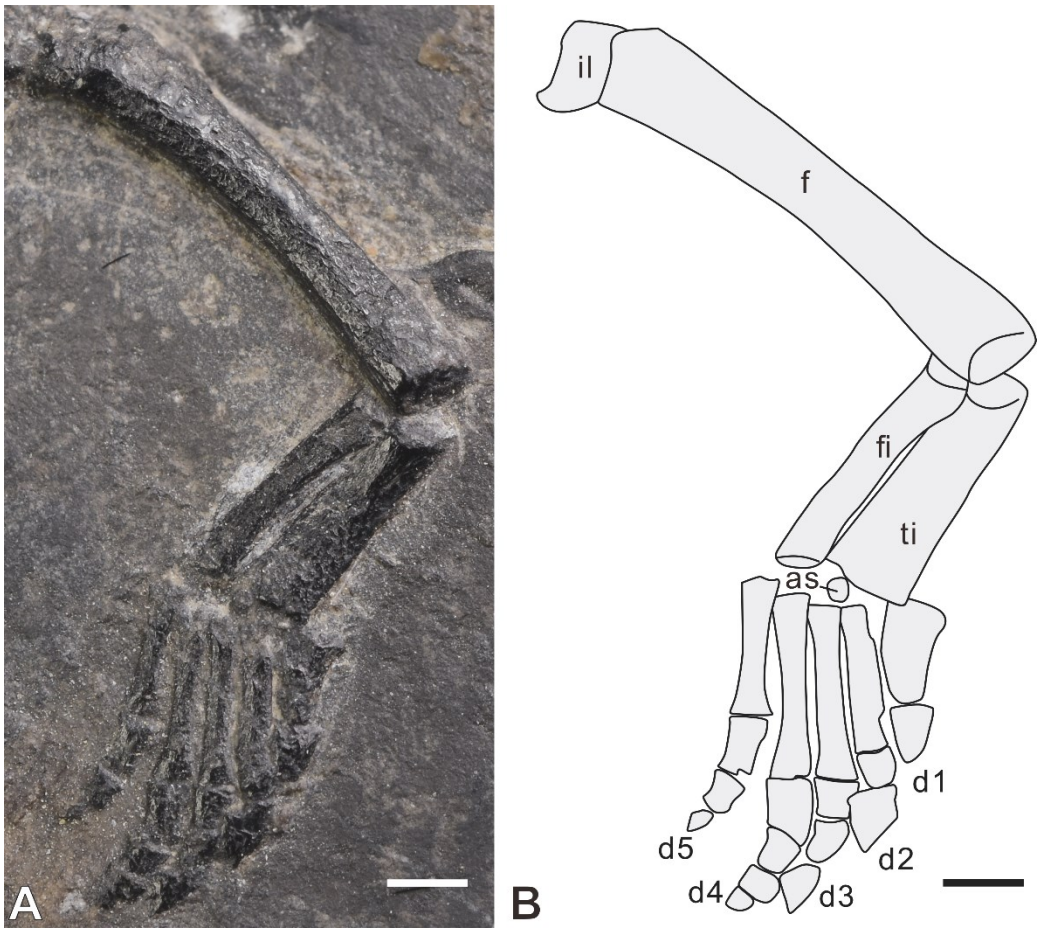

Figure 7. Right hindlimb of *Dianmeisaurus mutaensis* sp. nov. (HFUT MT-21-08-001). A. photo; B, interpreted drawing. Abbreviations: as, astragalus; d, digit; f, femur; fi, fibula; il, ilium; ti, tibia. Scale bars equal 1 mm.

Appendix B

Phylogenetic analysis

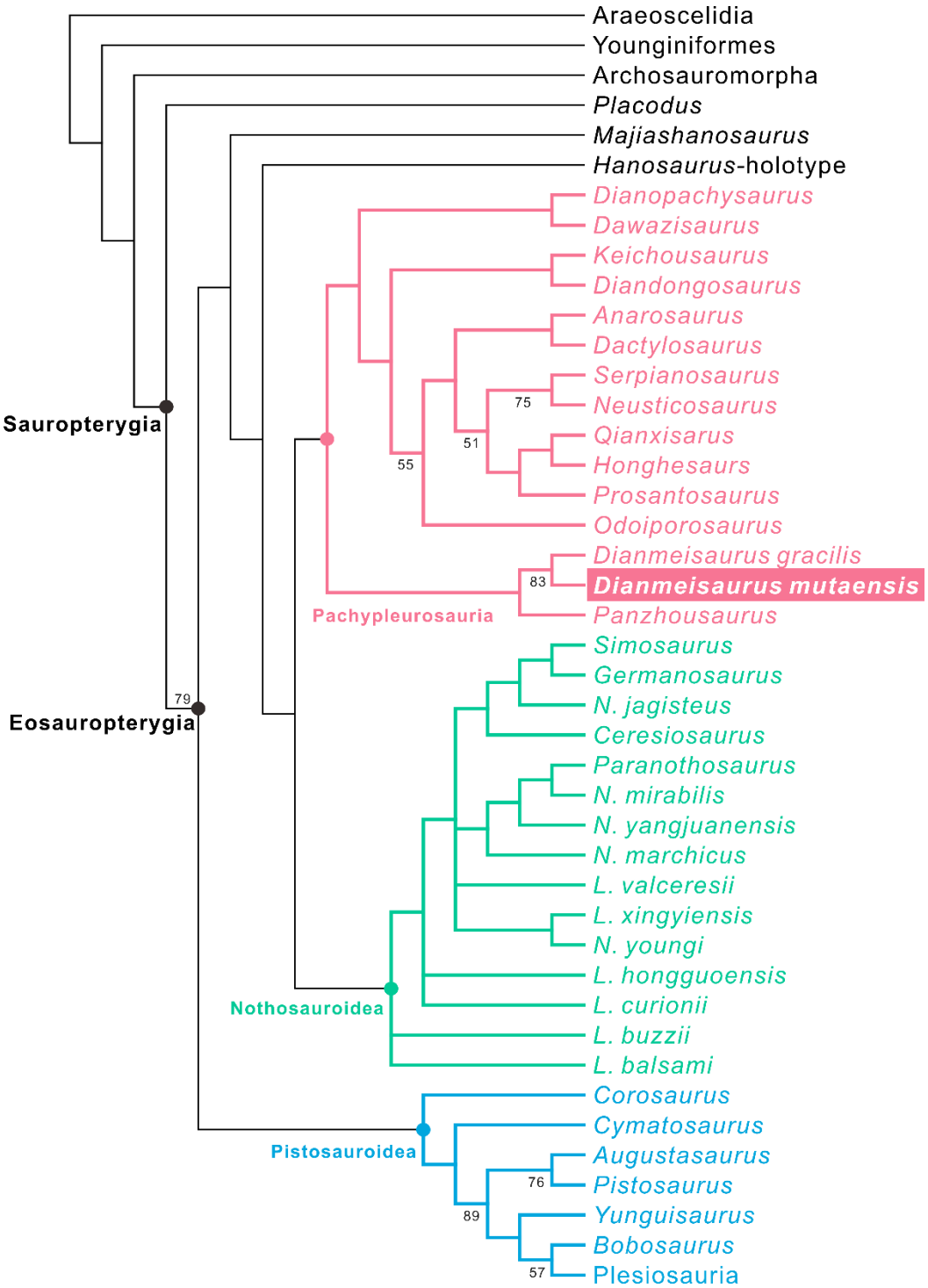

Figure 8. Strict consensus tree showing phylogenetic relationships of eosauropterygians. Bootstrap values over 50% (with 1000 replicates) are indicated in the tree.

To assess the phylogenetic position of *Dianmeisaurus mutaensis* among eosauropterygians, we compiled a new data matrix consisting of 203 characters, among

which 182 are informative, for 43 taxa. The matrix was based on a revised version of the one presented by Li and Liu (2020), and many new characters were added through a comparative study. We also coded several new taxa of eosauropterygians discovered in recent years, including *Qianxisaurus* (Cheng et al., 2012), *Odoiporosaurus* (Renesto et al., 2014), *Dianmeisaurus* (Shang & Li, 2015; Shang et al., 2017), *Dawazisaurus* (Cheng et al., 2016), *Panzhousaurus* (Jiang et al., 2019; Lin et al., 2021), *Honghesaurus* (Xu et al., 2022), and *Prosantosaurus* (Klein et al., 2022). In our phylogenetic analysis, Araeoscelidia, Younginiformes, Archosauromorpha, and *Placodus* were still selected as outgroups taxa as in Li and Liu (2020).

Heuristic searches of the new data matrix found five most parsimonious trees (tree length = 811, consistency index = 0.3169, retention index = 0.6139). *Dianmeisaurus mutaensis* forms the sister group to *D. gracilis*. The strict consensus tree recovered *Dianmeisaurus* as the sister group to *Panzhousaurus*. The clade consisting of *Dianmeisaurus* and *Panzhousaurus* occupies the basal-most position of Pachypleurosauria (Fig. 8). Meanwhile, the monophyly of Eusauropterygia is collapsed. Pistosauroidea, *Majiashanosaurus*, and *Hanosaurus* constitute the consecutive sister group to a monophyletic clade including Pachypleurosauria and Nothosauroidea. Our phylogenetic analysis recovered a monophyletic Pachypleurosauria clade, which is supported by six unambiguous synapomorphies: bones in the dermatocranium relatively smooth (character 1: 1); the ratio of longitudinal diameter of upper temporal divided by that of orbit is between 0.5-1 (character 45: 2); presence of a trough on the dorsal surface of retroarticular process (character 82: 1); anterolaterally expanded corners of clavicles present (character 128: 1); anterior preaxial margin of shaft of radius rather straight (character 190: 2); pes ungual phalanges extremely expanded (character 194: 1).

Discussion

Comparison with Dianmeisaurus gracilis

HFUT MT-21-08-001 is identified as a pachypleurosaur because of the presence of the following characteristics: the upper temporal fenestra distinctly smaller than the orbit, an anteriorly extended jugal that enters the ventral margin of the orbit, a distinct trough on the dorsal surface of the retroarticular process, pachyostotic pre- and postzygapophyses, and the reduced dorsal iliac blade. HFUT MT-21-08-001 also shares several derived characters with *Dianmeisaurus gracilis*: the postfrontal with distinct constriction behind the orbit; the width of interorbital septum distinctly shorter than the minimum length between external naris; the posterior margin of skull table deeply concave; the distal head of sacral ribs expanded.

Nevertheless, HFUT MT-21-08-001 shows many differences when compared with *Dianmeisaurus gracilis*. In *Dianmeisaurus gracilis*, the postnarial process of the premaxilla excludes the maxilla from the external naris, whereas in HFUT MT-21-08-001, the maxilla enters the external naris, which is similar to all other pachypleurosaurs (Rieppel., 2000; Cheng et al., 2012; Klein et al., 2022; Renesto et al,, 2014; Liu et al., 2011; Shang et al., 2011; Cheng et al., 2016). Also, the postfrontal extends backward beyond the frontal to a level close to the middle of the skull table in HFUT MT-21-08-001, a unique morphology among pachypleurosaurs, while it just reaches the posterior end of the frontal in *Dianmeisaurus gracilis*. Also, the postfrontal is excluded from the margin of the upper temporal fenestra in HFUT MT-21-08-001, but the postfrontal of *Dianmeisaurus gracilis* enters the upper temporal fenestra. Contrary to the presence of a distinct coronoid process in *Dianmeisaurus gracilis*, the coronoid process in HFUT MT-21-08-001 is absent.

There are even more differences in the postcranial morphology between HFUT MT-21-08-001and *Dianmeisaurus gracilis*. In contrast to the long and slender last dorsal rib in *Dianmeisaurus gracilis*, HFUT MT-21-08-001 has a stout last dorsal rib that is

shorter than the first sacral rib. The most significant difference is the number of sacral vertebrae, which is four in *Dianmeisaurus gracilis* but only two in HFUT MT-21-08-001. The phalangeal formula of the manus of HFUT MT-21-08-001 is 2-3-4-4-2 and that of the pes is 1-2-3-4-3, which are both less than the number of phalanges in *Dianmeisaurus gracilis* (manus: 2-3-5-5-3(?), pes: 2-3-4-5-5(?)).

Although HFUT MT-21-08-001 is a juvenile, these differences do not change during the development of the individual among reptiles, as far as we know (Currie, 1981; Currie & Carroll, 1984; Delfino & Sanchez-Villagra, 2010; Fröbisch, 2008; Griffin et al., 2021; Lin & Rieppel, 1998; Rieppel, 1992b; Rieppel, 1993a; Rieppel, 1993b; Rieppel, 1994; Sander, 1989). Therefore, we erected a new species for HFUT MT-08-001, i.e., *Dianmeisaurus mutaensis* sp. nov..

Phylogenetic implications to the interrelationships of eosauropterygians

Many eosauropterygian phylogenies were published after the comprehensive review of sauropterygians by Rieppel (2000). These phylogenetic analyses accompanied the description of *Dawazisaurus* (Cheng et al., 2016), *Diandongosaurus* (Liu et al., 2021; Liu et al., 2015; Sato et al., 2014a; Shang et al., 2011), *Dianmeisaurus* (Shang & Li, 2015; Shang et al., 2017), *Dianopachysaurus* (Liu et al., 2011), *Honghesaurus* (Xu et al., 2022), *Luopingsaurus* (Xu et al., 2023), *Majiashanosaurus* (Jiang et al., 2014), *Odoiporosaurus* (Renesto et al., 2014), *Panzhousaurus* (Jiang et al., 2019; Lin et al., 2021), *Prosantosaurus* (Klein et al., 2022), *Qianxisaurus* (Cheng et al., 2012), and *Yunguisaurus* (Cheng et al., 2006; Lu et al., 2021; Sato et al., 2010, 2014b; Shang et al., 2016; Wang et al., 2019; Zhao et al., 2008). But most of these phylogenetic analyses relied on the data matrix of Rieppel et al. (2002) or slightly modified versions. Recently, some novel data matrices for analyzing the interrelationship of eosauropterygians have been constructed to incorporate the morphological information available from new Chinese eosauropterygians (Li & Liu, 2020; Lin et al., 2021; Xu et al., 2023). In Li and Liu (2020), the monophyly of Eusauropterygia

collapsed, and Pachypleurosauria and Nothosauroidea constituted an unnamed clade. Our new phylogenetic analysis here also shows the collapse of the monophyly of Eusauropterygia, as in Li and Liu (2020), and suggests a new monophyletic clade comprising Pachypleurosauria and Nothosauroidea. Pistosauroidea, *Majiashanosaurus*, and *Hanosaurus* comprise the consecutive sister groups of the new clade. These results are consistent with those of Li and Liu (2020). However, the Early Triassic *Corosaurus* occupies the basal-most position of the Pistosauroidea in this study, as traditionally recognized (Rieppel 2000). This is in contrast to the phylogenetic result of Li and Liu (2020), which shows *Corosaurus* as the most basal member of Eosauropterygia. *Hanosaurus* is recovered in a relatively basal position within Eosauropterygia as in some previous analyses (e.g., Jiang et al., 2019; Li & Liu, 2020; Liu et al., 2015; Ma et al., 2015; Shang et al., 2017; Xu et al., 2022), rather than in a lineage leading to the Nothosauroidea (e.g., Cheng et al., 2012; Jiang et al., 2014; Sato et al., 2014a; Shang & Li, 2015), as a basal pachypleurosaur (e.g., Neenan et al., 2015), or even outside of the Sauropterygia clade (e.g., Cheng et al., 2016; Klein & Scheyer, 2014; Marquez-Aliaga et al., 2019; Neenan et al., 2013).

Monophyly and the palaeobiogeographic origin of Pachypleurosauria

The first cladistic analysis to test the monophyly of Pachypleurosauria was conducted by Storrs (1991). The monophyly of Pachypleurosauria was subsequently confirmed by a series of independent studies (reviewed in Rieppel, 2000). However, Holmes et al. (2008) restudied *Keichousaurus hui* and questioned the monophyly of Pachypleurosauria for the first time, which has been supported by several subsequent studies (e.g., Cheng et al., 2016; Jiang et al., 2014; Marquez-Aliaga et al., 2019; Shang et al., 2011; Wu et al., 2011). Nevertheless, some other studies still support the traditional view that Pachypleurosauria is monophyletic (e.g., Liu et al., 2011; Neenan et al., 2013).

A monophyletic Pachypleurosauria is also recovered here, as in several recent studies (Li & Liu, 2020; Lin et al., 2021; Liu et al., 2021). However, different from the traditional topology where *Dianmeisaurus* forms the sister group of *Diandongosaurus*, *Dianmeisaurus* forms the sister group of *Panzhousaurus*, and together they occupy the basal-most position of Pachypleurosauria in this study. *Dianopachysaurus* forms a monophyletic clade with *Dawazisaurus*, which comprises the sister group to all remaining pachypleurosaurs. *Keichousaurus* and *Diandongosaurus* form a monophyletic clade, comprising the sister group to a clade consisting of all European pachypleurosaurs. Our result further indicates that two middle Anisian pachypleurosaurs from South China, *Qianxisaurus* and *Honghesaurus,* are deeply nested in the European pachypleurosaurs, similar to the results of Xu et al. (2022, 2023). Compared with other Chinese pachypleurosaurs, *Qianxisaurus* and *Honghesaurus* exhibit some derived characters: the snout is elongated; the ratio of the longitudinal diameters of the upper temporal divided by that of the orbit is less than 0.5; the deltopectoral crest is well-developed; the posterior process of the postfrontal is close to the middle of the skull table.

Our phylogenetic analysis indicates that Chinese pachypleurosaurs, with the exception of *Qianxisaurus* and *Honghesaurus*, comprise the consecutive sister groups to all European pachypleurosaurs, supporting a hypothesis that Pachypleurosauria originated in the eastern Tethys (Liu et al., 2011; Renesto et al., 2014; Rieppel & Lin, 1995). However, the earliest known pachypleurosaur, *Dactylosaurus*, is from the early Anisian of the Germanic Basin (Rieppel & Hagdorn, 1997), which implies the existence of a ghost lineage in the eastern Tethys. The two unnamed pachypleurosaur skeletons from Myanmar (San et al., 2019), which could potentially be the oldest known pachypleurosaur, could falsify the existence of a ghost lineage. However, the geological age in the region where the Myanmar pachypleurosaur was collected still requires further study.

Conclusion

Dianmeisaurus mutaensis sp. nov. is established based on a newly discovered specimen from Muta village, Luxi county, Yunnan Province, China. *Dianmeisaurus mutaensis* exhibits several automorphic features, including the postfrontal extending posteriorly to the middle of the parietal table and being excluded from upper temporal fenestra, a stout last dorsal rib shorter than the first sacral rib, and two sacral vertebrae.

In addition, a novel data matrix was compiled to re-evaluate the interrelationships of eosauropterygians. Phylogenetic analysis shows the collapse of the monophyly of Eusauropterygia. Pistosauroidea, *Majiashanosaurus*, and *Hanosaurus* constitute the consecutive sister groups to a monophyletic clade comprising Pachypleurosauria and Nothosauroidea. Furthermore, the monophyly of Pachypleurosauria is supported by six synapomorphies. Our phylogenetic results provide further evidence to the eastern Tethys origin of pachypleurosaurs. However, early Anisian pachypleurosaurs from the eastern Tethys region are required to test the biogeographic hypothesis.

Institutional Abbreviations

HFUT, Hefei University of Technology, Hefei, Anhui, China; IVPP, Institute of Vertebrate Paleontology and Paleoanthropology, Chinese Academy of Sciences in Beijing, China.

Declarations

Availability of data and materials

All data generated or analyzed during this study are included in the Supplementary Data of this published article. HFUT MT-21-08-001 is stored at the Geological Museum of HFUT, Hefei, China, and publically accessed.

Competing interests

The authors declare that they have no competing financial interests.

Appendix B

Funding

This work was supported by the National Natural Science Foundation of China under Grant numbers 42172026 and 41772003.

Author's contributions

JL designed the research. YWH prepared all figures and tables. QL and YWH compiled the new data matrix, and YWH performed phylogenetic analyses. YWH and JL were the major contributors to writing the manuscript. All authors read and approved the final manuscript.

Acknowledgements

We thank A. S. Wolniewicz for early discussions, S.P. Jiang, and other members from the paleontological lab of HFUT for field assistance. We also acknowledge L. Y. Li for preparing this specimen. The associate editor N. Klein, reviewer S.N.F. Spiekman and another anonymous reviewer provided very helpful comments that significantly improved the manuscript.

Reference

Čerňanský, A., Klein, N., Soták, J., Olšavský, M., Šurka, J., & Herich, P. (2018). A Middle Triassic pachypleurosaur (Diapsida: Eosauropterygia) from a restricted carbonate ramp in the Western Carpathians (Gutenstein Formation, Fatric Unit): paleogeographic implications. *Geologica Carpathica*, *69*(1), 3-16.

Cheng, Y. N., Sato, T., Wu, X. C., & Li, C. (2006). First complete pistosauroid from the Triassic of China. *Journal of Vertebrate Paleontology*, *26*(2), 501-504.

Cheng, Y. N., Wu, X. C., Sato, T., & Shan, H.-Y. (2012). A new eosauropterygian (Diapsida, Sauropterygia) from the Triassic of China. *Journal of Vertebrate Paleontology*, *32*(6), 1335-1349.

Cheng, Y. N., Wu, X. C., Sato, T., & Shan, H.-Y. (2016). *Dawazisaurus brevis*, a new eosauropterygian from the Middle Triassic of Yunnan, China. *Acta Geologica Sinica - English Edition*, *90*(2), 401-424.

Currie, P. J. (1981). *Hovasaurus boulei*, an aquatic eosuchian from the Upper Permian of Madagascar. Palaeontologia Africana, 21, 99-168.

Currie, P. J., & Carroll, R. L. (1984). Ontogenetic changes in the eosuchian reptile *Thadeosaurus*. *Journal of Vertebrate Paleontology*, *4*(1), 68-84.

Dalla Vecchia, F. M. (2006). A new sauropterygian reptile with plesiosaurian affinity from the Late Triassic of Italy. *Rivista Italiana Di Paleontologia E Stratigrafia*, *112*(2), 207-225.

de Miguel Chaves, C., Ortega, F., & Pérez-García, A. (2018). New highly pachyostotic nothosauroid interpreted as a filter-feeding Triassic marine reptile. *Biology Letters*, 14(8), 20180130.

de Miguel Chaves, C., Ortega, F., & Pérez-García, A. (2020). The Iberian Triassic fossil record of Sauropterygia: an update. *Journal of Iberian Geology*, *46*, 445-464.

Delfino, M., & Sanchez-Villagra, M. R. (2010). A survey of the rock record of reptilian ontogeny. *Seminars in Cell & Developmental Biology*, 21(4), 432-440.

Fröbisch, N. B. (2008). Ossification patterns in the tetrapod limb--conservation and divergence from morphogenetic events. *Biological Reviews,*, *83*(4), 571-600.

Griffin, C. T., Stocker, M. R., Colleary, C., Stefanic, C. M., Lessner, E. J., Riegler, M., ... & Nesbitt, S. J. (2021). Assessing ontogenetic maturity in extinct saurian reptiles. *Biological Reviews*, *96*(2), 470-525.

Holmes, R., Cheng, Y. N., & Wu, X. C. (2008). New information on the skull of *Keichousaurus hui* (Reptilia: Sauropterygia) with comments on sauropterygian interrelationships. *Journal of Vertebrate Paleontology*, *28*(1), 76-84.

Hu, Y. W., & Liu, J. (2022). A new morphotype of nothosaurs (Sauropterygia: Nothosauridae) from the Middle Triassic of South China. *Historical Biology*, 1-10.

Jiang, D. Y., Lin, W. B., Rieppel, O., Motani, R., & Sun, Z. Y. (2019). A new Anisian (Middle Triassic) eosauropterygian (Reptilia, Sauropterygia) from Panzhou, Guizhou Province, China. *Journal of Vertebrate Paleontology*, *38*(4), 1-9.

Jiang, D. Y., Motani, R., Tintori, A., Rieppel, O., Chen, G. B., Huang, J. D., Zhang, R., Sun, Z. Y. & Ji, C. (2014). The Early Triassic eosauropterygian *Majiashanosaurus discocoracoidis*, gen. et sp. nov. (Reptilia, Sauropterygia), from Chaohu, Anhui Province, People's Republic of China. *Journal of Vertebrate Paleontology*, *34*(5), 1044-1052.

Jiang, D. Y., Motani, R., Hao, W. C., Rieppel, O., Sun, Y. L., Schmitz, L., & Sun, Z. Y. (2008). First record of Placodontoidea (Reptilia, Sauropterygia, Placodontia) from the Eastern Tethys. *Journal of Vertebrate Paleontology*, *28*(3), 904-908.

Kelley, N. P., Motani, R., Jiang, D. Y., Rieppel, O., & Schmitz, L. (2014). Selective extinction of Triassic marine reptiles during long-term sea-level changes

illuminated by seawater strontium isotopes. *Palaeogeography, palaeoclimatology, palaeoecology*, *400*, 9-16.

Klein, N., Furrer, H., Ehrbar, I., Torres Ladeira, M., Richter, H., & Scheyer, T. M. (2022). A new pachypleurosaur from the Early Ladinian Prosanto Formation in the Eastern Alps of Switzerland. *Swiss Journal of Palaeontology*, *141*(1), 12.

Klein, N., & Scheyer, T. M. (2014). A new placodont sauropterygian from the Middle Triassic of the Netherlands. *Acta Palaeontologica Polonica*, *59*(4), 887-902.

Li, Q., & Liu, J. (2020). An Early Triassic sauropterygian and associated fauna from South China provide insights into Triassic ecosystem health. *Communications Biology*, *3*(1), 63.

Lin, K. B., & Rieppel, O. (1998). Functional morphology and ontogeny of *Keichousaurus hui* (Reptilia, Sauropterygia). *Fieldiana (Geology) n.s.*, *39*, 1-39.

Lin, W. B., Jiang, D. Y., Rieppel, O., Motani, R., Tintori, A., Sun, Z. Y., & Zhou, M. (2021). Panzhousaurus Rotundirostris Jiang et al., 2019 (Diapsida: Sauropterygia) and the Recovery of the Monophyly of Pachypleurosauridae. *Journal of Vertebrate Paleontology*, e1901730.

Liu, J., Rieppel, O., Jiang, D. Y., Aitchison, J. C., Motani, R., Zhang, Q. Y., Zhou, C. Y. & Sun, Y. Y. (2011). A new pachypleurosaur (Reptilia, Sauropterygia) from the lower Middle Triassic of SW China and the phylogenetic relationships of Chinese pachypleurosaurs. *Journal of Vertebrate Paleontology*, *31*(2), 292-302.

Liu, Q., Yang, T., Cheng, L., Benton, M. J., Moon, B. C., Yan, C., An, C. B. & Tian, L. (2021). An injured pachypleurosaur (Diapsida: Sauropterygia) from the Middle Triassic Luoping Biota indicating predation pressure in the Mesozoic. *Scientific Reports*, *11*(1), 21818.

Liu, X. Q., Lin, W. B., Rieppel, O., Sun, Z. Y., Li, Z. G., Lu, H., & Jiang, D. Y. (2015). A new specimen of *Diandongosaurus acutidentatus* (Sauropterygia) from the Middle Triassic of Yunnan, China. *Vertebrata PalAsiatica, 53*(4), 281.

Ma, L. T., Jiang, D. Y., Rieppel, O., Motani, R., & Tintori, A. (2015). A new pistosauroid (Reptilia, Sauropterygia) from the late Ladinian Xingyi marine reptile level, southwestern China. *Journal of Vertebrate Paleontology*, *35*(1), e881832.

Marquez-Aliaga, A., Klein, N., Reolid, M., Plasencia, P., Villena, J. A., & Martinez-Perez, C. (2019). An enigmatic marine reptile, *Hispaniasaurus cranioelongatus* (gen. et sp. nov.) with nothosauroid affinities from the Ladinian of the Iberian Range (Spain). *Historical Biology*, *31*(2), 223-233.

Motani, R. (2009). The evolution of marine reptiles. *Evolution: Education and Outreach*, *2*(2), 224-235.

Neenan, J. M., Klein, N., & Scheyer, T. M. (2013). European origin of placodont marine reptiles and the evolution of crushing dentition in Placodontia. *Nature Communications*, *4*, 1621.

Neenan, J. M., Li, C., Rieppel, O., & Scheyer, T. M. (2015). The cranial anatomy of Chinese placodonts and the phylogeny of Placodontia (Diapsida: Sauropterygia). *Zoological Journal of the Linnean Society*, *175*(2), 415-428.

Piñeiro, G., Ferigolo, J., Ramos, A., & Laurin, M. (2012). Cranial morphology of the Early Permian mesosaurid *Mesosaurus tenuidens* and the evolution of the lower temporal fenestration reassessed. *Comptes Rendus Palevol*, *11*(5), 379-391.

Renesto, S., Binelli, G., & Hagdorn, H. (2014). A new pachypleurosaur from the Middle Triassic Besano Formation of Northern Italy. *Neues Jahrbuch für Geologie und Paläontologie - Abhandlungen*, *271*(2), 151-168.

Rieppel, O. (1989). A new pachypleurosaur (Reptilia: Sauropterygia) from the Middle Triassic of Monte San Giorgio, Switzerland. *Philosophical Transactions of the Royal Society of London B*, *323*(1212), 1-73.

Rieppel, O. (1992a). The skull in a hatchling of *Sphenodon punctatus*. *Journal of Herpetology*, *26*(1), 80-84.

Rieppel, O. (1992b). Studies on skeleton formation in reptiles. I. The postembryonic development of the skeleton in *Cyrtodactylus pubisulcus* (Reptilia: Gekkonidae). *Journal of Zoology*, *227*(1), 87-100.

Rieppel, O. (1993a). Studies on skeleton formation in reptiles. v. Patterns of ossification in the skeleton of *Alligator mississippiensis* DAUDIN (Reptilia, Grocodylia). *Zoological Journal of the Linnean Society*, *109*(3), 301-325.

Rieppel, O. (1993b). Studies on skeleton formation in reptiles: patterns of ossification in the skeleton of *Chelydra serpentina* (Reptilia, Testudines). *Journal of Zoology*, *231*(3), 487-509.

Rieppel, O. (1994). Studies on skeleton formation in reptiles. Patterns of ossification in the skeleton of *Lacerta agilis exigua* Eichwald (Reptilia, Squamata). *Journal of Herpetology*, *28*(2), 145-153.

Rieppel, O. (1999a). Phylogeny and paleobiogeography of Triassic Sauropterygia: problems solved and unresolved. *Palaeogeography Palaeoclimatology Palaeoecology*, *153*(1-4), 1-15.

Rieppel, O. (1999b). The Sauropterygian genera *Chinchenia*, *Kwangsisaurus*, and *Sanchiaosaurus* from the Lower and Middle Triassic of China. *Journal of Vertebrate Paleontology*, *19*(2), 321-337.

Rieppel, O. (Ed.). (2000). *Sauropterygia I* (Vol. 12A). Verlag Dr. Friedrich Pfeil.

Rieppel, O., & Hagdorn, H. (1997). Paleobiogeography of Middle Triassic Sauropterygia in central and western Europe. In M. Callaway Jack & L. Nicholls Elizabeth (Eds.), *Ancient Marine Reptiles* (pp. 121-144). Academic Press.

Rieppel, O., & Lin, K. (1995). Pachypleurosaurs (Reptilia: Sauropterygia) from the Lower Muschelkalk, and a review of the Pachypleurosauroidea. *Fieldiana (Geology) n.s.*, *32*, 1-44.

Rieppel, O., Sander, P. M., & Storrs, G. W. (2002). The skull of the pistosaur *Augustasaurus* from the Middle Triassic of northwestern Nevada. *Journal of Vertebrate Paleontology*, *22*(3), 577-592.

San, K. K., Fraser, N. C., Foffa, D., Rieppel, O., & Brusatte, S. L. (2019). The first Triassic vertebrate fossils from Myanmar: Pachypleurosaurs in a marine limestone. *Acta Palaeontologica Polonica*, *64*(2), 357-362.

Sander, P. M. (1989). The pachypleurosaurids (Reptilia: Nothosauria) from the Middle Triassic of Monte San Giorgio (Switzerland) with the description of a new species. *Philosophical Transactions of the Royal Society of London B*, *325*(1230), 561-666.

Sato, T., Cheng, Y. N., Wu, X. C., & Li, C. (2010). Osteology of *Yunguisaurus* Cheng et al., 2006 (Reptilia; Sauropterygia), a Triassic pistosauroid from China [Article]. *Paleontological Research*, *14*(3), 179-195.

Sato, T., Zhao, L. J., Wu, X. C., & Li, C. (2014a). *Diandongosaurus acutidentatus* Shang, Wu & Li, 2011 (Diapsida: Sauropterygia) and the relationships of Chinese eosauropterygians. *Geological Magazine*, *151*(01), 121-133.

Sato, T., Zhao, L. J., Wu, X. C., & Li, C. (2014b). A new specimen of the Triassic pistosauroid *Yunguisaurus*, with implications for the origin of Plesiosauria (Reptilia, Sauropterygia). *Palaeontology*, *57*(1), 55-76.

Shang, Q. H., Sato, T., Li, C., & Wu, X. C. (2016). New osteological information from a 'juvenile' specimen of *Yunguisaurus* (Sauropterygia; Pistosauroidea). *Palaeoworld*, *26*(3), 500-509.

Shang, Q. H., Wu, X. C., & Li, C. (2020). A New Ladinian Nothosauroid (Sauropterygia) from Fuyuan, Yunnan Province, China. *Journal of Vertebrate Paleontology*, e1789651.

Shang, Q. H., & Li, C. (2015). A new small-sized eosauropterygian (Diapsida: Sauropterygia) from the Middle Triassic of Luoping, Yunnan, southwestern China. *VERTEBRATA PALASIATICA*, *53*(4), 265-280.

Shang, Q. H., Li, C., & Wu, X. C. (2017). New information on *Dianmeisaurus gracilis* Shang & Li, 2015. *VERTEBRATA PALASIATICA*, *55*(2), 145-161.

Shang, Q. H., Wu, X. C., & Li, C. (2011). A new eosauropterygian from Middle Triassic of eastern Yunnan Province, southwestern China. *VERTEBRATA PALASIATICA*, *49*(2), 155-171.

Storrs, G. W. (1991). Anatomy and relationships of *Corosaurus alcovensis* (Diapsida: Sauropterygia) and the Triassic Alcova Limestone of Wyoming. *Bulletin of the Peabody Museum of Natural History*, *44*, 1-151.

Stubbs, T. L., & Benton, M. J. (2016). Ecomorphological diversifications of Mesozoic marine reptiles: the roles of ecological opportunity and extinction. *Paleobiology*, *42*(4), 547-573.

Sues, H. D., & Carroll, R. L. (1985). The pachypleurosaurid *Dactylosaurus schroederi* (Diapsida: Sauropterygia). *Canadian Journal of Earth Sciences*, *22*(11), 1602-1608.

Swofford, D. (2021). PAUP: phylogenetic analysis using parsimony (and other methods), version 4.0. 1998. *Sinauer Sunderland, MA*.

Wang, X., Lu, H., Jiang, D. Y., Zhou, M., & Sun, Z. Y. (2020). A new specimen of Yunguisaurus (Reptilia; Sauropterygia) from the Ladinian (Middle Triassic) Zhuganpo Member, Falang Formation, Guizhou, China and the restudy of Dingxiaosaurus. *Palaeoworld*, *29*(1), 137-150.

Wise, P. A., Vickaryous, M. K., & Russell, A. P. (2009). An embryonic staging table for in ovo development of *Eublepharis macularius*, the leopard gecko. *The Anatomical Record*, *292*(8), 1198-1212.

Wu, X. C., Cheng, Y. N., Li, C., Zhao, L. J., & Sato, T. (2011). New information on *Wumengosaurus delicatomandibularis* Jiang et al., 2008 (Diapsida: Sauropterygia), with a revision of the osteology and phylogeny of the taxon. *Journal of Vertebrate Paleontology*, *31*(1), 70-83.

Xu, G. H., Ren, Y., Zhao, L. J., Liao, J. L., & Feng, D. H. (2022). A long-tailed marine reptile from China provides new insights into the Middle Triassic pachypleurosaur radiation. *Sci Rep*, *12*(1), 7396.

Xu, G. H., Shang, Q. H., Wang, W., Ren, Y., Lei, H., Liao, J. L., Zhao, L. J. & Li, C. (2023). A new long-snouted marine reptile from the Middle Triassic of China illuminates pachypleurosauroid evolution. *Scientific Reports*, *13*(1), 16.

Zhao, L. J., Sato, T., & Li, C. (2008). The most complete pistosauroid skeleton from the Triassic of Yunnan, China. *Acta Geologica Sinica-English Edition*, *82*(2), 283-286.